# TIME DEPENDENT PROPERTIES OF SEMICRYSTALLINE POLY(ARYLENE ETHER ETHER KETONE) (PEEK) ABOVE AND BELOW THE GLASS TRANSITION

by

Vesselin Hristov Velikov

DISSERTATION SUBMITTED TO THE FACULTY OF
THE VIRGINIA POLYTECHNIC INSTITUTE AND STATE UNIVERSITY
IN PARTIAL FULFILLMENT OF THE REQUIREMENTS FOR THE
DEGREE
OF

**DOCTOR OF PHILOSOPHY**
**IN MATERIALS ENGINEERING SCIENCE**

Hervé Marand, Chairman
Garth L. Wilkes
Thomas C. Ward
Ronald G. Kander
Richie M. Davis

Blacksburg, Virginia
November 19, 1996

**Keywords:** Polymers, Melting, Annealing, Physical Aging, PEEK

# TIME DEPENDENT PROPERTIES OF SEMICRYSTALLINE POLY(ARYLENE ETHER ETHER KETONE) (PEEK) ABOVE AND BELOW THE GLASS TRANSITION

by

Vesselin Hristov Velikov

Hervé Marand, Chairman

Department of Chemistry

## (ABSTRACT)

Long time annealing of semicrystalline PEEK above the glass transition results in the observation of several time dependent phenomena - "physical aging", "secondary crystallization", "multiple melting" of lamellae with different thermal stability etc. Their interrelation - common origin and kinetics of development, is characterized extensively for the first time in this study.

The evolution of the crystallinity during the secondary crystallization process was monitored by DSC and density measurements. Crystallinity was characterized according to the standard two-phase model of semicrystalline polymers and analyzed with respect to the failure of the model to adequately describe the physical state of the polymer. A discrepancy was observed between DSC and density crystallinity values and their respective rates of development during the secondary crystallization stage.

WAXS reveals that the crystal density is not a physical constant, but depends on the crystallization and/or annealing temperature. Furthermore, the crystalline lamellae densify with time during crystallization and/or annealing. This observation leads to the conclusion that there is no one-to-one correspondence between density and crystallinity and necessitates the application of a revised equation for density crystallinity which accounts for the dynamics of crystal densification.

The characteristics of the low temperature endothermic peak in the DSC scan of PEEK (peak maximum, transition enthalpy etc.) were found to evolve with annealing time and temperature during the secondary crystallization process in a way similar to the kinetics of development of the enthalpy relaxation process in amorphous polymeric glasses.

This study reports for the first time in the literature the observation of "physical aging" above the glass transition in the case of PEEK (according to the definition of this term given by Struik). An extensive investigation of the "double melting"/"multiple melting" phenomenon, which is observed as a result of isothermal treatment of the polymer above $T_g$, was performed and several new observations reported.

After the end of the primary crystallization process, the semicrystalline polymer is a nonequilibrium system due to the fact that crystallinity is less than unity. The system's continuing approach to equilibrium and its response to mechanical perturbations follow kinetics similar to that of segmental relaxation below the glass transition.

This work is ultimately dedicated to ALL
MY TEACHERS, who taught me:

- to see the beauty of the world around through the eyes of a physicist;
- to appreciate the difference between knowledge and reality;
- to look for the right questions before going for the answers;

and especially - to those of them, who lead me into the amazing world of polymers, from which, as the first one of them told me, '...there is no return!'

"Past experience teaches us that it would be prudent to first establish the existence of a forest before trying to identify the trees."

L. Mandelkern, "The Crystalline State" (reference 9)

## ACKNOWLEDGMENTS

I wish to acknowledge the guidance, support, appreciation, and critical discussions for my work as provided during the last 5 years by:

- my advisor, Prof. Hervé Marand, whose patience and guidance were critical for the development of this work from a curiosity spurned wandering of my mind into a legitimate scientific research.

- Prof. Garth L. Wilkes, Prof. Thomas C. Ward, and Prof. Ronald G. Kander - the interactions with them, whether in a classroom or at seminars and discussions were extremely helpful and enjoyable lessons.

- Prof. Richie C. Davis, Prof. David Dillard and Dr. Allan R. Shultz with helpful guidance and discussions in the areas of their expertise.

- Dr. Abaneshvar Prasad through sharing his knowledge with me at a time I did not know how little my knowledge of polymers was.

- Vivek Prabhu and Dr. Milos Netopilic as they gave me critical assistance with some experiments.

- Dr. Brian Sauer, Dr. Ravi K. Verma, and Dr. Srinivas Srivatsan with helpful discussions.

- the fellow students in Prof. Marand's group, old and new, who created the lively and enjoyable atmosphere in which I lived (literally) for the last 5 years.

Special thanks to Julie "Joules" Vivirito, who worked with me on this project during a critical stage in its development in the summer of 1993 and gave me valuable support through restless work and everlasting good spirit. The work of Sinan Velioglu on the PBT experiments during the summer of 1994 is acknowledged too.

My family was a constant source of support for me. I couldn't have done it, if I didn't always feel from a distance, their love and support for me.

Many, many friends made life in Blacksburg during the years a wonderful environment to work and live. And thanks to U! I was able to overcome difficult times.

Now is the time to confess, that many ideas and experiments were born in my mind at random places and times, but always due to your critical presence - on a mountain hike, at a lakeside walk, at "The Cellar" or at the "Mill Mountain" coffee shop, even on Mt. Rogers!

And yes! That's how I spent most of my $$s, generously provided every year on April 16 by Dick and Jane to the National Science Foundation Science and Technology Center for High Performance Polymeric Adhesives and Composites, to be given to me as a research assistantship during my stay at Virginia Tech. Thank you, Dick! Thank you, Jane! Thank you, congressmen and senators!... America has gained a place in my heart and mind forever!

# TABLE OF CONTENTS

# List of Figures

# List of Tables

# CHAPTER 1. INTRODUCTION

## PEEK - INTRODUCTION

Poly(arylene ether ether ketone) (PEEK) is among few semicrystalline polymers, which in the last decade have been the subject of extensive applied as well as fundamental research due to their potential application as high performance thermoplastic matrix resins in advanced composite materials. PEEK exhibits a high glass transition temperature ($T_g$ ~ 145°C-155°C), high melting temperature ($T_m'$ ~ 335-345°C), and wide crystallization range ($T_m' - T_g \geq 200$ K). This allows for fast melt processing of a semicrystalline matrix, which due to its intermediate crystallinity (~ 30-45 %) has excellent properties. Table 1.1 summarizes some of the main physical properties and characteristics of PEEK, relevant to this study.

The properties of the polymer depend strongly on the morphology, which develops as a result of specific processing conditions. Therefore a better control of the processing condition variables and their effect on the morphology would allow for better control of the final properties of the neat PEEK material and its composites. An extensive review of the effect of processing and more specifically of thermal history on the properties of semicrystalline thermoplastic composites (with PEEK as an example) has appeared recently in the literature [1].

Crystallinity is one of the most important characteristics, which control the desired properties of the polymer. The effect of thermal history on the development of crystallinity in PEEK is a central part of this work and will be analyzed in detail later.

### *Goals:*

There are three main objectives of this work:

1. The original goal was to investigate the effect of chain mobility, molecular weight (MW), and molecular weight distribution (MWD) on the formation of a "second structure" (type II structure in the spherulites) in PEEK. According to polarized optical microscopy (POM) observations reported by Marand and Prasad,[2] this structure developed at long times

**Table 1.1** Physical properties and structural characteristics of PEEK.

Poly(arylene ether ether ketone) (PEEK)

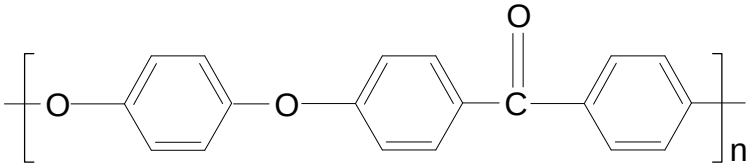


IUPAC Nomenclature:

Poly(oxy-1,4-phenylene-oxy-1,4-phenylene-carbonyl-1,4-phenylene)

| | |
|---|---|
| MW of repeat unit [g/mol] | 288.3 |
| Glass transition temperature, $T_g$ (at 10 K/min) | |
| amorphous | 145°C |
| semicrystalline | ~ 155°C |
| Melting temperature, $T_m$ (at 10 K/min) | ~ 335 - 345°C |
| Crystal unit cell | orthorhombic |
| Space group | Pbcn |
| Room temperature unit cell dimensions [a, b] | |
| a | ~ 7.8 Å |
| b | ~ 5.9 Å |
| c | ~ 10.0 Å |
| Density [g/cm$^3$] | |
| bulk melt crystallized (variable with conditions) | 1.300 - 1.310 |
| bulk amorphous | 1.263 - 1.265 |
| crystal density [a, b] | 1.365 - 1.415 |
| Heat of fusion, $\Delta H_m^0$ [ cal/g] [b] | 31.1 |

[a] Values reported from independent sources differ significantly beyond experimental uncertainties of the individual evaluations

[b] See section 3.2.3 for discussion on other literature values

and paralleled the formation and evolution of the low temperature melting endotherm of melt-crystallized PEEK. This original objective evolved into a thorough characterization of the conditions for development of the low-temperature annealing endotherm of PEEK and its evolution with time and temperature of thermal treatment. At a later stage of the research two more goals emerged:

2. Quantitative characterization of the development of secondary crystallinity in PEEK by various routine methods of crystallinity evaluation.

This characterization was done specifically in connection with the development of additional crystallinity during the long-time evolution of the low temperature annealing endotherm of PEEK. Furthermore, this long-term time dependence of the crystallinity of the polymer was correlated with the time dependence of several other structural characteristics of the polymer above $T_g$: a) the density of the unit cell of the crystalline lamellae and its time and temperature evolution; b) the crystallinity induced change in mobility of the amorphous regions in the semicrystalline polymer, as manifested by the change in the glass transition temperature with crystallization/annealing and the possible presence of a Rigid Amorphous Fraction (RAF) above $T_g$; and c) the phenomenon of "physical aging" above $T_g$ for semicrystalline PEEK. The ultimate goal was to test the compatibility of the standard two-phase model for the physical state of semicrystalline polymers with the development of secondary crystallization. Based on the results obtained during the realization of the objectives in item 2) and the study of a large volume of literature data on the subject of "multiple melting" and "annealing endotherm(s)" in other polymers, the third and most complex and challenging goal emerged:

3. To study and present evidence for the universality of some of the conclusions of this work for the entire spectrum of semicrystalline polymeric materials: linear homopolymers, crystallizable blends and copolymers, liquid crystalline polymers, natural polymers etc.

## *Overview of this study:*

Chapter 2 presents a review of several subjects which are important for this study:

- a very brief review of structure and morphology of semicrystalline polymers,

- the two-phase model of the physical state of semicrystalline polymers and its deficiencies from the point of view of current knowledge of the subject,

- a brief introduction into the subject of secondary crystallization,

- review of the phenomenon known as "double melting" (or "multiple annealing endothermic peaks") in the case of PEEK and for other polymers as well,

- review of the structural relaxation in semicrystalline and amorphous polymers, known as "physical aging", with particular attention to the effect of "physical aging" above the nominal glass transition of semicrystalline polymers.

Chapter 3 describes the materials used, their preparation conditions and the methods of characterization employed. The fractionation procedure and the MW characterization of the PEEK fractions are described there too.

At the beginning of chapter 4 the results from the melting studies of the PEEK fractions are presented so as to emphasize the development of the goals of this study. The next sections of chapter 4 present the results from the four main areas of investigation: characterization of the low temperature annealing endotherm in the heating scan of PEEK and examples for few other polymers - isotactic polystyrene (i-PS) and poly(butylene terephthalate) (PBT); crystallinity evaluation by density and DSC (Differential Scanning Calorimetry) on three different sets of semicrystalline PEEK samples and supporting results from wide angle X-ray scattering (WAXS) measurements; the results from the small strain creep studies of the "physical aging" of semicrystalline PEEK below and above its nominal $T_g$, and calorimetric investigation of the glass transition of semicrystalline PEEK.

Chapter 5 is devoted to summary and discussions of the results presented in chapter 4. The development with time and temperature of crystallization of the DSC and density crystallinities for the three sets of crystallized samples and observed discrepancies are discussed. The final results are analyzed and compared with similar studies of poly(phenylene sulfide) (PPS). Based on this discussion, conclusions about the density of the amorphous phase in semicrystalline PEEK are drawn and the connection of these results with

a model of the development of secondary crystallinity, currently developed, is presented. The conclusions from the "physical aging" study about the effect of isothermal annealing on the slowing down of the retardation are presented and their connection with the results from the crystallinity study is established.

At the end of chapter 5, the results of several experiments, deemed "controversial" from the point of view of the current model for the low temperature melting endotherm and secondary crystallinity, are presented. These results and their analysis naturally point out some ideas for future work, which should be undertaken in order to resolve the controversial conclusions stemming from these experiments.

Considering the goals presented above, the reader might certainly judge, that some of the objectives are not fully realized at the end, and that more studies are necessary in order to completely cover several of the objectives and justify some of the conclusions. This is especially true in regard to the third goal above - the universality of some of the phenomena and conclusions and their validity for other polymers with quite different chemistry and architecture. The purpose of this work is not to give a definitive proof. Certainly, after more than 30 years of research on the subject of annealing effects on semicrystalline polymers and especially multiple melting endotherms, resulting from isothermal annealing conditions, such a task will be enormous even if taken alone. This work merely attempts to bring together a few examples for the major commercial linear polymers and a few examples from several different groups of polymeric materials. It exposes the similarities between the results from these studies, as opposed to the original treatment in each of the investigations, which predominantly had chosen to focus only on a single polymer or a single class of polymers. In support of this part of the study only a few original results are reported.

Regarding the study of crystallinity, one might argue that it is limited in scope, providing extensive analysis of the results from only two methods - DSC and density crystallinities. In defense of this choice it can be said that the two methods chosen are two of the most routine methods for determination of crystallinity. It was considered important to limit this study to only those methods, for which their application and interpretation of results seems straightforward from the point of view of the two-phase model of crystallinity and is

not a subject of fundamental controversy. The starting assumption was that the results uncovered will then lead straight to conclusions about the physical state of the polymer, and not about the inherent limitations and controversial points of the method itself.

The study of the effects of molecular weight on the development of the low temperature melting endotherm of PEEK was abandoned after the initial qualitative results were obtained. This was deemed necessary for two reasons: the practical one - to be able to investigate the problems stated in goals 1) and 2) above with large quantities of commercially available material; and for the reason of clear and "clean" methodology - to be able to discard the possibility, that any unusual (from the point of view of previous knowledge) behavior uncovered might be due to flaws in the synthesis, fractionation and conversion of the material studied. If the results and conclusions of this work are accepted, certainly there is a lot of work which can be done with the fractionated material, namely - quantitative investigation of the effect of MW and MWD on the development of the low temperature annealing endotherm and the structural relaxation phenomena above $T_g$.

# CHAPTER 2

# REVIEW

Most macromolecules can exist in either of two states - crystalline or amorphous, which are characterized by the degree of conformational order within the chain and the degree of order of the chains relative to one another.

In the unoriented *amorphous* state the chains are randomly arranged and the overall conformational state of the individual chain is the random coil state. The properties of polymers in the high temperature limit of this state are the properties of common viscous liquids. An important characteristic of the amorphous state, relevant to this study, is the glass transition temperature, $T_g$, of a polymer. This is a kinetic characteristic used to characterize the dramatic increase upon cooling of the relaxation time of a polymer (by several orders of magnitude within a narrow temperature interval). The molecular mechanism for the glass transition phenomenon is the loss of the ability for thermally activated cooperative motion in the liquid state upon cooling. In practical terms, $T_g$ is defined as the temperature where the relaxation times are of the order of $10\text{-}10^2$ s. Alternatively, $T_g$ is defined as the temperature at which the viscosity of the liquid reaches the value of $10^{13}$ Poise, or as the point of discontinuity in the plots of the first derivatives of the volume and enthalpy against temperature, respectively - $\alpha_T(T)$ and $C_P(T)$. Below this temperature the kinetic restraints lead to the realization of a nonequilibrium amorphous state - the glassy state.

The *crystalline* state of macromolecules is the subject of the rest of this review.

## 2.1 Semicrystalline Polymers

The crystalline state of polymers is characterized by three dimensional intermolecular order. Due to the fact that, by their nature, polymers are composed from repeating sequences of covalently bonded atoms, any thermally stable polymer with reasonable degree of regularity within the sequences of repeat units will be able to exist in an ordered state - the crystalline state, thermodynamically more stable than the amorphous state below the equilibrium melting temperature. Because the morphology resulting from the crystallization process is controlled

by kinetics, rather than by thermodynamics, polymers never crystallize completely. The morphology resulting from crystallization is a partially crystalline and therefore metastable state in which ordered crystalline regions coexist with regions of disordered chains.

In the following, some of the features of the physical state of semicrystalline polymers will be presented: the two-phase model of the physical state of semicrystalline polymers, a general review of the kinetics of crystallization with emphasis on the two-stage break up into primary and secondary crystallization processes, the concepts of crystallinity, crystal-amorphous interphase, rigid amorphous fraction (RAF) and certain time dependent phenomena, developing beyond the completion of the primary crystallization process.

Under quiescent conditions most polymers crystallize forming spherulites on the macroscopic level. The spherulites grow radially until the bulk of the polymer is filled. On the microscopic level the spherulites consist of lamellar crystals, formed by chain folding (figure 2.1). The lamellae are separated by regions of amorphous material, which could consist of free, uncrystallized polymer chains, free ends of chains partially included in the crystalline lamellae, tight (short) or loose (long) chain folds and tie molecules which constitute bridges between lamellar crystals (figure 2.2).

For evaluation of the extent to which a polymer has been able to crystallize, the parameter crystallinity - $\chi_c$ ("crystallinity index", "percent crystallinity") is introduced. It is usually expressed as the fraction (or alternatively as the percentage) of the total volume or mass of the material, which exhibits crystalline order. Except where denoted, for reasons of consistency and clarity in this work only the weight fraction crystallinity will be considered (further mentioned simply as "crystallinity"), expressed as a fractional number:

$$\chi_c = \frac{m_c}{m_a + m_c} \qquad (2.1)$$

where $m_c$ is the mass of the crystalline phase and $m_a$ - the mass of the amorphous phase. The definition makes use of the idea [3] that any intensive property $P^i$ of a semicrystalline polymer could be represented by an average of the "partial properties" of the crystalline and the amorphous components - $\overline{P}_c^i$ and $\overline{P}_a^i$:

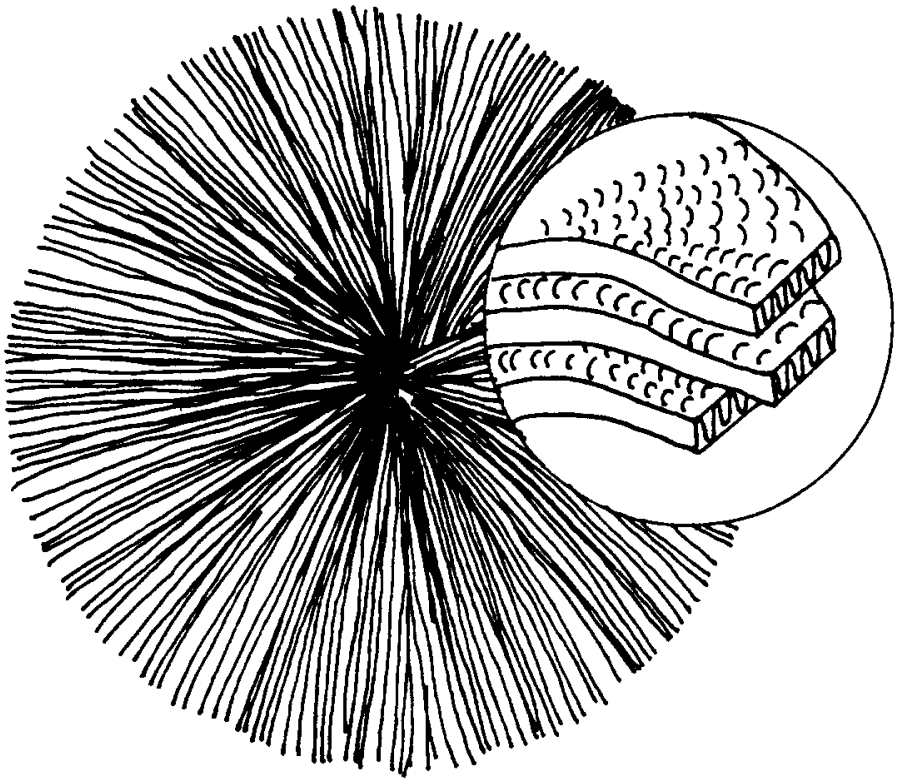

**Figure 2.1** Semicrystalline morphology - spherulite with chain folded lamellae (from reference 4).

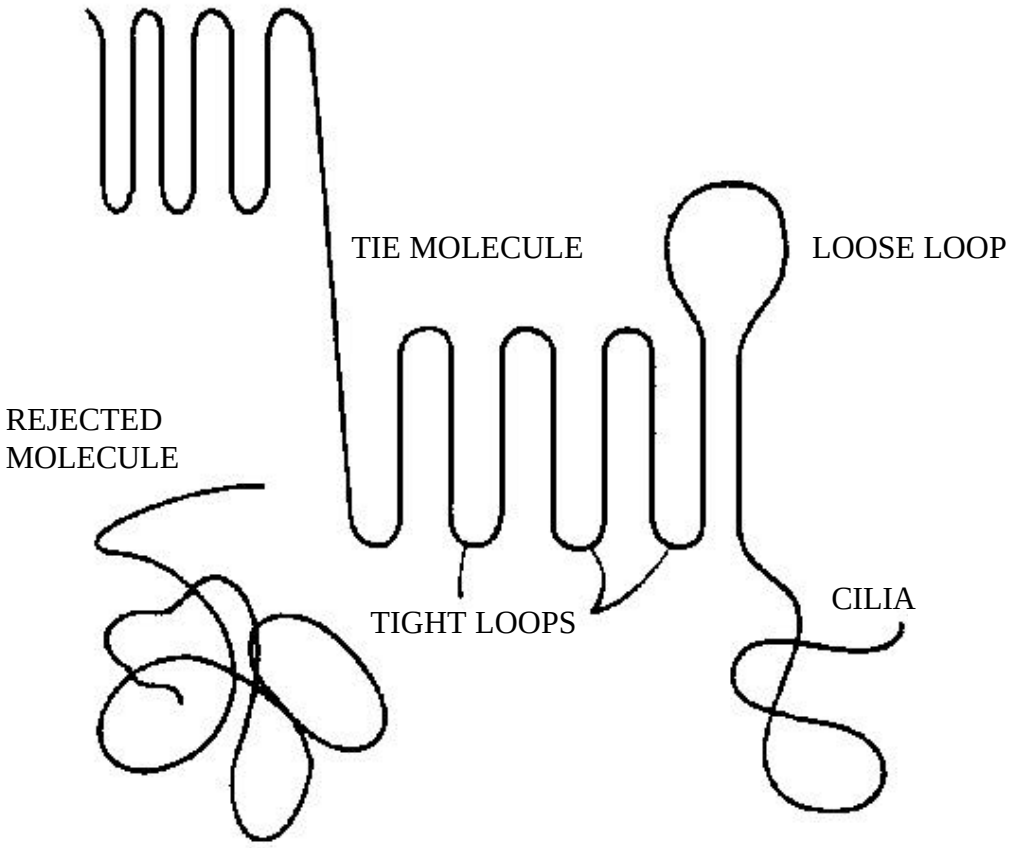


**Figure 2.2** Local structure within the sperulites: crystalline lamellae and intercrystalline amorphous regions (from reference 7).

$P^i = \chi_c \, \overline{P}_c^i + (1-\chi_c)\, \overline{P}_a^i$ . Therefore

$$\chi_c = \frac{P^i - \overline{P}_a^i}{\overline{P}_c^i - \overline{P}_a^i} \qquad (2.2)$$

For example, density crystallinity $\chi_c^{Dens}$ is derived from the relationship between the density of the polymer $\rho$ and the densities of the amorphous and the crystalline phases, respectively $\rho_a$ and $\rho_c$, if we use as an intensive property the specific volume $\overline{v}$:

$$\chi_c^{Dens} = \frac{\overline{v}_a - \overline{v}}{\overline{v}_a - \overline{v}_c} = \frac{(1/\rho_a) - (1/\rho\ )}{(1/\rho_a) - (1/\rho_c)}$$

$$\chi_c^{Dens} = \frac{\rho_c}{\rho} \frac{\rho - \rho_a}{\rho_c - \rho_a} \qquad (2.3)$$

where $\rho_a$ and $\rho_c$ are taken as the standard reference values for the ideal amorphous and crystalline phases respectively.

If the property $P^i$ is related (linearly) to the crystalline phase only (e.g. in equation (2.2) $\overline{P}_a^i$ = 0), as in the case of the enthalpy of fusion, then the crystallinity becomes a simple ratio between the measured property and its value for the pure crystalline phase. Thus DSC crystallinity $\chi_c^{DSC}$ is expressed as:

$$\chi_c^{DSC} = \frac{\Delta H_m}{\Delta H_m^0} \qquad (2.4)$$

where $\Delta H_m^0$ is the melting enthalpy for a 100% crystalline polymer.

Crystallinities defined through other properties, sensitive to the difference between the crystalline and amorphous phase, can be used too: WAXS crystallinity, IR (infrared spectroscopy) crystallinity, NMR (nuclear magnetic resonance) crystallinity, SAXS (small angle X-ray scattering) crystallinity etc.

In routine evaluations of crystallinity the importance of the fact that, in addition to the value of the property $P^i$ obtained from the experiment, the values of the partial properties $\overline{P}_a^i$

and $\overline{P}_a^i$ are required, is seldom rigorously examined. In fact, their determination for a sample with a given crystallinity level is rarely possible. Thus, usually one has to determine them from extrapolations to the limiting cases of the perfectly amorphous and the perfectly crystalline polymer. [3] One exception is the case when $P^i$ is the specific volume. The partial specific volume of the crystalline phase $\overline{v}_c$ can be evaluated directly from X-ray measurements of the volume of the unit cell. Yet, despite the fact that, for many polymers, there are significant differences between literature values for $\overline{v}_c$, the determination of $\overline{v}_c$ is rarely done in situ. For evaluations of $\chi_c^{Dens}$, an "accepted" value for $\overline{v}_c$ is usually taken from literature sources.

This study concentrates on the fundamental investigation of the two most commonly used routine methods for evaluation of crystallinity - DSC and density. A more detailed review of crystallinity from an experimental point of view is given in chapter 3.1.3.

## 2.2 The Two-Phase Model of the Physical State of Semicrystalline Polymers

From a theoretical point of view, it is important to note that the above definitions of crystallinity assume the semicrystalline polymer is an *ideal two-phase* system. The interface between the crystalline and amorphous phases is assumed sharp and effectively substituted with an infinitesimally thin dividing surface, and the two phases are homogeneous and stable. That is, the partial properties of the amorphous and the crystalline phases are those of the *ideal crystalline* phase and the *ideal amorphous* phase.

These are, in fact, the premises of the simple *two-phase model* of the physical state of semicrystalline polymers. [3] It is somewhat peculiar to realize, that the two-phase model's assumptions, a "standard" for the application of the definition for crystallinity [5, 6] - equation (2.1) and any particular form of equation (2.2), are in fact reminiscent of the old fringed micelle model for the physical state of semicrystalline polymers. The fringed micelle model was among the first models of semicrystalline polymers to illustrate the ideas, that crystalline polymers are only partially crystalline and the size of the individual crystals is smaller than the chains' length (figure 2.3). It emerged as an elegant operative idea about how molecular

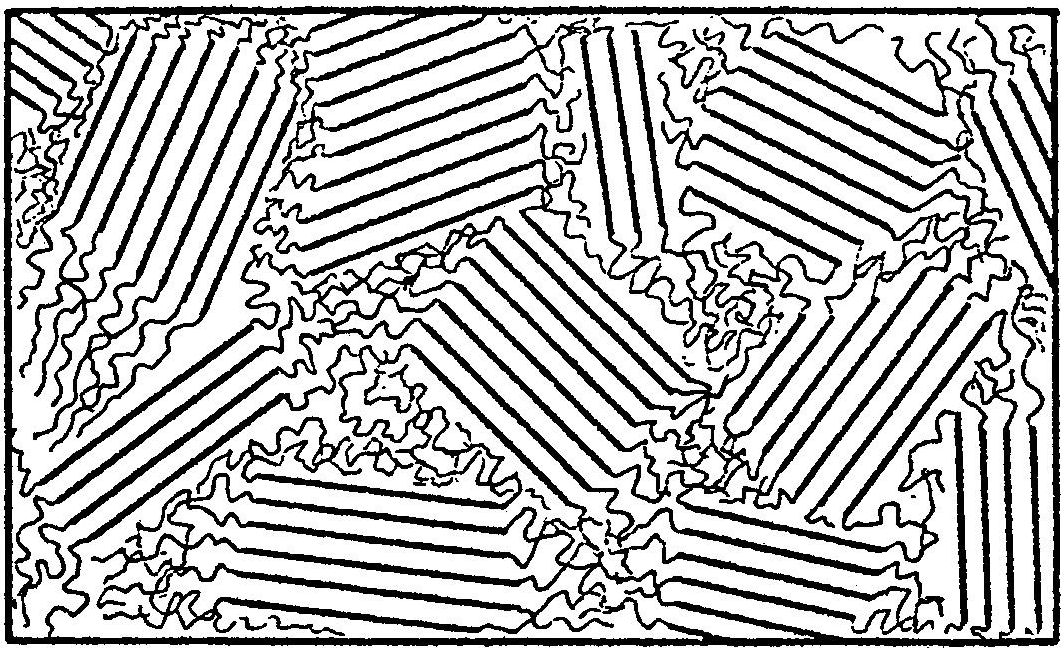

**Figure 2.3** The "fringed micelle" model of semicrystalline polymers (from reference 8).

order is formed and dissipated at microscopic level so as to justify the observed sizes of crystalline regions in polymers. It is not difficult to envision why the question about the nature of the interfacial regions doesn't even have to be asked in the case of the fringed micelle model - all chain segments emerging from the crystal surface and diffusing into the amorphous regions are in a similar state. Order is continuously diffused out from the crystalline surface and not too far away from the crystalline surface the amorphous regions are homogeneous.

However, the nature of molecular organization in polymer crystals is misrepresented by this model. After the discovery of the fact that linear flexible and semiflexible polymers crystallize by the mechanism of chain folding, the simplistic two-phase fringed micelle model was abandoned, except in few special areas, mostly - the polymers to which it was applied initially: rubber, cellulose, and polymers with very low crystallinity. [5]

The idea of the simple two-phase model was kept, however, for the purpose of its great operative value in the analysis of crystallinity. It would be then reasonable to state that the shortcomings of the simple two-phase model represent the problems and shortcomings of the concept of crystallinity itself too.

## 2.3 Deficiencies and Problems of the Two-Phase Model

In this section several theoretical problems of the two-phase model from the point of view of current knowledge about polymer crystalline architecture will be presented. In addition, a critical examination of the literature on semicrystalline polymers reveals a large number of interrelated experimental studies, all consistently pointing towards limitations and inconsistencies of the two-phase model. To clearly relay these to the reader several concepts and results need to be introduced, namely: the concept of *rigid amorphous fraction* (RAF), *secondary crystallization*, *multiple melting* endotherms, and structural relaxation ("*physical aging*") above the nominal glass transition temperature of semicrystalline polymers.

### *2.3.1 General problems*

Out of the variety of shortcomings of the two-phase model and its associated concept of crystallinity (p. 110 in reference 5) several are of importance for the subject of this work.

Those are the inherent problems in describing the crystalline phase, the amorphous regions and lack of description of the interphase between them:

- nature of the interfacial transition layer between the ordered crystalline regions and the disordered amorphous zones,

- constraints on the intercrystalline amorphous regions; transient and permanent entanglements, which perturb them from the "ideal" truly amorphous polymer,

- crystallite perfection.

From the coexistence of the chain folded crystalline lamellae and amorphous regions arises the question about the nature of the interfacial region between them. The nature of the interfacial zone is illustrated schematically in figure 2.2 and with more detail - in figure 2.4. Its unique feature, lacking in the fringed micelle model, is the special state of disorder in the basal planes where the chain folding occurs. The molecules, which protrude and occupy the interfacial zone can belong to a variety of diverse populations: short (tight) folds, long (loose) folds, taut and loose tie molecules, connecting adjacent crystals, free ends (cilia).

Quite obviously, at least the presence of relatively short folds at the interface and their absence from the bulk of the amorphous phase brings us to the conclusion that the disordered regions cannot be considered homogeneous. Therefore a caution must be exercised when an unique property is assigned to the amorphous phase as a whole. That property should be considered as an apparent property of the amorphous phase instead. The second conclusion is that due to this inhomogeneity of the disordered regions and the fact that the interfacial zone could possess unique properties, it cannot be considered infinitesimal anymore.

Allowance must be made also for the different mobility which chains with various degree of attachment to the rigid crystalline lamellae might have. The constraints the crystalline phase imposes on the mobility of short folds are stronger than those on loose folds. Shorter tie molecules would have less conformational freedom than longer ones. The effect of the crystalline lamellae on the cilia and free unattached chains is only in terms of a macroscopic spatial constraint at relatively low levels of crystallinity. At higher crystallinities the interconnectedness of the crystalline lamellae through rather taut tie molecules

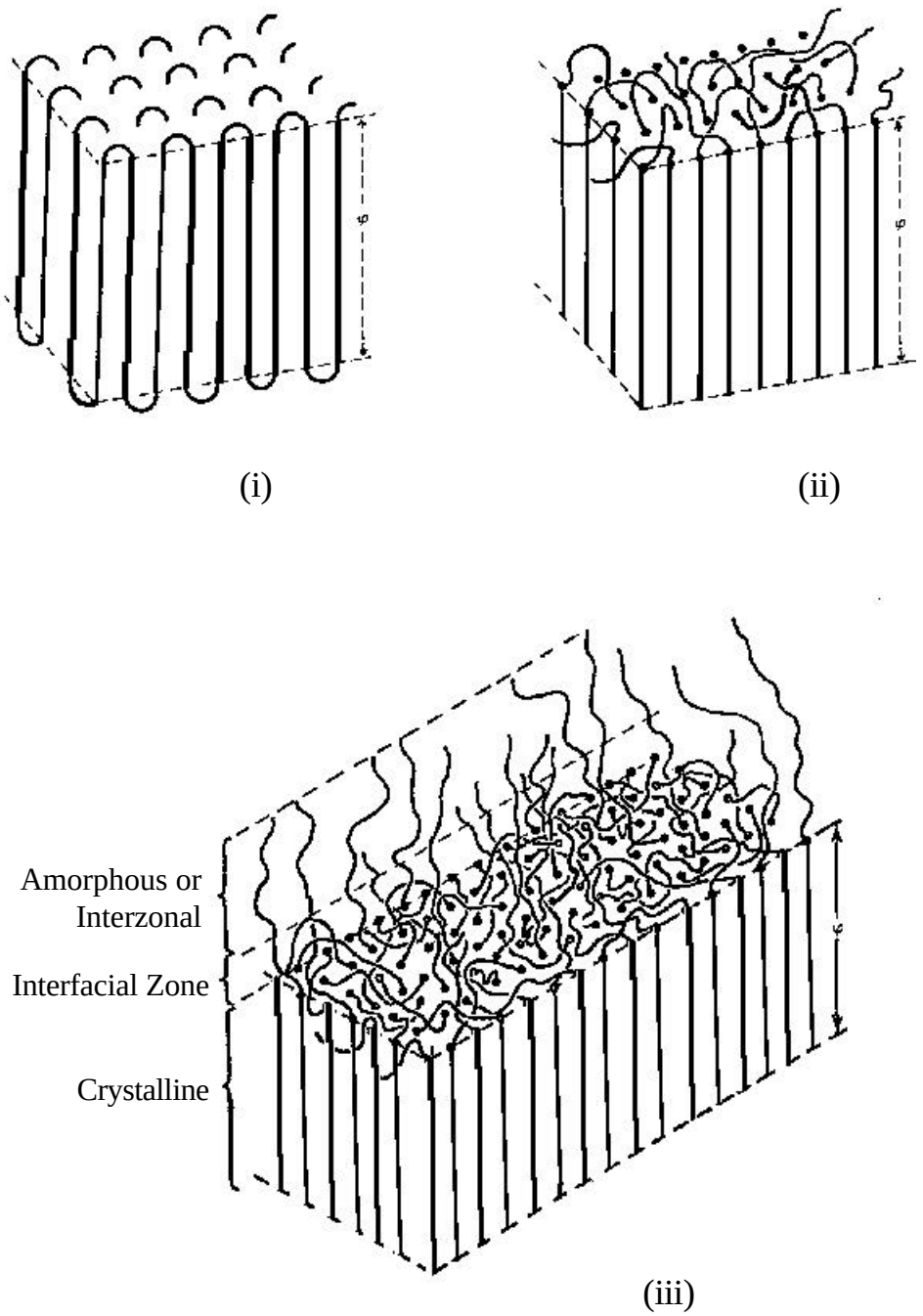


**Figure 2.4** Various models for the nature of the interfacial chain-fold surface layer: (i) - regular folds (adjacent reentry), (ii) - nonadjacent reentry (switchboard model), (iii) - nonadjacent reentry with tie molecules (from reference 9).

could lead to the effective embedding of the free amorphous regions into a rigid semicrystalline matrix. Such an idea has been suggested in fact long ago by Boyer.[7]

Finally one must note that the two-phase model (and its treatment of crystallinity) does not address the static and dynamic aspects of the issue of crystalline perfection. Intracrystalline defects are present in the crystalline lamellae. In general, these defects lead to changes in the values of the partial properties considered for the definition of crystallinity. By considering these partial properties to be the ones for the "ideal" polymer crystal the two-phase model fails to take that change into account. Such a change could be considered a static effect - a weighted change due to certain concentration of defects. Yet dynamic treatment of the problem could be necessary too, if the crystalline perfection changes with environmental conditions (and therefore partial properties and ultimately - crystallinity, are affected).

### *2.3.2 Rigid Amorphous Fraction (RAF)*

The concept of RAF is introduced when the physical state of the polymer within the two phase semicrystalline structure is considered in reference to the two characteristic temperatures $T_g$ - the glass transition and $T_m^{'}$ - the melting temperature of the polymer. Above the $T_m^{'}$ there is a single phase - the polymer is in the liquid state. In this state the chains are mobile and in dynamic equilibrium. If from this state the polymer is successfully quenched without crystallizing below $T_g$ it is in the metastable glassy state. The freezing of the cooperative motions of the chain molecules below the glass transition temperature leads to a rigid behavior. The release of these cooperative molecular motions when going up in temperature through the temperature region of the glass transition leads to the relaxation from a rigid glassy state to a mobile supercooled liquid state. The result of this relaxation when the polymer is probed with various techniques is that a change in physical properties typical for a second order transition is observed: a break in the slope of the temperature dependence of enthalpy, volume etc. and a stepwise change in their first derivatives - respectively $C_P$ (the heat capacity at constant pressure), $\alpha_T$ (the volume coefficient of thermal expansion) etc. The

magnitude of this stepwise change can be used as a characteristic of the strength of this relaxation in the glass transition region.

As most linear polymers with a fair degree of chain regularity are able to crystallize in the temperature window between $T_g$ and $T_m$ it follows that above the glass transition of the polymer a fraction of the material crystallizes and for all practical purposes remains with properties similar to the properties of the rigid glassy state up to the melting temperature of the crystalline lamellae. Therefore from the point of view of the two phase model described above one can state that below $T_g$ the rigid fraction $f_r$ of a semicrystalline polymer is equal to the sum of the crystalline fraction - the crystallinity $\chi_c$ and the glassy fraction below $T_g$ - (1- $\chi_c$) e.g. equal to unity. Above $T_g$ the rigid fraction of the polymer should consist only of the crystalline fraction: $f_r = \chi_c$ and the amorphous fraction of the polymer above $T_g$ should be mobile.

Therefore, according to the well known properties of the glass transition of polymers, the magnitude of $\Delta C_P$ - the change of the heat capacity at $T_g$ is a measure of the strength of the relaxation for calorimetric probing of the material. It had been found however, [10, 11] that for many semicrystalline polymers only part of the amorphous fraction as measured by (1- $\chi_c$) participates in the glass transition, that is, above $T_g$:

$$f_r = 1 - \frac{\Delta C_P}{\Delta C_P^0} \quad > \quad \chi_c$$

where $\Delta C_P$ is the measured heat capacity change for the semicrystalline polymer and $\Delta C_P^0$ is the measured heat capacity change for a completely amorphous polymer.

This had lead to the suggestion that above $T_g$ the amorphous phase in the polymer can be subdivided into a “mobile” (MAF) and “rigid” amorphous fraction (RAF). [10] Therefore above $T_g$:

$$f_r = 1 - f_{MAF} = 1 - \frac{\Delta C_P}{\Delta C_P^0} \quad = \quad \chi_c + f_{RAF} \qquad (2.5)$$

The existence of rigid amorphous fraction above $T_g$ has been observed in high crystallinity flexible chain polymers such as poly(oxymethylene) (POM),[12] polyethylene (PE),[11] isotactic polypropylene (i-PP),[13] poly(caprolactone),[170] as well as semi-flexible chain polymers, such as polymers with aromatic rings in the backbone or sterically hindering side groups, attaining intermediate crystallinities: poly(butylene terephthalate) (PBT),[14] poly(ethylene terephthalate) (PET),[113, 170] i-PS, [206] nylon-6 and nylon-6,6, [170] poly(phenylene sulfide) (PPS), [15, 62] and PEEK. [16] For PEEK, according to the calorimetric study of Cheng et al., [16] the amount of the overall rigid fraction above $T_g$ is:

$$f_r = 1 - \frac{\Delta C_P}{64.8} \quad [C_P \text{ in mcal/deg*g}] \qquad (2.6)$$

After the original discussions of the existence of RAF from calorimetric studies of semicrystalline polymers by Wunderlich and co-workers, its existence has been confirmed using the same basic principle as described above through other techniques. For example, by using dielectric spectroscopy (DS) it has been found that the strength of the dielectric relaxation at $T_g$ is less than what is expected on the basis of the known crystallinity of the polymer; hence the RAF $f_{RAF}^{DS}$ above $T_g$ is being evaluated. Cebe and Hong [17] and Kalika and Krishnaswamy [18] have examined and confirmed the existence of RAF for PEEK by dielectric relaxation techniques. Similarly by studying transport properties of dichloromethane vapor in PEEK at low activity a higher than expected fraction of the polymer is found to be impermeable to the vapors above $T_g$. [19] The fractional amount of impermeable polymer in excess of the crystallinity evaluated is associated with the RAF - $f_{RAF}^{Diff}$ .

The proposed existence of a rigid amorphous fraction in the polymer above the glass transition region is a clear deviation from the standard two phase model of semicrystalline polymers. This phenomenon - the effective immobilization of portion of the amorphous material in a semicrystalline polymer, has been attributed to the constraining effect of the crystalline lamellae on the amorphous regions between the crystals. [10] With this statement in mind it is not difficult to suggest as a first step in exploring the molecular origin of the RAF, that its existence could be connected with the failure of the simple two-phase model to take

into account the existence of a finite interphase with unique properties between the crystal and the amorphous polymeric liquid (figure 2.4). While further studies to characterize its exact location and molecular nature in the overall semicrystalline morphology are necessary it should not be forgotten that detailed analysis of the RAF content depends strongly on the precision and consistency in the evaluation of crystallinity by the standard methods employed.

### *2.3.3 Secondary Crystallization*

The overall crystallization kinetics of a polymer can be modeled with the Avrami equation:

$$1-\chi_c(t)=\exp(-kt^n) \qquad (2.7)$$

where $\chi_c(t)$ is the mass fraction of the material transformed into the crystalline state at time *t* and *n* is an exponent characteristic for the mode of nucleation, growth geometry and the growth control process.[3] After taking a double logarithm and proper manipulation, equation (2.7) can be linearized to give the exponent *n* and the constant *k* from a linear plot. From experimental studies of several polymers it has been known that, at some stage of the crystallization process, the crystallinity vs. time double logarithmic curves exhibit large negative deviations from the predictions of the Avrami equation.[3] This is illustrated on figure 2.5, which presents the double logarithmic plot of crystallinities derived from dilatometry and DSC (crystallization enthalpy and melting enthalpy) for polyethylene fraction (MW = 85,000 g/mol) crystallized from the melt at 127.5°C.[20] The initial part of the plots is indeed linear (with a slope corresponding to *n* =2.5) as expected from equation (2.7). The later part of the curve shows that the crystallization process significantly slows down - the slope of the curves drops down to about 0.5.

This type of observation for PE and other polymers has lead to the formal break up of the crystallization process into two processes: *primary crystallization*, characterized by the Avrami kinetics, and *secondary crystallization* - the crystallization which takes part after the primary one is completed.[3] The secondary crystallization process is generally characterized as the slow process of completion of crystallization. It could occur in inter-spherulitic amorphous regions - in the material trapped between impinged spherulites, which crystallizes

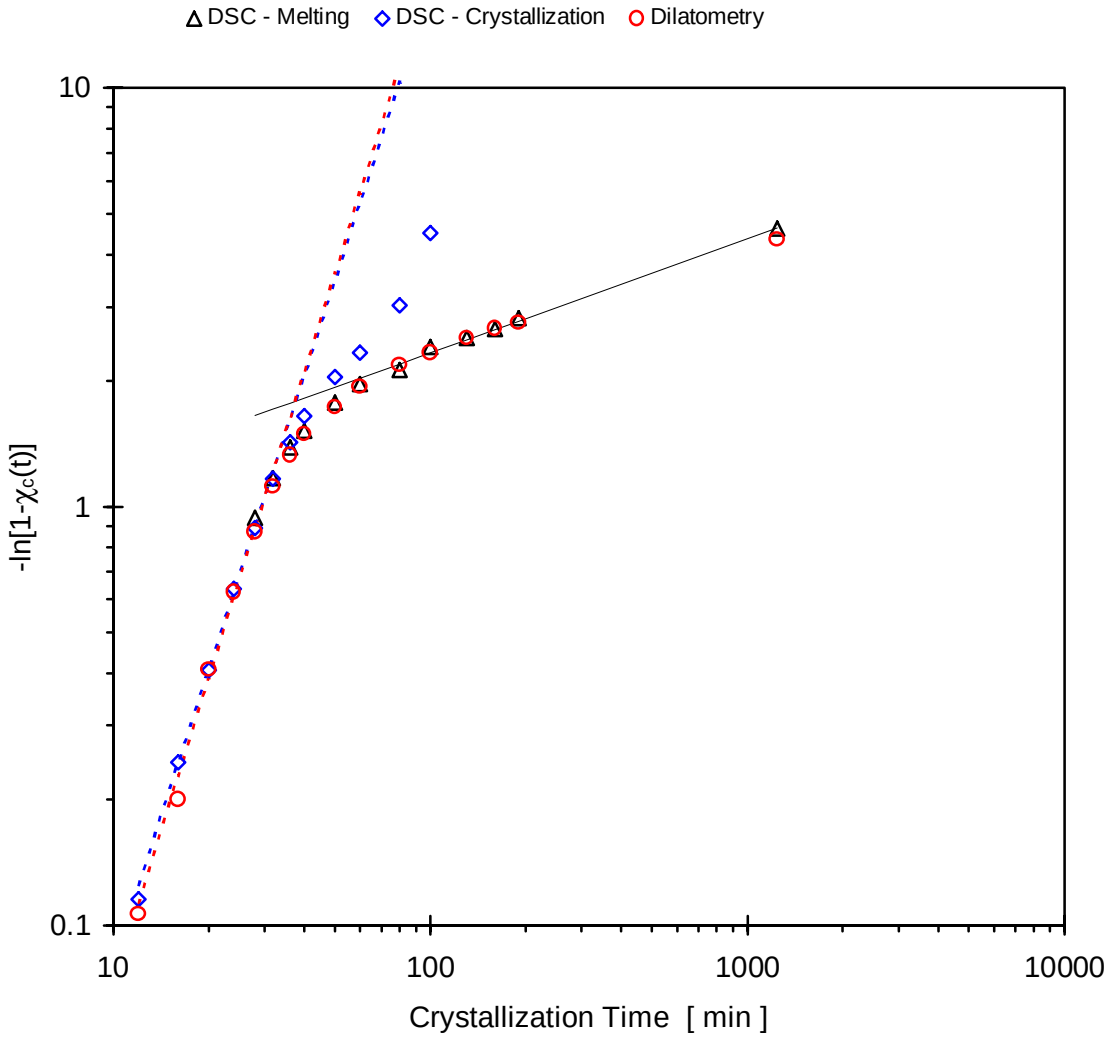


**Figure 2.5** Primary and secondary crystallization in polyethylene at $T_x$ = 127.5°C from DSC and dilatometric evaluation of crystallinity (data from reference 123).

more slowly than the previously formed mature spherulites due to its full enclosure into the rigid semicrystalline matrix of the previously formed spherulites. [3]

Secondary crystallization could also occur in the intra-spherulitic amorphous regions. This could proceed through one of two possible mechanisms - incorporation of the intra-spherulitic amorphous material into: 1) existing crystals, 2) newly formed crystals. [3]

Most often in the literature the long-time evolution of crystallinity through the secondary crystallization stage has been associated with the "lamellar thickening" mechanism.[21-23] This conclusion appeared from the results of studies of the effect of annealing on semicrystalline polymers of high crystallinity, mostly - linear PE. It has been reported to occur following a log-time kinetics. [24-29] Fischer and Schmidt [27, 29] have reported from SAXS studies, that upon annealing the long period of single crystals of linear PE changes according to the following equation:

$$L = L_0 + K \log\left( t / t_0 \right) \qquad (2.8)$$

where $L$ and $L_0$ are respectively the values of the long period after annealing at times $t$ and $t_0$. The rate of increase of crystallinity with $\log(t_x)$ decreases with increasing undercooling, [21, 30] suggesting a mobility controlled process.

It is important to note that all of the studies quoted above have been somewhat limited in scope - they investigated annealing effects and lamellar thickening above the $\alpha$-relaxation temperature range of PE and at relatively low undercoolings or upon direct crystallization from the melt.

In polymers with medium and low levels of crystallinity the effect of long annealing on crystallinity, morphology and properties is much less understood. This is partly due to the much larger variety of polymers studied and the much wider range of methodologies applied. While this should have been beneficial, in reality the interpretation of results from differing techniques or combinations of techniques has lead some authors to arrive at conflicting conclusions.

For example, isotactic polypropylene (i-PP) has a crystalline α-relaxation process at about 100°C, [88, 136-138] which is above the glass transition temperature ($T_g$ = -10°C [13]). Annealing effects at room temperature have been studied mostly from a material properties point of view [31-35] and independently from the long time melt crystallization and annealing above the crystalline α-relaxation.

In contrast to i-PP, poly(ethylene terephthalate) (PET), which has a glass transition temperature above ambient conditions has been studied over the entire range from $T_g$ to $T_m^{'}$. A wide variety of mechanisms for the long time effect of annealing on the crystal structure and morphology have been suggested: lamellar thickening, [36] crystallization of new populations of lamellae, [37] combination of thickening and recrystallization, [36] and crystal perfection. [38, 40, 41] The thermal transitions and the morphological changes observed upon heating up from the isothermal crystallization or annealing temperature have been attributed to melting and recrystallization [39] or the melting of separate populations of lamellae. [36, 37]

It is highly unlikely, however, that lamellar thickening is the mechanism of secondary crystallization of semi-rigid chain polymers such as PET, PBT, PEEK, PPS or materials with bulky side groups like i-PS. For these polymers the chain rigidity is unfavorable to reorganization at the lamellar fold surface, which is required if isothermal lamellar thickening is to occur. A partial indication for this is the fact that, unlike PE and i-PP, no crystalline α-relaxation process (resulting in relaxation of the crystal-amorphous interface) has been detected for these polymers. [136]

In summary - from the review presented above, it follows that secondary crystallization is an indirect confirmation of the shortcomings of the simple two-phase model. The deviations from the theoretical predictions of the Avrami model and the changes in the morphology of the semicrystalline matrix on a long time scale indicate the non-equilibrium nature of the structure formed during what is for most polymers the "practical" crystallization step - the relatively short primary crystallization process.

## 2.4 Double Melting

One of the deficiencies of the two-phase model is associated with the phenomenon of "multiple melting". Regardless of the physical nature of this phenomenon, the possibility, that its associated enthalpy is related to reorganization processes upon heating or to melting of populations with different stability poses a serious question about the ability of the static picture drawn by the two-phase model to describe properly the semicrystalline state of polymers.

Multiple endothermic transitions above $T_g$ in the DSC thermograms of pure and thermally stable linear polymers could be the result of a number of possible reasons. A multiple endothermic melting scan, for example, could reflect the well separated melting traces of fractions of the polymer with different molecular weight, successively crystallized in time or upon change in temperature, an indication of a transformation between different crystal modifications of the polymer, the separate melting transitions of different crystal phases or the overall effect of melting-recrystallization-remelting processes. [42] In a liquid-crystalline polymer the successive endothermic transitions reflect successive phase transformations upon heating from a crystalline to liquid-crystalline order and from liquid crystalline to isotropic liquid state.

### *2.4.1 Double Melting in Semicrystalline Polymers*

This review and the following report will be limited strictly to the investigation of multiple endothermic transitions resulting from the *isothermal* annealing and/or crystallization of semicrystalline polymers from the glassy state or from the melt.

Typical multiple melting trace in the case of PEEK is shown on figure 2.6. It has been widely stated in the literature [1] that in the “double melting” scan of PEEK the low temperature endotherm is the result of isothermal crystallization and/or annealing between $T_g$ and $T_m$ of the polymer. Upon such a thermal treatment the DSC melting scan of the polymer shows, in addition to the broad melting endotherm in the 280-350°C range, a small low temperature endotherm appearing just above the temperature of isothermal treatment.

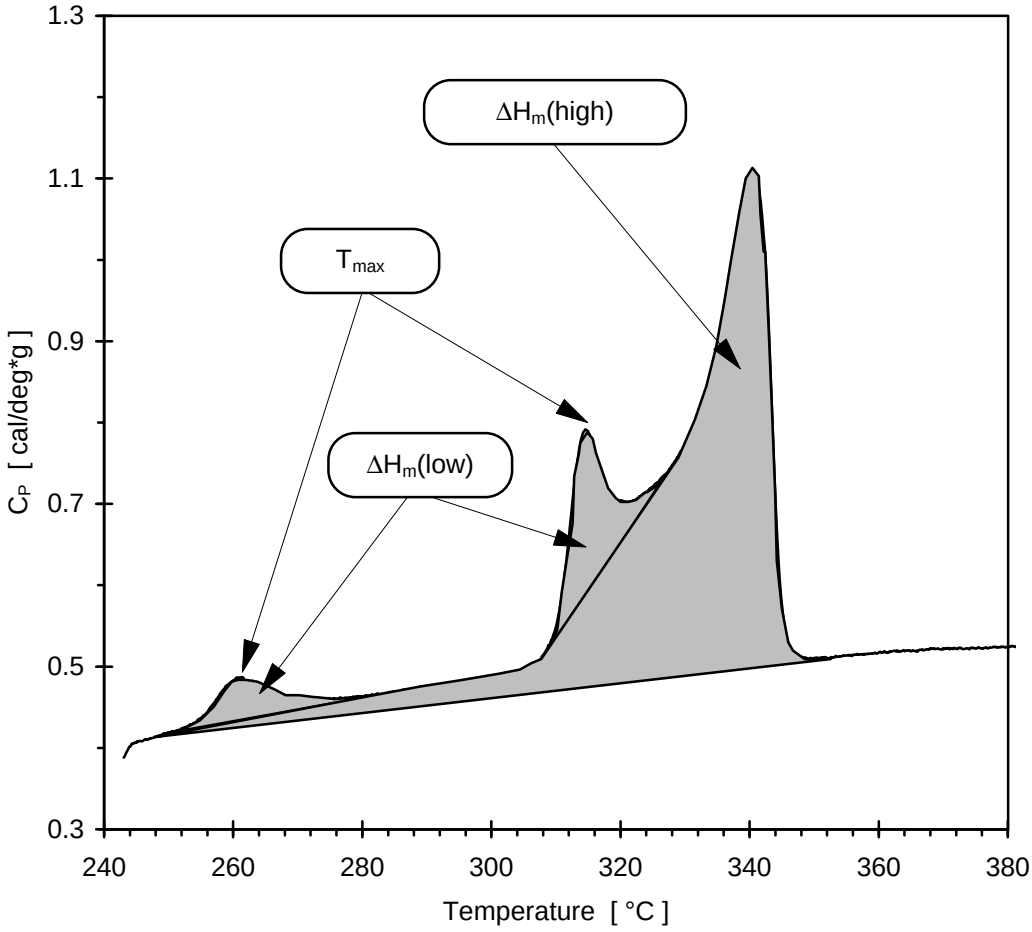


**Figure 2.6** Multiple melting of semicrystalline PEEK after crystallization at 305°C for 60 min followed by annealing at 245°C for 60 min.

More importantly, it needs to be emphasized, that this multiple melting behavior is a universal phenomenon, observed for many flexible chain polymers crystallized or annealed below their crystalline α-relaxation and for semi-rigid chain polymers crystallized or annealed at any temperature between $T_g$ and $T_m^{'}$. Before the final melting, one or more endothermic transitions, which result from similar conditions, namely - subjection of a polymer to a single step or multiple step isothermal treatment, have been observed for many polymers, regardless of the differences and complexity of their chain architecture, chain mobility, crystal structure(s), crystal morphology, and thermochemical stability:

- polyethylene (PE), [43]

- isotactic polypropylene (i-PP), [13, 44-47, 161, 172-175]

- isotactic polystyrene (i-PS), [48-50, 176-180]

- poly(vinyl chloride) (PVC), [51-53, 183]

- polyamides (several even numbered nylons), [37, 54-56, 180-182]

- polyesters - poly(ethylene terephthalate) (PET) [36-40, 57, 184-190] and poly(butylene terephthalate) (PBT), [14, 58-60, 189-192] poly(hydroxybutyrate) (PHB) and its copolymers with hydroxyvalerate, [202]

- poly(phenylene sulfide) PPS [15, 61, 124, 193] and poly(arylene ether ketone)s with poly(arylene ether ether ketone) (PEEK) as a representative of the class, [2, 16, 63-82]

- liquid crystalline polymers, [218]

- blends of some of the above mentioned polymers with other semicrystalline or amorphous polymers. [129, 132, 176, 191, 194-196]

Some original experimental evidence for the multiple melting of different semicrystalline polymers will be presented in section 4.2.2.

Holdsworth and Turner-Jones [39] suggested that, for PET, the multiple endotherms are the result of the melting of the lamellae originally formed at the crystallization temperature and their further recrystallization during heating followed by the final melting of the recrystallized

lamellae. This model was later challenged by Groeninckx et al. [36] who upon a more detailed investigation of the effect of various thermal treatments on the crystallinity, melting behavior and morphological features suggested a complex model involving crystal perfection without thickening, partial melting, and recrystallization with or without thickening of the lamellae depending on the conditions of crystallization and annealing. They suggest a possible failure of the two phase model to relate the morphological parameters with the melting behavior of the polymer. Lin and Koenig [188] and Zhou and Clough, [185] based on little other evidence, but the results of few original experiments, attribute the low temperature "annealing endotherm" in the multiple melting peak scan of PET to the melting of small imperfect lamellae, formed during the secondary crystallization process.

Lemstra et al. [48] in a study of the triple endothermic melting behavior of isothermally crystallized i-PS identify the upper two endotherms in the DSC scan with the process of melting-recrystallization, but fail to provide a well supported model for the low temperature "annealing endotherm" observed in the melting scans of all isothermally crystallized samples. They suggest that one possible reason for the small annealing endotherm could be a process of “densification”, possibly a secondary crystallization, without specifying the mechanism for it.

In a study on multiple melting of Nylon 6,6 , Bell et al. [55] suggest the coexistence of two different morphological forms of the polymer which melt correspondingly at different temperatures; one - kinetically favored, the other - thermodynamically favored.

As was mentioned above, in all these polymers the multiple melting/annealing endotherms share unique common features. Therefore, an explanation of the observed phenomena must not be limited to narrowly staged experiments on one polymer. A model will have to include the whole field of semicrystalline polymers mentioned above. Such a general model requires a much broader approach. This study will be limited to the establishment of certain controversies surrounding the multiple melting phenomenon from the point of view of the two-phase model with PEEK as an example. It will suggest a working model which is currently being explored with studies on other polymers as well. With this in mind we can continue with the analysis of the experimental work on the multiple melting behavior of PEEK and the models proposed for its explanation.

### *2.4.2 Double Melting in PEEK*

For the purpose of this discussion, it needs to be stated in advance that, in the case of PEEK, sources of multiple melting such as fractionation during crystallization, [2, 70] thermal degradation [2] and the melting of different crystallographic phases [74, 83] have been ruled out. Thus only two models are being presently considered: the "melting-recrystallization model" and the "bi-modal lamellar population model".

The first report on the "double melting" thermograms of PEEK comes in a work by Blundell and Osborn. [63] Following experimental procedures similar to these used previously on PET, [39, 171] they identify the presence of two melting endotherms in the DSC scans of both cold and melt crystallized PEEK samples. A larger endotherm appears in the temperature region between 280°C and 340°C and a smaller one - just above the crystallization or the annealing temperature.

Following the model proposed by Holdsworth and Turner-Jones for PET [39] the authors suggest that the small low temperature endotherm is due to the melting of the crystalline lamellae formed during the isothermal crystallization. Therefore, it represents the melting process of the majority of crystals present at any temperature below the crystallization temperature, that is - including the ones at room temperature.

Upon heating, a process of continuous melting and recrystallization is suggested to occur above the original crystallization temperature. In the study of Lee and Porter [66] the upper peak is identified as the maximum of the combined endothermic melting and exothermic recrystallization peaks of the continuously reorganizing crystalline regions. This model's main strength lies in the explanation of the heating rate dependence of the double melting DSC scan for samples annealed at fairly high temperatures. [66]

The dual lamellar population model was simultaneously developed by Cebe and Hong [71] and by Bassett et al. [70] and further expanded upon with morphological evidence by other authors. [73, 84, 85] Cebe and Hong studied the melting behavior of PEEK by applying a cyclic thermal treatment in the DSC on a previously crystallized sample. They demonstrated, that the upper melting endotherm remained unchanged as a result of successive heatings above the

temperature of the previous treatment, followed by immediate cooling down of the sample. The only feature of the DSC heating scans which changed during this particular treatment was the position and intensity of the low temperature endotherm, which appeared just above the highest previous thermal treatment temperature.

Based on this observation it was suggested that the low endotherm represents the melting of a secondary population of less perfect, thus less stable, lamellae which melt just above the isothermal crystallization temperature. Additional evidence against the melting-recrystallization model has been provided in a work on thermal properties of PEEK by Cheng et al. [16] and by the study of Bassett et al. [70] A sequence of DSC heating scans of samples which were isothermally melt-crystallized for various times unequivocally shows that the upper melting endotherm develops first and should, therefore, be associated with the melting of primary PEEK lamellae. The low temperature endotherm appears only at later times after significant part of the material has crystallized. However, Cheng et al. suggest, that regardless of the thermal history, a process of continuous melting occurs for PEEK in a very broad temperature region and do not exclude the possibility of partial recrystallization of the material, which melts at low temperature, especially in the case of samples crystallized from the glassy state.

According to the study by Bassett et al. [70] the two peaks in the typical double melting scan of PEEK represent the melting of different components within the spherulitic morphology, formed at different stages of the crystallization process and situated at physically different locations within the spherulitic structure.

At the earlier stage - primary crystallization, primary lamellae develop so as to occupy but not fill up the spherulitic superstructure. Upon heating in the DSC, the melting of these occurs at the high temperature main endotherm. At the later stage (secondary crystallization) a population of secondary lamellae develops from the melt between the primary ones. These secondary lamellae are smaller and stable only up to a temperature slightly above the crystallization/annealing temperature. The constraining effect of the primary lamellae is pointed out as the reason for the slowing down of the secondary stage of crystallization and for the lower thermal stability of the secondary lamellae. The authors are cautious in

assigning a specific molecular mechanism for the secondary crystallization. Rather they assign its name merely according to the time factor - from the fact that it represents the development of new lamellae *after* the formation of the dominant primary ones. Finally they point out that such a model of sequential crystallization would be applicable to the crystallization mechanism of other chain folding polymers of intermediate crystallinity values, namely i-PS and PET.

The two models for the double melting behavior of PEEK described above have been considered and expanded in several later studies. In calorimetric studies by Lee et al., [65, 66] crystallinity studies by Jonas et al. [67] and WAXS and SAXS studies by Jonas et al. [68] the authors defend the melting recrystallization model. However further work by other groups has shown irreconcilable inconsistencies of the melting-recrystallization model. New evidence provided in calorimetric studies by Chang, [72] electron microscopy by Lovinger et al., [83] Lattimer et al., [73] optical microscopy by Marand and Prasad, [2] and morphological studies by Wide and Small Angle X-ray Scattering by Wang et al., [85] Hsiao et al., [84] and Kruger and Zachmann [74] supports and expands on the bi-modal lamellar population model.

## 2.5 Structural Relaxation and "Physical Aging"

It is a known and accepted fact in the literature on polymers, that structural relaxation occurs in both semicrystalline and amorphous polymers below their respective $T_g$. [86,87,164,166,197] The phenomenon is commonly known as *physical aging* in the literature. For certain semicrystalline polymers with $T_g$ below ambient conditions (i-PP, HDPE, LDPE) studies in the temperature range encompassing room temperature and above have shown viscoelastic response similar to the physical aging of polymeric glasses below $T_g$. [46, 47, 87-93] Preliminary reports from our group have shown, that the same effect is observed in the case of PEEK. [81] Before presenting the results, a brief introduction on the subject of physical aging is due.

### *2.5.1 Origin of "Physical Aging" Below the Glass Transition*

The term *physical aging* has been commonly used in the polymer literature [86] to denote the isothermal changes in structure sensitive properties of polymeric glassy materials with time, which are not accompanied by chemical changes (i.e. no chemical aging). These

changes are due to the nonequilibrium nature of the glassy state and are characteristic for all glassy materials - ceramic, organic, inorganic, metal etc. [87]

During the formation of the glassy state by cooling an amorphous or a semicrystalline polymer, a temperature range is reached in which the molecular relaxation times begin to exceed experimental timescales associated with the cooling process. Therefore cooling below this range leaves a structure which is unable to relax and retain its equilibrium properties. The temperature range in question is the range of the glass transition of the polymer. More commonly used is the designation of a glass transition temperature $T_g$ below which the amorphous polymer or the noncrystalline fraction of a semicrystalline polymer depart from equilibrium.

The relaxation of the excess free volume and enthalpy of the polymer towards their equilibrium values at a given temperature in the glassy state is governed by a broad distribution of molecular relaxation times. In the case of the decrease of the quenched free volume, this change is directly observed in the long term densification of the polymer upon annealing at temperatures below $T_g$. In the case of the decrease of the excess enthalpy upon isothermal annealing below $T_g$, the changes are observed indirectly through the calorimetric observation of the enthalpy recovery peak at or below $T_g$, when the material is heated through the glass transition.

As the availability of free volume governs the molecular mobility, the structural relaxation leads to an increase of molecular relaxation times (e.g. physical aging is a self-retarding process). In addition to enthalpy and volume relaxation effects, aging is observed in the change of the linear viscoelastic response of the glass both in isothermal dynamic mechanical and isothermal transient tests. The type of test utilized in this study is the linear creep response, widely used in the studies of physical aging by Struik. [87-91] It is a transient method in which the effect of structural relaxation on the short term creep response of the polymer is studied through a series of {aging-loading-creep-recovery} profiles designed in such a way, that the test time $t$ after an elapsed aging time $t_a$ ($t_e$ in Struik's notation) satisfies the requirement $t << t_a$ (i.e. momentary creep response data is collected after elapsed aging

time $t_a$). This design is necessary in order to minimize the effect of isothermal aging during the creep test time.

### *2.5.2 Analysis and Interpretation of the Results*

The Kohlrausch-Williams-Watts (KWW) function is one of several mathematical expressions utilized to model an important characteristic of the relaxation behavior of glasses below $T_g$ - the nonexponentiallity of the response to external changes. In the opinion of I. Hodge, [200] it is a "... widely used, versatile, convenient, and generally accurate decay function."

The KWW function (the "stretched exponential" function) has been used for describing the relaxation function of polymers and other materials. Its general form (for a decay function):

$$\Phi(t) = \Phi_0 \exp\left[-\left(\frac{t}{\tau_0}\right)^{\beta}\right] \qquad (2.9)$$

is a result of the following equation for the rate of relaxation (originally proposed by Kohlrausch):

$$d\Phi(t) = -\Phi(t)\frac{dt}{\tau'(t)} \qquad \text{where} \quad \tau'(t) = \frac{\tau_0^{\beta} t^{1-\beta}}{\beta}$$

An alternative form of the rate equation, which illustrates the essence of the non-exponentiallity, is:

$$d\Phi(t') = -\Phi(t')d[t']^{\beta} \qquad \textit{where} \quad t' = \frac{t}{\tau_0}$$

In general, it has been recognized, that the experimental manifestations of nonexponentiallity can not be described by a single relaxation time and, therefore, require a distribution of relaxation times. The Laplace transform of the KWW-function represents an asymmetric distribution of relaxation times, in which $\tau_0$ is related to the average relaxation

time - the first moment of the distribution [1] and β reflects the breadth and asymmetry of the relaxation spectrum - the broader the spectrum, the lower the value of β. [200]

Other mathematical expressions have been used to describe the nonexponentiality. These are also empirical and are selected mainly for the simplicity of their functional form in the respective domain of work (real time, retardation/relaxation time, or frequency domains) and, therefore, the ease of analysis and manipulation of data: log-normal distribution function of relaxation times (Moynihan [210]), box distribution (Tobolski [211]), wedge and double box distributions of relaxation times (Kovacs and Hutchinson [212]), and several functions used in the frequency domain studies by dielectric spectroscopy - the Davidson-Cole function (having convenient form in the time domain as well), the Cole-Cole function, and the Havriliak-Negami function. [200] Some of these expressions (namely the Davidson-Cole function and the log-normal distribution) give results, that are very close to a KWW function with an exponent of 0.5. [200]

Struik has suggested [86] that, for physical aging of polymeric glasses, the creep compliance *J(t)* may be approximated with the following form of the KWW function:

$$J(t) = J_0 \, exp\left[\left(\frac{t}{\tau}\right)^{\beta}\right] \qquad (2.9a)$$

The limitation of this equation is that it is useful for describing only the early stages of the creep response - when $t < \tau$. Upon physical aging below $T_g$, $\tau$ becomes dependent on the aging history - $\tau = \tau(t_a, T_a)$. This is reflected in the observation, that if one plots $J(t, t_a)$ vs. *log(t)* the creep compliance curves can be superposed onto a master curve by shifting them horizontally along the *log(t)* axis. To illustrate this we can write the ratio of the creep compliances $J(t, t_a)$, expressed through equation (2.9a), measured at two different aging times - $t_a$ and a reference aging time $t_{ar}$:

$$\frac{J(t,t_a)}{J(t,t_{ar})} = \frac{J_0(t_a)}{J_0(t_{ar})} exp\left[\left(\frac{t}{\tau}\right)^{\beta} - \left(\frac{t}{\tau_r}\right)^{\beta}\right] \qquad (2.10)$$

Equation (2.10) can be rewritten as:

$$\frac{J(t,t_a)}{J(t,t_{ar})} = \frac{J_0(t_a)}{J_0(t_{ar})} \exp\left[\left(\frac{t*\frac{\tau_r}{\tau}}{\tau_r}\right)^{\beta} - \left(\frac{t}{\tau_r}\right)^{\beta}\right] \qquad (2.10a)$$

If we rescale the time axis of the data collected at aging time $t_a$ by choosing a new time scale $t' = t*\frac{\tau_r}{\tau} = \frac{t}{a}$, which is equivalent to:

$$\log(t') = \log(t) - \log(a) \qquad (2.11)$$

then equation (2.10a) becomes an identity provided the pre-exponential factor does not change with aging time. The mathematical manipulation just described is equivalent to shifting of the curve $J(t, t_a)$ by an amount $log(a)$ on a logarithmic time axis. After this shift it coincides with the creep compliance curve $J(t, t_{ar})$, measured after aging time $t_{ar}$. In physical terms, this interpretation states that the slowing down of the molecular relaxation processes during aging is equivalent to a shift of the relaxation spectrum to longer relaxation times. This effect of isothermal annealing below $T_g$ has been observed for many glassy amorphous polymers, for nonpolymeric glasses as well as for semicrystalline polymers. [86] Quantitatively the slowing down of the molecular relaxation is described by the horizontal shift rate

$$\mu = \frac{\partial\, log(a)}{\partial\, log(t_a)} \qquad (2.12)$$

Its value is decreasing with decreasing temperature of aging at temperatures well below $T_g$, but approaches a value of 1 at temperatures not too far away from the glass transition region. Upon further approach to the glass transition region the value of $\mu$ falls down to zero again. [86] The description of the effect of physical aging on the response of the glassy polymer, given so far, is universal for all polymers at temperatures below $T_g$, whether they are fully amorphous or partially crystalline. A functional form of the relaxation behavior of polymers similar to the KWW function has been derived by Ngai and coworkers on the basis of the coupling model. [200, 207-209]

The use of a nonexponential relaxation function is essential in order to successfully describe the "memory effect" in the relaxation of glasses. As Hodge has pointed out, "... the memory effect occurs in any non-exponentially relaxing system, regardless of (although

modified by) any possible non-linearity in the system... ", [200] where the latter (non-linearity) is reflected in the time-temperature-structure dependence of the average relaxation time (described by the Tool-Eichlin, Gordon-Narayanaswamy, Moynihan, Adam-Gibbs, and KAHR approaches, for example - see references quoted in reference 200).

The use of the KWW function is not limited to the retardation function in small strain creep studies (Struik [86-91]). It had been used also in the following relaxation studies of polymers:

- enthalpy relaxation (Moynihan et al., [210] ten Brinke et al., [213] references by Hodge [200])

- dielectric relaxation (Williams et al. [214])

- studies of relaxation near the glass transition through the decay of nonlinear optical properties (NLO) (Verbiest et al. [215])

- neutron scattering (Richter [209])

It is important to note the difference between the trivial phenomenological justification of the KWW function and its use in specific applications (the latter has been discussed by Echeveria et al. in a study of "physical aging" in polyetherimide (PEI) [203]):

A response to a Heavyside perturbation function with magnitude $\sigma_0$ at time "zero" results in a change in the measurable property $\varepsilon(t)$ described by:

$$J(t)=\frac{\varepsilon(t)}{\sigma_0}=J_U+(J_R-J_U)*\{1-\Phi(t)\}=J_U+(J_R-J_U)\left\{1-\exp\left[-\left(\frac{t}{\tau_0}\right)^{\beta}\right]\right\} \quad (2.13)$$

(Note: For creep in polymeric glasses and semicrystalline polymers, an additional linear term describing viscous flow is omitted as viscosities in these systems are very high.)

Thus the response is characterized by 4 parameters: the initial unrelaxed ("instantaneous") value $J_U$, the relaxed ("equilibrium") value $J_R$, and the parameters of the retardation function - $\tau_0$ and $\beta$. Knowledge of these parameters is essential for deriving analytical (rather than visual or "by hand") parameters of the time-temperature superposition, that is, the horizontal and vertical shifts of the response curves to a master curve.

From these parameters, if the experimental time-scale is shorter than the relaxation time-scale (as is often the case in creep studies), only $J_U$ can be determined with a reasonable accuracy. It would be unreasonable to assume, that correct values of $\tau_0$ and $\beta$ can be derived by probing only the early times response (i.e. without a reasonable approach to the vicinity of the limiting $J_R$ value).

Thus, for practical derivation of the shift parameters from "short time" response curves often other analytical expressions are used. In general these ignore the limiting value of $J_R$ and are based only on an initial value $J_U^{'}$ (assumed to be close to $J_U$) and a simple functional dependence on time, which involves a "characteristic time", to be used in the horizontal shifting procedure.

With these approximate methods horizontal and vertical shifts can still lead to the building of a master curve. However, it is important to note, that due to the limited knowledge of the relaxation curve, such master curves and the information they contain, should be considered valid only in the time range studied. [203]

For example, Echeveria et al. [203] used the Andrade form of the creep compliance curves at short times in order to derive the master curve for an amorphous PEI:

$$J(t) = J_g + \beta * t^{1/3} \qquad (2.14)$$

Struik's use of the KWW function for superposition onto a master curve also omits the limiting value of the creep compliance and is, therefore, confined only to times shorter than the average retardation time. The functional form used by Struik [88]:

$$J(t) = J_0 \exp\left[\left(\frac{t}{\tau_0}\right)^{\beta}\right] \qquad (2.9a)$$

is approximately equivalent to the full response function above, equation (2.13), under the following assumptions: $t << \tau_0$ and $J_0 = J_U = (J_R - J_U)$.

The first assumption above is reasonable if it can be deduced, that one is far away from reaching the limiting compliance values. The second assumption, however, is generally not

valid and, therefore, would result in values of $\tau_0$ and $\beta$, significantly different from the actual ones.

Nevertheless, after applying the horizontal and vertical shifts specific to the analytical approximation method used (or by hand), a master curve can be obtained, and the time-temperature dependence of the shifts can be analyzed. The derived shifts, shift rates and their temperature dependence would be expected to break only in the immediate vicinity of a relaxation temperature, where the assumption of $t << \tau_0$ will no longer be valid. In this range, the full retardation function must be used. Horizontal and vertical shifts can be derived and a master curve can be built, if a single relaxation mechanism is active in the temperature range studied.

### *2.5.3 "Physical Aging" of Semicrystalline Polymers Above the Glass Transition*

In more recent years several groups of researchers have drawn considerable attention to the peculiar response of two of the most common commercial polymers, PE and i-PP, to room temperature annealing - a thermal treatment which naturally occurs within the lifetime of exploitation of these two polymers. When unmodified by chemical or any other means both polymers are highly crystalline - with crystallinity $\chi_{cr} > 0.6$. For both polymers the glass transition temperature is generally identified as the $T_\beta$ relaxation temperature, which for both falls below room temperature. The highest relaxation temperature - $T_\alpha$ is associated with the crystalline phase and is about 50°C for linear PE and about 100°C for i-PP [88] (for low frequency and transient experiments). Therefore the room temperature annealing falls naturally in the temperature region between $T_\beta$ and $T_\alpha$ for both polymers.

As $T_\beta$ is the glass transition temperature, it is expected, based on the two-phase model of semicrystalline polymers, that the amorphous fraction of the polymer will be liquid-like above its glass transition and will be completely relaxed. On the time scale of the transient creep experiment designed for testing physical aging of glassy polymers the response should be featureless - the response of a liquid-like mobile amorphous phase should be fast and the

distribution of relaxation times, expected to be very narrow, should not change with time (e.g. no horizontal shift of the response with annealing time should be observed).

An extensive study of these two polymers in the region between $T_g$ and $T_\alpha$ by Struik [86-91] has shown that this is not the case! The transient response of the two semicrystalline polymers to small stress is a creep compliance curve indicative of long relaxation times and the effect of isothermal annealing is similar to the one observed upon annealing of glassy polymers below their $T_g$ - the creep compliance curves measured at different annealing times are displaced uniformly and superpose onto one another by horizontal shifts along the *log(t)* axis with a finite logarithmic horizontal shift rate - $\mu > 0$. In addition to the horizontal shifts, small vertical shifts are required in order to superpose the curves at various annealing times. The vertical shifts imply that in addition to the slowing down of the relaxation by annealing, an absolute change in the observed material property (in this case - the initial creep compliance $J_0$) is observed. The nature of these vertical shifts is somewhat ambiguous. [90, 91] However, at this point in the review it is important to note, that the creep compliance curves at various isothermal annealing times and at various temperatures do comply in general with the universal form of equation (2.9a) and can not be brought together to a universal master curve just by vertical shifts alone. [90, 91]

Thus two facts have been unambiguously established by Struik's pioneering work: 1) i-PP and PE "physically age" above their glass transitions (at least in the phenomenological sense of this term [86]); 2) the observed physical aging above $T_g$ cannot be explained by change in the limiting value of the observed material property alone - instantaneous (unrelaxed) or relaxed creep compliance. The explanation of the effect of isothermal annealing above $T_g$ must involve both - a slowing down of the relaxation process (horizontal shifting) and the change in the instantaneous creep compliance (vertical shifting).

### *2.5.4 Models for the "Physical Aging" of Semicrystalline Polymers Above the Glass Transition*

In order to explain the observation of "physical aging" in semicrystalline polymers above their nominal glass transition temperatures Struik has proposed a model, which is

similar to the model designed to explain the effect of hard inclusions on the properties of filled rubbers. [87, 90]

In this model the crystals disturb the amorphous phase and reduce the segmental mobility of the amorphous chains in their immediate vicinity. The properties of the amorphous phase become identical to the properties of the fully amorphous polymer only at large distances from the crystalline lamellae. This leads to a broadening and extension of the glass transition to higher temperatures. Effectively there is a distribution of glass transition temperatures in the polymer depending on the proximity and connectivity of amorphous chains to the crystalline lamellae.

Thus at a given annealing temperature above what is considered to be the nominal glass transition temperature, there are, according to Struik, regions of the amorphous phase, which are completely relaxed, other, which are immobilized by the adjacent crystalline phase and effectively glassy, and still other regions, which are just passing through their glass transition. In a slightly more simplistic representation of the model, designed to better illustrate the characteristic response of the semicrystalline polymer to annealing ("physical aging") at different temperatures, [90] Struik reduces the above consideration to the existence of two distinct $T_g$'s: lower $T_g$ - $T_g^L$, identifiable with the nominal $T_g$ of the polymer, and upper $T_g$ - $T_g^U$, which is the $T_g$ of the fraction of the amorphous phase, constrained by the proximity of the crystalline lamellae. The idea certainly is not new and it is pointed out by the author that such a model had been suggested earlier by Boyer [7] in relation to the complex relaxation behavior of a variety of semicrystalline polymers. Struik draws further support for his model from the concept of "rigid amorphous fraction" in semicrystalline polymers as originally proposed by Wunderlich on the basis of calorimetric measurements at $T_g$ (see section 2.3.2).

Thus at any temperature the creep compliance is determined from the sum of contributions from the less constrained and the more constrained amorphous fractions:

$$J(t) = J_1(t) + J_2(t) = J_{1U} + \Delta J_1 * \Phi_1(t) + J_{2U} + \Delta J_2 * \Phi_2(t) \qquad (2.15)$$

From the above equation, generally, it follows that the viscoelastic response of the semicrystalline polymer is no longer thermorheologically simple, [200] and therefore, the time-

temperature superposition, which is characteristic for the single phase amorphous polymer, must fail. Struik proposed that the response of the heterogeneous amorphous fraction can be uncoupled in temperature regions where the contribution of one of the amorphous fractions has insignificant time dependence compared to the contribution of the other amorphous fraction. These temperature regions are defined by the characteristic temperatures of the two amorphous fractions $T_g^L$ and $T_g^U$. The uncoupling is described schematically as a procedure for visual ("by hand", rather than analytical )superposition. The temperature scale is divided into four characteristic regions of behavior, labeled respectively, "Region 1" - "Region 4". [88]

For Region 1 ($T < T_g^L$) and Region 2 ($T \rightarrow T_g^L$) the time dependence of $J_2(t)$ is very small and for all practical purposes produces only a vertical shift in the total compliance values with aging. Regions 1 and 2 are separated only formally by the temperature limit of applicability of equation (2.9a). In Region 3 ($T_g^L < T < T_g^U$) $J_1(t)$ is at the end of the glass-rubber transition and is no longer sensitive to aging. At the lower temperature end of Region 3 (just above $T_g^L$), $J_1(t)$ is leaving the glass transition and entering the "rubbery plateau". Its complex time dependence (decreasing logarithmic slope) can not be uncoupled from $J_2(t)$ and leads to failure of the time-temperature superposition. Region 4 ($T > T_g^U$) is characterized by an uniform behavior of the amorphous fraction, all of which is rubbery. Aging effects disappear, however crystallization upon annealing can produce changes in the creep compliance with annealing time.

Struik's model has been challenged by several authors. [46, 47, 92-95] In the studies of Read et al. [92, 93] and Chai and McCrum [94, 95] the main challenge is the questioning of the existence and nature of the combination of vertical and horizontal shifts, necessary for the superposition of the creep curves at different aging times for i-PP and HDPE aged between $T_\beta$ ($T_g$) and $T_\alpha$ (in Struik's notation - between $T_g^L$ and $T_g^U$). Both studies suggest that the observed downward vertical shifts of the compliance are due to a mere "geometric construction". [92] They propose, that the vertical shifts are due to change in the relaxation strength of the β-process with time. It has been acknowledged by both groups, however, that aging must result in a shift of the retardation spectrum to longer times - a fact, which sometimes is not well understood and misrepresented in the literature. [47]

(Note: Read et al. and Chai and McCrum attempt to show that changes in relaxation strength are responsible alone for the observed aging effect, but their results do not support this, or at least are inconclusive and tend to give possible dual explanations, thus not disproving unequivocally Struik's statement, that aging produces a shift of the retardation spectrum. Both studies acknowledge this to a different extent in their respective discussion sections, but the abstracts of the papers are somewhat incomplete and misleading on this issue! In a recently published study Hellinckx [47] has ignored this and stated that Read's results ascribe the effect of aging solely to change "in the magnitude [...] rather than the retardation times".)

Hellinckx [47] provides a model for the aging of i-PP between $T_g$ and $T_\alpha$, which incorporates both - changes in magnitude as well as in the retardation spectrum of the observed relaxation with aging time.

The physical aging of i-PP has also been studied through transport properties, [33, 34] yield stress, [31, 34] and stress relaxation measurements of annealed fibers. [32]

All the studies on i-PP mentioned above either do not address the possibility of secondary crystallization upon annealing of i-PP and/or HDPE above $T_g$ or refer to it as highly unlikely as a mechanism for the observed "physical aging". Recently, however, Hutchinson and Kriesten [46] pointed out, that if structural relaxation is observed by creep recovery, then enthalpic recovery should be observed too. Their set of experiments attempts to correlate the rate of development of the creep compliance curves with the rate of development of density and the DSC endothermic peak just above the aging temperature, which results from isothermal annealing. The conclusions drawn by Hutchinson and Kriesten are in favor of some "type of ordering or partial crystallization", in effect - secondary crystallization, as the origin of "physical aging".

In addition to i-PP several other polymers exhibit "physical aging" above their respective nominal glass transitions. Struik has demonstrated, that at least in a narrow temperature interval above $T_g$ PET and several polyamides (Nylon-6 and Nylon-12) exhibit finite horizontal shift rates close to unity i.e. annealing of these polymers above their $T_g$'s is slowing down their structural relaxation in a manner similar to i-PP. [91] These observations have received little attention in the literature on physical aging of semicrystalline polymers,

perhaps because Struik's results on these polymers are limited to only 20-30 K above the nominal $T_g$. Another reason could be the fact, that these polymers have glass transition temperatures well above ambient conditions and "physical aging" above $T_g$ has not been perceived as having such practical implications as in the case of PE and i-PP.

### *2.5.5 "Physical Aging" of PEEK*

Physical aging of amorphous and semicrystalline PEEK had been the subject of several studies in the literature. [96-101] Kemmish and Hay [96] studied the effect of annealing below $T_g$ on the enthalpy relaxation and the change in ultimate mechanical properties of the material. In a separate study Hay [102] investigated the kinetics of enthalpy relaxation of neat PEEK and PEEK-PEI (polyetherimide) compatible blends. The transient and dynamic mechanical responses as a function of aging time below $T_g$ have been studied by Ogale and McCullough, [97, 98] Wang and Ogale, [100] and Carfagna et al. [99] Ogale and McCullough have investigated the transient creep response and the enthalpy relaxation as a function of aging time and temperature in a narrow temperature interval just below $T_g$ - 130-150°C. They report no observation of enthalpic relaxation after aging of semicrystalline samples with crystallinities 0.22 and 0.33, [97] but this is in contradiction with the findings of Hay [102] and Cheng et al. [16] and is probably due to poor resolution in their measurements. The horizontal shift rate $\mu$ reported by Ogale and McCullough, derived from tensile creep experiments, follows in general the theoretical predictions and the experimental findings for other polymers: at the lowest investigated temperature below $T_g$ $\mu$ is close to unity and decreases sharply as $T_a$ approaches $T_g$ of the samples. Wang and Ogale [100] reported a value of 1.0 for the horizontal shift rate of semicrystalline PEEK for aging done at 130°C from stress relaxation and dynamic mechanical testing in shear mode.

All of the studies mentioned above were limited to the effects of annealing below $T_g$ on the properties of PEEK. Jar and Kausch [101] investigated the effect of post-crystallization annealing above $T_g$ on the mechanical properties of semicrystalline PEEK. They report, that annealing above $T_g$ results in a post-yield hardening of samples tested at 120°C, independent on how the samples were crystallized initially. The result is analyzed in connection with the

crystallinity and morphology studies of the effect of annealing above $T_g$, [63, 70, 71] namely - with the studies of the "low temperature melting endotherm" resulting from such a thermal treatment of PEEK.

The results of Jar and Kausch appear to indirectly support the secondary lamellar formation model for the low temperature melting of PEEK. [70, 71] Their study is not fully representative of the effect of isothermal annealing on the microstructural changes in the polymer as the testing is done well beyond the region of the linear viscoelastic response. The large deformations involved in the experiments of Jar and Kausch do not guarantee, that the structure, the response of which is recorded at the yield point and beyond, is the same as the original structure, resulting from the isothermal annealing treatment. The importance of this work, however, is that it acknowledges, that the mechanism of the development of the low temperature annealing endotherm of PEEK must play a role in determining the observed changes in mechanical properties of PEEK, which result from annealing above $T_g$.

In summary, the studies of physical aging of PEEK, reviewed above, had been somewhat limited in the scope of their investigations. With the exception of the work of Ogale and McCullough [97] in all the other studies physical aging had been investigated at a single temperature, chosen at about 15-20 K below $T_g$ for a maximum amplitude of the observed effects. The work by Hay [102] is an exception too, but limited to enthalpy relaxation studies. Furthermore, as mentioned above, there has been a controversial statement regarding the physical aging of semicrystalline PEEK as studied by DSC - that no enthalpic relaxation occurs upon annealing of semicrystalline PEEK below $T_g$. [97] In addition to that, the only study, which addresses the effects of structural relaxation upon annealing above $T_g$, is limited to an indirect method of investigation. [101]

From the perspective of the substantial level of research on physical aging of i-PP above $T_g$ and certain similarities of the effect of long time annealing of PEEK above $T_g$ to the enthalpic relaxation phenomenon in the glassy state, [78] a more in-depth study of "physical aging" of PEEK is due, encompassing a wide range of temperatures below and above the glass transition region. The results of a straightforward application of Struik's experimental approach to semicrystalline PEEK are reported in section 4.4 and discussed in section 5.4.

The results of a rather unorthodox approach to "physical aging" by DSC studies are presented at the end of the discussion chapter in section 5.6.3 due to their controversial nature.

# CHAPTER 3

# EXPERIMENTAL

This chapter describes the methods of characterization used, the equipment and conditions of characterization, and the preparation of the samples used.

## 3.1 Materials - Preparation

The material used for the studies of the low temperature annealing endotherm and for the crystallinity and creep studies is commercial PEEK grade 450G ($M_w$ = 38,300 g/mol). Few crystallization and annealing experiments in the DSC were performed also on isotactic polystyrene (i-PS) and poly(butylene terephthalate) (PBT). The i-PS material was obtained from Dr. J. Rieke from Dow Chemical ($M_w$ = 486,000 g/mol, $M_w/M_n$ = 6.6). Dr. H. D. Iler kindly provided a small amount of purified material, from which the atactic and low MW fractions have been extracted [103] ($M_w$ = 1,030,000 g/mol; $M_w/M_n$ = 2.4). The PBT was obtained from Dr. E. Raschke from Amoco and used without any modification except drying for 24 hours in a vacuum oven at 100°C in order to remove traces of water.

For the studies of the effect of molecular weight on the melting behavior of PEEK a precursor polymer poly(ether ether ketimine) (PEEKtmn), kindly supplied by the laboratory of Prof. J. E. McGrath at Virginia Tech, was fractionated, characterized by solution techniques and hydrolyzed to poly(ether ether ketone) fractions.

The preparation and thermal histories of the samples used for the studies of the low temperature annealing endothermic peak, for crystallinity studies, for creep studies, and the preparation and MW characterization of the narrow molecular weight PEEK fractions are described in the following sections.

### *3.1.1 Fractionated PEEK*

In order to study the effect of MW on the melting behavior of PEEK fractions with molecular weights between 3,200 g/mol and 43,300 g/mol were prepared by a method similar to one described in the literature by Roovers et al. [104]

PEEK is insoluble in most common solvents. [105-107] Solubility has been reported only in strong acids such as concentrated sulfuric acid, [105, 106] hydrofluoric acid, [106] chlorosulfonic acid [105] or in high boiling point solvents at temperatures close to the melting point of the polymer, such as some high boiling point esters, benzophenone, diphenyl sulfone, phenol/trichlorobenzene, and α-chloronaphthalene. [105-107] Solution characterization to estimate molecular weights has been most commonly carried out in concentrated $H_2SO_4$ [105,106] and also in $HSO_3Cl$. [105] This type of characterization has been shown to lead to the sulfonation of the polymer at the diether substituted ring. [105, 106] In effect, after the characterization a new ionic polymer is formed, whose properties are expected to be quite different from the properties of the original PEEK. This poses an especially difficult problem when one works with small quantities of the polymer.

After Mohanty et al. [108] reported on a method to develop amorphous precursor polymers for poly(arylene ether ketones), Roovers et al. [104] applied the idea to obtain narrow molecular weight fractions poly(ether ether ketone).

The fractionation method used by Roovers et al. [104] is fractional precipitation of a precursor polymer poly(arylene ether ether ketimine) by non-solvent addition. The solvent/non-solvent pair is benzene/n-hexane. In this study benzene was substituted with toluene due to the much lower toxicity and therefore easier handling of the latter. The MW characterization will show, that this substitution does not affect the efficiency and quality of the fractionation.

The starting PEEKtmn material was synthesized by Dr. K. Lyon. It had molecular weight averages $M_n$ = 20,000 g/mol and $M_w$ = 39,000 g/mol, as determined from GPC with universal calibration, e.g. polydispersity ratio (PDR) as expected for a step-growth process PDR = 2.0. Its intrinsic viscosity at 25°C in THF is $[h]_{THF}^{25^\circ C}$ = 0.295 dl/g.

After several initial fractionations to establish and test the procedure a batch fractionation was done in a 1000 ml flask on a 500 ml 1% w/w solution of PEEKtmn in toluene. The need for a flask much larger than the initial volume of the solution comes from two factors: 1) the cumulative addition of up to 50 ml nonsolvent before the last fraction is

obtained, 2) the need to account for the thermal expansion of the solution during step 2 below.

The fractionation procedure consisted of the following steps:

1) Drop-wise addition of prescribed amount of nonsolvent (table 3.1) in the stirred solution at room temperature until the solution became turbid.

2) Raising the temperature of the solution in a water bath until the precipitated material dissolved back and the solution became clear again.

3) Slow cooling upon which the precipitation of the highest molecular weight chains present in the solution occurred.

4) The solution was left to reach room temperature and held there until the polymer rich phase precipitated at the bottom of the flask and the solvent rich phase became completely transparent.

5) The solvent rich phase was poured out of the flask. This was facilitated by the fact, that the polymer rich phase was a sticky gel-like mass, which was deposited on the bottom side of the flask during agitation of the solution with a magnetic stirrer.

6) The current fraction was dissolved in chloroform and precipitated with methanol. The precipitate was filtered with a filter, the choice of which depended on the fraction obtained (e.g. molecular weight). With the first fractions, a filtering flask with large filtering funnel and a filtering paper (pore size 25 μm) was sufficient as the final precipitate consisted of rather large particles and it was not necessary to apply high pressure. For the last fractions (with MW less than 15,000 g/mol) small funnels with support between the funnel and the filtering paper were used.

7) The fractions were dried in vacuum oven at 160-180°C for 12-24 hours.

The cycle described above was applied nine times and nine fractions were obtained. The last one was obtained with the addition of a relatively large amount of nonsolvent (in effect - an excess amount of nonsolvent was applied). Despite this, the remaining solution still had a light yellow color, indicative of the fact that the smallest MW fractions of the

initial polymer (possibly oligomers) could not be removed. As a result, the last fraction was expected to have a relatively higher polydispersity ratio as will be confirmed by gel permeation chromatography (GPC).

Another peculiar aspect of the fractionation procedure was the fact, that the first amount of nonsolvent addition produced a fraction, containing a very small amount of material. The first fraction is expected to contain the highest molecular weight chains present in the solution. Its appearance was slightly different from that of the later produced fractions. Its color was more intense dark yellow as opposed to the light yellow color of the other fractions. It is possible, that the first step extracted not only material with molecular weight at the high end of the MW distribution curve, but maybe also some crosslinked material, present in small amounts in the starting polymer. The amount of this first fraction obtained was too small for practical purposes and it was not characterized or hydrolyzed to PEEK.

Thus effectively eight ketimine fractions were obtained - denoted further in the study as KTMN4-2, ..., KTMN4-9. Table 3.1 gives the quantitative parameters of the fractionation procedure: starting material, amount of nonsolvent added at each step, and mass yield for each fraction.

The MW characterization of the fractions by various solution techniques (GPC, vapor phase osmometry (VPO), solution viscosity is discussed in section 3.2.1.

After the PEEKtmn fractions were thoroughly characterized for MW and polydispersity they were hydrolyzed to PEEK fractions. The hydrolysis was done through the experimantal procedure, recommended by Dr. A. Brink from Prof. J. S. Riffle's laboratory at Virginia Tech [109]:

1) A 5% solution of the ketimine polymer was prepared in dried NMP. 2) A small amount of water was added in a ratio to ensure 4-fold excess of water vs. repeat units (as recommended).

3) The solution was equilibrated at 85°C.

4) A small amount of HCl was dissolved in NMP in a ratio to ensure 1.53 fold excess of repeat units vs. HCl.

**TABLE 3.1** Parameters and results of the batch fractionation of poly(arylene ether ether ketimine).

| | |
|---|---|
| **method:** | fractional precipitation by nonsolvent addition |
| **solvent/nonsolvent pair:** | toluene/n-hexane |
| **starting material:** | $M_n$ = 20,000 g/mol, $M_w$ = 39,000 g/mol |
| | $[h]_{THF}^{25^\circ C}$ = 0.295 dl/g |
| **starting amount:** | 4.2 g PEEKtmn, ~ 1 % w/w solution, 500 ml |

| Step # | Amount Nonsolvent [ ml ] | Fraction* | Fraction Yield** [ g ] |
|---|---|---|---|
| 1 | 5.0 | KTMN4-1 | 0.011 |
| 2 | 8.4 | ***KTMN4-2*** | 0.313 |
| 3 | 12.4 | KTMN4-3 | 0.830 |
| 4 | 14.8 | KTMN4-4 | 0.418 |
| 5 | 17.5 | ***KTMN4-5*** | 0.404 |
| 6 | 21.5 | KTMN4-6 | 0.397 |
| 7 | 27.0 | KTMN4-7 | 0.231 |
| 8 | 50.0 | ***KTMN4-8*** | 0.231 |
| 9 | excess | ***KTMN4-9*** | 0.304 |

* Fractions in bold italics denote material, which after hydrolysis to PEEK has been used in crystallization and melting studies

** Total yield efficiency - 75 %

5) The HCl solution was syringed into the polymer solution. The PEEK polymer precipitated into fine light gray particles.

6) The solution was precipitated into water, filtered and washed twice with water to ensure the removal of the HCl.

7) The PEEK fractions thus obtained were dried in vacuum oven for 24 hours.

The PEEK fractions are labeled as PEEK4-2, ..., PEEK4-9, following the numeric notation of the ketimine fractions.

The ketimine fractions were completely hydrolyzed to PEEK fractions. This was tested by thermogravimetric-mass spectral (TGA-MS) analysis. Following the method of Roovers et al., [104] the abundance of the ions with *m/z* = 93, 94, and 103 (aniline, phenol, and benzonitrile respectively) was monitored upon degradation. The benzonitrile is practically absent from the traces. The relative ratio of the aniline and phenol ions for the hydrolyzed PEEK fractions is much lower than that for pure PEEKtmn and is practically the same as in the trace of the commercial PEEK sample submitted with them for reference.

The amount of PEEK material available from each fraction can be estimated from the theoretical ratio of the molecular weights of the repeat units of PEEK and the ketimine polymer:

$$m(\text{PEEK4-X}) = m(\text{KTMN4-X}) \times R \quad \text{where}$$

$$R = \frac{M_{r.u.}^{PEEK}}{M_{r.u.}^{PEEKtmn}} = \frac{288.3}{363.3} = 0.793 \qquad (3.1)$$

### *3.1.2 Commercial Grade PEEK*

The polymer used initially for the studies of the long crystallization from the melt was in the form of semicrystalline pellets with density of 1.303 g/cm$^3$ measured by the density gradient column technique. Small samples the size of the DSC pans with weights of about 5.0-10.0 mg (± 0.1 mg) were cut and melted in the DSC at 385°C for 5 min, then subjected to various thermal histories, which will be presented in detail in section 3.2.2. PEEK's apparent equilibrium melting temperature is quoted in the range of 385-395°C. [64, 66, 129] The effect of

thermal degradation has been shown to be significant in samples annealed above 400°C under nitrogen and above 380°C in air. [110] Therefore care has been taken to melt the samples under nitrogen whenever possible. When melting was done in air, the melting times have been minimized.

After the goal of the study was set to the investigation of the development of crystallinity with annealing or crystallization above $T_g$, the same grade material (450G) was ordered in the form of amorphous sheets, 0.51 mm thick, supplied by Atlantic Plastics, Roanoke, Virginia, USA. The sheets have been processed by Westlake Plastics, Westlake, OH. Their initial density is 1.264 g/cm$^3$, which indicates the possibility of a very small amount of crystallinity present ( $c_c^{Dens} < 0.008$). Further DSC studies with this material were done on disk shaped samples 4.5-5.5 mm in diameter (10.00-20.00 mg weight depending on crystallinity and sample size).

### *sample preparation for the crystallinity studies:*

Three different types of samples were investigated for the crystallinity studies: 1) melt-crystallized samples, which were crystallized for various times $t_x$ at given crystallization temperature $T_x$, 2) cold-crystallized samples, annealed from the amorphous glassy state to a given crystallization temperature $T_c$, for various crystallization times $t_c$, and 3) cold-crystallized samples, annealed from the glass to various crystallization temperatures $T_c$, for the same crystallization time $t_c$. The temperature profiles are illustrated in section 3.2.2. The importance of the parameters of the various thermal histories will be discussed in the following paragraphs as well as in section 3.2.2.

The melt-crystallized samples are disks, the size of a microscope cover slip, cut from the amorphous sheets. Those were placed between thin brass shim support plates, melted at 385°C for 4 min and subsequently crystallized in the furnace of a LINKAM hot stage (model 600-THM) under nitrogen gas flow. The melt-crystallization temperatures were chosen so that to ensure fast primary crystallization - $T_x$ = 300°C is the lowest possible temperature at which upon quenching from the melt the sample could be thermally equilibrated before

significant crystallization begins. The crystallization times $t_x$ are 4 min, 8 min, 16 min, 30 min, 60 min, 120 min, 240 min, 960 min, 1920 min, and 3840 min. After the crystallization time elapsed, the samples were fast cooled in the hot stage by applying through the cooling circuit of the hot stage a high flow rate of nitrogen gas, chilled by passing through a liquid nitrogen trap. The cooling rate of the hot stage furnace was estimated to be in excess of 200 K/min. This was done to ensure that upon cooling to room temperature all samples were subjected to the same cooling conditions, preventing them from prolonged further crystallization upon cooling (if such crystallization indeed happens). This provides conditions under which the crystalline lamellae should have formed and grown isothermally at the given crystallization temperature only.

The cold-crystallized samples were annealed in a Carver hot press and subsequently cooled down to room temperature by quenching into ice-water mixture. The series, cold-crystallized at various temperatures, were annealed for 60 min at several $T_c$s: 163°C, 183°C, 203°C, 223°C, 243°C, 263°C, 272°C. The other cold-crystallized series of samples were annealed at 243°C for various times: 1 min, 2 min, 4 min, 8 min, 16 min, 30 min, 60 min, 120 min, 240 min, 960 min, 1920 min, 3840 min, 7680 min, 15480 min, and 21550 min.

### *sample preparation for the creep experiments:*

The material used in this study is PEEK grade 450G, supplied in the form of amorphous sheets. From this starting material, plates 1.8 mm thick were prepared by molding at a temperature above the melting temperature of PEEK (at 370°C). A lower temperature than the 385°C temperature used in the melt-crystallization studies was chosen in order to avoid the possibility of degradation as the molding was done in air. In addition, it was found that slightly lowering the temperature of the melt greatly reduced the formation of voids, which were present in great numbers in plates pressed at 385°C.

As the presence of voids would make meaningless and incomparable the results of a mechanical test, a greater importance was placed on the preparation of a series of homogeneous samples, produced from one batch. Not raising the melt temperature enough could have the effect of preserving some nuclei in the unrelaxed melt, which could affect the

ability of the samples to crystallize upon entering the temperature window of crystallization upon cooling. The homogeneity of the samples and the subsequent equal annealing conditions still justify the reliability of the results and conclusions, because what is monitored is the difference in the response of these samples to annealing long after their initial crystallization.

The plates were quenched into ice/water. This cooling procedure was not sufficient to produce amorphous plates, as was evidenced by the lack of transparency of the resulting material. In order to ensure homogeneity within the plates and similar thermal prehistory, samples with size 1.8 mm × 24 mm × 11 mm were cut and annealed for 35 min at 305°C and quenched immediately. This treatment ensures that primary crystallization is completed under similar conditions throughout each sample and in all of the samples. Although the crystallization history of the samples is a complex one (fast and incomplete melt crystallization upon cooling followed by annealing at 305°C), the thermal history of all the samples is the same. The last prolonged thermal treatment, before the tests, results in the annealing of the lamellae, which might have formed upon fast cooling, and in the cold-crystallization of the remaining uncrystallized material. The temperature range of testing is well below the 305°C annealing temperature. Therefore, it is expected that any changes upon annealing at temperatures below 305°C will not cause significant reorganization of primary morphology already formed at the higher temperature and will result only in "secondary" effects.

## 3.2 Characterization Methods

### *3.2.1 MW Characterization*

In order to be able to justify the correlation between the observed variations in the melting behavior of the fractions and molecular weight, a careful characterization of the molecular weight distribution of each fraction is needed. There are two objectives in this study: 1) to determine the efficiency of the fractionation procedure, and 2) to determine the molecular weight and polydispersity ratio (PDR) of the fractions.

The efficiency of the fractionation in this study is estimated based on the following criteria [111]:

- narrow molecular mass distribution of the fractions (small PDR),

- no fraction reversal (in the case of fractional precipitation, after every step a fraction with MW lower than the previous fraction's MW should be obtained).

- good fraction yield.

The evaluation of the first two criteria comes directly from the molecular weight characterization of the fractions. The last is a practical one - to obtain a sufficient number of fractions and sufficient amount of material from each fraction in order to be able to satisfy the objective of the fractionation procedure. The data in table 3.1 suggest, that the parameters of the fractionation (solvent/nonsolvent pair, concentration of the solution, number of steps, and amount of nonsolvent at each successive step) were chosen properly in order to satisfy the set goals - to obtain approximately 5-15 % of the starting amount for the different fractions.

The goal in the molecular weight characterization of the ketimine polymer fractions was to obtain reliable values for the MWs through efficient, but routine methods, which would not lead to the loss of significant amount of material. This lead to the choice of the following methods of characterization:

- gel permeation chromatography (GPC),

- intrinsic viscosity (IV) measurements,

- vapor phase osmometry (VPO).

Although light scattering from solution of the polymer at multiple angles and concentrations would have lead to the best results as it determines the absolute molecular weight of a polymer (utilizing the Zimm plot [3]), that method was not deemed proper for this study, as it would have required large amount of each fraction to be used (in fact most of the mass available for each fraction). A recovery of the fractions from the solutions is possible, but still a fractional loss at each of the multiple solution concentrations needed would have lead to the possibility for significant loss of material.

A fast routine determination of the viscosity average molecular weights would have been possible from the experimental intrinsic viscosities $[\eta]$ of the fractions in given solvent at certain temperature if the Mark-Houwink-Sakurada (MHS) equation for the polymer for that solvent and temperature is known. Roovers et al. [104] have determined the MHS relationship between $[\eta]$ in tetrahydrofuran (THF) at 25°C and the molecular weights of their fractions:

$$[\eta]_{THF}^{25^\circ C} = 6.3_4 \times 10^{-4} \; M^{0.61_7} \qquad (3.2)$$

For the determination of the polydispersity of the fractions, additional characterization is needed. The number average molecular weights $M_n$ were determined by GPC and VPO and the weight average molecular weights $M_w$ by GPC. The intrinsic viscosities of the samples were compared under the same conditions with the MHS equation of Roovers et al.

***intrinsic viscosity***

The intrinsic viscosities of the ketimine polymer fractions in THF at 25°C $[\eta]_{THF}^{25^\circ C}$ were determined with an Ubbelohde capillary viscometer from the efflux times of the pure solvent - $t_0$ and of solutions of the fractions with different concentrations $c$ - $t(c)$, based on the following relations [8]:

relative viscosity $$\eta_r(c) = \frac{\eta}{\eta_0} \cong \frac{t}{t_0} \qquad (3.3a)$$

specific viscosity $$\eta_{sp}(c) = \eta_r - 1 = \frac{\eta - \eta_0}{\eta_0} \cong \frac{t - t_0}{t_0} \qquad (3.3b)$$

reduced viscosity $$\eta_{red}(c) = \frac{\eta_{sp}}{c} \qquad (3.3c)$$

inherent viscosity $$\eta_{inh}(c) = \frac{\ln(\eta_r)}{c} \qquad (3.3d)$$

intrinsic viscosity $$[\eta] = \lim_{c \to 0}(\eta_{red}) = \lim_{c \to 0}(\eta_{inh}) \qquad (3.3e)$$

The intrinsic viscosities of the ketimine fractions are reported in table 3.2. Their values decrease continuously with increasing fraction number. This indicates, that there is no fraction reversal.

***gel permeation chromatography***

GPC characterization was carried out in THF at 25°C on a Waters 150-C GPC with Viscotek 100 in-line viscometer and a Chromatics KMX-6 low angle light scattering (LS) detector. The outputs of these are correspondingly: concentration, viscosity, and single angle LS intensity against retention volume $V_r$. This gave three possible ways of determination of the molecular weights:

1) conventional calibration,

2) universal calibration,

3) "absolute" MW.

The method of the conventional calibration of GPC is based on calibrating the retention volumes observed for different molecular weights by running several narrow molecular weight distribution polystyrene standards. This method provides relative weight average MW - $M_w^{GPC-CONV}$ and the polydispersity ratio PDR, listed in the first two rows of data in table 3.3. The molecular weights are only relative and not absolute, because the rough assumption is made, that the retention of the ketimine polymer in the columns is the same as that of a-PS with the same molecular weight. Such an assumption is obviously a gross simplification of the problem. From the single concentration chromatogram runs, however, at least one important quantitative conclusion was established - the observation of narrow unimodal peaks in the chromatograms, separated on the retention volume scale was a guarantee, that the fractionation was efficient.

The universal calibration method is based on the invariance of the hydrodynamic volume $V_H$ of the chains for different polymers - $V_H = [h] \times M$. MHS parameters in THF at 25°C for the PS standards used in the calibration were taken from the equation by Meyerhoff, as recommended by Kurata et al. [112]:

**TABLE 3.2** Intrinsic viscosities of the poly(arylene ether ether ketimine) fractions in THF at 25°C.

| **Fraction** | $[h]_{THF}^{25^{\circ}C}$ **[ dl/g ]** |
|---|---|
| KTMN4-2 | 0.514 |
| KTMN4-3 | 0.411 |
| KTMN4-4 | 0.334 |
| KTMN4-5 | 0.286 |
| KTMN4-6 | 0.255 |
| KTMN4-7 | 0.205 |
| KTMN4-8 | 0.176 |
| KTMN4-9 | 0.130 |

**TABLE 3.3** Results from the molecular weight characterization of the poly(arylene ether ether ketimine) fractions: GPC conventional calibration - $M_w^{GPC-CONV}$, polydispersity ratio (PDR), GPC universal calibration - $M_w^{GPC-UNIV}$, GPC with in-line light scattering - $M_w^{GPC-LS}$, VPO - $M_w^{VPO}$ (product of $M_n^{VPO}$ and PDR from GPC).

| Fraction | $M_w^{GPC-CONV}$ | $PDR$ | $M_w^{GPC-UNIV}$ | $M_w^{GPC-LS}$ | $M_w^{VPO}$ * | $M_w^{PEEK}$ |
|---|---|---|---|---|---|---|
| KTMN4-2 | 73 000 | 1.35 | 54 600 | - | - | 43 300 |
| KTMN4-3 | 61 600 | 1.35 | 39 800 | 35 000 | - | 31 600 |
| KTMN4-4 | 42 900 | 1.2 | 29 700 | 25 700 | - | 23 600 |
| KTMN4-5 | 33 600 | 1.2 | 22 900 | - | - | 18 200 |
| KTMN4-6 | 26 700 | 1.2 | 16 900 | 14 400 | 16 100 | 13 400 |
| KTMN4-7 | 18 000 | 1.2 | 13 300 | 12 000 | 12 100 | 10 600 |
| KTMN4-8 | 12 500 | 1.2 | 8 000 | 9 000 | 10 500 | 6 300 |
| KTMN4-9 | 6 100 | 1.45 | 4 000 | - | 3 500 | 3 200 |

* $M_w^{VPO} = M_n^{VPO} \times PDR$

$$[h]_{THF}^{25^{\circ}C} = 13.63 \times 10^{-4} \; M^{0.714} \qquad (3.4)$$

From the chromatograms of the a-PS molecular weight standards a calibration file is created, which gives the correspondence between $V_H$ and molecular weight.

The simultaneous recording of dual - viscosity and concentration, chromatograms allows the determination of the hydrodynamic volume of the fractions, from which their molecular weights are determined. The values of the molecular weights of the ketimine fractions from the universal calibration in GPC are listed in the third row of data in table 3.3. The polydispersity ratio, calculated from the universal calibration differs very little from the one, calculated from the conventional calibration and is not listed separately.

The simultaneous calculation of the concentration chromatogram and the low angle light scattering chromatogram from the in-line light scattering detector allows the determination of a value for the molecular weight, which is closer to the true absolute molecular weight. It is still not the absolute molecular weight as no extrapolation to zero concentration and angle is made (the LALS chromatogram is taken at fixed angle). The values of the molecular weights calculated from the concentration and LALS chromatograms are listed in the fourth column of table 3.3.

***vapor phase osmometry***

The molecular weights measured by the method of VPO are absolute number average molecular weights $M_n$. Measurements were performed on dilute solutions of the fractions in toluene at 50°C on Wescan 233 vapor phase osmometer. Calibration was carried out with PS standards. The limit of the instrument in detecting molecular weights with toluene as a solvent is approximately 50,000 g/mol.

The resulting values of the molecular weights $M_n^{VPO}$ multiplied by the polydispersity ratio (PDR) from GPC are reported in the fifth row of data in table 3.3. The multiplication by the PDR factor was done in order to make comparison between the same type of MW averages, calculated from different methods.

The molecular weight standards used in the GPC and VPO characterization are narrow molecular weight distribution anionic atactic polystyrenes with molecular weights ranging from 580 g/mol to 2,950,000 g/mol (GPC) and from 1,500 g/mol to 15,000 g/mol (VPO).

***analysis of the molecular weight data***

Analysis of the values reported in table 3.3 leads to the conclusion, that the molecular weights from GPC-conventional calibration are much higher than the rest of the values. The molecular weights determined from GPC-universal calibration and GPC-LS are in close agreement. The number average molecular weight values for the low MW fractions determined from VPO, when multiplied by the polydispersity ratio from GPC, give weight average values $M_w^{VPO}$ close to these, calculated from GPC-LS and GPC-universal calibration.

From the intrinsic viscosity values reported in table 3.2 and the GPC-universal calibration molecular weights from table 3.3 the Mark-Houwink-Sakurada relationship between $[h]_{THF}^{25^\circ C}$ and $M$ was calculated:

$$[h]_{THF}^{25^\circ C} = 6.5_9 \times 10^{-4} M^{0.61_3} \qquad (3.5)$$

Comparison with equation (3.2) shows, that the MHS coefficient and exponent determined in this study are close to the values by Roovers et al. [104]

The final conclusions from the MW characterization of the poly(arylene ether ether ketimine) fractions are:

- the fractionation of PEEKtmn resulted in narrow molecular weight distribution fractions,

- the molecular weights determined by GPC-universal calibration are in close agreement with the values expected from the intrinsic viscosities data and the MHS relationship determined by the independent study of Roovers et al., [104]

- for future reference routine characterization of PEEKtmn narrow molecular weight fractions can be done by GPC-universal calibration and intrinsic viscosity measurements.

The last raw of data in table 3.3 reports the number average molecular weights of the PEEK fractions, obtained from equation (3.1) and the ketimine fractions' molecular weights reported in row 3 (GPC-universal calibration).

### *3.2.2 Thermal Properties*

The investigation of the thermal properties of PEEK is the major part of this study. The main technique of investigation is differential scanning calorimetry (DSC). The additional studies of the small strain creep compliance, density, and WAXS could be classified formally as "thermal properties" studies too. They share a common methodology with the DSC studies, which is investigation of the effect of long isothermal treatment of semicrystalline and amorphous PEEK above $T_g$ on the physical properties of the polymer.

DSC studies were done on a Perkin Elmer differential scanning calorimeter model 2-C. The principle of operation of the DSC is described in the literature. [113] Various heating rates were used: 5 K/min, 10 K/min, 20 K/min. Studies of the transition enthalpies for crystallinity determination were done at 20 K/min. Calibration of the melting scans was done with indium ($T_m$ = 156.61°C) and lead ($T_m$ = 327.5°C) standards. Crystallization and annealing temperatures in the DSC, reported in this study are about 0.8-0.9 K above the actual temperature of the DSC cell. This is to be expected when calibration of the DSC is done in such a way as to have the melting scan at 10 K/min of a DSC standard material exhibit an onset temperature equal to the thermodynamic melting temperature of the standard material.

A linear horizontal baseline of the DSC signal was obtained before the beginning of each series of DSC scans. This corrects for the difference between the heat flow output of a blank DSC pan and the reference pan to zero or a constant. The samples were encapsulated in pans with the same weight (± 0.05 mg). The heat flow output for the sample was obtained after subtraction of the baseline heat flow from the recorded output for that sample.

In the early stages of the investigation of the low temperature endothermic peak of PEEK, calibration of the heat flow output was done with the melting enthalpies of lead and

indium. Later, for all the crystallinity studies calibration of the heat flow was done with a sapphire standard. [113, 114]

After application of the sapphire correction, the $C_P(T)$ trace is very close to the Advanced Thermal Analysis System (ATHAS) recommended values for $C_P(T)$ of PEEK below and above $T_g$. [16, 115] The application of the sapphire correction is a lengthy process involving several scans and computation procedures outside the DSC computer program control environment. Therefore, the sapphire correction was calculated only before the beginning of a series of DSC scans for a given experiment. As such an experiment could involve the recording of up to a dozen of DSC scans or more and last accordingly up to 24 hours, possible drifts of the baseline during the experiment would lead to systematic error in the heat flow output and make inapplicable the sapphire correction to the heat flow. In order to correct for this, the baseline was monitored during the duration of the experiment. The observed drifts of the baseline were usually linear with temperature. For a given DSC scan the appropriate baseline for the scan was subtracted. Alternatively, if a baseline was not recorded immediately before or after a given DSC scan, but the baselines at the beginning and the end of a series of scans recorded in one batch experiment exhibited a drift linear with temperature, an adjustment of the slope of the scans was made before applying the sapphire correction.

With this approach a large number of sequential DSC scans belonging to a single experiment were recorded in a short time. This avoided large drifts in the baseline and temperature calibrations which are observed if the experiment becomes too long.

Figure 3.1 presents the DSC heating scan (at 20 K/min) of initially amorphous PEEK after baseline subtraction, slope adjustment and sapphire correction. Also plotted are the recommended heat capacities of the glassy PEEK below $T_g$ and liquid PEEK above the final melting [16, 115] and their extrapolations to the rest of the scanned region. The correspondence between the single run result from this study and the results of Cheng et al. [16, 115] is very good. Notice, that the $C_P$ of the supercooled liquid PEEK just after $T_g$, but below the beginning of the cold-crystallization exotherm, matches the extrapolated values of the $C_P$ of the melt. This observation, also mentioned by Cheng et al. [16] and Seguela, [116] allows the $C_P(T)$ of the

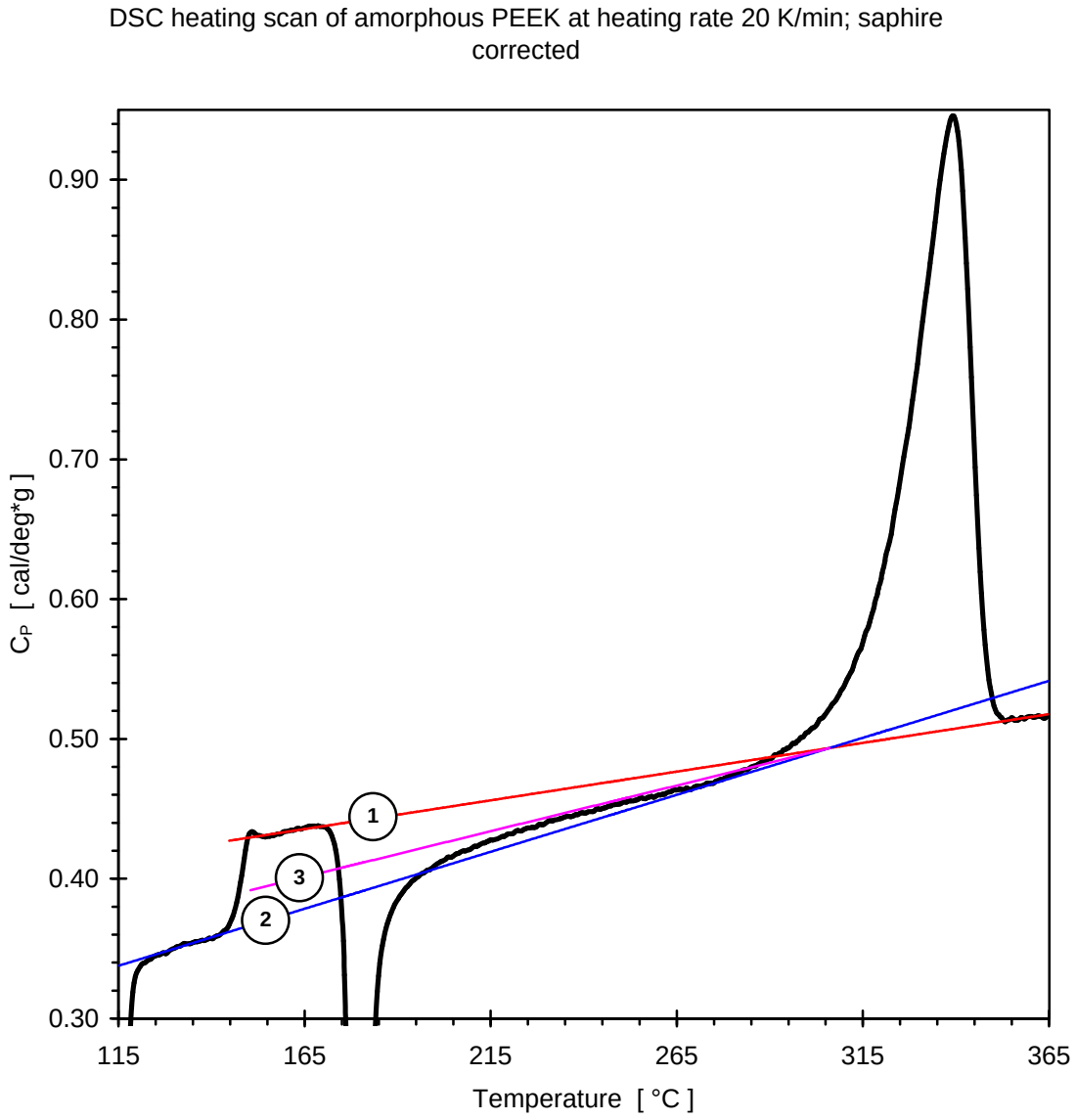


$C_p(\text{liquid}) = 0.2554 + 0.00041*T$

$C_p(\text{glass}) = 0.0213 + 0.00082*T$

} ATHAS data (references 16 and 115)

T in K, $C_p$ in cal/deg*g

**Figure 3.1** DSC heating scan of amorphous PEEK at 20 K/min. Also included are: (1) $C_P$ of the melt, extrapolated to lower temperatures, (2) $C_P$ of the glass (extrapolation to $T > T_g$ taken as $C_P$ of crystalline phase), and (3) the $C_P$, which a material with 60% rigid fraction must have between $T_g$ and melting region.

semicrystalline state between $T_g$ and the beginning of the melting region to be reasonably well approximated as a linear combination of the heat capacities of the mobile amorphous fraction and the rigid fraction (crystalline and RAF). As an illustration the expected heat capacity of PEEK with $f_r = 0.6$ is plotted too.

The following parameters of the physical transitions of PEEK samples with various thermal histories were investigated:

- $T_m^{'}$ - the observed melting temperature,

- $T_{max}$(low) - the temperature of the low temperature endothermic peak resulting from isothermal crystallization and/or annealing above $T_g$,

- $\Delta H_m$ - the total melting enthalpy of a sample,

- $\Delta H_m$(low) - the enthalpy of the low temperature endothermic peak,

- $T_g$ - the glass transition temperature,

- $\Delta C_P(T_g)$ - the magnitude of the change in $C_P$ at the glass transition temperature.

Figure 3.2 illustrates the above mentioned parameters for the heating scan of PEEK with the following thermal history: crystallization from the melt at $T_x$ = 305°C for $t_x$ = 300 min and subsequent annealing at $T_a$ = 210°C for $t_a$ = 60 min.

The melting temperature $T_m^{'}$ is determined as the maximum temperature of the "high" temperature final endothermic (melting) transition.

The position of the low temperature endothermic transition is characterized by the maximum of the endothermic peak(s) $T_{max,i}$. The index "i" (where i = 1, 2, ...) denotes the number of the peak in the order it was produced during the thermal treatment of the sample if the thermal history of the sample includes multiple isothermal steps (see figures 3.4 and 3.5).

The glass transition temperature $T_g$ is measured as the temperature at which the $C_P(T)$ trace of the sample in the glass transition region is equidistant from the extrapolated traces of the glassy and the rubbery amorphous or semicrystalline state. [16, 113] The difference between these extrapolated traces at $T_g$ is $\Delta C_P(T_g)$.

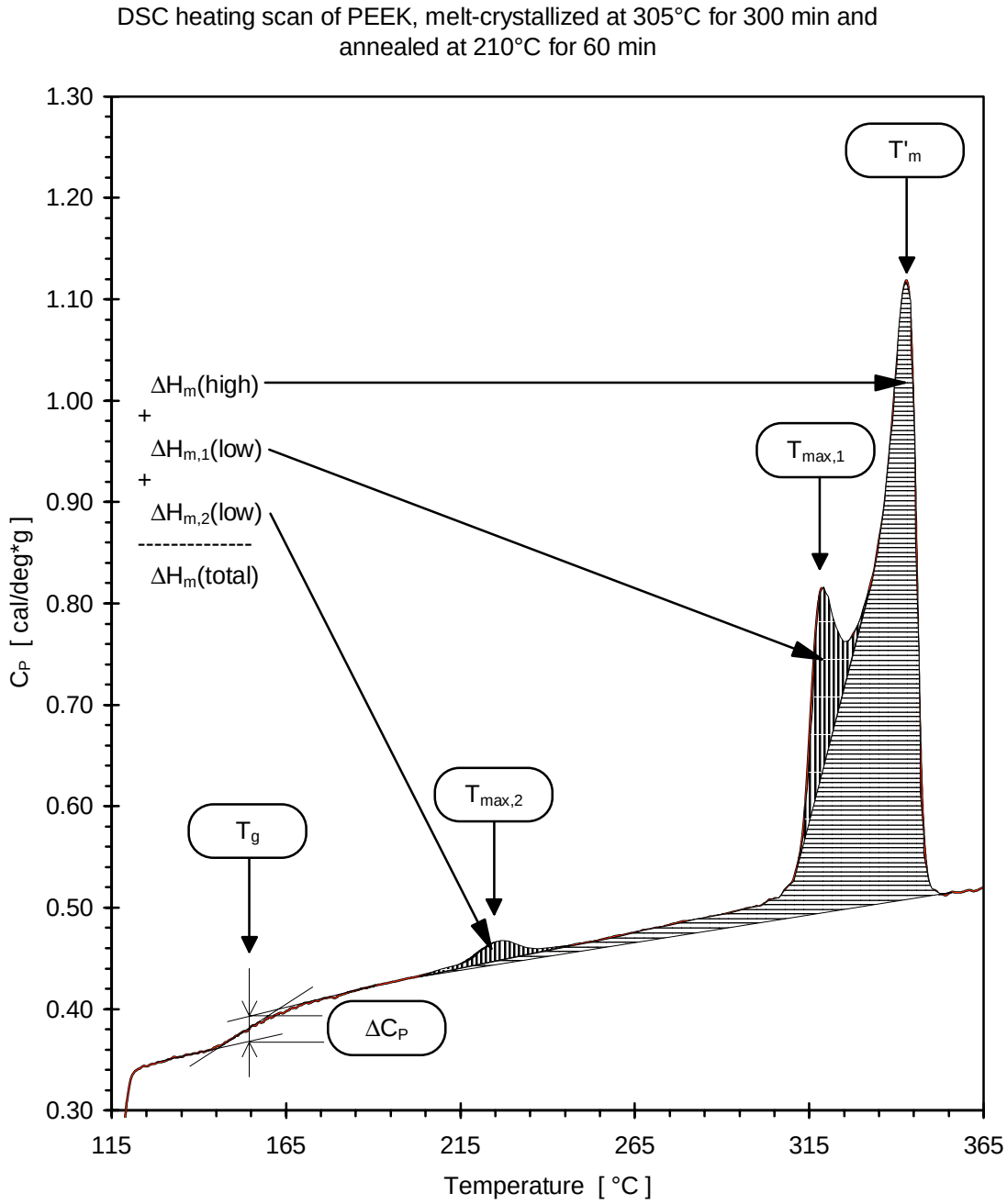


**Figure 3.2** Thermal characterization of PEEK by DSC - investigated parameters.

The calculation of the transition enthalpies carries certain difficulty due to the fact, that the choice of the local "baseline" in reference to which they are measured is not always straightforward. In light of the assumption, that the low temperature endothermic transition represents the melting of crystalline lamellae (see section 2.4.2) the total melting enthalpy $\Delta H_m$ is evaluated between the temperature of the last isothermal treatment of the sample and the temperature at which the final trace of melting disappears in the $C_P(T)$ scan. A local "baseline" could be defined as the $C_P(T)$ trace the sample would have if the melting peak was not present (or separated). This local baseline would reflect the subtraction of the heat flow due to the heating of a sample with continuously increasing amorphous fraction from the integrated heat flow. The rate of increase of the amorphous fraction is governed by the rate of melting of the sample. Therefore, the evaluation of the enthalpy of melting would be impossible without the knowledge of the crystallinity e.g. the enthalpy of melting:

$$Q_t(T_1 \to T_2) = \Delta H_m + \int_{T_1}^{T_2} C_p(T)\,dT = \Delta H_m + \int_{T_1}^{T_2} \left\{ c_c(T) * C_{p,c}(T) + \left[1 - c_c(T)\right] * C_{p,a}(T) \right\} dT$$

$$\Delta H_m = Q_t(T_1 \to T_2) - Q_{12}(\Delta T) \qquad (3.6)$$

where $Q_t(T_1 \to T_2)$ is the integrated heat between $T_1$ and $T_2$ and $Q_{12}(\Delta T)$ is the heat due to the raising of the temperature of the sample between $T_1$ and $T_2$.

This problem has been circumvented in many *different* ways in the literature. [6] In order to be able to routinely calculate the melting enthalpies from many DSC scans, a linear local baseline has been applied in this study by connecting the $C_P$'s between the points of evaluation and calculating the area of the curve above it in the DSC scan (see figure 3.2). Analysis of the absolute error associated with this choice of baseline is done in section 3.2.3a.

The choice of local baseline for the calculation of $\Delta H_m$(low) - the enthalpy of the low temperature endothermic peak, is even more complicated. The following general rule was applied for the calculation of $\Delta H_m$(low): the choice of the local baseline was made consistent with the behavior of the $C_P(T)$ before and after the low temperature endotherm. Thus in the case of $\Delta H_{m,2}$(low) on figure 3.2, a linear baseline between the beginning and the end of the peak appears a natural choice. In the case of $\Delta H_{m,1}$(low), however, the choice of a linear

local baseline is a gross simplification and would lead to an erroneous value. There is no other justification for it except the simplicity and ease of calculation.

Two better approaches are possible - to apply a non-linear local baseline or to resolve the low temperature endotherm from the high temperature final melting peak. Whichever approach one chooses, a justification for the choice and an explanation of the method is needed for comparison with independent studies.

For PEEK, Cheng et al. [16] quote the calculated enthalpies of the low temperature endothermic peak. However, the method of separation of the high and low temperature endotherms is not described. From the magnitude of the values associated with the low temperature endotherm it seems as if in the case of low temperatures of crystallization and/or annealing approximately a linear local baseline has been applied for the low temperature peak. But the high values associated with the low temperature peak in the case of high crystallization temperatures could not have been obtained with a linear local baseline. It seems, that the two peaks (high and low) have been separated through an unspecified peak fitting (peak resolving) routine.

In the case of PBT Nichols and Robertson [59] developed a method, which models the appearance of the low-temperature endothermic peak from the annealing of a starting distribution of lamellae with different melting points. Their method predicts at least qualitatively the appearance of multiple endotherms when PBT is annealed in the temperature range 170-205°C. However, the method does not allow for the variation of the low temperature endotherm with time and seems to fail to account for the appearance of multiple peaks when the annealing temperature is too high (figure 13 in reference 60).

The separation of the low temperature endotherm and the calculation of its enthalpy will be presented in detail in section 4.2.1. At this point it suffices to say, that a linear local baseline has been applied in most cases. This leads to an underestimate of the value of $\Delta H_m$(low) when the low temperature endotherm appears as a shoulder on the broad higher temperature endotherm. It must be noted that in few special cases - the melting of the series of samples for crystallinity studies and the post-crystallization annealing of PEEK close to the final melting, the low temperature peak has been resolved by fitting $C_P(T)$ in its vicinity

with a 3-parameter peak fitting routine, which will be justified at the end of section 4.2.1. The enthalpy $\Delta H_m$(low) was then calculated as the enthalpy of the best fit.

Careful evaluation of the above mentioned parameters is needed in order to give a quantitative description of the evolution of the low temperature endotherm and accurate evaluation of small changes in crystallinity with change in thermal history. Yet the accurate evaluation of the above mentioned parameters will be of little use if the thermal histories of the samples are unknown or ill specified.

Figures 3.3 - 3.7 illustrate the different types of thermal histories to which the different series of PEEK samples have been subjected in this study.

The general features of these thermal histories are:

- in all studies where the first step was crystallization from the melt, the material was melted at 385°C for 4 min; this was done in order to begin with a homogeneous melt and ensure similar starting conditions for all samples within a series,

- the primary crystallization of the melt was completed (except in case b on figure 3.6) and the effect of crystallization and/or annealing time and temperature monitored thereafter,

- when thermal treatment was carried out in the DSC, samples were scanned with or without quenching below $T_g$; in the former case these samples may crystallize further during cooling, in the latter case the length of the experiment was minimized time-wise, but no information on the variation of $T_g$ with thermal history was obtained,

- the samples for the studies of crystallinity were quenched below $T_g$ after the prescribed crystallization or annealing times elapsed; the quenching was done as fast as possible in order to prevent further crystallization upon cooling.

Note: This last step is markedly different from the thermal histories applied in the study of Cheng et al. [16] In that study all the samples were cooled very slowly (at a rate -0.31 K/min) from the temperature of the last isothermal treatment to room temperature. For example, samples annealed at 270°C and 250°C for 120 min were nonisothermally annealed above $T_g$ during cooling for respectively 380 min and 320 min. Such a treatment could allow significant additional slow crystallization upon cooling and could make it difficult to

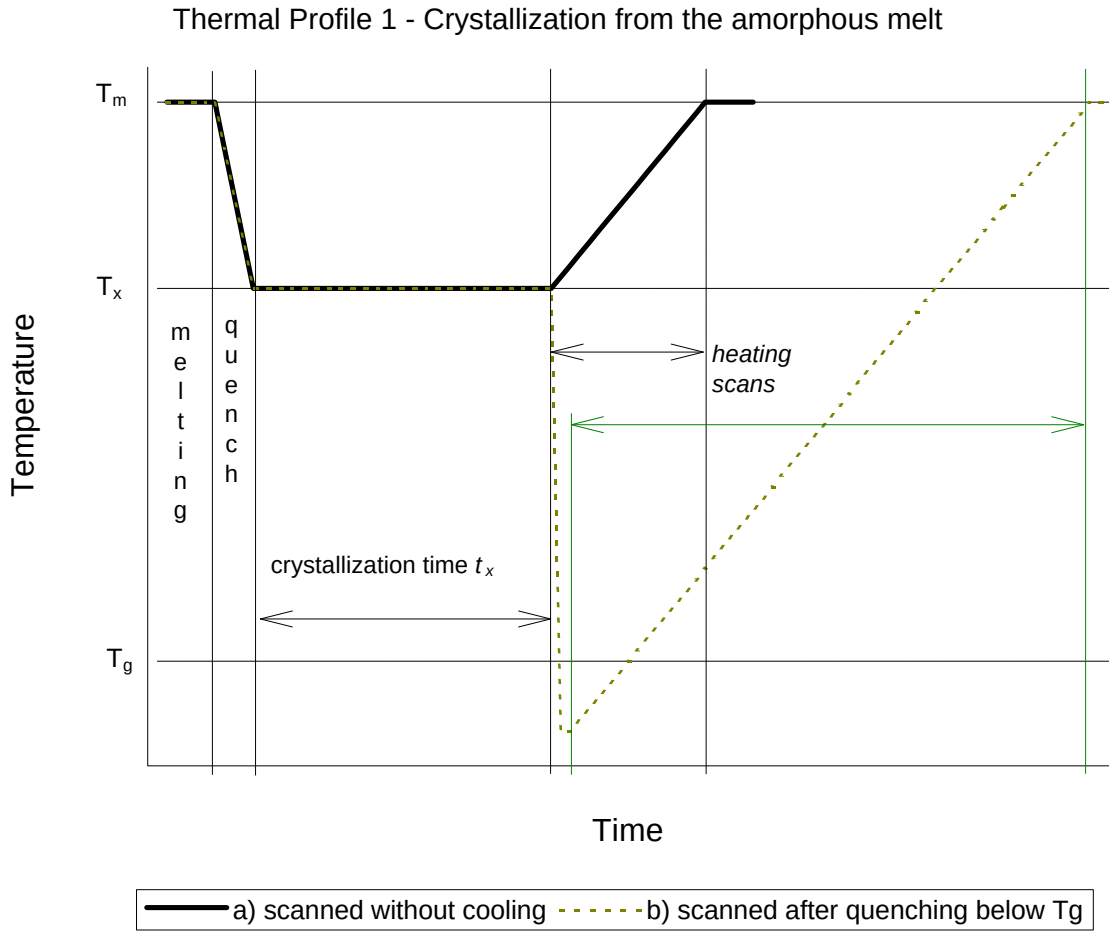


$T_m$ = 385°C $t_m$ = 5 min

quenching rate = as fast as allowed instrumentally

$T_x$ = 300-330°C $t_x$ = 4 min - 7,680 min (3 decades)

scanning rate = 10 K/min; 20 K/min

**Figure 3.3** Crystallization from the melt till completion of primary crystallization and beyond.

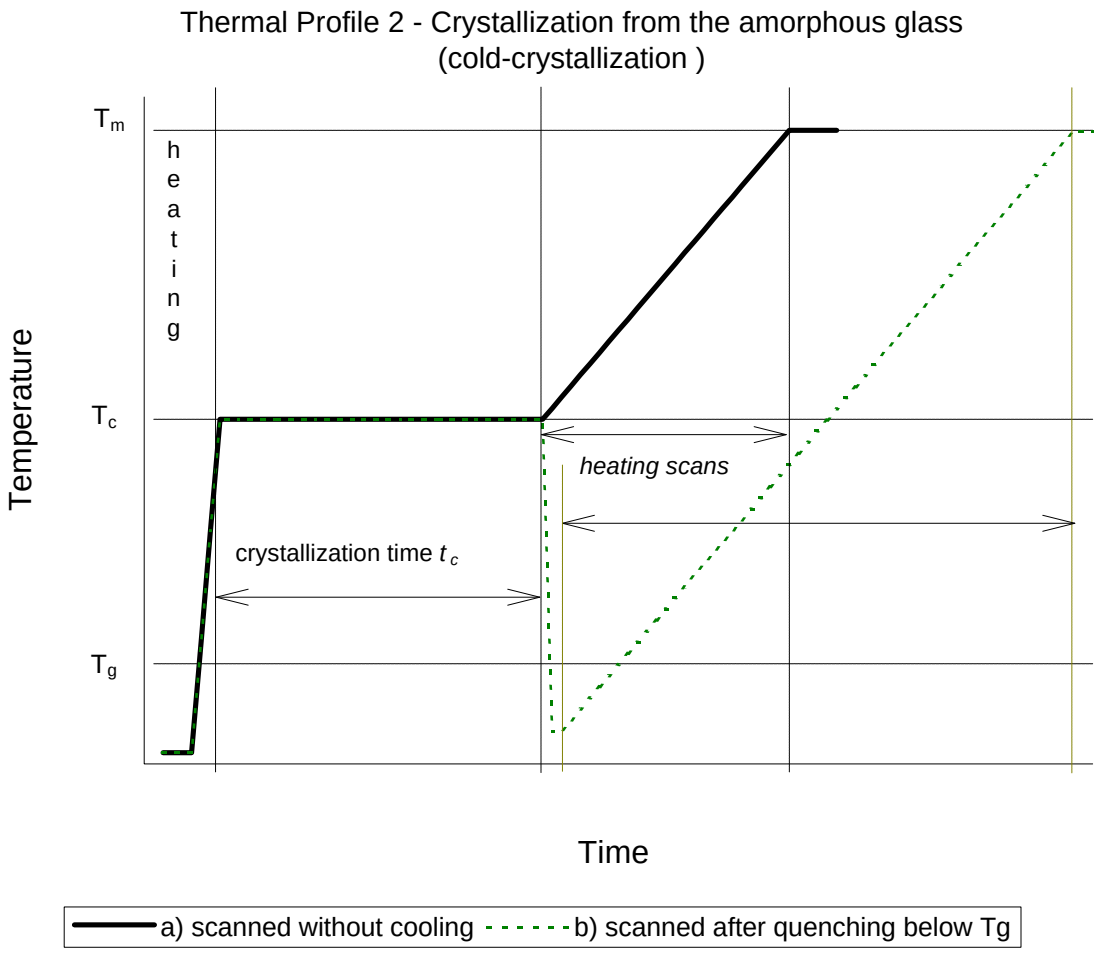


Initial conditions - as is (amorphous sheet)

initial heating rate (up to $T_c$) = fast

$T_c$ = 160-345°C $t_c$ = 1 min - 25,000 min (4.5 decades)

scanning rate = 5 K/min, 10 K/min; 20 K/min

**Figure 3.4** Dynamic crystallization from the glassy state followed by isothermal annealing.

distinguish between the effect of isothermal annealing from the effect of slow cooling. It comes as no surprise then, that in the DSC crystallinity analysis of Cheng et al., the contribution of the low melting crystallinity formed upon cooling plays a major role in the balance of the rigid fraction (crystalline + RAF) vs. mobile fraction above $T_g$.

The type of thermal history depicted on figure 3.3 (Thermal Profile 1) was used to monitor the development of the low temperature endotherm upon isothermal crystallization from the melt. The effects of crystallization temperature $T_x$ and time $t_x$ were studied.

Thermal Profile 2 (figure 3.4) was applied to monitor the effect of time $t_c$ and temperature $T_c$ of cold-crystallization or annealing on the low temperature endotherm. An initially amorphous sample was quickly brought up to a given $T_c$ and annealed there for the prescribed length of time. As figure 3.1 shows, crystallization from the amorphous glassy state upon heating occurs very fast - most of the dynamic crystallization is completed within about 40 seconds between recorded temperatures of the DSC cell 170°C and 185°C (note, that actual sample temperature is slightly lower due to thermal lag). Thus for most of the lower part of the temperature interval studied ($T_c$ = 160-260°C) this allows us to examine *only* the effect of isothermal annealing after the fast cold crystallization of the sample upon heating. In the interval between 300°C and 345°C, where melting of the cold-crystallized material occurs, heating to $T_c$ will result in the melting of a part of the crystallized material. Therefore, at the beginning of the high temperature annealing a fraction of the crystalline material will melt and then recrystallize. In few experiments this thermal history was applied to samples, which have been pre-crystallized.

Thermal Profile 3 (figure 3.5) was applied to monitor the development of the low temperature endotherm upon annealing up of pre-crystallized samples. The initial crystallization from the melt was done at low temperatures ($T_x$ = 290°C-315°C) until the completion of the primary crystallization process. After that the samples were heated and the development of the low temperature endotherm monitored with annealing time and temperature. The annealing temperature was chosen at or above the maximum of the low temperature peak, which results from the crystallization step alone.

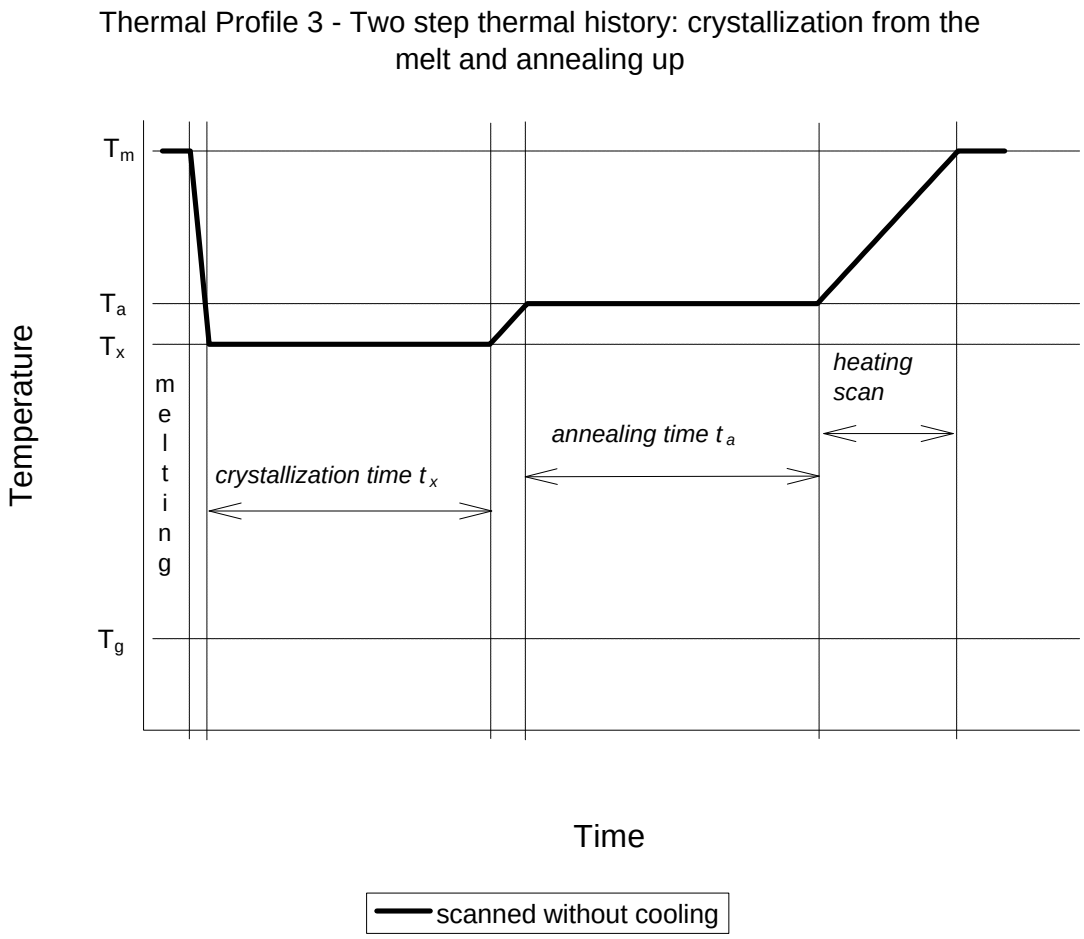


$T_m$ = 385°C $t_m$ = 5 min

quenching rate = as fast as allowed instrumentally

$T_x$ = 290-315°C $t_x$ = 15 - 480 min (till completion of primary crystallization)

$T_a$ = 300-345°C $t_a$ = 1 min - 3,840 min (2.5 decades)

scanning rate = 10 K/min

**Figure 3.5** Two step thermal history: crystallization from the melt till completion of primary crystallization and annealing up.

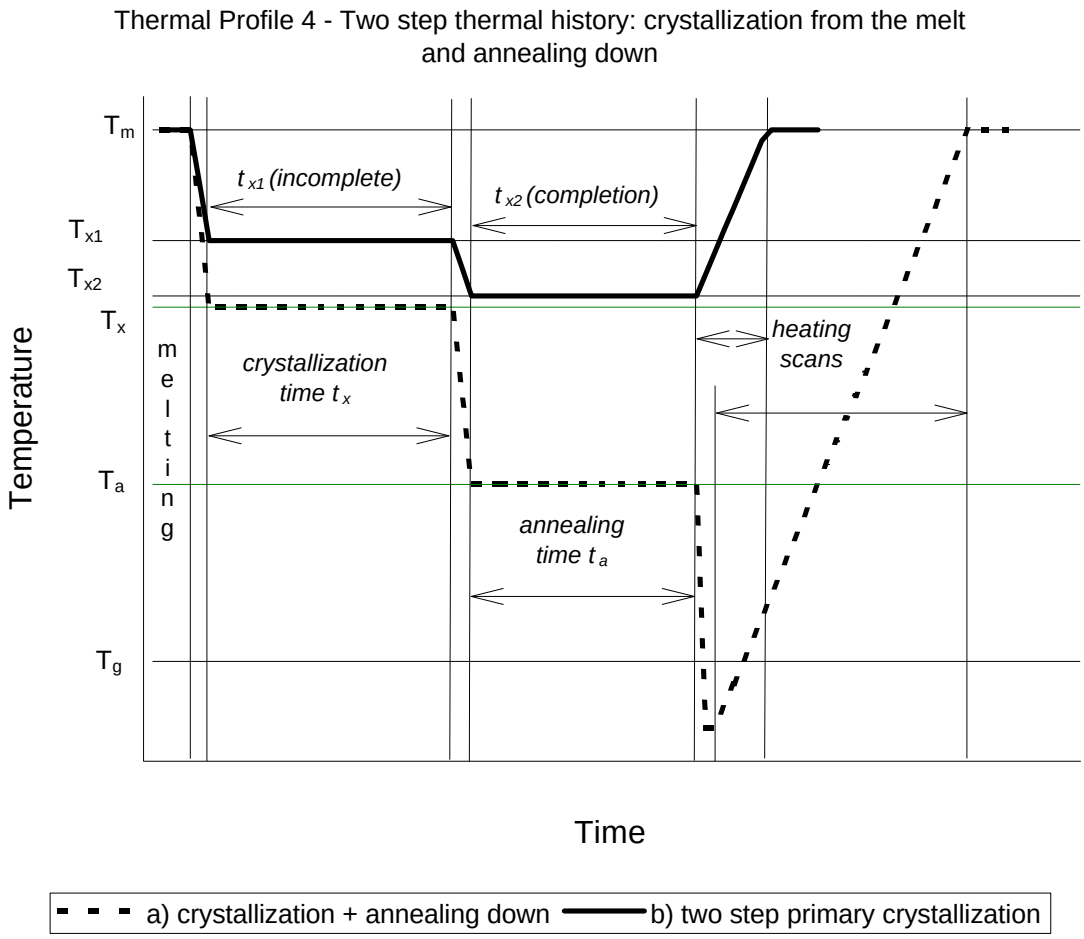


$T_m$ = 385°C $t_m$ = 5 min

$T_x$ = 300-310°C $t_x$ = 30 min - 300 min (primary crystallization is completed)

$T_a$ = 300-345°C $t_a$ = 4 min - 7,680 min (2.5 decades)

$T_{x1}$ = 330-320°C $t_{x1}$ = 60 min - 480 min (primary crystallization is incomplete)

$T_{x2}$ = 290-310°C $t_{x2}$ = 15 min - 480 min (primary crystallization is completed)

scanning rate = 10 K/min

**Figure 3.6** Two step thermal history - crystallization from the melt and: a) annealing down, b) crystallization down.

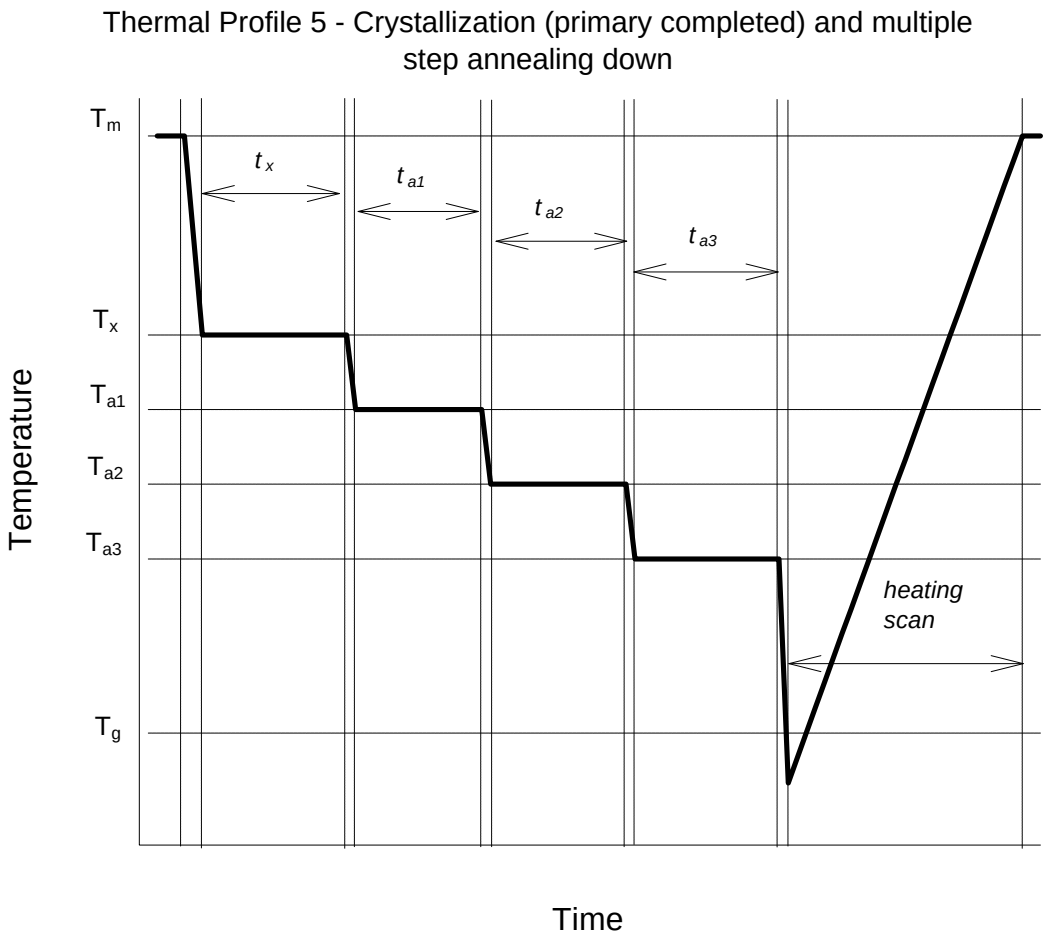


$T_m$ = 385°C $t_m$ = 5 min

$T_x$ = 300-310°C $t_x$ = 30 min - 120 min (primary crystallization is completed)

$T_{a,i}$ = 185 - 275°C $t_{a,i}$ = 30 min - 960 min

scanning rate = 10 K/min

**Figure 3.7** Multiple step thermal history: crystallization from the melt till completion of primary crystallization and multiple step annealing down.

In Thermal Profile 4 (figure 3.6) the multiple step annealing is carried out down from the initial melt crystallization temperature. In case (a) the first step is a complete primary crystallization from the melt. Annealing below $T_x$ at different annealing temperatures and for various times follows. In case (b) the initial crystallization was carried out at relatively high temperatures for such times, that a significant part of the material was left uncrystallized. The next step is annealing down during which the primary crystallization is completed.

Thermal Profile 5 (figure 3.7) is a multiple step annealing down from the melt. This treatment is similar to the one described by Chang [72] and Lattimer et al. [73] except that the time and temperature of the first step allow for completion of the primary crystallization.

The importance of the various parameters of the thermal histories described above will be analyzed when the results from them are reported in section 4.2.1.

### *3.2.3 Crystallinity*

Crystallinities of the samples described in section 3.1.2 were characterized by density and DSC measurements. The application of the corresponding equations for the crystallinities - equations (2.3) and (2.4) from section 2.1, does not involve any other assumptions than the basic assumptions of the two-phase model of the semicrystalline state. The measured quantities - density and melting enthalpy are directly derived from routine experimental techniques. These two methods are the most widely used routine methods of crystallinity determination. It was considered, that with their choice the impact of this study on the two phase model and crystallinity determination will be more pronounced than if more sophisticated techniques were chosen.

As was stated in the introduction, the purpose of this study is to report on some inconsistencies in the evaluation of crystallinity on the basis of the two phase model by DSC and density measurements. Therefore a special attention needs to be paid to each step of the process followed to derive crystallinity values from the raw data. We will analyze some of these critical steps before we proceed to reporting of the results.

The analysis of the two techniques follows in the subsequent sections. As the knowledge of the reference value $r_c$ - the crystal density, is required in equation (2.3) for the density crystallinity, the characterization of the unit cell parameters of PEEK by WAXS is described also in this section.

### *3.2.3a Crystallinity by Differential Scanning Calorimetry (DSC)*

The evaluation of the DSC crystallinity is done according to equation (2.4):

$$c_c^{DSC} = \frac{\Delta H_m}{\Delta H_m^0} \qquad (2.4)$$

The evaluation of the total melting enthalpy $\Delta H_m$ was described in section 3.2.2 above. It involves the construction of a linear baseline between points $C_P(T_1)$ and $C_P(T_2)$, where $T_1$ is at the beginning of melting and $T_2$ after the end of melting. $T_1$ is chosen as the lower of 260°C and $T_x$-10 K or $T_c$-10 K; $T_2$ is about 350-360°C. The melting enthalpy is evaluated from the area between the baseline and the $C_P(T)$ scan.

This simplification leads to a systematic error, the magnitude of which depends strongly on the magnitude of the temperature interval of evaluation (i.e. on the choice of $T_1$) and weakly on the possible variations in the value of $C_P(T_1)$ with crystallinity.

For $T_1$ = 260°C and $T_2$ = 360°C the magnitude of the error introduced by using a linear baseline in a sample with crystallinity $c_c$ = 0.40 is about $d(\Delta H_m)$ = 0.28 cal/g. If the crystallinity of a series of samples changes little, there will be a small variation of the error due to variation of $C_P(T_1)$ with crystallinity. For change of crystallinity of about $d(c_c)$ = 0.05 the magnitude of this variation of the error is 0.05 cal/g and is, therefore, negligible. Thus we can assume, that the use of a linear baseline between 260°C and 360°C introduces a constant, positive systematic error of about 0.25 cal/g, which leads to overestimate of crystallinity of all samples evaluated within given temperature interval by about $d(c_c)$ = 0.01.

A variation in $T_1$ (due to the occurrence of the low temperature endotherm over wide temperature interval) leads to a larger variation of the error. If we assume, that a series of

samples has approximately the same crystallinity (and therefore - the same $C_P(T)$ between $T_g$ and the beginning of melting) the evaluation of $DH_m$ with a baseline drawn in progressively wider intervals ($T_1$, $T_2$) leads to larger positive errors being introduced. Thus with a linear baseline drawn between $T_1$ = 180°C and $T_2$ = 360°C for a sample with $c_c$ = 0.40 the error is 0.76 cal/g. The crystallinity is overestimated by 0.025.

From the analysis above it is clear, that:

- the use of linear baseline for series of samples with approximately close crystallinities, for which the melting transition occurs in the same temperature interval, leads to a constant positive, but small, shift of the crystallinities.

- the use of linear baseline for a series of samples with approximately close crystallinities, for which the melting transition begins at lower and lower temperatures, leads to a positive shift of the crystallinities, which increases in magnitude with widening of the melting interval.

The error, introduced by the use of linear baseline, could be described approximately by the equation:

$$d(\Delta H_m) = f_r\left[0.42 + 0.01 \times (260 - T_1)\right] \quad [\text{ cal/g }] \qquad (3.7)$$

where $f_r$ is the rigid fraction and $T_1$ is in [°C].

From the values of the enthalpies, the DSC crystallinities were calculated by using a reference value of $\Delta H_m^0$ = 31.1 cal/g [63] for the enthalpy of a fully crystalline PEEK. This value was derived by Blundell and Osborn from an extrapolation of the relationships between $\Delta H_m$ and the density and WAXS crystallinities $c_c^{WAXS}$ and $c_c^{Dens}$ to 100 % crystallinity. It has been the most widespread reference value, used by many investigators. [16, 17, 19, 69-71, 116]

Other values for $\Delta H_m^0$ have been suggested or reported in the literature:

- Jonas et al. [67] have used the value of Blundell and Osborn, and suggested that a higher value of $\Delta H_m^0$ might explain some (but not all) discrepancies between crystallization and melting enthalpies of samples of different crystallinities.

- Chang [72] suggested, that the value of 31.1 cal/g could be underestimating $\Delta H_m^0$ due to the fact, that Blundell and Osborn used a value for $r_c$ 1.4005 g/cm$^3$ - lower than the maximum observed value for PEEK, which is 1.415 g/cm$^3$.

- Mehmet-Alkan and Hay [75] have suggested a value of 29.3 cal/g based on a consideration of a thermal cycle of cooling, crystallization, heating, and melting. However, their method of taking into account the heat capacities of the crystalline and amorphous fractions is based on some questionable assumptions.

- Lee et al. [65] arrived at a value of 39.5 cal/g from extrapolation of a $\Delta H_m$ vs. density plot to the highest crystal density measured - $r_c$ = 1.415 g/cm$^3$. [118] The latter is the crystal density derived from WAXS of highly oriented PEEK fibers. It differs from most of the other WAXS values for $r_c$ in the literature only in the significantly reduced value of the *c*-axis parameter of the unit cell. It is thus not clear whether one could use such a value for the extrapolation.

- Zoller et al. [117] derived a value of $\Delta H_m^0$ = 38.5 cal/g from P-V-T measurements of the dependence of the melting temperature of PEEK on pressure (the Clapeyron equation):

$$\frac{dT_m^{'}}{dP} = T_m^{'} \frac{DV_m}{DH_m^0} \qquad (3.8)$$

They used the equation to relate the variation of the observed melting point $T_m^{'}$ with applied pressure $P$ to $\Delta V_m$ and $\Delta H_m^0$. $DV_m = V_a(T_m^{'}) - V_c(T_m^{'})$ is the difference between the measured volume of the melt at $T_m^{'}$ and the extrapolated volume of the crystal at $T_m^{'}$.

In order to be able to compare the results for the DSC crystallinity with the largest possible sample of independent studies, the value quoted by Blundell and Osborn was chosen. Use of any of the other quoted values will reduce all the DSC crystallinity values determined in this study by a corresponding factor equal to the ratio of the currently used value of $\Delta H_m^0$ and the new one.

### *3.2.3b Crystallinity by Density*

Densities of the samples were measured at 25°C in a density gradient column prepared with NaBr/water solution. Calibration of the column was done with glass standard floats of density known within ±0.0001 g/cm$^3$. The resolution of the column was about 0.0001-0.0002 g/cm$^3$. Measurements were done on relatively large probes, selected and cut from visibly void free regions of the samples.

The two steps in determining the density crystallinity according to equation (2.3):

$$c_c^{Dens} = \frac{r_c}{r}\frac{r - r_a}{r_c - r_a} \qquad (2.3)$$

are the absolute determination of the bulk density of the sample and the proper choice or measurement of the constants $r_c$ and $r_a$.

Possible sources of error in determining the bulk density are air bubbles on the surface of the sample and voids within the sample. Therefore only probes with no air bubbles attached on the surface were used for calculating density. Whenever possible several probes from one sample were used. If there was a small scatter in their positions in the density column, the average of the densities of the different probes was used. If there was a significant difference in densities (some samples with much lower apparent density), that was assumed to be an indication of the presence of voids in the probes and only those with the highest density (lowest position in the column) were used.

Equation (2.3) suggests that there is one-to-one correspondence between the measured density and crystallinity within the concept of the two phase model of crystallinity. The parameters $r_c$ and $r_a$ are considered as constants, physical characteristics of the crystalline and amorphous phases, correspondingly. There is significant scatter in the values reported in the literature, especially for $r_c$.

The following different values of $r_a$ are reported in the literature: 1.258 g/cm$^3$, [18] 1.261 g/cm$^3$, [75] 1.262 g/cm$^3$, [116] 1.263 g/cm$^3$, [63, 65, 66] and 1.264 g/cm$^3$. [120] Some of the above values are for "as received" amorphous films. This could be the explanation for the scatter of the literature data. In most studies, where no determination of the amorphous density was

done, a value of 1.263 g/cm$^3$ was chosen. Direct measurements in our laboratory on amorphous samples quenched from the melt also gave a value of 1.263 g/cm$^3$. Consequently, this is the value we chose to use in equation (2.3).

The values of the crystal density, however, differ much more - they range from 1.378 g/cm$^3$ [120] to 1.425 g/cm$^3$. [123] Values of 1.394 g/cm$^3$, [121] 1.4005 g/cm$^3$, [63] 1.405 g/cm$^3$, [119] 1.370 - 1.412 g/cm$^3$, [122] 1.378 - 1.425 g/cm$^3$, [123] and 1.415 g/cm$^3$ [118] have been reported.

Wakelyn, [122] Hay et al., [123] and Zimmerman and Konnecke [198] have shown that the room temperature density of the unit cell of PEEK crystallized from the glass depends on the temperature of crystallization $T_c$. The magnitude of increase of the room temperature crystal density with increase in $T_c$ is quite significant and completely covers the "uncertainty range" of values of $r_c$ reported above. Similar effect has been reported by Chung et al. [124] for PPS. In addition to the effect of $T_c$, Chung et al. report also an effect of $t_c$ on $r_c$ - the density of the unit cell of PPS increases with increase in log($t_c$).

The values of $r_c$ derived by Hay et al., [123] Zimmermann and Konnecke, [198] and by Wakelyn [122] differ only slightly (see table 3.4), while the scatter in the data reported by the latter is much lower. Our own results, which will be reported in section 4.2.3b and used in section 4.2.3c, are closer to the results of Wakelyn.

A recent synchrotron WAXS study of cold-crystallized and annealed PEEK by Jonas et al. [68] suggests that the annealing time dependence of the unit cell density (seen in PPS [124]) is observed in cold-crystallized PEEK as well. In conclusion, in the case of the cold-crystallized samples at various crystallization temperatures and for different times at a given temperature, equation (2.3) must be applied in a corrected form:

$$c_c^{Dens}(T_c,t_c) = \frac{r_c(T_c,t_c)}{r(T_c,t_c)} \frac{r(T_c,t_c)-r_a}{r_c(T_c,t_c)-r_a} \qquad (2.3a)$$

The density crystallinity, calculated according to equation (2.3a), is referred to as *corrected* density crystallinity, whereas $c_c^{Dens}$, calculated according to equation (2.3) is referred to as *uncorrected* density crystallinity. The effect of the time dependence of $r_c$ on

**TABLE 3.4** - Dependence of the crystal unit cell density $r_c$ on crystallization temperature $T_c$ from WAXS data on cold-crystallized PEEK ($t_c$ = 60 min) after Wakelyn[122] and Hay et al.[123].

Wakelyn [122]

| $T_c$ [°C] | 189 | 216 | 241 | 264 | 282 | 306 | 323 |
|---|---|---|---|---|---|---|---|
| $r_c$ [g/cm$^3$] | 1.367 | 1.370 | 1.384 | 1.390 | 1.385 | 1.408 | 1.412 |

$r_c(T_c, t_c = 60\ \text{min}) = 1.3545_{\pm 0.0123} + 0.00034_{\pm 0.00005}*(T_c\text{-}160)$

$R^2 = 0.9115$

Hay et al. [123]

| $T_c$ [°C] | 184 | 217 | 248 | 250 | 303 | 323 |
|---|---|---|---|---|---|---|
| $r_c$ [g/cm$^3$] | 1.374 | 1.388 | 1.408 | 1.375 | 1.424 | 1.424 |

$r_c(T_c, t_c = 60\ \text{min}) = 1.3641_{\pm 0.0314} + 0.00037_{\pm 0.00012}*(T_c\text{-}160)$

$R^2 = 0.6949$

density crystallinity for PEEK will be presented in section 4.2.3c and analyzed in the discussion chapter - section 5.3.

The values of 1.263 g/cm$^3$ for the amorphous density [63, 65, 66] and 1.400 g/cm$^3$ for the crystalline density [63] are most often quoted and have been adopted by most investigators. These values are used to calculate the density crystallinities of the cold-crystallized series referred to as "uncorrected crystallinities". These values are supplied for a comparison with data from previous studies of the density crystallinity of PEEK.

### *3.2.3c Wide Angle X-Ray Scattering*

Wide angle X-ray diffraction studies were initially performed on a Nicolet diffractometer operating at 40 kV and 30 mA, with Nickel filtered $CuK_\alpha$ radiation ($\lambda$ = 1.542 Å), for the purpose of crystallinity determination by WAXS. Data was collected at 0.05° increments between $2q$ 10° and 35°. Analysis was carried out by the method of Hermans and Weidinger:

$$c_c^{WAXS} = \frac{I_c}{I_a + I_c} \qquad (3.9)$$

where $I_c$ is the integral scattering from selected crystalline peaks and $I_a$ is the amorphous scattering. [3] The data collection and analysis was done using the Siemens polycrystalline software package. It utilizes subtraction of background (Compton) scattering and resolving of the relatively sharp crystalline peaks from the broad amorphous halo.

Applying this method to the series of melt-crystallized samples revealed, that the estimated uncertainty and scatter of the method were larger than the absolute magnitude of the change in $c_c^{WAXS}$ expected to be seen in these samples. Furthermore, it was suggested, that Ruland's method for computation of crystallinities needs to be applied for a more accurate evaluation of $c_c^{WAXS}$. [125] Therefore the method of Hermans and Weidinger was not employed anymore and WAXS studies concentrated on crystal unit cell parameters determination for use in equation (2.3a).

Wide angle X-ray scattering studies for unit cell parameters determination were carried out using a Scintag XDS2000 diffractometer operated at 40 kV and 30 mA, using a copper $CuK_\alpha$ radiation ($\lambda$ = 1.542 Å) and a combination of slits: 5/3/0.5/0.3 mm. The radius of the focusing circle of the goniometer is $R$ = 290 mm.

Samples were scanned in reflection mode within the angular range of 10°-35°, where the strongest and best resolved reflections for PEEK, indexed as (110), (111), (200), and (211), are positioned. Intensities were recorded in step-mode every 0.01° for times ranging between 2 s and 8 s.

The peak positions were calibrated using silicon as an external standard. Care was exercised to mount the samples flat and reproducibly on the holder for a reliable use of the external standard. Correction for the shift of the peak positions due to the transparency of the samples was also applied. [126]

Peak positions were determined from the best fit of the peaks with a PEARSON type VII function [127]:

$$I(q) = \frac{I_{\max}}{\left[1+\frac{1}{m}\left(\frac{q-q_{\max}}{a}\right)^2\right]^m} \qquad (3.10)$$

where $q = \frac{2\sin(q)}{l}$, $I_{max}$ is the height of the peak, $a$ is related to the width of the peak, and $m$ is a positive number from 1 to infinity. From the positions of the peak maxima, the corresponding $d$-spacings are calculated according to Bragg's law:

$$l = 2d_{hkl}\sin(q^{hkl}_{\max}) \qquad (3.11)$$

PEEK has an orthorhombic crystal unit cell, which is determined by 3 parameters - $a$, $b$, and $c$. The equations for the $d$-spacings and the volume and density of the unit cell are:

$$\frac{1}{d^2_{hkl}} = \frac{h^2}{a^2}+\frac{k^2}{b^2}+\frac{l^2}{c^2} \qquad (3.12)$$

$$V = abc$$

$$r_c = \frac{M_{u.c.}}{V} = \frac{638.28}{V} \qquad (3.13)$$

where V is in Å$^3$ and $r_c$ - in g/cm$^3$.

Therefore at least three equations for the *d*-spacings are needed in order to determine the lattice parameters and correspondingly the crystal density $r_c$. In reality, an overdetermined system of equations is always used in lattice parameters determination. [128] The reason for this is, that the statistical nature of the process of emission, diffraction, and counting diffracted radiation leads to fluctuations in the values along the peak profiles. These fluctuations in intensity could lead to fluctuations of the fitted peak maxima and the resulting *d*-spacings. The statistical nature of the fluctuations should lead to a random error in the *d*-spacings and cell parameters and therefore should not be of highest concern. One should note, however, that the Lorenz polarization factor affects intensities registered with a diffractometer in such a way, that for polymers, for all practical purposes, the low angle peaks are subject to much less fluctuation, than the peaks at higher angle. The latter are reduced in intensity due to the Lorenz polarization factor. Therefore a bias is possible if one of the Miller indices appears infrequently in the low angle peaks.

The statistical fluctuations, together with the systematic error from instrumental conditions, lead to deviations of the peak positions from the ideal ones, described by Bragg's law - equation (3.11). Therefore, the unique solution of a well determined system of Bragg law equations will be different from the true one.

There are different types of systematic errors, caused by instrumental conditions. In the case of diffractometry, which is of interest for this study, the more important sources of systematic error are listed below and their effect on this study analyzed [126, 128]:

- Use of a flat specimen instead of one with the curvature of the focusing circle leads to negative shift of $2q_{max}$, which is inversely proportional to the square of the radius of the goniometer circle and proportional to the irradiated length of the sample. [126] The latter was minimized by optimizing the need for larger intensity and the need for reducing the horizontal divergence, using an appropriate choice of slits.

- Axial divergence of the beam leads also to negative shift, which is minimized by the use of soller slits. [126]

- The error due to displacement of the sample from the axis of rotation of the goniometer is positive when the sample lies inside the focusing circle and negative when it is outside [126, 128]:

$$d(2q_{\max})[rad] = \frac{2S\cos(q)}{R} \qquad (3.14)$$

where $S$ is the displacement measured in the same units as the goniometer radius $R$. This error is subject to the most unpredictable variation from sample to sample. For this reason, samples were always mounted with extreme care to ensure that they were as close as possible to the focusing plane as defined by the sample holder.

- The most significant error in samples of low absorption, such as polymers, is the transparency error. It is due to the small extinction of the incident beam and exponentially decreasing contributions to the reflection from layers, which are below the surface and, therefore, displaced from the goniometer axis (outside the focusing circle). Its functional dependence differs from the displacement error in equation (3.14) by $S$ becoming a function of the sample thickness $t$, the linear absorption coefficient $m$, and the diffraction angle [126]:

$$d(2q_{\max})[rad] = -\frac{2t\cos(q)}{R}\left\{\frac{\sin(q)}{2mt} - \frac{1}{\exp\left[\frac{2mt}{\sin(q)}\right]-1}\right\} \qquad (3.15)$$

In highly crystalline materials this error is usually minimized by the choice of very thin samples. In polymers this would lead to significant decrease of the absolute intensities and is not an option. Therefore, for precise determinations of crystallinity the systematic error described by equation (3.15) needs to be accounted for.

The linear absorption coefficient of the PEEK samples was determined from their measured density $r$ and the mass absorption coefficient $\left(\frac{m}{r}\right)_{PEEK}$. The latter was determined

from listed mass absorption coefficients of the elements present in the repeat unit of PEEK [128]:

$$\left(\frac{m}{r}\right)_{PEEK} = w_H\left(\frac{m}{r}\right)_H + w_C\left(\frac{m}{r}\right)_C + w_O\left(\frac{m}{r}\right)_O = 5.19 \text{ cm}^2/\text{g}.$$

With the density values measured in this study - $r$ = 1.278 - 1.308 g/cm$^3$, the linear absorption coefficient is about $m$ = 6.6 - 6.8 cm$^{-1}$. Typical transparency corrections are on the order of $d(2q_{\max})_{transp}$ [deg] = 0.04 - 0.06°.

The only other correction applied was the external Si-standard correction. Samples were mounted carefully, as close as possible to the way the Si-standard was mounted on the sample holder. It was assumed, that this would justify the use of the displacement correction for the Si-standard, extrapolated to the PEEK angular range.

In light of this, and the fact that care has been taken to correct for the other main source of systematic error - the sample's transparency, an approach somewhat different from the standard calculation procedures [128] has been taken. In essence the calculation method outlined by Wakelyn [122] was applied. The method consists in the following steps:

- The positions of the peak maxima were determined from a PEARSON VII fit of the Bragg peaks after local baseline subtraction. The calculations were performed with the Scintag DMS2000 diffraction management system software, which is used with the Scintag XDS2000 diffractometer for operation and data analysis.

- The peak maxima were corrected with the extrapolated shifts, derived from a Si-standard diffractogram.

- Transparency correction shift - the negative of the result from equation (3.15), was applied.

- The *d*-spacings were calculated using the $CuK_\alpha$ wavelength $\lambda(CuK_\alpha)$ = 1.5418 Å.

- From the three *d*-spacings $d_{110}$, $d_{111}$, $d_{211}$ and equation (3.12) the lattice parameters were determined: $a_1$, $b$, $c$.

- Using $d_{200}$, a second value for the $a$ is determined - $a_2 = 2*d_{200}$.

- The final value $a_{av}$ is computed as weighted average of the previous two using 1 to 3 weighing ratio. [122]

- The crystal density is determined from equation (3.13).

### *3.2.4 Small Strain Creep*

Tests were done in a bending mode in a DuPont Instruments DMA model 983. The bending mode is a mixed mode of deformation, approximately 90 % shear and 10 % tensile.

The creep studies were performed using a methodology well described in the literature. [86, 87, 90] The samples (described in section 3.1.2) were heated from room temperature to the aging/annealing temperature. The creep compliance of a sample is measured during a part of a cycle of successive isothermal aging-load-recovery-aging steps.

After the initial aging time $t_{a1}$, a small constant stress is applied and from the resulting strain the bending creep compliance $J(t)$ is recorded during the creep time $t_{creep}$. The applied stress is small in order to ensure linear viscoelastic response during the creep test. The ratio of the creep time $t_{creep}$, during which the creep compliance is measured, and the preceding aging time $t_a$ was always kept 1:10. Thus effective aging during the measurement period is negligible and the creep compliance is a momentary creep compliance with respect to the aging process, representative of the state of the sample as a result of the elapsed aging time $t_a$.

The load is then released and a recovery time follows, during which the strain relaxes exponentially and the sample continues to age isothermally. The recovery time is approximately 15 times the creep time, allowing for complete recovery of the strain, and approximately 1.5 - 1.8 times the previous aging time. After the prescribed recovery time has elapsed, at a time during the experiment at which $t = 3*t_{a1} = t_{a2}$ the load is applied again and the cycle is repeated. With the increase in aging time, the creep times increase from cycle to cycle allowing larger parts of the retardation spectrum to be probed. Figure 3.8 illustrates the temperature, stress and strain profiles during the time of the experiment.

The samples were tested at the following temperatures, from below $T_g$ to about 100 K above $T_g$: 120°C, 140°C, 160°C, 180°C, 200°C, 220°C, 240°C, and 260°C. The aging times

employed in the experiment are 0.23 hr, 0.67 hr, 2 hrs, 6 hrs, and 18 hrs (plus 54 hrs for the sample tested at 200°C). The analysis of the momentary creep compliance curves and their aging time dependence follows the approach of Struik [88] and has been reviewed in section 2.5.2.

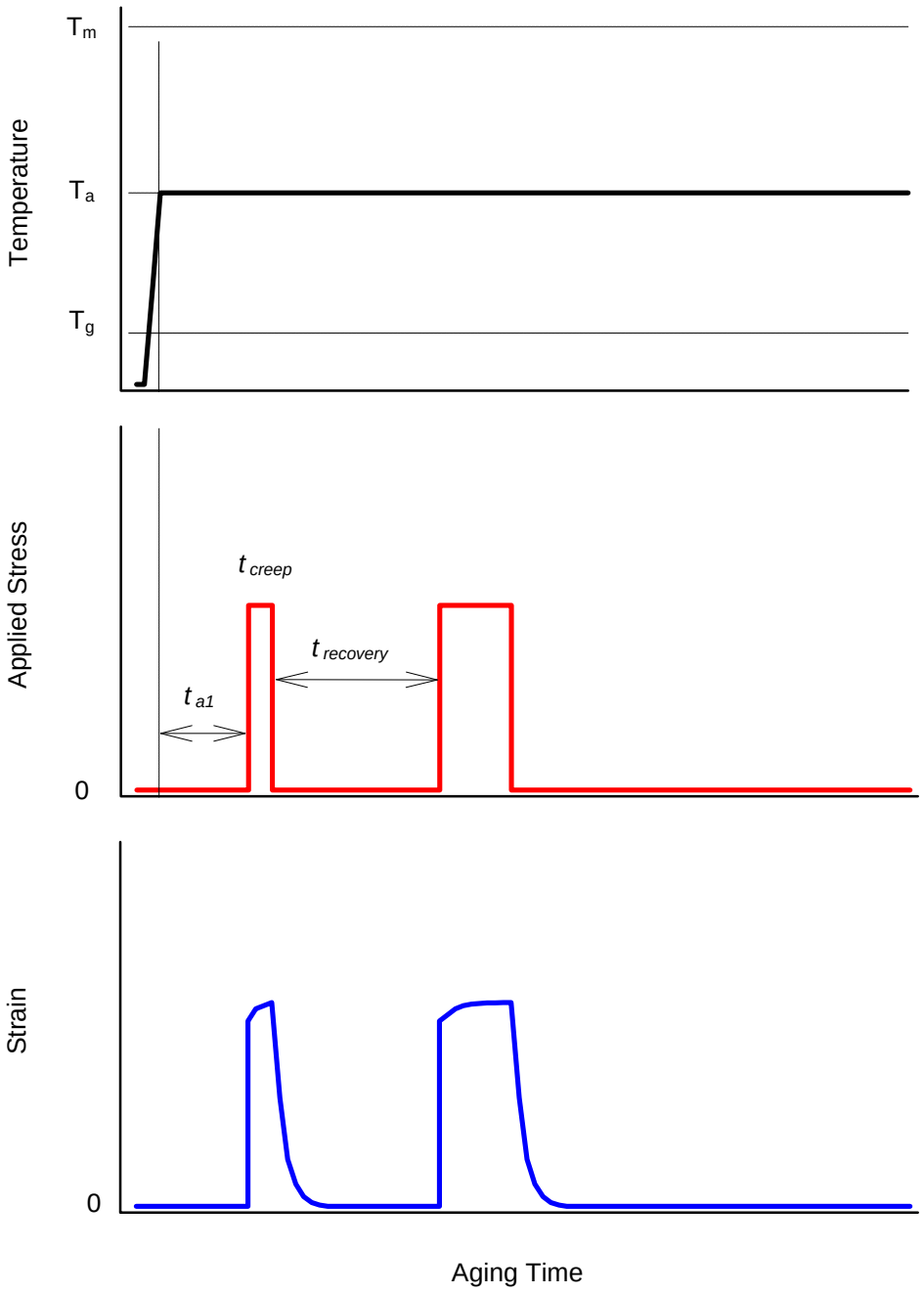


$T_a$ = 120°C, 140°C, 160°C, 180°C, 200°C, 220°C, 240°C, 260°C

$t_a$ = 0.23 hrs, 0.67 hrs, 2 hrs, 6 hrs, 18 hrs, 54 hrs.

**Figure 3.8** Temperature, applied stress, and resulting strain profiles during the creep experiments.

# CHAPTER 4

# RESULTS

## 4.1 Thermal Characterization of Commercial PEEK and PEEK Fractions

Samples from the fractions were melted in the DSC and quenched into the amorphous glassy state below $T_g$. Heating scans from below $T_g$ to the end of melting were recorded at 10 K/min. The results from these scans are reported in table 4.1 together with results from the heating scan of commercial PEEK. Increasing the molecular weight from 6,300 to 43,300 g/mol results in an increase of the glass transition temperature from 124°C to 147°C. Figure 4.1 compares the results from this study with the data on identically obtained PEEK fractions by Day et al. [130] From the extrapolation of the $T_g$ vs. $1/M_n$ plot, according to the Fox-Flory equation:

$$T_g = T_g^{\infty} - \frac{K}{M_n} \qquad (4.1)$$

the intercept with the vertical axis on the figure gives the value of $T_g^{\infty}$ - the apparent glass transition temperature of infinite molecular weight PEEK $T_g^{\infty}$ (10 K/min) = 149°C. The results of this study are slightly lower than those from reference 130 and the value of $T_g^{\infty}$ is subject to a larger uncertainty, due to a smaller number of fractions analyzed.

The lowering of $T_g$ with MW results in lowering of the low temperature limit of the crystallization window. The temperatures at the onset and maximum rate of the cold crystallization process - $T_{c,\,onset}$ and $T_{c,\,max}$, are also lowered with decreasing the MW.

The enthalpy of the cold crystallization exotherm - $\Delta H_c$, decreases with increasing MW. As in the case of commercial PEEK, its value is lower than the enthalpy of the melting endotherm at the end of the heating scan. This indicates additional crystallization or reorganization above the cold-crystallization exotherm during the heating scan. The final crystallinity of the samples just before the beginning of melting, as measured by the value of the melting enthalpy $\Delta H_m$ increases with decrease in MW. DSC crystallinities, calculated

**TABLE 4.1** Thermal characterization of PEEK fractions and commercial grade PEEK 450G from heating scans of amorphous samples at 10 K/min.

| $M_w$ [ g/mol ] | **3 200** | **6 300** | **18 200** | **43 300** | 38 300* |
|---|---|---|---|---|---|
| $T_g$ [ °C ] | **124** | **132** | **141** | **147** | 145 |
| $T_{c,\,onset}$ [ °C ] | **145** | **150** | **168** | **175** | 170 |
| $T_{c,\,max}$ [ °C ] | **157** | **162** | **173** | **188** | 175 |
| $\Delta H_c$ [ cal/g ] | **8.0** | **8.0** | **9.0** | **6.9** | 6.0 |
| $T_m^{'}$ [ °C ] | **328** | **346** | **349** | **333** | 339 |
| $\Delta H_m$ [ cal/g ] | **15.0** | **15.4** | **13.2** | **9.9** | 9.9 |
| $c_c^{DSC}$ | **0.48** | **0.50** | **0.43** | **0.32** | 0.32 |
| $c_{c,in}^{DSC}$ ** | **0.52** | **0.49** | **0.47** | **0.37** | - |

* commercial grade PEEK 450G, $M_w/M_n \sim 2.0$

** initial DSC crystallinity of the hydrolyzed material

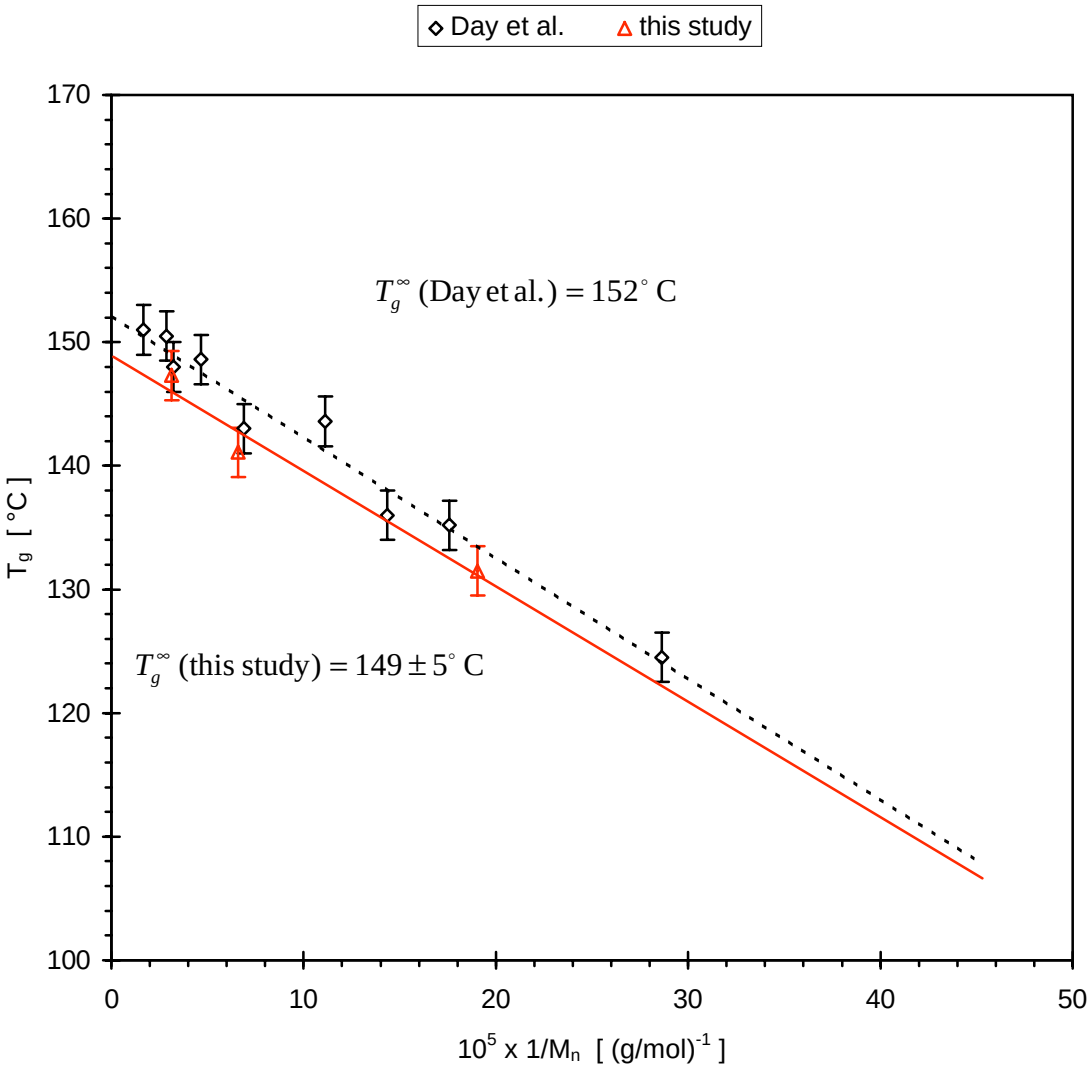


**Figure 4.1** MW dependence of the glass transition of PEEK fractions (from DSC at heating rate 10 K/min). Comparison with data by Day et al. [130].

according to equation (2.4), change from about 0.32 for $M_w$ = 43,300 g/mol to 0.50 for $M_w$ = 6,300 g/mol. The difference between the melting enthalpy and the crystallization enthalpy is 3 cal/g for the high MW sample and 7-7.5 cal/g for the low MW samples. This indicates, that reorganization or additional crystallization during the heating scan is much more pronounced in the low MW fraction. The melting peak changes in magnitude and width with decreasing MW, becoming narrower and steeper at the end of the melting trace.

The temperature of the maximum of the melting peak $T_m^{'}$ shows a more complex behavior with variation in MW. Its characterization for isothermal crystallization from the melt state is the subject of the next section.

### *4.1.1 Hoffman-Weeks Plots and the Equilibrium Melting Temperature*

The Hoffman-Weeks analysis has been widely used to evaluate the apparent equilibrium melting point of a polymer of finite molecular weight from the dependence of the melting temperature of isothermally formed thin lamellae on the temperature of crystallization. [4] It is based on the prediction of the Hoffman-Lauritzen kinetic theory of crystallization, that at relatively small undercooling a linear relationship exists between the observed melting temperature of the crystalline lamellae - $T_m^{'}$, and $T_x$:

$$T_m^{'} = T_m\left(1-\frac{1}{g}\right) + \frac{1}{g}T_x \qquad (4.2)$$

where $T_m$ is the equilibrium melting temperature and *g* is the coefficient of thickening of the lamellae. The equilibrium melting temperature is determined in a $T_m^{'}$ vs. $T_x$ plot from the intercept of the extrapolated linear relationship between $T_m^{'}$ and $T_x$ with the line $T_m^{'} = T_x$.

Several studies have examined the equilibrium melting temperature of commercial PEEK through a Hoffman-Weeks analysis. A study by Lee and Porter [66] determined a value $T_m$ = 389°C, and a later study by Chen and Porter arrived at a value of 384°C. [129] Hsiao and Sauer [132] derived a $T_m$ value of 382°C. The extrapolation of the $T_m^{'}$ = *f*($T_x$) line to about 50 K above the highest $T_x$ at which crystallization occurs within reasonable time is expected to

lead to a relatively large uncertainty. The values quoted above are well within the limits of this uncertainty.

Figure 4.2 shows the Hoffman-Weeks plot of the commercial PEEK polymer. The dependence of $T_m'$ on $T_x$ is characterized by a linear part between about 315°C and 330°C. Linear extrapolation over this part of the plot leads to $T_m$ = 384±5°C - within the range of the other reported values.

Isothermal crystallization from the melt above 330°C takes more than 12 hours to complete and was not attempted. Crystallization below 310-315°C leads to a deviation of the $T_m' = f(T_x)$ dependence from a straight line. This has been also observed by other investigators [16, 65, 129, 132] and explained with reorganization or melting, followed by recrystallization, of the original lamellae, formed at these lower $T_x$. [129] The lamellae, which are formed at high undercooling, become unstable as the temperature is raised upon heating. This could lead to nonisothermal thickening upon heating, which would cause an increase of the thickening coefficient *g* and make the latter dependent on $T_x$. [129] As a result, the inverse of *g* - the slope of the $T_m'$ vs. $T_x$ dependence, decreases with decrease of $T_x$. Another possible scenario is that after the melting of the fraction of the primary lamellae, corresponding to the lower temperature end of the broad melting endotherm of PEEK, these lamellae have enough time to recrystallize into thicker and more stable lamellae. The latter melt at higher temperature, and thus raise the apparent melting temperature corresponding to this low $T_x$.

Chen and Porter [129] reported, that the deviation from straight line in the Hoffman-Weeks plot occurs for $T_x$ < 303°C. In this study the deviation occurs at higher crystallization temperatures. This is possibly due to the fact, that the results of Chen and Porter are from DSC melting scans at a heating rate of 20 K/min, whereas the results from figure 4.2 were obtained at a heating rate of 10 K/min. When the heating rate is increased, the lamellae have less time to reorganize or recrystallize after melting during the heating scan and the observed $T_m'$ for lower crystallization temperatures will be closer to the true $T_m'$ of the isothermally formed lamellae.

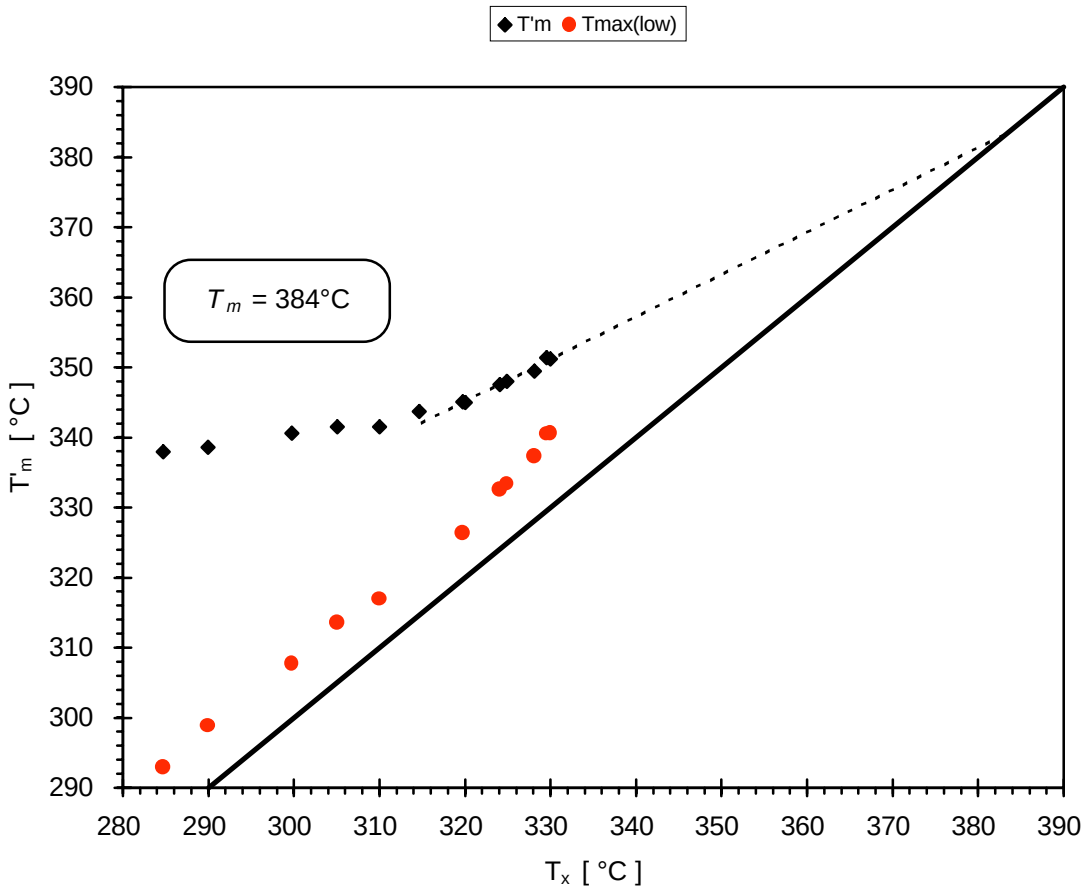


**Figure 4.2** Hoffman-Weeks plot for commercial PEEK 450G. Extrapolation based on the upper, linear part of the $T'_m$ vs. $T_x$ relationship.

This problem is directly related to the controversy about the heating rate dependence of the high temperature melting endotherm, which in turn, has been a central point in the debate about the plausibility of the melting-recrystallization model for the dual melting behavior of PEEK, [63, 65, 66] reviewed in section 2.4.2. This issue will be analyzed in greater detail in section 5.6.1. At this point it suffices to say that Lee and Porter [65] claimed that the $T_m^{'}$ of PEEK, cold-annealed at 220°C (which appears to be independent from $T_x$ as shown in references 16 and 65), is decreasing with increasing heating rate, while $T_m^{'}$ of PEEK, melt-crystallized at 318°C and 323°C is independent of heating rate. However Bassett et al. [70] have shown, that $T_m^{'}$ of PEEK, melt-crystallized at 310°C for 1 hour, decreases with increasing heating rate in the DSC.

Therefore, it seems logical that a proper determination of the equilibrium melting temperature, $T_m$, should involve extrapolation of $T_m^{'}$ data from several heating rates to infinite heating rate, calibration of the thermal lag correction with the heating rate dependence of the melting of a standard, and then application of the Hoffman-Weeks extrapolation.

With this in mind, the reported literature values for $T_m$ of PEEK from Hoffman-Weeks plots must be considered as "*heating rate specific*". Ignoring the heating rate dependence may introduce a significant uncertainty in the value for the equilibrium melting temperature.

Figures 4.3 and 4.4 show the Hoffman-Weeks plots for the PEEK fractions. Due to the limited amount of material available for this study, the melting of the samples was recorded only at heating rate of 10 K/min. Only the points from the linear part of the $T_m^{'} = f(T_x)$ dependence are shown. Extrapolation to the point of intercept with the $T_m^{'} = T_x$ curve, shown as a thick bold line, leads to the values of the apparent equilibrium melting temperature, $T_m$, of the fractions reported in table 4.2. The dependence of $T_m$ on molecular weight is plotted on figure 4.5b.

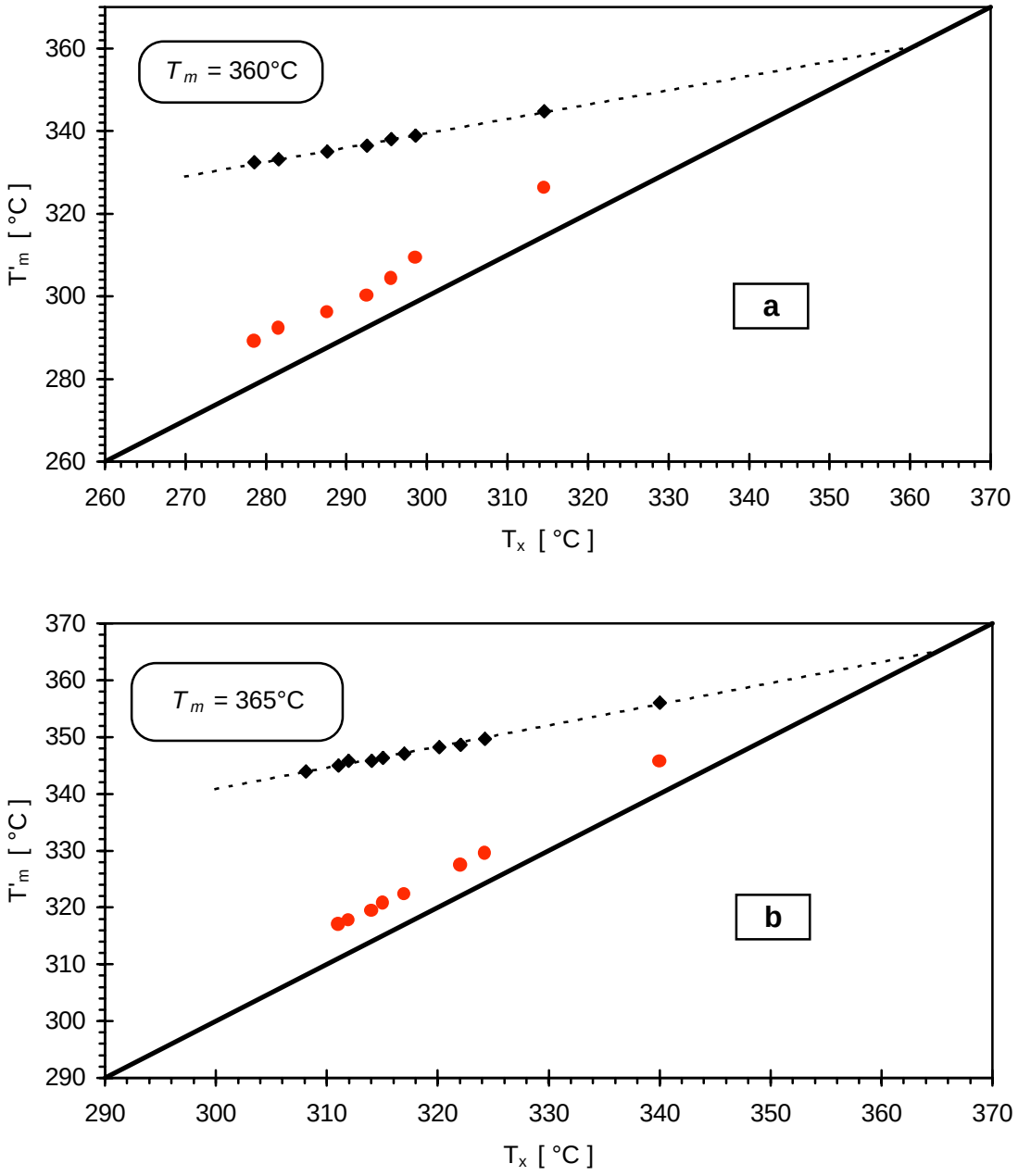


**Figure 4.3** Hoffman-Weeks plots for fractions: a) PEEK4-2 (43.3 K), b) PEEK4-5 (18.2 K).

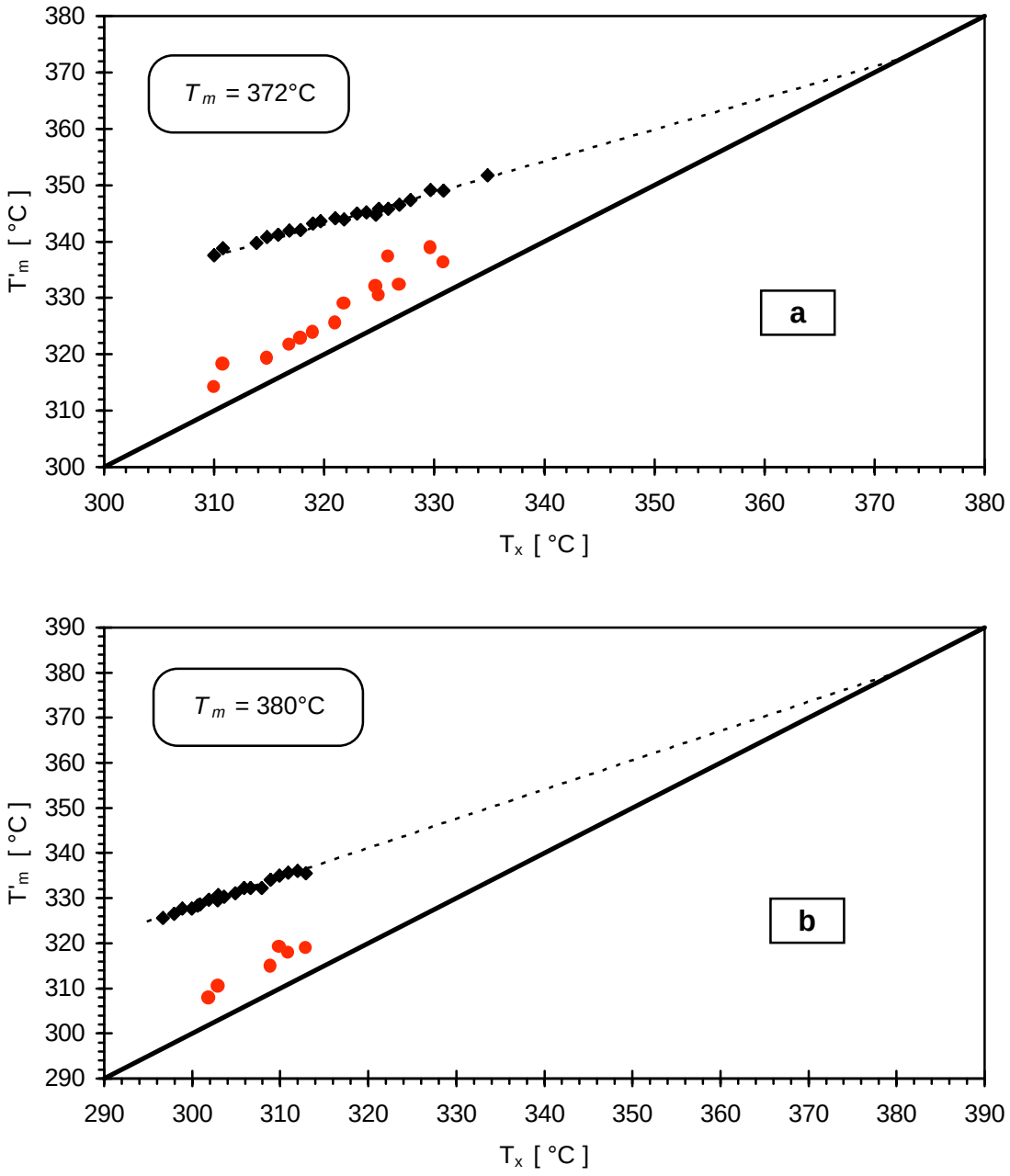


**Figure 4.4** Hoffman-Weeks plots for fractions: a) PEEK4-8 (6.3 K), b) PEEK4-9 (3.2 K).

**TABLE 4.2** Results from Hoffman-Weeks analysis of the melting temperatures of isothermally crystallized PEEK fractions and commercial grade PEEK 450G.

| $M_w$ [ g/mol ] | **43 300** | **18 200** | **6 300** | **3 200** | 450G [a] |
|---|---|---|---|---|---|
| $M_n$ [ g/mol ] | **32 100** | **15 200** | **5 300** | **2 200** | |
| $\frac{1}{g}$ [b] | **0.35** | **0.37** | **0.56** | **0.65** | 0.606 |
| $g$ [c] | **2.9** | **2.7** | **1.8** | **1.5** | 1.7 |
| $T_m$ [d] [ °C ] | **360** | **365** | **372** | **380** | 384 |

[a] commercial grade PEEK 450G, $M_w$ = 38 300 g/mol, $M_w/M_n$ ~ 2.0

[b] slope of the linear part of the Hoffman-Weeks plot

[c] thickening coefficient

[d] apparent equilibrium melting temperature (derived from melting scans at 10 K/min)

The results are quite unexpected from the established views and literature data on the MW dependence of $T_m$. [42] The apparent equilibrium melting temperature increases with decrease in MW: from 384°C for the fraction with $M_n$ = 2,200 g/mol to 360°C for the fraction with $M_n$ = 32,000 g/mol. The opposite behavior is usually expected for the MW dependence of $T_m$. For example, in the analysis of the growth rate studies of similarly obtained PEEK fractions, Day et al. [130] and Deslandes et al. [131] have used values of $T_m$, loosely based on the observed coefficient of dependence of $T_m$ on $1/M_n$ for unfractionated PPS with different MW, from data by Lopez and Wilkes. [133] From the Hoffman-Weeks result for $T_m$ of commercial PEEK with $M_n$ = 15,000 g/mol and the above mentioned coefficient for PPS, they calculated, that $T_m$ would increase from 382°C for a fraction with $M_n$ = 7,000 g/mol to 404°C for a fraction with $M_n$ = 60,200 g/mol.

The observations of this study are consistent with another result by Day et al. [130] and Deslandes et al. [131] At all crystallization temperatures the crystallization rates of the low MW PEEK fractions are higher than those for the high MW fractions. This would be an indication, that secondary nucleation effects do not dominate the crystallization mechanism even at low undercooling, but an explanation as to why this occurs has not been given. Furthermore, their result concerns only the crystallization process, but not the thermal stability of the crystalline lamellae.

The unexpected MW dependence of $T_m$ becomes somewhat more comprehensible if we abstract ourselves for a moment from the Hoffman-Weeks analysis and consider the actual values of $T_m'$ observed in figures 4.3 and 4.4 and their corresponding crystallization temperatures. In order to visually illustrate and ease the comparison, the data are plotted on a single plot - figure 4.5a. The lines in the figure represent the fit over the linear part of the $T_m'$ vs. $T_x$ dependence for $T_x$ ranges of values, where isothermal crystallization is attainable. Two observations immediately become clear when the fractions with MW from 3.2K to 18.2 K are compared:

1) with increase in MW the upper limit of the crystallization window increases.

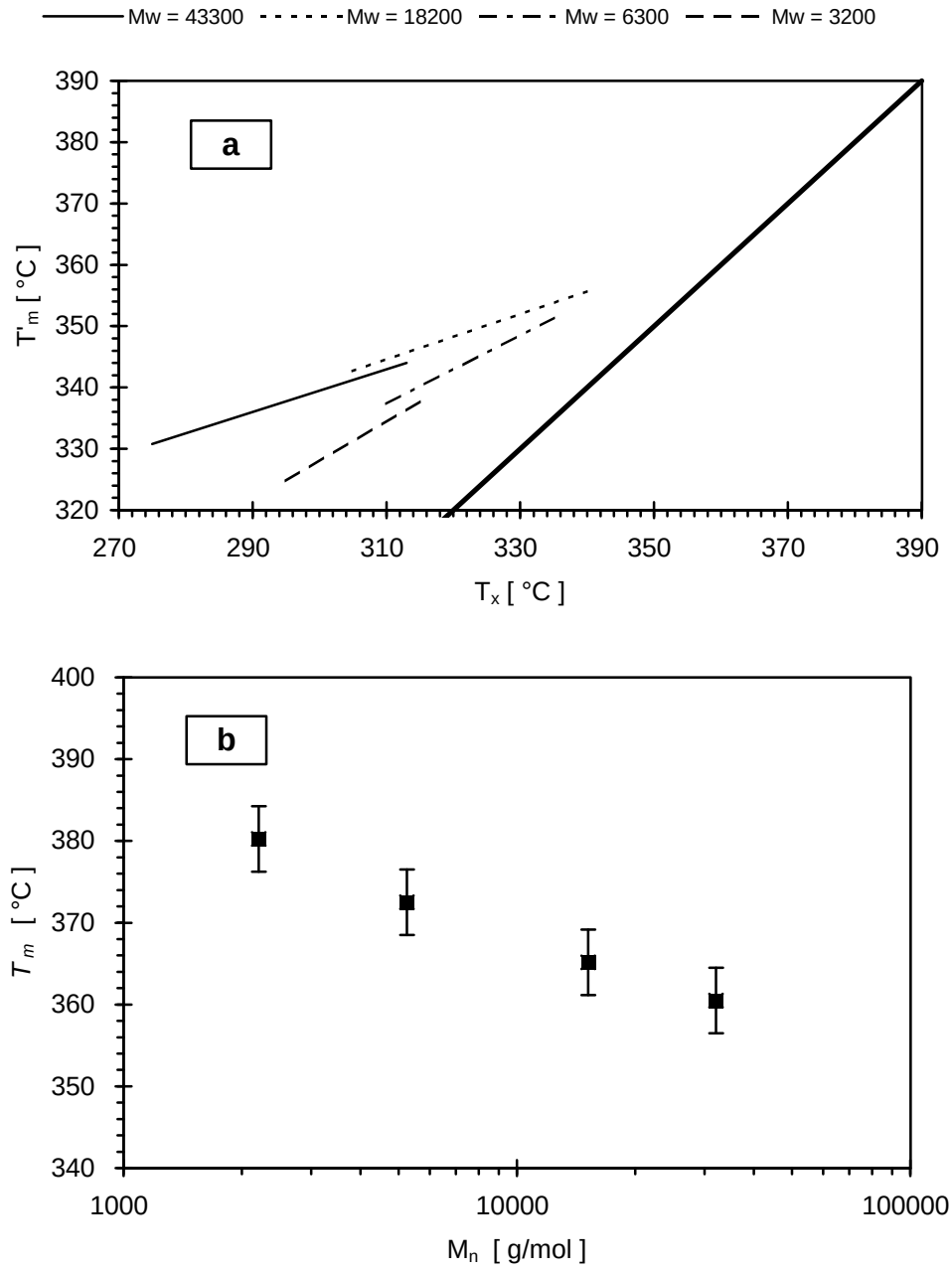


**Figure 4.5** Results from Hoffman-Weeks analysis of the PEEK fractions: a) limits of isothermal crystallization from the melt and melting; b) dependence of the apparent equilibrium melting temperature $T_m$ on MW.

2) for every crystallization temperature, the *actual* melting temperature of the fractions increases with increase in MW. In the narrow range around $T_x$ = 310°C, where all fractions are able to crystallize isothermally (at different rates), the values of $T_m^{'}$ for the 43.3 K fraction are also higher than $T_m^{'}$ for the 3.2 K and 6.3 K fractions, although slightly lower than the values for the 18.2 K fraction.

These two results are in perfect agreement with the expectations for the variation of melting temperatures and crystallization conditions (undercooling) with MW - the lower the MW, the lower the melting temperature and the higher the undercooling needed for inducement of crystallization. Thus the nearest to $T_m$ observable crystallization and melting temperatures appear to be thermodynamically controlled and in line with the expectations.

The situation is reversed only when the assumptions of the Hoffman-Weeks analysis are applied and *extrapolation* is made to crystallization temperatures $T_x$, which for increasing MW are progressively higher. Only then (that is only for the *expected*, but unattainable crystallization temperatures) is the *extrapolated* melting temperature trend with MW reversed. The geometrical explanation of the effect is that the increasingly higher slopes of the $T_m^{'} = f(T_x)$ lines for fractions with lower MW cause the reversal of the extrapolated melting behavior from the observed one. The formal interpretation of the higher slope effect in terms of the Hoffman-Weeks analysis is a lower thickening coefficient *g* for the lower MW fractions.

It is quite possible, however, that the Hoffman-Weeks analysis is not applicable for the low MW fractions. One of the assumptions of the Hoffman-Weeks analysis is low undercoolings. If the $T_m$ of the commercial PEEK is taken as a reference, then the undercoolings involved in the analysis of the fractions are about 40 K to 70 K at best. These values are certainly not small, but are similar in magnitude to the undercoolings employed in the analysis of other polymers. The other assumption is a constant, independent from $T_x$, value of the thickening coefficient *g*. This approximation could be expected to fail with decrease in MW as the deviation from the macromolecular character of the chains increases. The number average molecular weights of the low MW fractions (see table 4.2) correspond to

number average chain lengths of 8 and 18 repeat units and 120 Å and 270 Å respectively. The observed melting temperatures of the lowest MW fraction (3.2 K) are indeed very close to the melting temperature of a highly crystalline ( $\Delta H_m = 29.75\,\text{cal/ g}$ ) PEEK oligomer with $M_n$ = 1,500 g/mol - 320°C. Under such conditions the Hoffman-Weeks analysis, which applies to the chain-folding of long macromolecules, might not be applicable.

These arguments can not explain the low values of $T_m$ and the apparent reversal of the expected MW trend for the two fractions with higher molecular weight. One alternative is to test the Hoffman-Weeks values of $T_m$ by examining the dependence of the observed melting temperature on lamellar thickness $l_c$ (derived from SAXS) and extrapolate this dependence to infinite thickness. The basis of this analysis is the Gibbs-Thomson-Tamman equation [42] which describes the melting point depression due to small crystal size. Such an investigation is quite demanding in terms of amount of material for the SAXS experiment and was not attempted due to the limited amount of material available in this study.

### *4.1.2 Effect of Molecular Weight on Crystallinity - Kinetics of Secondary Crystallization and Morphology*

The effect of MW on crystallinity and crystallinity dependent mechanical properties of PEEK has been examined in the literature in the case of several unfractionated PEEK samples with different MW between 15,000 and 50,000 g/mol. It was found, that crystallinity decreases with increase in MW and so does the mechanical strength (tensile modulus and yield strength for example). [134]

The small amounts of fractionated PEEK available does not allow an extensive evaluation of the dependence of crystallinity and material properties on MW for PEEK fractions. In the following two sections a qualitative description of the effect of MW on the melting behavior by DSC and morphology by polarized optical microscopy (POM) will be provided.

### *4.1.2a Development of "Double Melting" in PEEK Fractions*

The effect of molecular weight on the ability of the PEEK fractions to isothermally crystallize from the melt was shown already on figures 4.3, 4.4 and 4.5a in the preceding section. Qualitatively the effect of MW on DSC crystallinity was reflected in the values quoted in table 4.1 (derived for samples dynamically crystallized from the glass). In agreement with the results from other studies, [130, 131, 134] it was found that an increase in MW has a restrictive effect on both the crystallinity attained (table 4.1) and the rates at which the material crystallizes. With decreasing MW, the width of the isothermal melt-crystallization windows decreases (see figure 4.5a). The latter illustrates the fact that, as the crystallization temperature drops, the crystallization rates increase faster for the low MW fractions.

One particular aspect of the isothermal crystallization behavior of PEEK fractions, which the above mentioned studies [130, 131, 134] have not investigated, is the "double melting" behavior, which results from isothermal crystallization conditions.

All of the fractions investigated in this study showed the "double melting" DSC trace, characteristic of isothermally crystallized PEEK (see the review in section 2.4.2). On their Hoffman-Weeks plots (figures 4.3 and 4.4), in addition to the melting temperatures $T_m^{'}(T_x)$, the positions of the peak maximum of the low temperature endotherm - $T_{max}(T_x)$ is shown. As in the case of the commercial polymer [16, 65, 129, 132] (see also figure 4.2 above), the general trend of the dependence of $T_{max}$(low) on $T_x$ is a line almost parallel to the $T_m^{'} = T_x$ line. The scatter in the case of the low MW fractions (figure 4.4) is due to variations in the crystallization times employed.

Figures 4.6 and 4.7 show the effect of isothermal crystallization temperature on the low temperature endotherm in the melting scans of the fractions. The low temperature peak increases in magnitude and shifts in position with crystallization time. [1, 66, 70, 72, 76] Thus, in order to produce well resolved low temperature endothermic peaks, all the melting traces shown on figures 4.6 and 4.7 are the result of long isothermal crystallization. The temperatures were chosen in such a way as to represent the upper section, the lower section, and the middle of the isothermal melt-crystallization window, shown on figure 4.5a.

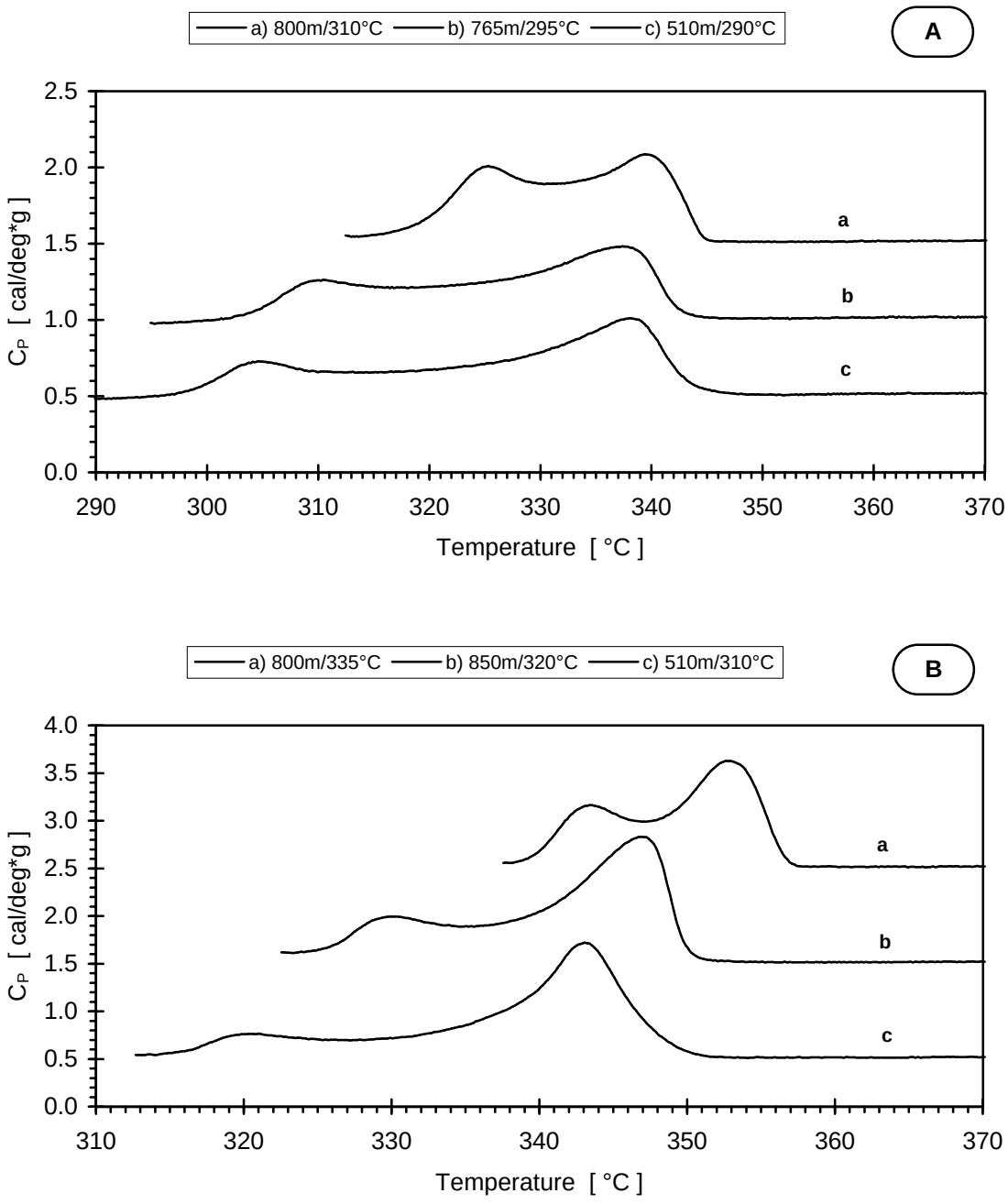


**Figure 4.6** DSC melting scans after long time crystallization from the melt: A) fraction PEEK4-2 (43.3 K), B) fraction PEEK4-5 (18.2 K).

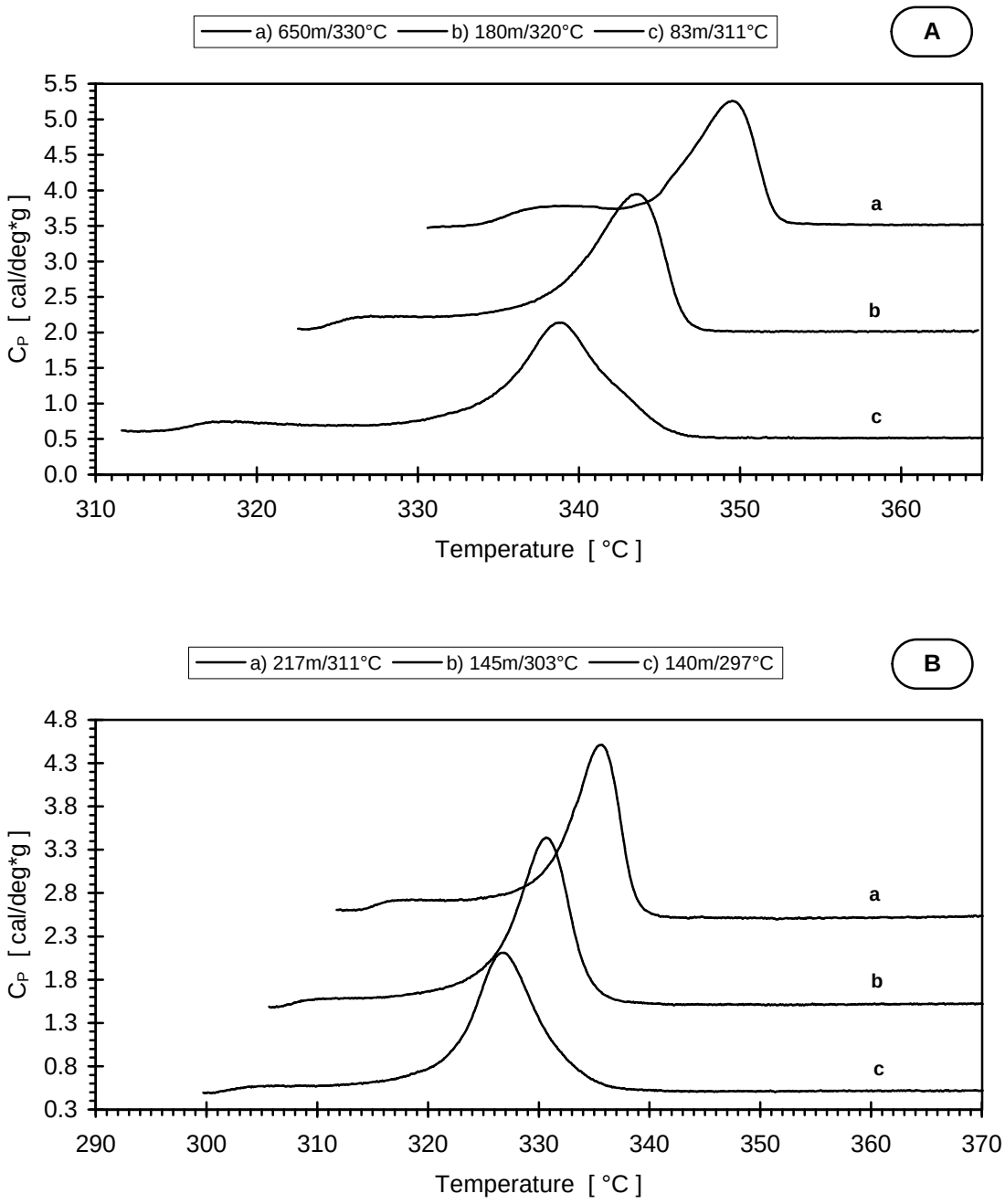


**Figure 4.7** DSC melting scans after long time crystallization from the melt: A) fraction PEEK4-8 (6.3 K), B) fraction PEEK4-9 (3.2 K).

Figure 4.6a shows the typical double peak shape of the melting scans of fraction PEEK4-2 (43.3 K) after long crystallization at $T_x$ = 290°C, 295°C, and 310°C; figure 4.6b - fraction PEEK4-5 (18.2 K) at $T_x$ = 310°C, 320°C, and 335°C; figure 4.7a - fraction PEEK4-8 (6.3 K) at $T_x$ = 311°C, 320°C, and 330°C; and figure 4.7b - fraction PEEK4-9 (3.2 K) at $T_x$ = 297°C, 303°C, and 311°C.

With a decrease in the molecular weight, the high temperature melting peak becomes narrower, but increases in magnitude. The former reflects the fact that, with decreasing MW, the distribution of sizes or degree of perfection of the crystalline lamella population becomes more narrow and uniform. The high temperature melting peak of the low MW fractions (figure 4.7) is almost symmetrical. The latter is an indication of the increase of the DSC crystallinity with decrease in MW. Crystallinity increases from 0.22 for fraction PEEK4-2 (43.3 K), crystallized at 300°C for 345 min, to 0.48 for fraction PEEK4-9 (3.2 K), crystallized at 313°C for 140 min.

The effect on the low temperature peak is opposite. With decreasing MW the peak becomes less and less pronounced till for the fraction with the lowest MW it appears as a very small "irregularity" in the DSC trace. In a single run experiment for this fraction one would hardly characterize it as a "peak", but rather describe it as a "step", "$C_P$ change" etc. Such characterization of the low temperature endothermic peak resulting from isothermal conditions above $T_g$ has indeed been done in the case of high crystallinity polymers - for example i-PP, where a change in the DSC trace with similar appearance has been labeled "dual glass transition". [13] An investigation under various thermal conditions and the observation of the trend of change of the low temperature peak with MW undoubtedly show, that the small endothermic shift in the heat flow is a manifestation of a very weak "double melting" in the case of the lowest MW fraction. Indeed, this shift appears just above the crystallization temperature as does the low temperature endothermic peak for the other fractions and commercial PEEK.

Figures 4.8 and 4.9 show the effect of crystallization time on the melting scans of the PEEK fractions. Melting scans recorded after three different crystallization times are shown for each fraction at a given crystallization temperature (denoted in the figure captions).

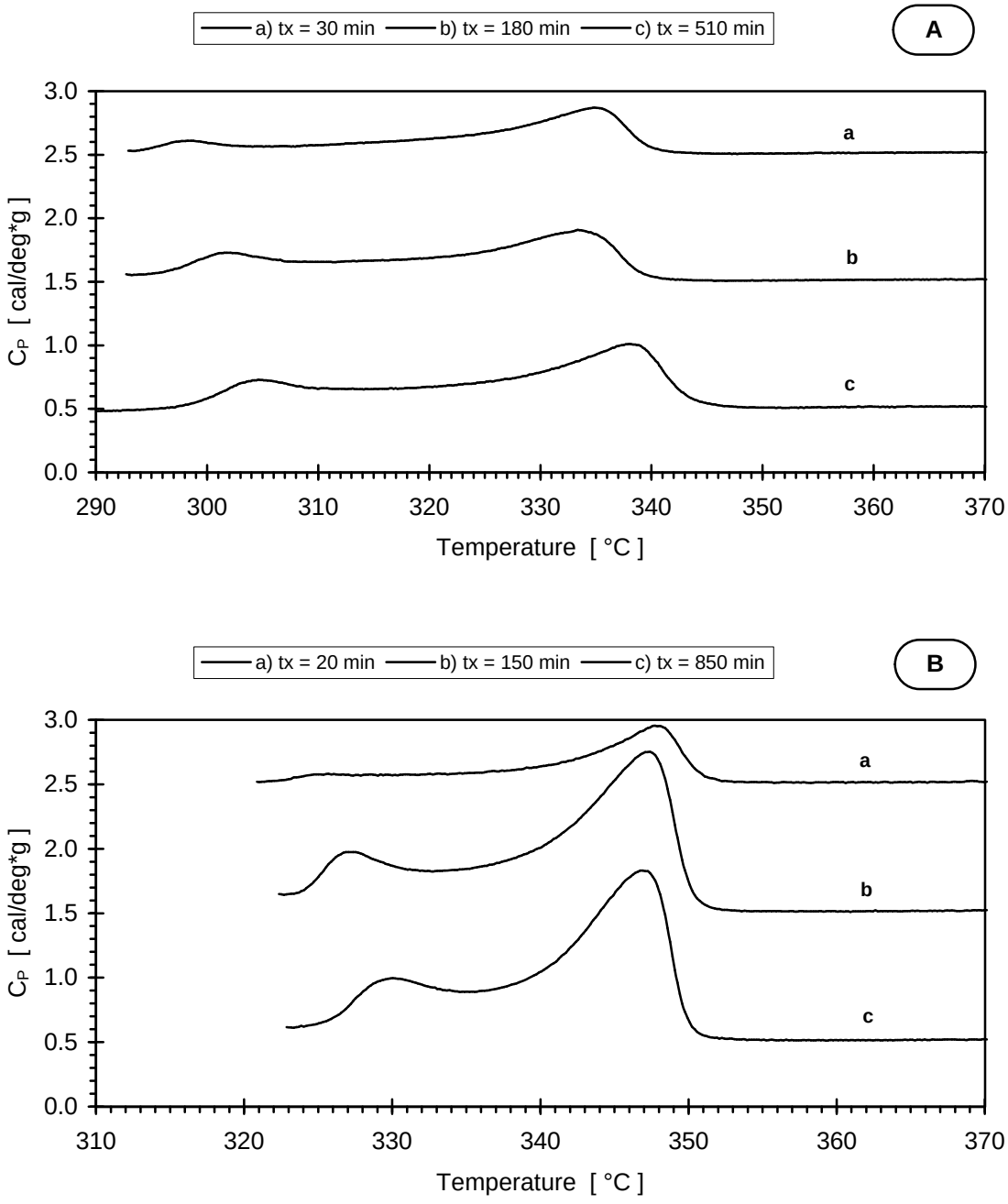


**Figure 4.8** DSC melting scans after crystallization from the melt for: A) fraction PEEK4-2 (43.3 K) at $T_x$ = 290°C, B) fraction PEEK4-5 (18.2 K) at $T_x$ = 320°C.

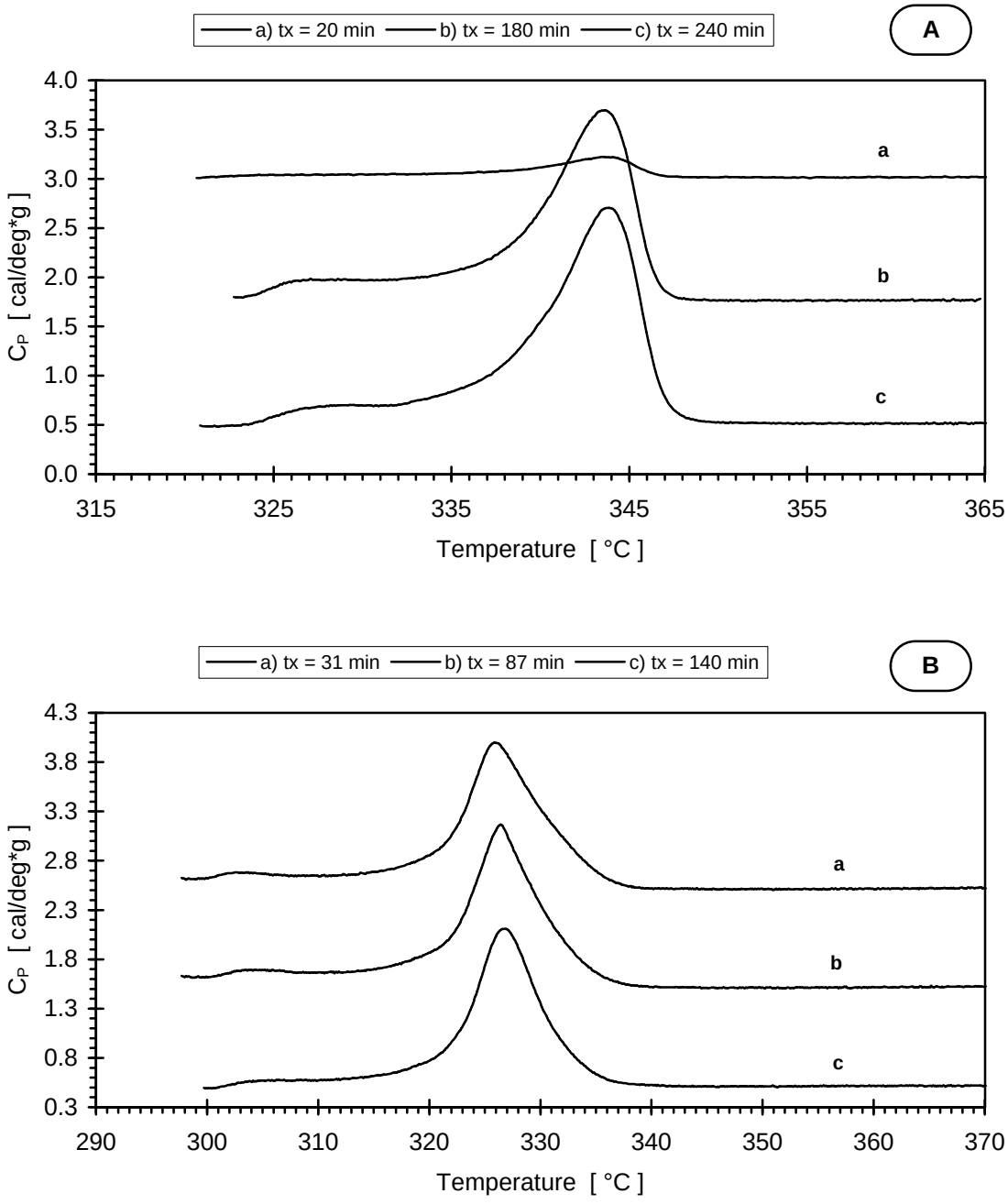


**Figure 4.9** DSC melting scans after crystallization from the melt for: A) fraction PEEK4-8 (6.3 K) at $T_x$ = 320°C, B) fraction PEEK4-9 (3.2 K) at $T_x$ = 297°C.

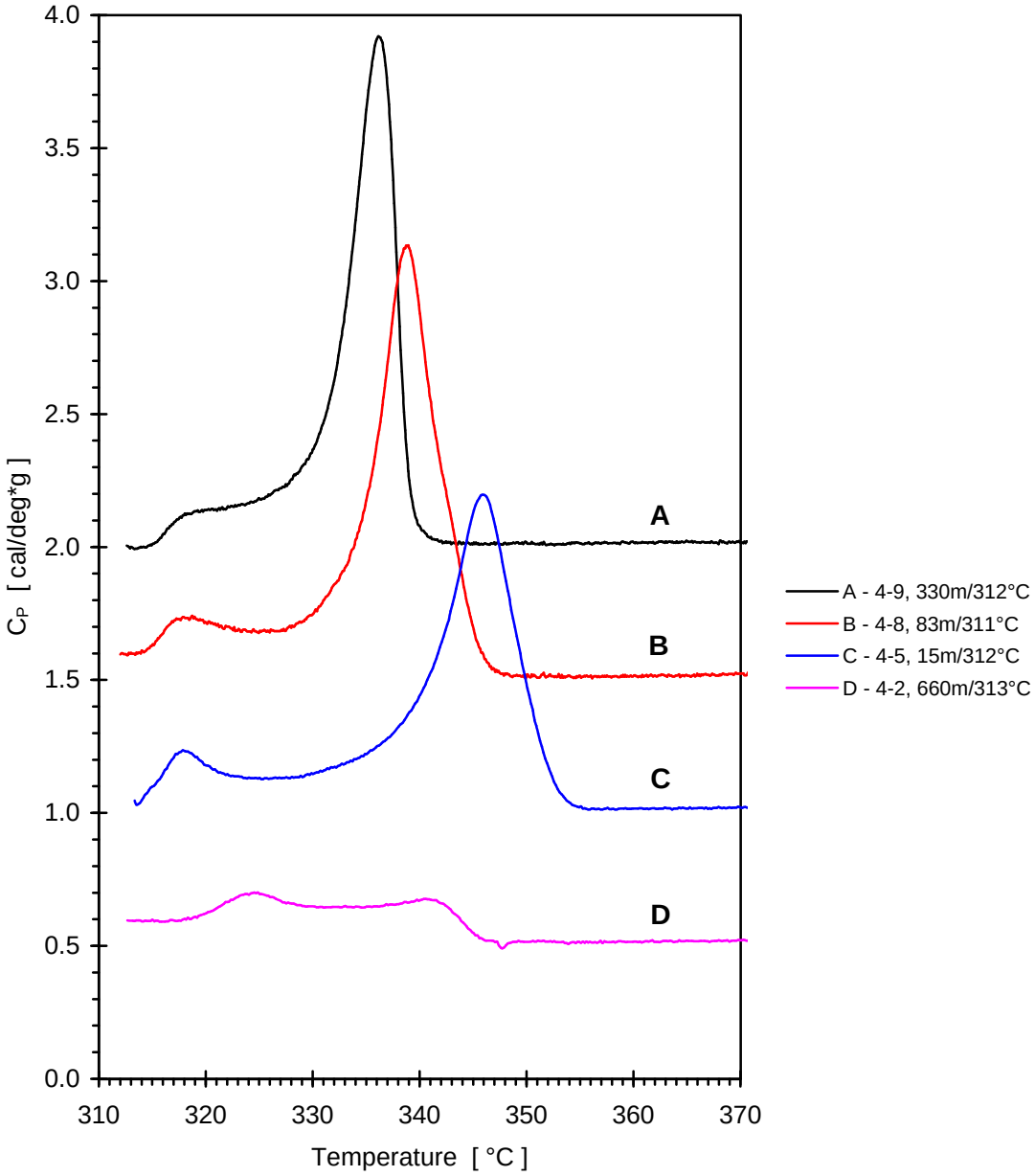


**Figure 4.10** DSC melting scans of PEEK fractions, crystallized from the melt at 312±1°C for different times.

It is clear, that similarly to commercial PEEK, with increase of crystallization time for each of the fractions $T_{max}$(low) shifts to higher temperatures and the area of the low temperature peak increases. As we have reported earlier (figure 1 in reference 77) this qualitative feature of the low temperature peak becomes more easily resolved if large relative changes in $t_x$ are employed. A quantitative description of the dependence of the parameters of the low temperature endotherm on time and temperature of thermal treatment for commercial PEEK will be given in section 4.2.1.

As the crystallization times and temperatures used in figures 4.6 - 4.9 are different for each fraction a final comparison between "double melting" of the fractions is made in figure 4.10. It shows the melting scans of all four fractions after crystallization at $T_x$ = 312±1°C. The fact, that the crystallization times used are quite different and vary by an order of magnitude does not diminish, but rather emphasizes, the effect of MW on the development of the low temperature endothermic peak. The peak position on the temperature scale varies in strict accordance with the crystallization time used. The peak area increases with increase in MW from 3.2 K to 18.2 K even though the crystallization times decrease in this sequence. The highest MW fraction PEEK4-2 (43.3 K) has a much smaller DSC crystallinity due to its slow crystallization rate at 313°C. The enthalpy of the low temperature peak for this fraction exhibits the highest ratio to the total enthalpy of the melting scan among all fractions and thus confirms the relative and absolute trend of increase in the enthalpy of the low temperature endotherm with increase in MW.

In summary, the results from this section unequivocally show, that the "double melting" phenomenon is manifested in PEEK fractions with various molecular weights with all its characteristics known up to date.

It is tempting to draw a relation between the effect of MW on the low temperature endotherm and on DSC crystallinity and crystallization rates. The decrease in the enthalpy, associated with the low temperature endotherm, with decreasing MW is opposite to the effect on crystallinity and crystallization rates. [130, 131, 134] This observation was a factor in the development of an earlier hypothesis [78] that the low temperature endothermic peak in PEEK was not a *melting* peak, but a manifestation of a phenomenon solely related to the amorphous

fraction of the polymer, namely - an enthalpic relaxation caused by the "physical aging" of the rigid amorphous fraction (RAF) of semicrystalline PEEK above the nominal glass transition of the mobile amorphous fraction of the polymer. [78-80]

### *4.1.2b Evolution of the "Second Structure" (Type II Spherulitic Morphology)*

In the introductory chapter of this study it was mentioned, that the goal of this investigation of the crystallization and melting behavior of PEEK originated at the early stage from an observation through polarized optical microscopy by Marand and Prasad [2] of a peculiar new morphology in the sperulitic growth of the polymer. At high temperatures and at long crystallization times, the spherulitic growth became non-linear and slowed down very significantly, although large uncrystallized regions could still be observed. Moreover, in parallel with this effect, the growth of a new morphological pattern was observed (labeled by the authors as "type II structure"). At the edges of the spherulites a crystalline superstructure developed. It had much higher birefringence than regions observed in the central parts of the spherulites.

Furthermore, upon heating in the microscope, a marked drop in the birefringence of the type II structure was observed about 10 K above the crystallization temperature. This contrasted with the continuous decay of the birefringence of the rest of the spherulite (the type I structure) upon melting. Type II structure melted completely (e.g. disappeared completely) just a degree or so away from the final melting of the type I structure.

The authors noted the fact that the temperature and time dependence of the new morphological feature can be qualitatively correlated with that of the "double melting" behavior of PEEK. In the latter, the low temperature endotherm develops in time only after the development of a significant part of the high temperature peak. The enthalpy of the low temperature endotherm becomes a significant fraction of the total melting enthalpy only at long times or at high crystallization and/or annealing temperatures. The maximum of the transition is located about 10-20 K above the crystallization temperature.

Despite the qualitative character of the correlations between the two phenomena, the strength of their multiple similarities lead the authors to propose that the low temperature endotherm in the DSC scan must manifest some transformation in the type II structure during the heating scan in the microscope hot stage.

Following the investigation of the melting behavior of the PEEK fractions by DSC, a polarized optical microscopy study was undertaken. Samples were prepared by a procedure, described in the literature [2] - thin films were cast from a 0.22 % w/w solution in benzophenone and dried at 160°C under vacuum. Samples were melted under nitrogen in the microscope's hot stage at 385°C for 5 minutes and isothermally crystallized at two temperatures. The crystallization temperatures were chosen at the upper and lower end of the temperature windows of isothermal melt-crystallization, depicted in figure 4.5a.

Figure 4.11 shows the polarized micrographs of fraction PEEK4-2 (43.3 K) after long crystallization for: a) 200 min at 260.5°C, b) 67.5 hrs at 310.8°C. At 260.5°C high nucleation and fast growth are observed and crystallization is completed within 3 hrs. At the higher $T_x$ of 310.8°C nucleation density is lower, linear growth stops before impingement and a large fraction of the type II morphology develops thereafter.

Similar effects are observed for fraction PEEK4-5 (18.2 K) - figure 4.12. At the lower temperature of 305.7°C crystallization is completed within 6 hours - figure 4.12a. At the higher $T_x$ of 325.9°C linear growth stops before impingement and the type II morphology develops - figure 4.12b.

In fractions 4-5 and 4-8 this new morphological form is observed in the periphery as well as inside the spherulites. The new morphology is represented less in the lower molecular weight fractions. In fractions 4-8 and 4-9 crystallization is completed at any temperature, but increasing inhomogeneity and coarseness of the already formed sperulitic structure at long times is an indication of the formation of type II structure. Upon heating in the microscope, at about 10-15 degrees above $T_x$ a change in the birefringence of the type II regions is observed in the higher MW fractions.

The results support the observations of Marand and Prasad [2] that the development of the type II morphology parallels that of the low temperature endotherm in the DSC scan.

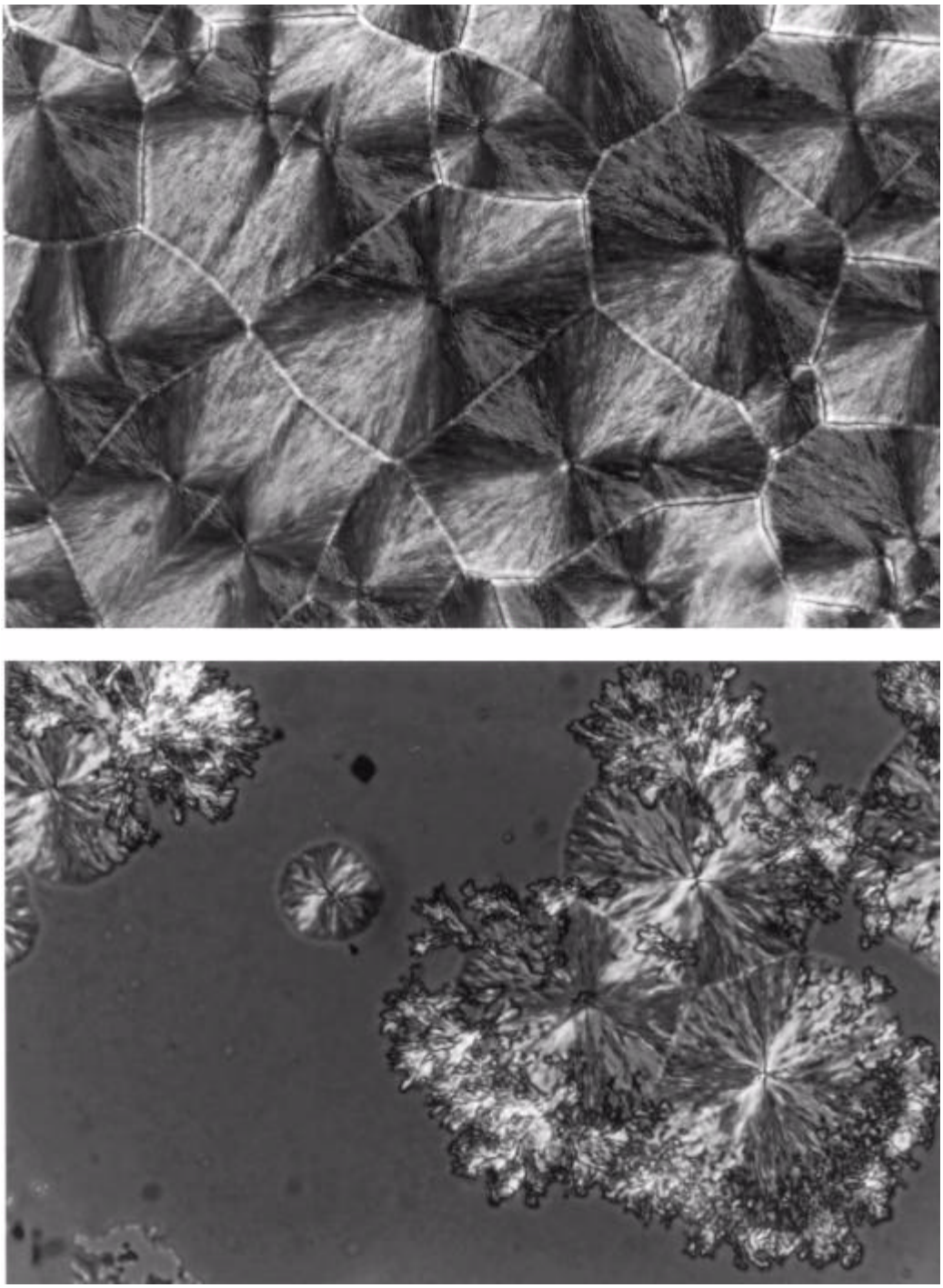


**Figure 4.11** Photomicrograph of fraction PEEK4-2 ($M_w$ = 43,300 g/mol), isothermally crystallized for long times: A) at $T_x$ = 260.5°C for 200 min, B) at $T_x$ = 310.8°C for 4050 min. Type II morphology overlays the spherulites after radial growth stops.

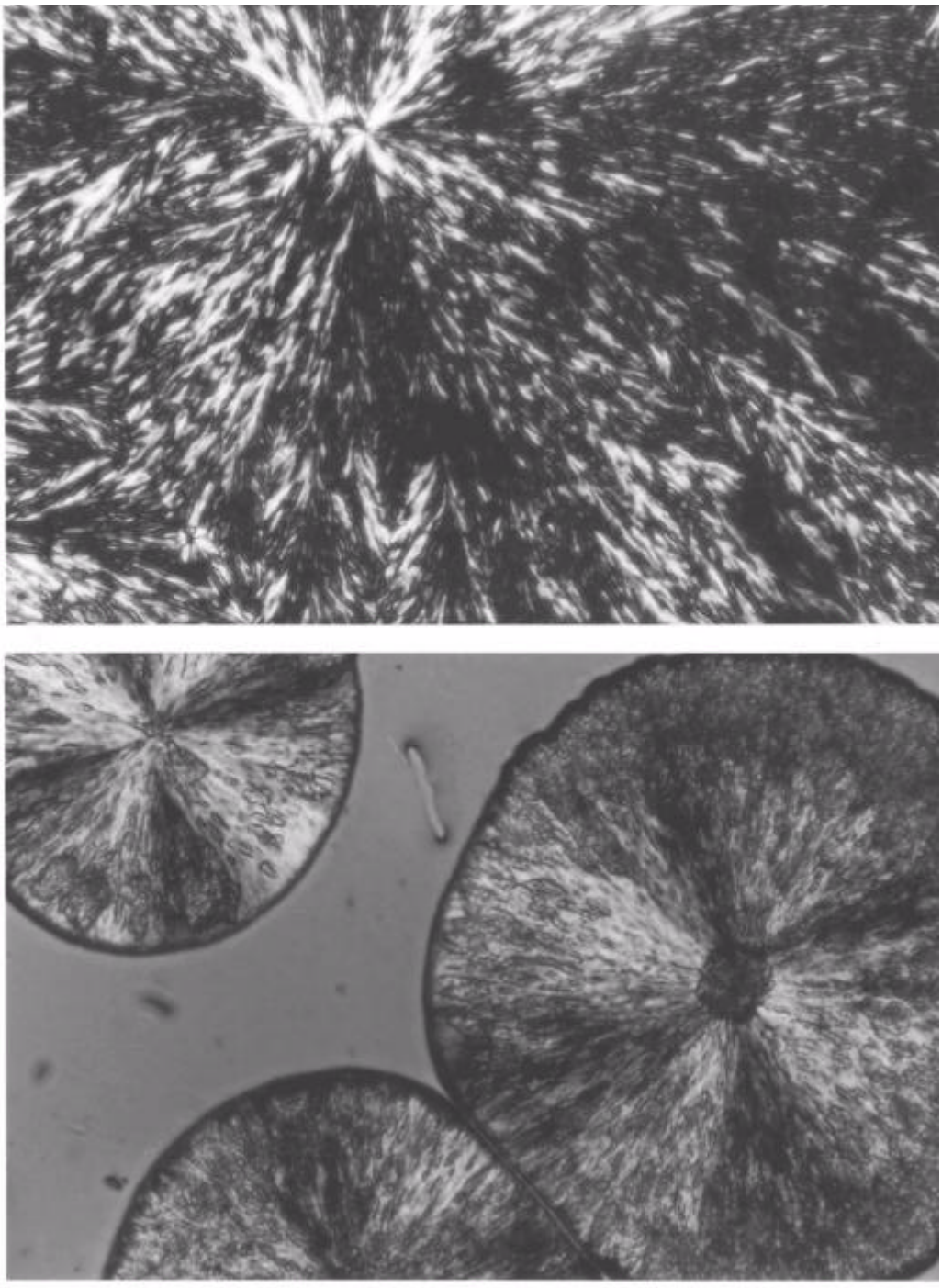

**A**

**B**

**Figure 4.12** Photomicrograph of fraction PEEK4-5 ($M_w$ = 18,200 g/mol), isothermally crystallized for long times: A) at $T_x$ = 305.7°C for 400 min, B) at $T_x$ = 325.9°C for 2850 min. Type II morphology is less significant than in figure 4.11-B.

The observation of increasingly less type II structure and lower low temperature peak enthalpies with decreasing MW does not support the hypothesis of Marand and Prasad, that type II structures correspond to growth from completely relaxed and type I (regular sperulitic growth) - from unrelaxed amorphous phase. If that explanation was correct, the lower MW fractions would have exhibited more type II morphology and higher low endotherm enthalpies as lower MW results in more cilia and less chain loops and tie molecules at the crystal-amorphous interface.

## 4.2 Effects of Annealing Time and Temperature

In this section results from the studies of the effects of annealing time and temperature on the crystallization and melting behavior of PEEK are provided. Section 4.2.1 examines the effect of the crystallization and/or annealing time and temperature on the development of the low temperature endothermic peak under all of the thermal history profiles listed in the experimental section (figures 3.3 - 3.7). Section 4.2.2 provides few examples for the observation of the same effects in other polymers. Section 4.2.3 investigates the effect of the same parameters on the crystallinity development, section 4.2.4 - the effect on the small strain creep of PEEK, and section 4.2.5 - the effect on the calorimetric glass transition temperature of semicrystalline PEEK.

### *4.2.1 Characterization of the Crystallization/Annealing Low Temperature Endotherm of PEEK*

Figure 4.13 shows the DSC heating scans (at heating rate 20 K/min in the interval 115°C - 365°C) of samples, cold-crystallized in the Carver hot press for 60 min from the amorphous glassy state at different temperatures above $T_g$. In addition, the recorded heating scan of completely amorphous PEEK sample and the NATAS [16, 115] recommended data for the measured and extrapolated heat capacities of glassy and liquid PEEK are plotted. The scans are corrected by baseline subtraction and heat flow calibration and presented as $C_P$ vs. $T$. The plot is similar in appearance to results from other studies of the melting of cold-crystallized PEEK. [16, 63, 64, 67, 68, 70]

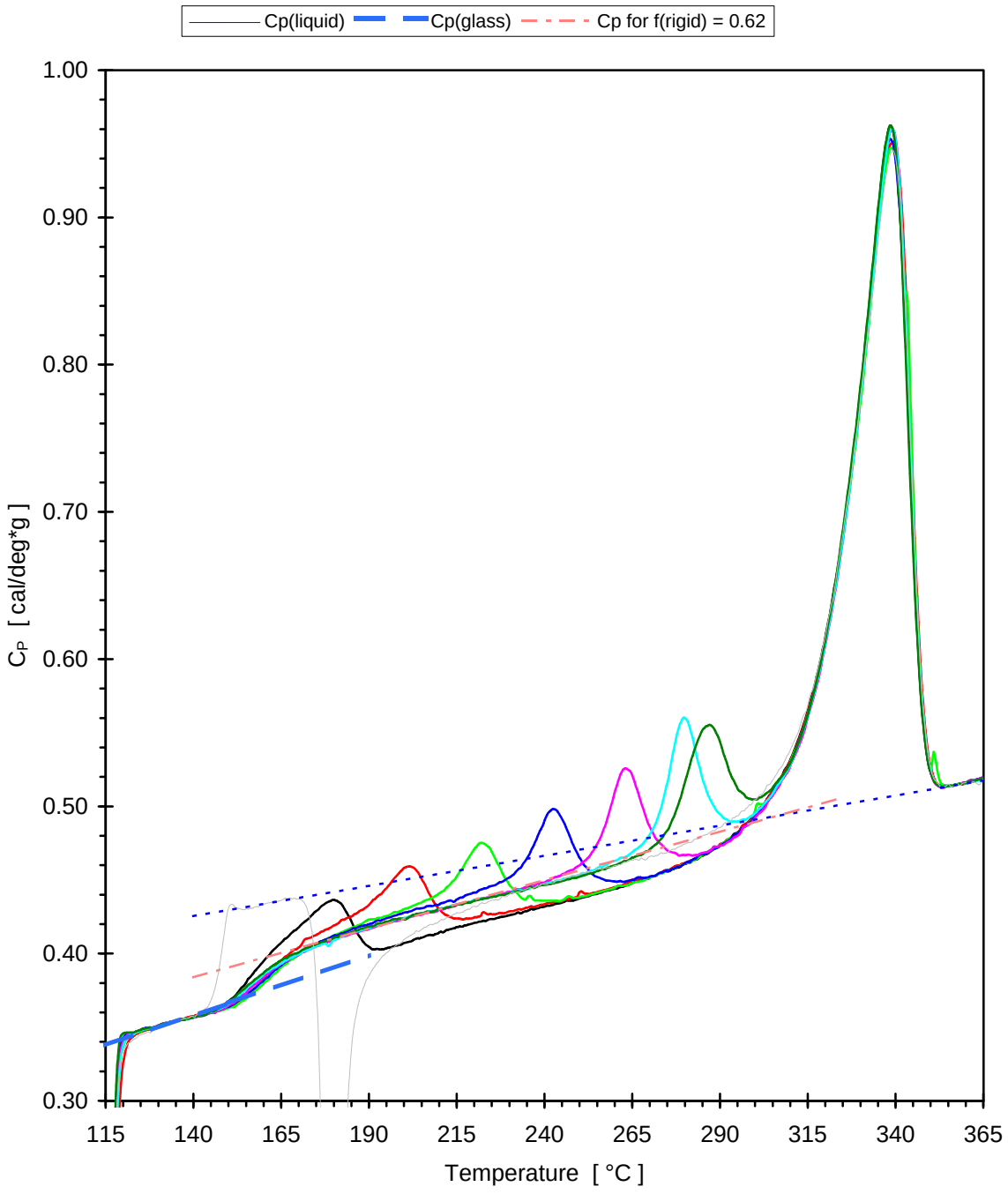


**Figure 4.13** DSC heating scans of PEEK samples, cold-crystallized for 60 min at: 163°C, 183°C, 203°C, 223°C, 243°C, 263°C, 272°C and a scan of amorphous sample from the glassy state. For the other lines - see the legends above.

The dynamic crystallization during the heating of the amorphous sample in the DSC at 20 K/min occurs within 10-15 K (e.g. 30-45 seconds) between 175°C and 185-190°C. Therefore the volume-filling (primary) crystallization from the amorphous glassy state is completed within no more than 1 min from setting a crystallinity studies sample (see section 3.1.2) in the hot press for all the samples except possibly the one crystallized at 163°C. Thus the effective thermal history of these samples is fast isothermal crystallization upon thermal equilibration of the sample in the press, followed by the annealing at the corresponding $T_c$. However, for reasons of clarity in the comparisons with other thermal history profiles these samples are labeled as "cold-crystallized" and the corresponding time and temperature time are labeled $t_c$ and $T_c$.

For each sample a broad high temperature endothermic peak is observed in the range of approximately between 275-285°C and 350°C. As can be seen in the plot, this peak adopts almost exactly the position and shape of the melting peak obtained in the scan of the initially amorphous sample. Therefore, during the scan for every sample the physical state just before the beginning of the "final" melting is the same.

The only differences observed are in the temperature region below the melting range. For every sample a second, low temperature, endothermic peak is observed in the heating scan just above $T_c$. Figure 4.14-A shows the position of the peak maximum of the low and high temperature peaks - $T_{max}$(low) and $T_m^{'}$, as a function of $T_c$ in a Hoffman-Weeks plot. $T_m^{'}$ is a constant, whereas the data for $T_{max}$(low) lies on a line, almost parallel to the $T_m^{'} = T_c$ line. The slope of the line is slightly less than one, therefore, for annealing at higher temperatures the low endotherm peak maximum appears slightly closer to $T_c$ than at lower ones. Figure 4.14-B shows the dependence of the enthalpy of the low temperature endotherm on cold-crystallization temperature $T_c$.

A closer look at the $C_P$(T) traces before and after the low temperature peak allows two more observations:

1) When well separated from the high melting peak and from the step change of $C_P$ at $T_g$, the low temperature peak is almost symmetrical in shape.

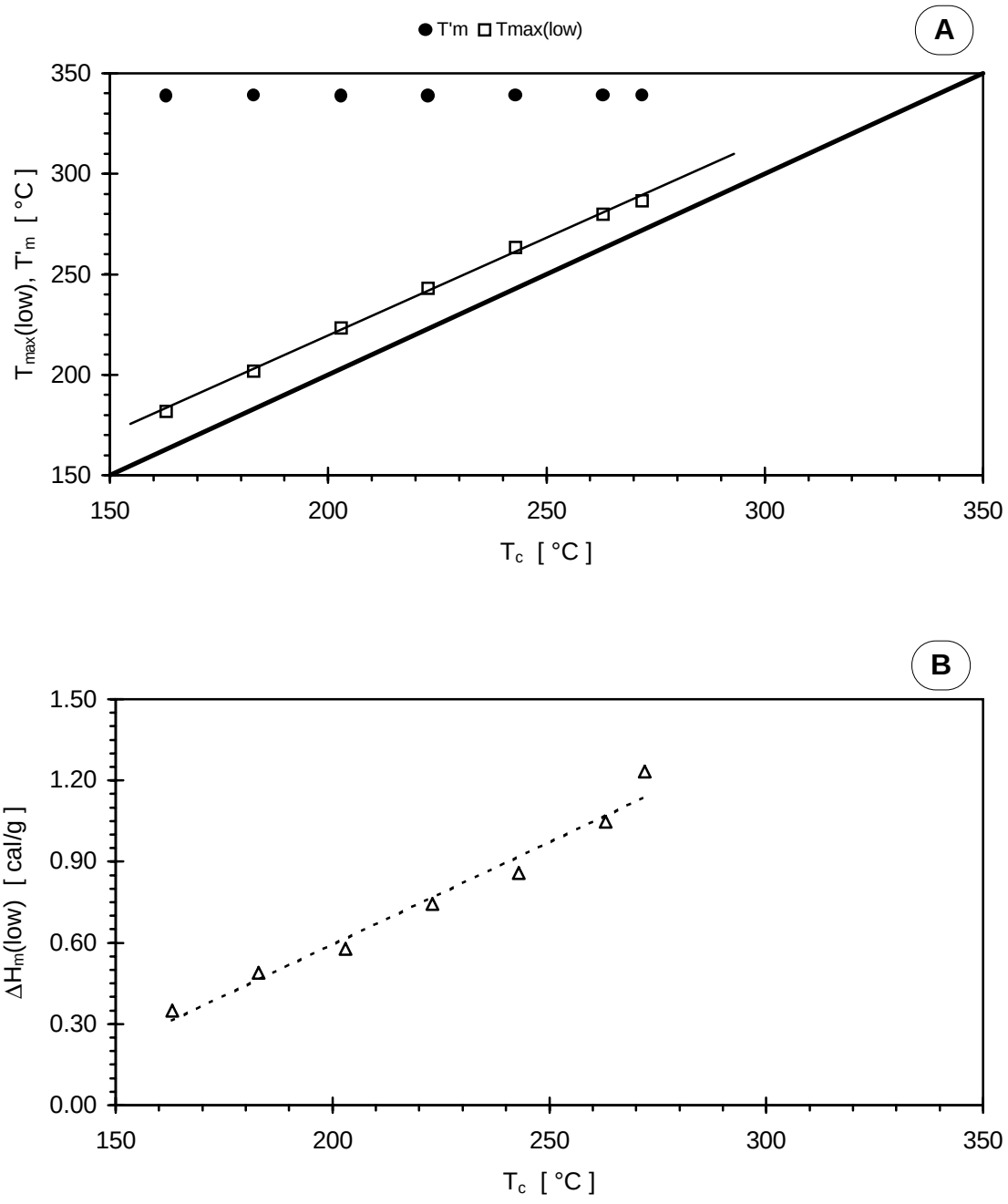


$T_{max}(low) = 0.971*(T_c-155) + 175.3$

$\Delta H_m(low) = 0.282 + 0.0068*(T_c-155)$

} at heating rate 20 K/ min

**Figure 4.14** Dependence of the low temperature endothermic peak's parameters on the cold crystallization temperature $T_c$: A) $T_{max}$(low), B) $\Delta H_m$(low).

2) The "local baseline", which defines the peak is non-linear. $C_P(T)$ before the peak is higher than $C_P(T)$ after the peak. The $C_P(T)$ lines before and after the peak are different in position, but almost identical for all samples. The only difference between the scans is the shift of the low endotherm at higher temperatures along the two separate "baselines" - the one before and the one after the peak. The traces after the peak coincide with one another with remarkable precision. The traces before the peak shift down slightly in magnitude with increasing $T_c$. This observation can also be made in the work of Cheng et al. (figure 10 in reference 16). The change in baseline after the peak corresponds to an exothermic deviation. More analysis of this peculiar feature will be provided later in the discussion chapter.

Figure 4.15 shows the DSC heating scans (at heating rate 10 K/min in the interval from $T_x$ to 370°C) of samples, melt crystallized in the DSC for 480 min at various temperatures. The plot is similar to figure 7B in reference. [2]

As in the case of the cold-crystallized samples in figure 4.13, a second endothermic peak is observed in the melting trace, just above $T_x$. The peak maximum and enthalpy are plotted against $T_x$ on figure 4.16. Figure 4.16-A is similar to the Hoffman-Weeks plot of the commercial PEEK polymer on figure 4.2. The high temperature peak, corresponding to the final melting, shifts to higher temperature with increasing $T_x$, following the expected Hoffman-Weeks behavior. The use of same crystallization times $t_x$ results in a $T_{max}$(low) vs. $T_x$ dependence, which is a line, parallel to the $T_m' = T_x$ line, similar to the result for cold-crystallized samples on figure 4.14-A. The enthalpy of the low temperature endotherm increases with increasing $T_x$, following approximately linear relationship (figure 4.16-B).

The results presented above describe features of the low temperature endotherm, already known from the literature studies on PEEK melting. The peak appears above the temperature of isothermal treatment, its magnitude increases with increase of $T_c$ or $T_x$, and its position is on a line, parallel to the $T_m' = T_x$ line on the Hoffman-Weeks plot. For samples with similar thermal history (e.g. cold-crystallized samples, melt-crystallized samples), $\Delta H_m$(low) exhibits a linear dependence on temperature.

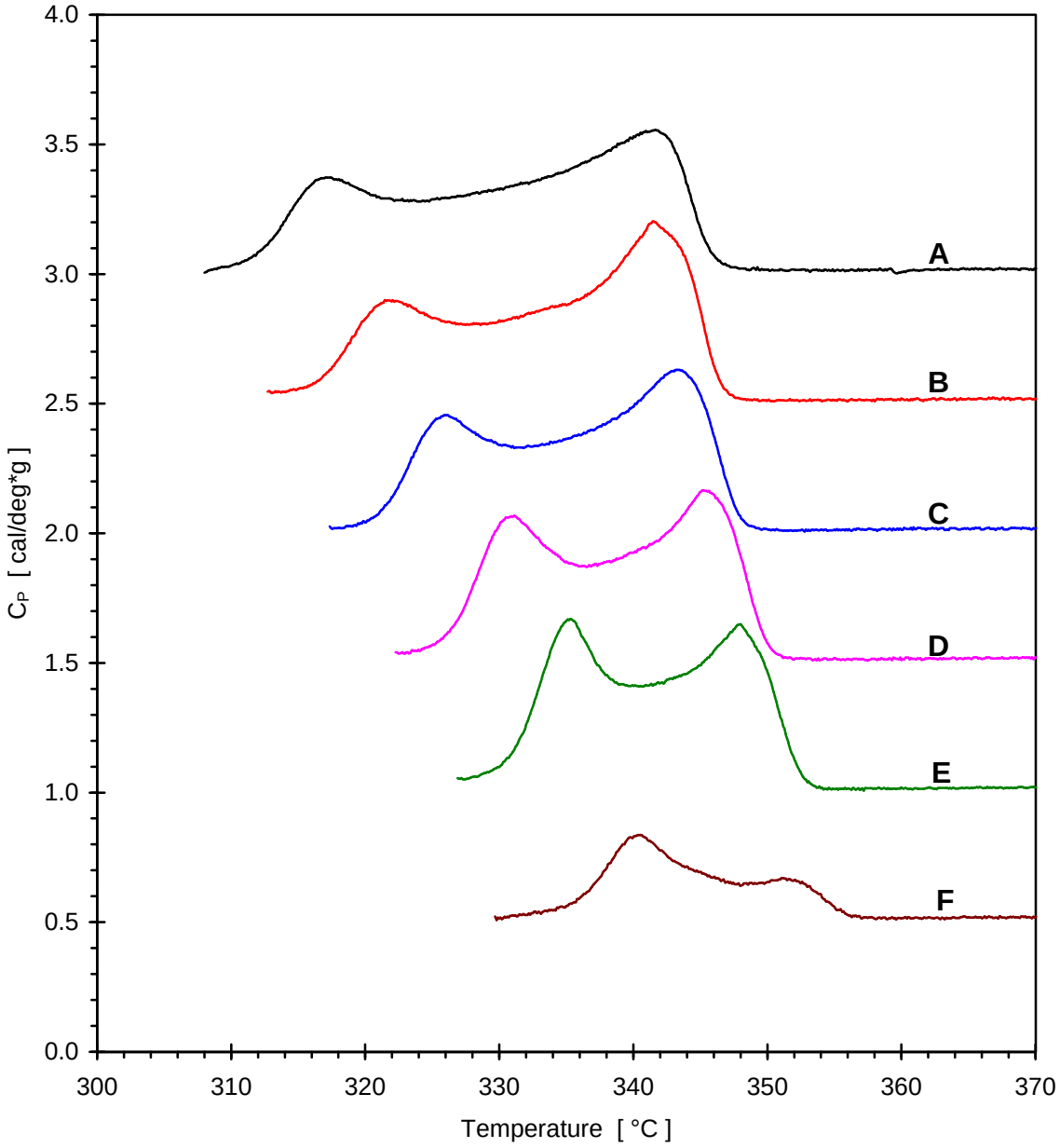


**Figure 4.15** Melting scans of PEEK samples, melt-crystallized in the DSC for 480 min at: A) 305°C, B) 310°C, C) 315°C, D) 320°C, E) 325°C, F) 330°C. All scans are shifted up from the last one for clarity.

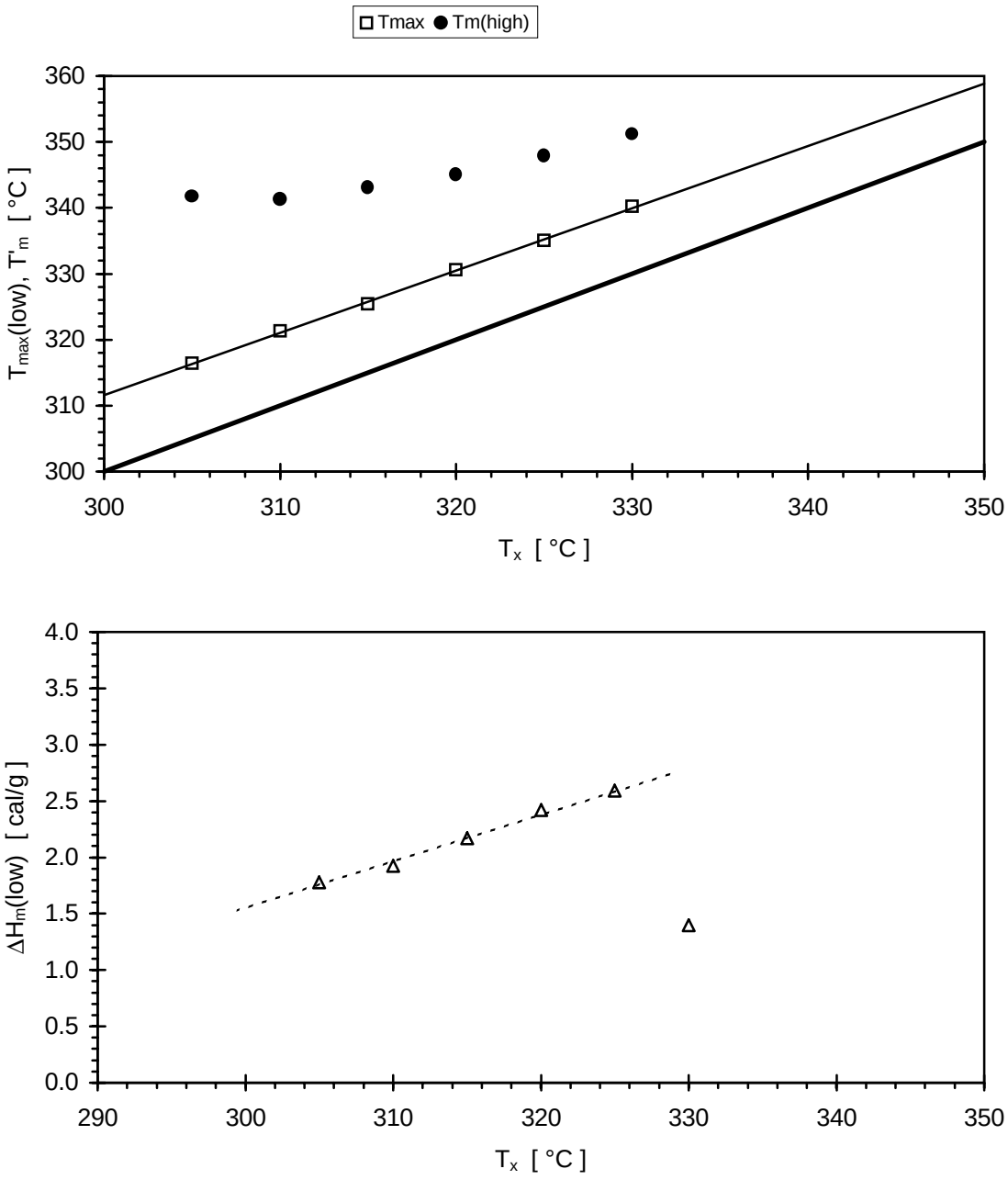


$$\left.\begin{aligned} T_{max}(\text{low}) &= 0.9455*(T_c\text{-}300) + 311.6 \ [°C] \\ \Delta H_m(\text{low}) &= 1.53 + 0.0425*(T_x\text{-}300) \ [\text{cal/g}] \end{aligned}\right\} \text{at heating rate } 10\ K / min$$

**Figure 4.16** Dependence of the low temperature endothermic peak's parameters on the temperature of isothermal crystallization from the melt $T_x$ ($t_x$ = 480 min).

Studies of the sequence in which the high and low temperature endotherms arise in time after isothermal crystallization from the melt, have shown, that the high temperature peak appears before the low temperature one. [2, 16, 70] Figure 4.17 illustrates this observation in more detail, than given in the literature. It shows the melting scans of PEEK samples, crystallized isothermally at 307°C for short times. After the times indicated on the plot elapsed, the isothermal crystallization was interrupted and the melting scan collected immediately. The times were selected in a way as to cover various points along the isothermal crystallization exotherm of PEEK, crystallized at 307°C. The scanning rate is relatively low - 5 K/min, allowing some additional crystallization to occur in the first 10-15 K (2-3 min) during the scan, if the sample has not crystallized completely at 307°C for the given $t_x$. The first time - 110 s, is too short and only a small fraction of the material was able to crystallize. Significant additional crystallization occurs during the first 2-3 min of the scan, up to about 320°C, which is represented by a large exothermic deviation, well below the $C_P(T)$ trace of a fully amorphous PEEK. With increase in crystallization time, a larger fraction of the material is able to crystallize isothermally and the magnitude of the exothermic deviation at the beginning of the scan decreases. At the end of the interval between 255 s and 300 s most of the primary crystallization is completed and no exothermic deviation is observed in the 300 s scan. In the same time interval the low temperature endothermic peak begins to develop. The scans for 300 s, 400 s, and 600 s show its first appearance and gradual development.

In the earlier reports on PEEK melting, it has been shown, that the low temperature endotherm continues to develop after long times of crystallization or annealing, [16, 66, 72] but the nature of the dependence of $T_{max}$(low) and $\Delta H_m$(low) on $t_x$ or $t_a$ has not been investigated for long crystallization times.

Examination of our early studies of the isothermal crystallization of the PEEK fractions (figure 1 in reference 77) suggested, that increase of the crystallization time by a factor of 2 produces continuous increase of the enthalpy of the low temperature endotherm and shifts up the peak maximum by approximately equal amounts.

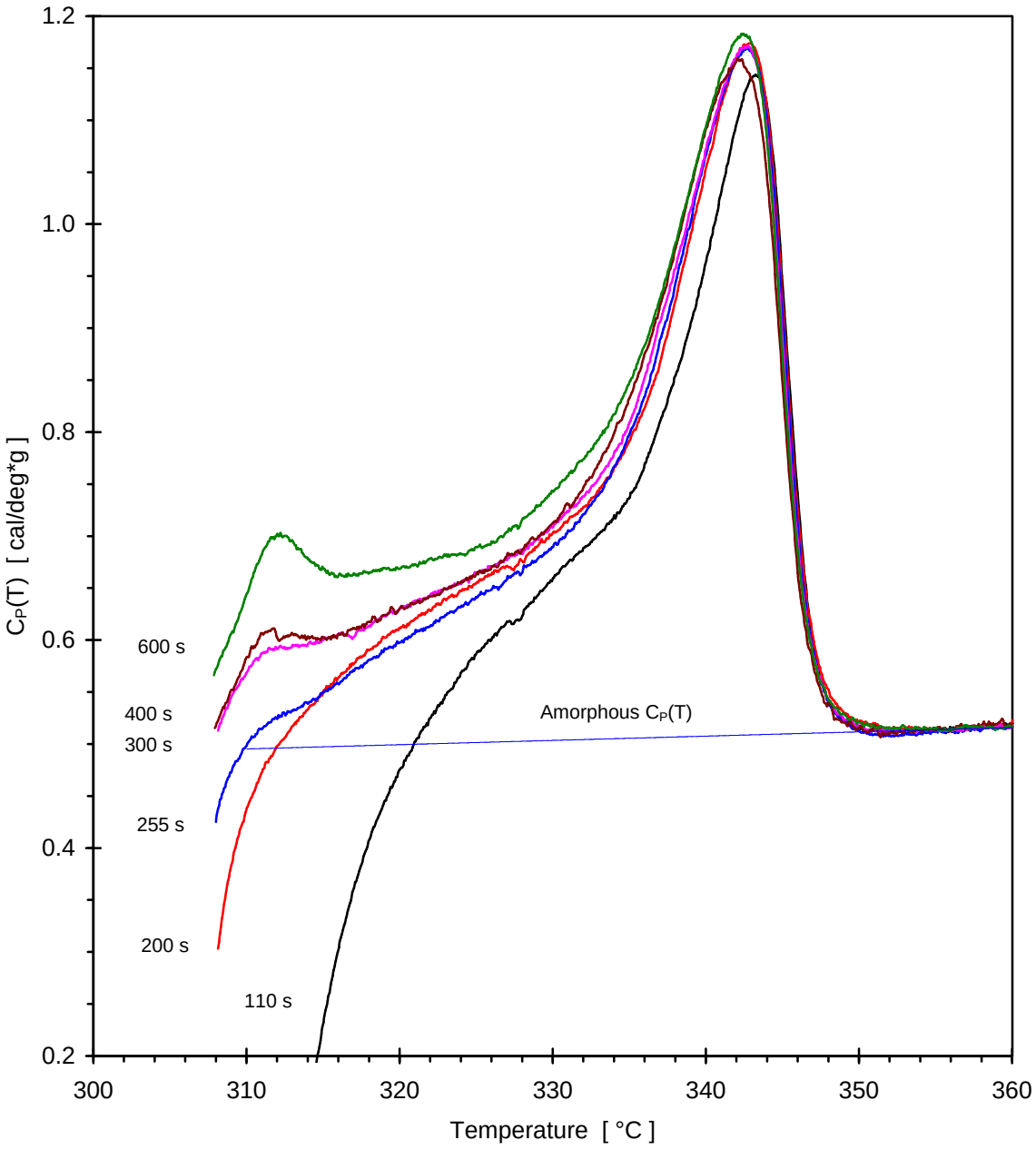


**Figure 4.17** Melting scans of PEEK samples, melt-crystallized in the DSC at 307°C for short crystallization times. Heating rate is 5 K/min. Crystallization times are indicated next to the scans.

This observation suggests that in order to investigate effectively the time dependence of the low temperature endotherm, a logarithmic time scale of observation must be chosen. In almost all of the experiments reported in this study the logarithmic increment in time was chosen by multiplying the first time by a power of 2.

Figure 4.18 shows the melting scan of PEEK samples crystallized in the DSC at $T_x$ = 310°C for times increasing approximately in geometric progression with a factor of 2. The high melting endotherm in the scans remains almost unchanged as the lowest time was chosen close to the end of the exothermic crystallization peak observed upon isothermal crystallization at 310°C. From one scan to the next the low temperature peak gradually shifts to higher temperatures and increases in area. The same crystallization experiment was repeated in the entire interval, where PEEK can crystallize at close to isothermal conditions - 300°C - 330°C at intervals of 5 K. A similar development of the melting scans with time was observed in all cases. The only difference is due to the slowing down of the nucleation process for the development of primary crystallization. With increase in $T_x$ the crystallization half-time and the time for completion of the primary crystallization process increase. [63] Therefore, the first observation of the low temperature endothermic peak (according to the results from figure 4.17), is shifted to longer times.

Figure 4.19-A shows the positions of $T_{max}$(low) for three different crystallization times at the various crystallization temperatures on a Hoffman-Weeks plot. For every given $t_x$ the lines through the $T_{max}$(low) datapoints are almost parallel to the $T_m' = T_x$ line. With a logarithmic increase of $t_x$ these lines are shifted vertically away from the $T_m' = T_x$ line.

Figure 4.19-B shows the development of the peak maximum $T_{max}$(low) with crystallization time $t_x$ on a log-time scale, on which the times, chosen in geometric progression are equidistantly placed on the abscissa. For all crystallization temperatures $T_{max}$(low) increases linearly with log($t_x$). To a first approximation the different $T_{max}$(low) vs. log($t_x$) lines are almost parallel and vertically spaced at equal intervals. A closer look at the dependence shows, that it is of the form:

$$T_{max}(low) = T_x + A + B * log(t_x) \qquad (4.3)$$

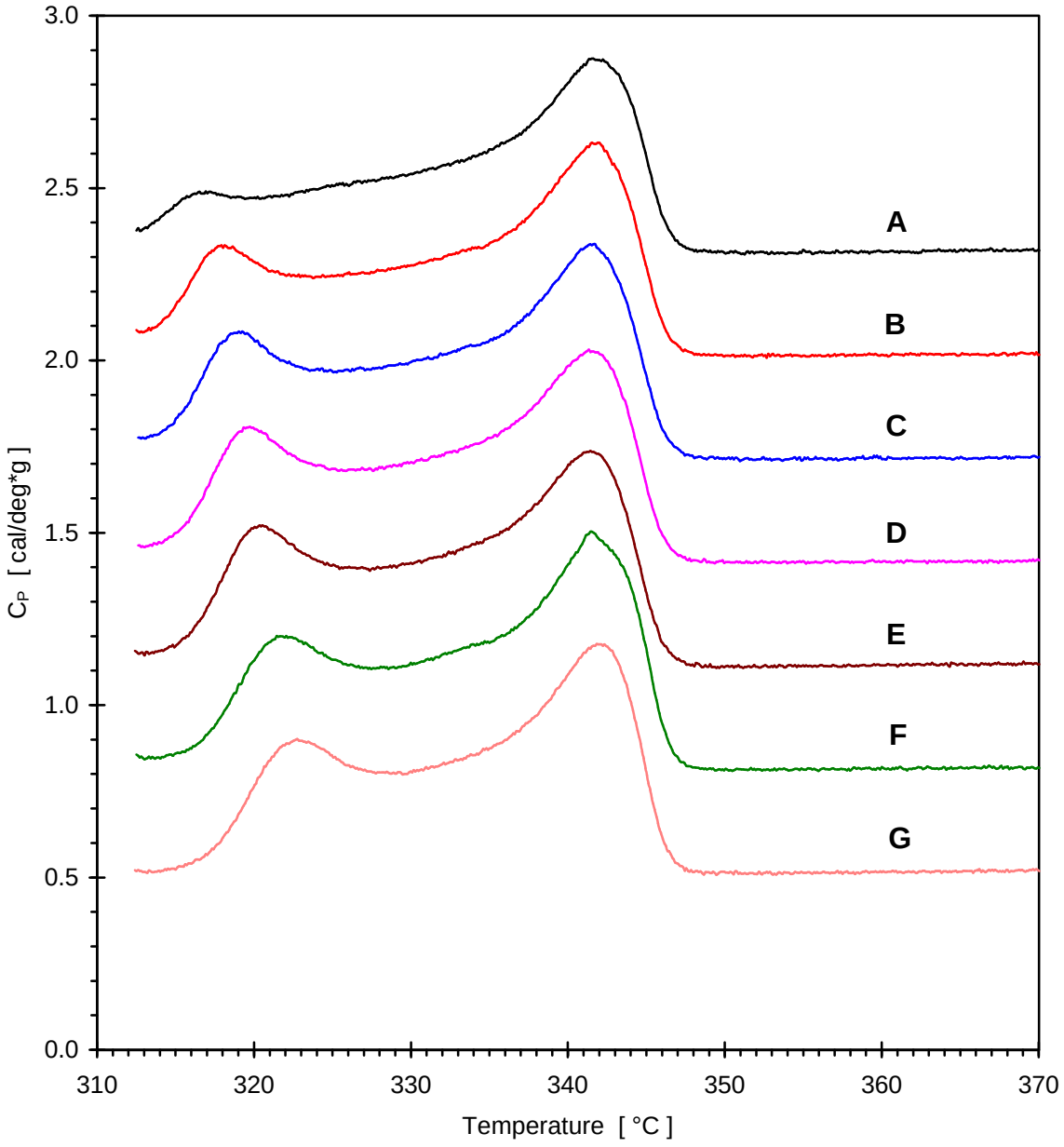


**Figure 4.18** Melting scans of PEEK samples, melt-crystallized in the DSC at 310°C for: A) 10 min, B) 31 min, C) 68 min, D) 130 min, E) 240 min, F) 512 min, G) 978 min. All scans are shifted up from the last one for clarity.

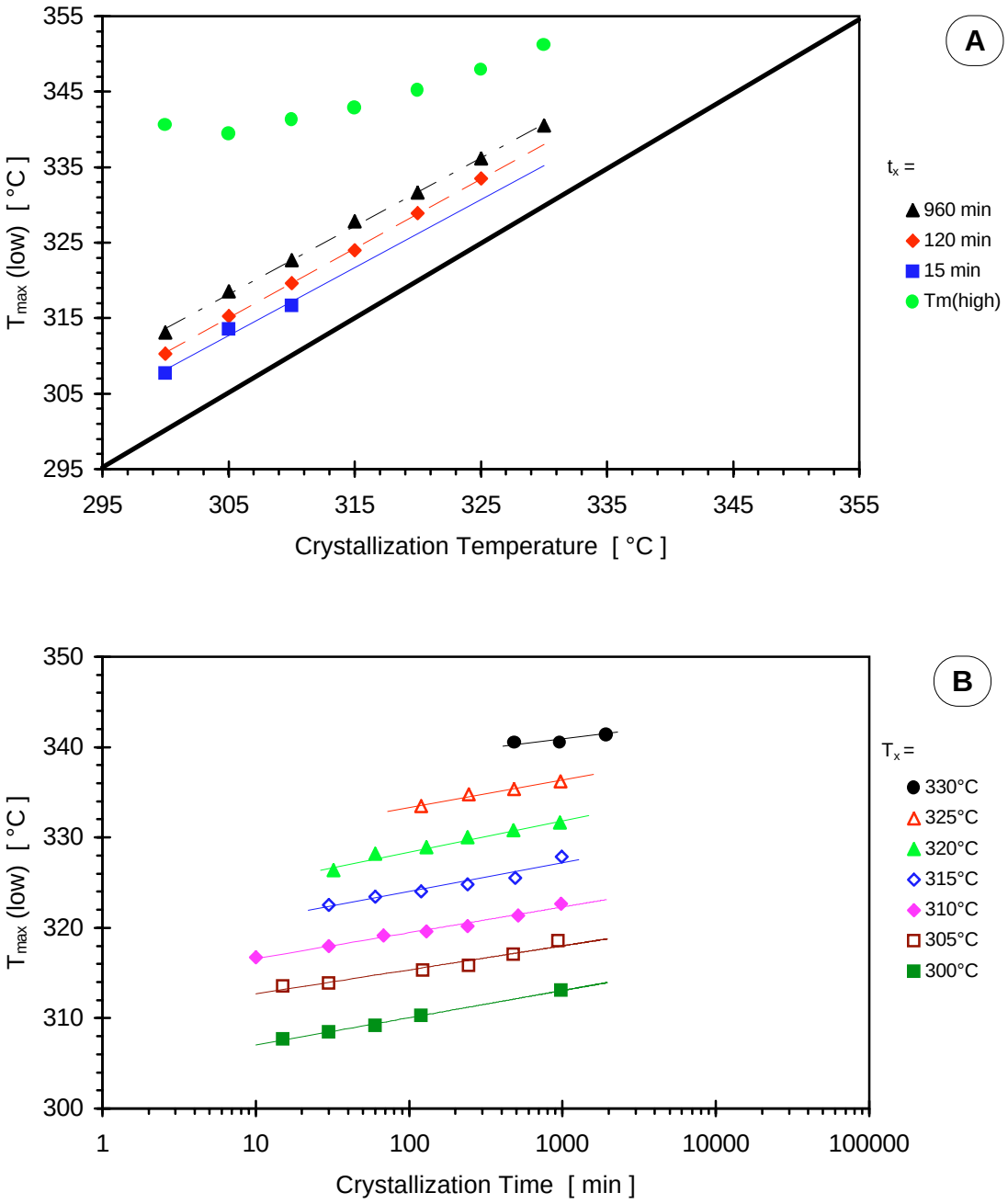


$T_{max}(low) = T_x + A\,(T_x) + B\,(T_x) * \log(t_x)$

**Figure 4.19** Dependence of the low temperature endothermic peak maximum on the time and temperature of crystallization from the melt: A) Hoffman-Weeks plot ($T_x$-dependence), B) $\log(t_x)$ dependence.

where the parameters *A* and *B* are functions of $T_x$.

The results from a straightforward linear fit of the dependence of $T_{max}$(low) on log($t_x$) do not show a clear trend in the dependence of the slope and coefficient with $T_x$ and the correlation coefficient of the least squares fit is not very good (generally around 0.95 for $T_x$ > 305°C). When an induction time, appropriate for the corresponding $T_x$ is subtracted from $t_x$ for the series of datapoints at each $T_x$, the correlation is greatly improved and a trend of decrease in the values of *A* and *B* with $T_x$ is observed. This type of correction is in agreement with the results from figure 4.17, which show, that the development of the low temperature peak begins after an initial induction time, corresponding to the development of a certain fraction of the primary crystallinity.

(Note: The applied induction time values are smaller than the times for the leftmost datapoints for each $T_x$ on figure 4.19B; their precise determination is impractical for the high $T_x$ series, as staging an experiment similar to the one shown on figure 4.17 at a higher $T_x$ would require many long DSC scans.)

Figure 4.20 shows the dependence of the parameters *A* and *B* on $T_x$. Despite the scatter, the results clearly indicate a decrease in the values of the slope *B* and the intercept at $t_x$ = 1 min - *A*. This means, that with an increase in $T_x$, the low temperature endothermic peak, which develops after isothermal annealing (i.e. crystallization) time $t_x$: 1) appears closer to $T_x$, 2) shifts up in position on the temperature axis at a slower rate.

The use of conditions of isothermal crystallization from the melt has a limiting effect on the precision of the quantitative analysis of the development of the low temperature endotherm with time and temperature of isothermal treatment. Two of the limiting factors are due to the observation of a non-negligible induction time for the development of the low temperature endotherm. For example, the correction with an induction time determined to be 20±5 min from the datapoints at long times: 240 min, 480 min, 960 min etc., will have a negligible effect on the uncertainty of these datapoints on the horizontal axis, but the uncertainty on the datapoints at shorter times: 120 min, 60 min, 30 min will be very large and increase dramatically with decrease of $t_x$. Therefore, with an increase in $T_x$ (and therefore an increase in induction time) more and more datapoints are determined with insufficient

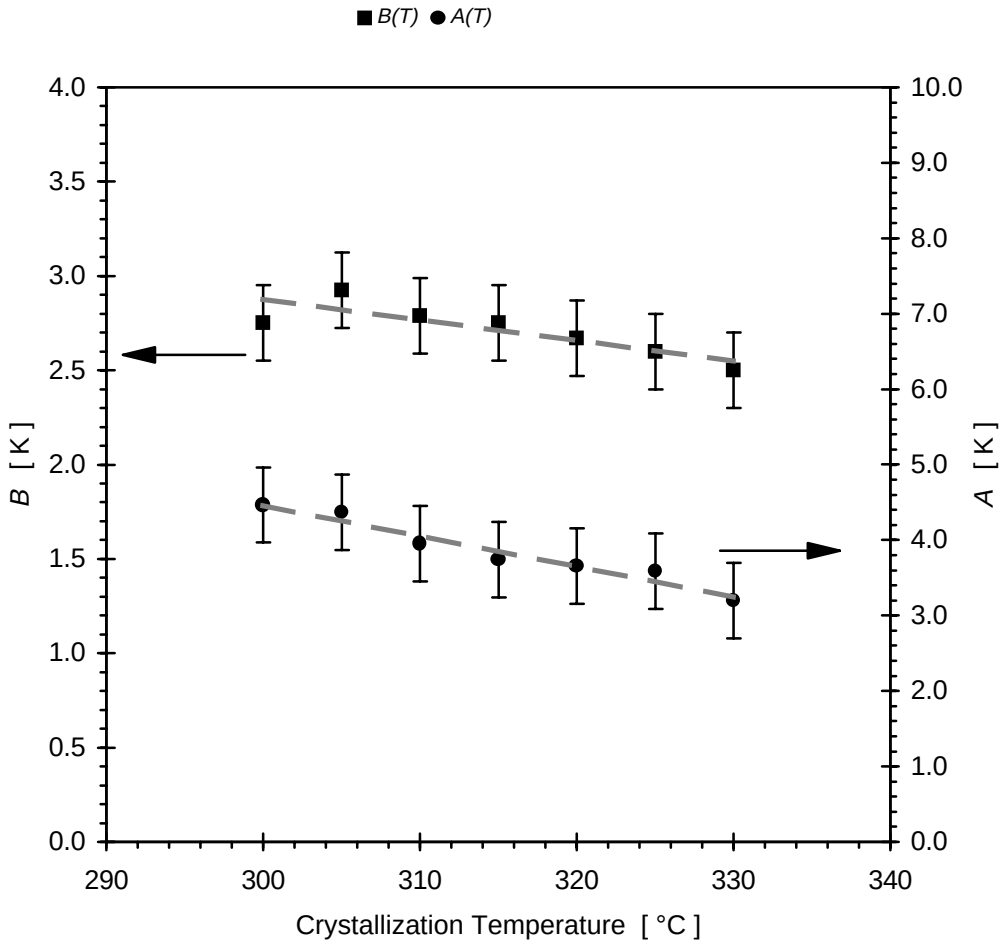


$$T_{max}(low) - T_x = A(T_x) + B(T_x) * \log(t_x - t_{ind})$$

**Figure 4.20** Dependence of the parameters of the linear relationship between $T_{max}(low)$ and $\log(t_x)$ on crystallization temperature $T_x$ for samples, isothermally crystallized from the melt.

accuracy on the log($t_x$) axis. The second reason arises from the increase in the induction time with increase in $T_x$. This pushes the experimentally useful crystallization times at higher $T_x$ to even larger values. The use of datapoints at longer times, however, is limited by practical reasons - the times must increase in geometric series and in order to cover sufficient number of decades of time one must go to times which are too long for practical purposes. Furthermore, long exposure of the polymer melt at high temperatures even in an inert atmosphere could lead to thermal degradation, [110] which in turn would introduce yet another possible uncertainty.

Another uncertainty in the quantitative analysis of the time and temperature dependence of the low temperature endothermic peak is the fact, that with increase in $T_x$, the peak appears closer to the high temperature melting peak. This is evident from the DSC scans of figure 4.15 and the plot of $T_{max}$(low) and $T_m^{'}$ vs. $T_x$ on figure 4.19-A. With the merging of the two peaks the use of a correct procedure for resolving their separate contributions to the melting scan becomes increasingly important. Large errors in the values of $T_{max}$(low) could be introduced if improper "local baseline" (i.e. separation procedure) is used. The relative error in the values of $\Delta H_m$(low) would be even higher.

Some of these difficulties were partially resolved with the studies of the melting scans of PEEK samples with somewhat different thermal histories from the ones described above. Thermal histories as the ones described in figures 3.5 - 3.7: two step crystallization followed by annealing up (figure 3.5) or down (figure 3.6) and isothermal crystallization, followed by multiple step annealing down (figure 3.7), result in multiple endotherms in the DSC heating scan of PEEK. Partial studies of these observations have been reported previously by Cheng et al., [16] Chang, [72] and Lattimer et al. [73]

Figure 4.21 compares the melting scans of samples with thermal history as shown in figure 3.5 with the melting scans resulting from isothermal crystallization. The thermal histories are summarized in the figure caption. Isothermal crystallization at 315°C for 120 min results in melting scan (A). It is characterized by a high temperature melting peak with $T_m^{'}$ = 345°C and a low temperature one with $T_{max}$(low) = 324°C. Melting scans (C-G) are

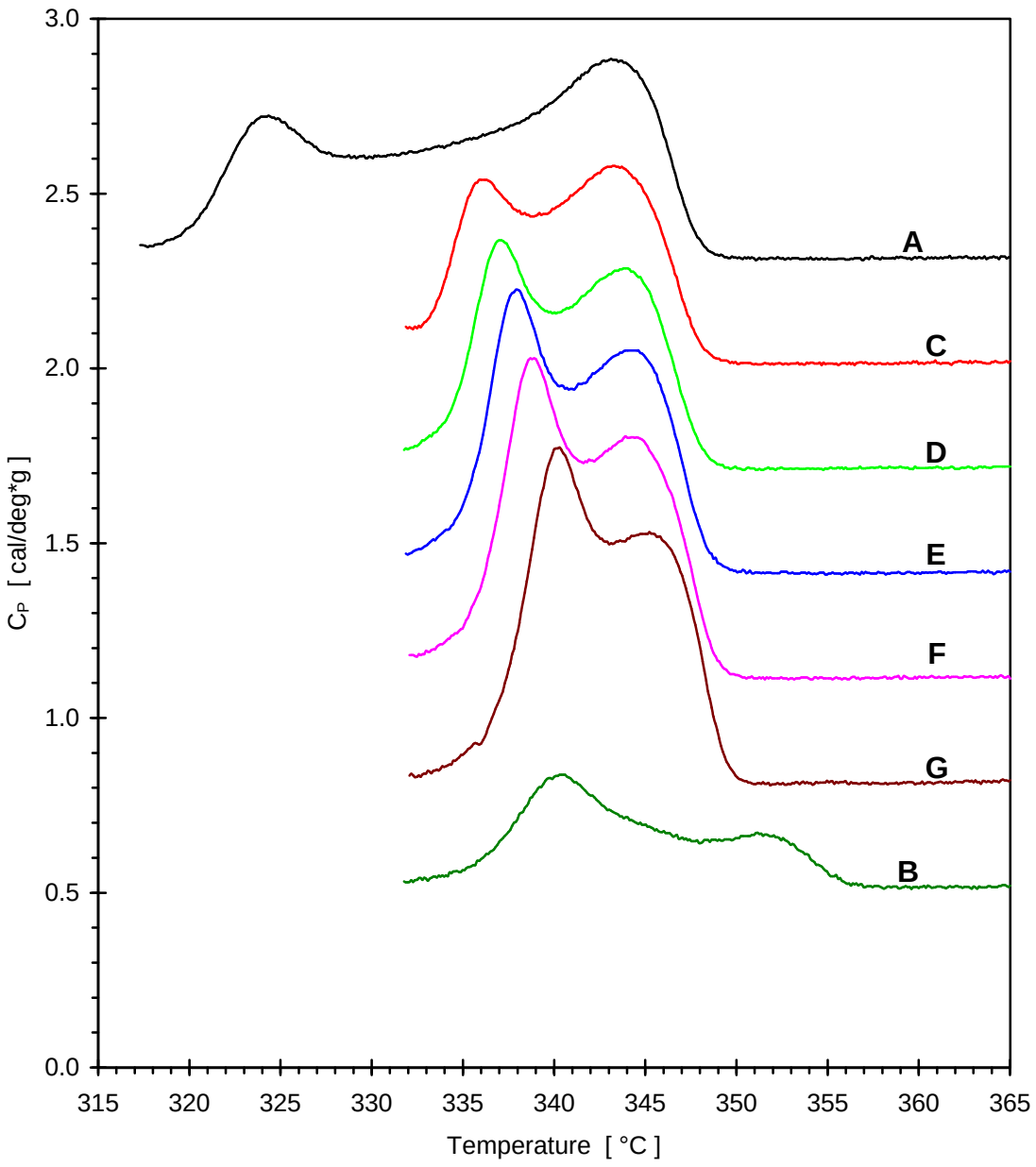


**Figure 4.21** DSC melting scans of PEEK samples, isothermally crystallized from the melt at: A) 315°C for 120 min, B) 330°C for 488 min; C-G - isothermally crystallized at 315°C for 120 min and annealed at 330°C for the following times: C) 1.9 min, D) 7.5 min, E) 30 min, F) 120 min, G) 497 min.

produced when the isothermal crystallization at 315°C for 120 min is followed by annealing at 330°C for various times. This amounts to interrupting melting scan (A) at a point after the low temperature peak and annealing there. The resulting scans have a high temperature melting endotherm, which is at the same position as the one produced from the isothermal crystallization at 315°C alone. The annealing at 330°C introduces an additional, low temperature, endotherm, which shifts up in position an increases in magnitude in a similar fashion as the one, resulting from isothermal crystallization alone (figure 4.18). Scan (G), which is the result of $t_a$ = 497 min can be compared against scan (B), which results from isothermal crystallization from the melt at 330°C for approximately the same time - $t_x$ = 488 min. Isothermal crystallization at 330°C is limited by the slow nucleation from the amorphous melt. The result is a small melting endotherm with $T_m^{'}$ = 351°C, positioned in accordance with the Hoffman-Weeks analysis of the melting temperature of PEEK (figure 4.2). There is also a broad low temperature endothermic peak, which is the result of the long annealing during the crystallization process. Its $T_{max}$ is close to that of the low temperature peak produced by annealing of the same duration at 330°C - scan (G).

Another important result is, that annealing times as low as 1.9 min (110 s) still produce a low temperature endotherm. This result and additional studies in our laboratory (not reported here) lead to the conclusion that, for all practical purposes, the induction time for development of the low temperature endotherm is zero, when annealing of already semicrystalline PEEK is investigated. This is in sharp contrast with the isothermal crystallization results (figures 4.17 - 4.19), which showed, that induction times as high as 100-200 min are observed.

Figure 4.22 compares the development of the peak maximum position of the low temperature endotherm - $T_{max}$(low), for samples, isothermally crystallized or annealed at one and the same temperature. A linear relationship between $T_{max}$(low) and log(t) is observed over three decades of time for the samples, annealed up at 320°C and 330°C. The correlation between the datapoints is much better, than for the isothermally crystallized samples at the same temperatures. This is probably due to the fact, that the induction time for the annealed samples is practically zero and, therefore, does not produce large errors in the positions of the

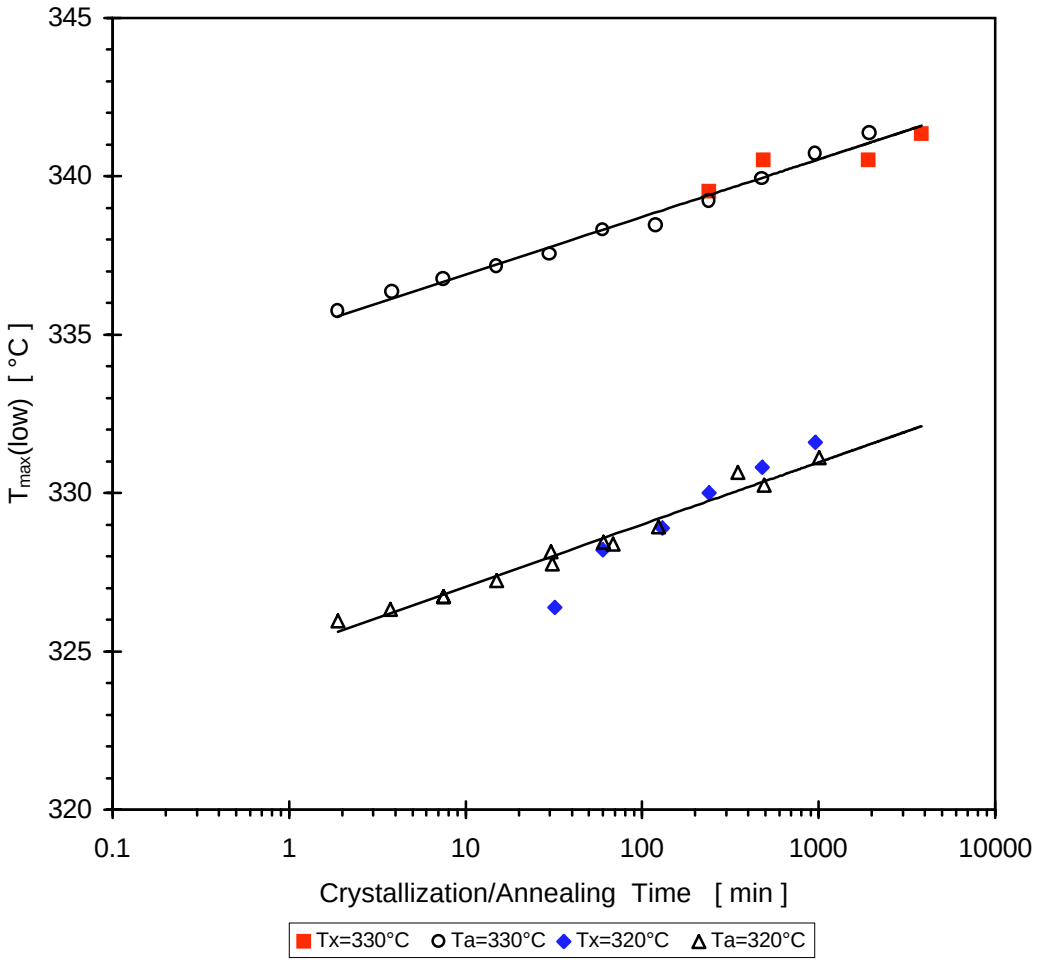


**Figure 4.22** Development of $T_{max}$(low) with time for PEEK samples, isothermally crystallized from the melt at 320°C and 330°C, and samples, crystallized from the melt and annealed up: {$T_x$ = 300°C/$t_x$ = 30 min, $T_a$ = 320°C}; {$T_x$ = 315°C/$t_x$ = 120 min, $T_a$ = 330°C}.

datapoints on the abscissa. If an induction time of 20 min is subtracted from the values of $t_x$ for the samples with $T_x$ = 320°C, this corrects the curvature of their $T_{max}$(low) vs. log($t_x$) relationship to a straight line, coincident with that for the samples, annealed at 320°C.

Thus, the prolonged annealing of semicrystalline PEEK either during the isothermal crystal growth or after an initial pre-crystallization produces a low temperature endothermic peak in the melting scan. The position of the peak seems to be unaffected by the previous thermal history and is controlled only by:

- the required presence of crystallinity,

- the temperature of annealing or crystallization,

- the time of isothermal treatment at this temperature.

The difference in the conditions, prior to the isothermal treatment, results only in differences in the shape of the peak and in its enthalpy.

Figure 4.23 shows the DSC heating scans of PEEK samples, resulting from isothermal crystallization at 305°C, followed by multiple step annealing down at steps of 30 K. The scan in figure 4.23-A is for constant crystallization or annealing times of 30 min. In figure 4.23-B the annealing time at every step down in temperature is increased several times relative to the annealing time at the previous step in order to increase the magnitude of the multiple peaks, resulting from the annealing at lower temperatures. The time at the first step, which is effectively isothermal crystallization from the amorphous melt, is long enough to allow for almost complete primary crystallization. If this condition is not satisfied, the result of a multiple annealing down is rather complicated.

Figure 4.24 shows the DSC melting scans of samples from fraction PEEK4-5 (18.2 K), which have been isothermally crystallized from the melt in a two-step process. The two crystallization temperatures are 325°C and 310°C. Scans A and B correspond to isothermal crystallization for two different times at 310°C - 11 min and 20 min, and annealing up at 325°C for one and the same time - 154 min. The shorter time at 310°C - 11 min, allows very little crystallization at this temperature. The crystallization of the sample is completed at 325°C during the 154 min annealing. This scenario is indicated by the presence of two

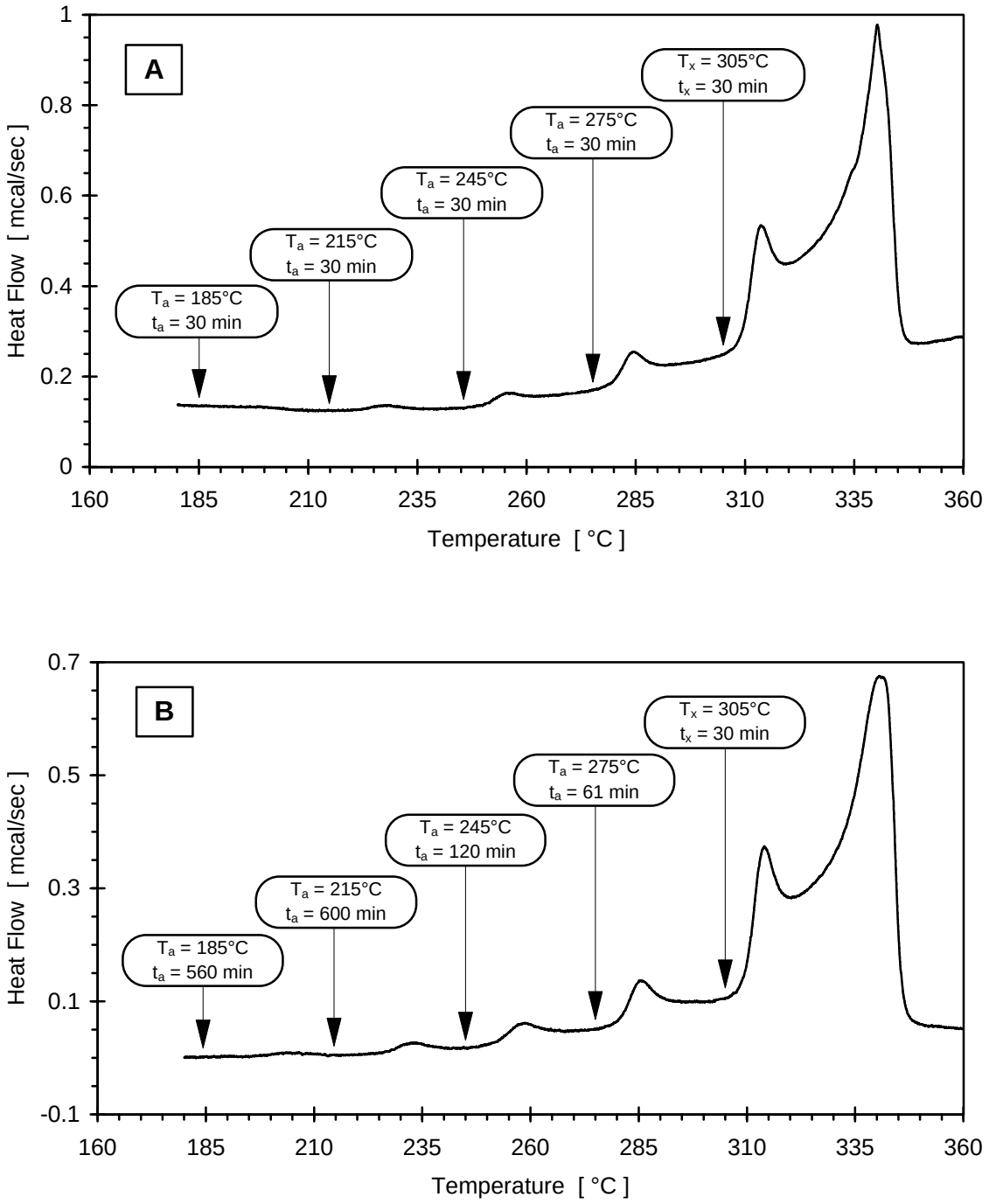


**Figure 4.23** DSC melting scans of PEEK samples, isothermally crystallized from the melt at 305°C for 30 min and annealed down at several temperatures: A) $t_a$ = 30 min, B) $t_a$ is increased as $T_a$ decreases.

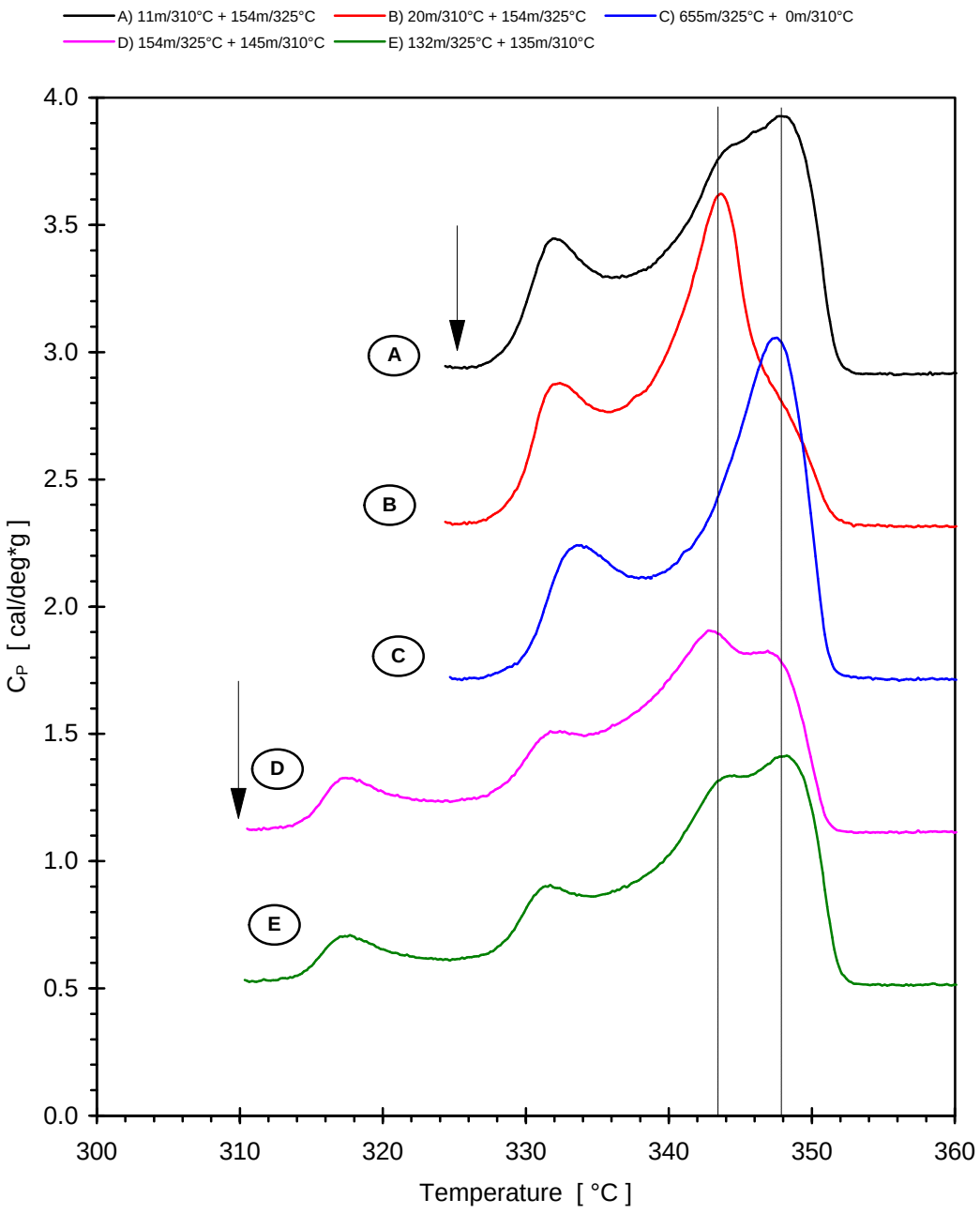


**Figure 4.24** Two-step crystallization from the melt at the indicated sequence of crystallization temperatures and times.

peaks in the broad high temperature part of the scan. Their positions correspond to the Hoffman-Weeks dependence of $T_m^{'}$ on $T_x$ for this fraction (figure 4.3-B). The low temperature peak is the result from the long annealing at 325°C during the long crystallization at this temperature. In scan B the longer crystallization time at 310°C has lead to crystallization of most, but not all of the sample. Some additional crystallization has occurred at 325°C. This can be detected by the small shoulder on the high temperature side of the strong peak, corresponding to the melting for $T_x$ = 310°C. The intensity and position of the low temperature peak in this scan are the same as in scan A as the crystallization time at 325°C for both samples is the same.

Scan C shows the melting of sample, which has been isothermally crystallized at 325°C for a long time - 655 min. $T_m^{'}$ is the same as the one observed in scan A and the low temperature peak has a higher $T_{max}$ and higher enthalpy, due to the longer crystallization time.

In all of scans A-C no low temperature peak is observed for the crystallization at 310°C. This is due to the fact, that the second crystallization step is done above the $T_{max}$(low) expected for the crystallization at 310°C.

In scans D and E the order of crystallization is reversed. The sample is first crystallized at 325°C for times close to those in scans A and B, and then annealed below at 310°C. The crystallization is interrupted at 325°C and completed at 310°C. $T_m^{'}$ of the two high temperature peaks again can be identified as those expected from the Hoffman-Weeks plot for the fraction. The difference between these two scans and the previous ones is in the observation of two low temperature peaks - one for the crystallization at 325°C and another one below it for the crystallization at 310°C. A sharp difference is observed in the intensities of the 325°C low temperature peaks in scans A-B vs. scans D-E. This can be explained by the fact, that during the annealing at 325°C, the first two samples had higher degree of crystallinity as the crystallization was completed at the early stages of the annealing. In samples C and D the material was not crystallized to its maximum attainable crystallinity as obviously crystallization continued at 310°C.

In summary, up to four endothermic peaks can be observed in the melting scans of samples, subjected to a two-step thermal history. These can be identified as two high temperature melting peaks and one or two low temperature peaks. Their time and temperature behavior is as expected from the known behavior of $T_m^{'}$ and $T_{max}$(low) with time and temperature of isothermal treatment.

The scans in figures 4.23 and 4.24 show, that annealing down after initial isothermal crystallization produces an endothermic peak, which is similar in nature to the one observed after isothermal crystallization from the melt or cold-crystallization from the amorphous glassy state. The peak increases in magnitude and shifts up in temperature with increasing time as observed in both experiments shown on figures 4.18 and 4.21 - isothermal crystallization and crystallization followed by annealing up. The presence of up to four endothermic peaks as in figure 4.24 can complicate enormously the task of resolving the enthalpies and $T_{max}$ for the low temperature peaks. Thus, in order to simplify the analysis, in all two step experiments the initial crystallization step was chosen long enough, so that primary crystallization is almost completed.

Upon annealing down (figure 4.23) the low temperature endothermic peak is much smaller in magnitude and the multiple peaks present can be well resolved in order to determine the local baseline for each of them, only if a proper choice of the parameters for the experiment (two-step crystallization, followed by annealing down) is made.

The results from such an experiment are presented in figures 4.25 - 4.27. The conditions of the experiment are as follows. The initial material was pressed into 0.5 mm thick sheets and isothermally crystallized from the melt at 310°C for 300 min in a Pasadena SP210C hot press. This was done in order to avoid prolonged crystallization in the DSC for each separate sample, which would have prolonged the experiment. The temperature of the Pasadena hot press is reported as set by the dial of the temperature controller of the press. Small samples were cut from the center of the sheets and annealed separately for different times at the center of a Carver hot press maintained at 210°C. The temperature of the Carver hot press was observed with a thermocouple inserted between the plates of the press. Small variations of the annealing temperature were observed during the annealing. These were

possibly due to variations in the power input, set by the temperature controller of the press. They lead to a temperature control, which is poorer than that of the DSC. The actual annealing temperature is expected to be $T_a$ = 210±2°C. After annealing the samples were fast cooled below $T_g$ in ice-water. DSC scans were then recorded in one batch under the conditions, described in the experimental section (section 3.2.2). The heating rate was 20 K/min. Baseline subtraction and heat flow calibration with sapphire standard were applied.

The heating scans of selected samples from 115°C to 365°C are shown of figure 4.25. As expected, they show:

- a broad glass transition in the range 140°C - 170°C,

- a linear increase of $C_P$ with temperature in the range 170°C-290°C,

- an endothermic peak, superposed on the linear $C_P(T)$ trace in this range, which is the result of the annealing at 210°C,

- an endothermic peak resulting from the isothermal crystallization at 310°C, which is superposed to the broad melting in the interval 290°C - 355°C.

The differences in the position of the low temperature endotherm in the 305°C - 330°C range, which results from the isothermal crystallization, are random with respect to the annealing times at 210°C. A careful examination of the way the samples were cut from the sheet shows that the farther away the sample was from the center of the sheet, the lower the position of this peak was. We know, that the position of the peak is dependent on the isothermal crystallization or annealing temperature. Therefore we can securely claim, that this variation is due to thermal gradient in the Pasadena hot press. Comparison of the DSC scans from unannealed samples and from samples, which have been isothermally crystallized in the DSC for 300 min in the same temperature range (300°C - 310°C), showed, that the actual temperature of isothermal crystallization was 306±2°C. There is no difference in the remaining part of the DSC scans in the melting range above 325°C, therefore we assume, that this variation of $T_x$ would have no effect on the initial crystallinity of the samples and on the development of the low temperature endotherm, which results from the annealing at 210°C. With this in mind, we concentrate on the analysis of the $C_P(T)$ trace in the temperature interval 170°C - 290°C, in the middle of which the second annealing endotherm is observed.

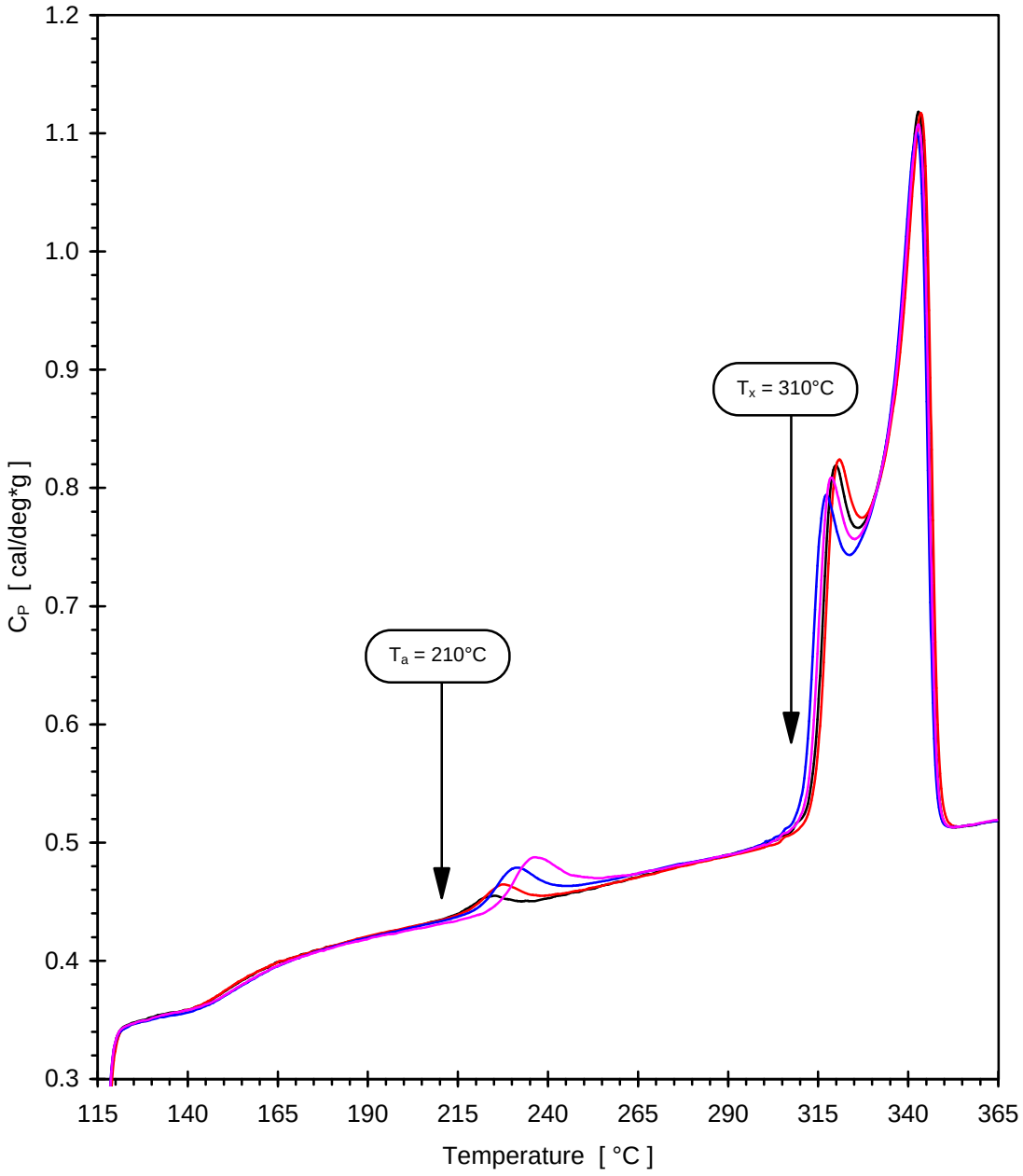


**Figure 4.25** DSC heating scans of PEEK samples, melt-crystallized at $T_x$ = 310°C for $t_x$ = 300 min and subsequently annealed at $T_a$ = 210°C for: 8 min, 30 min, 960 min, and 7680 min.

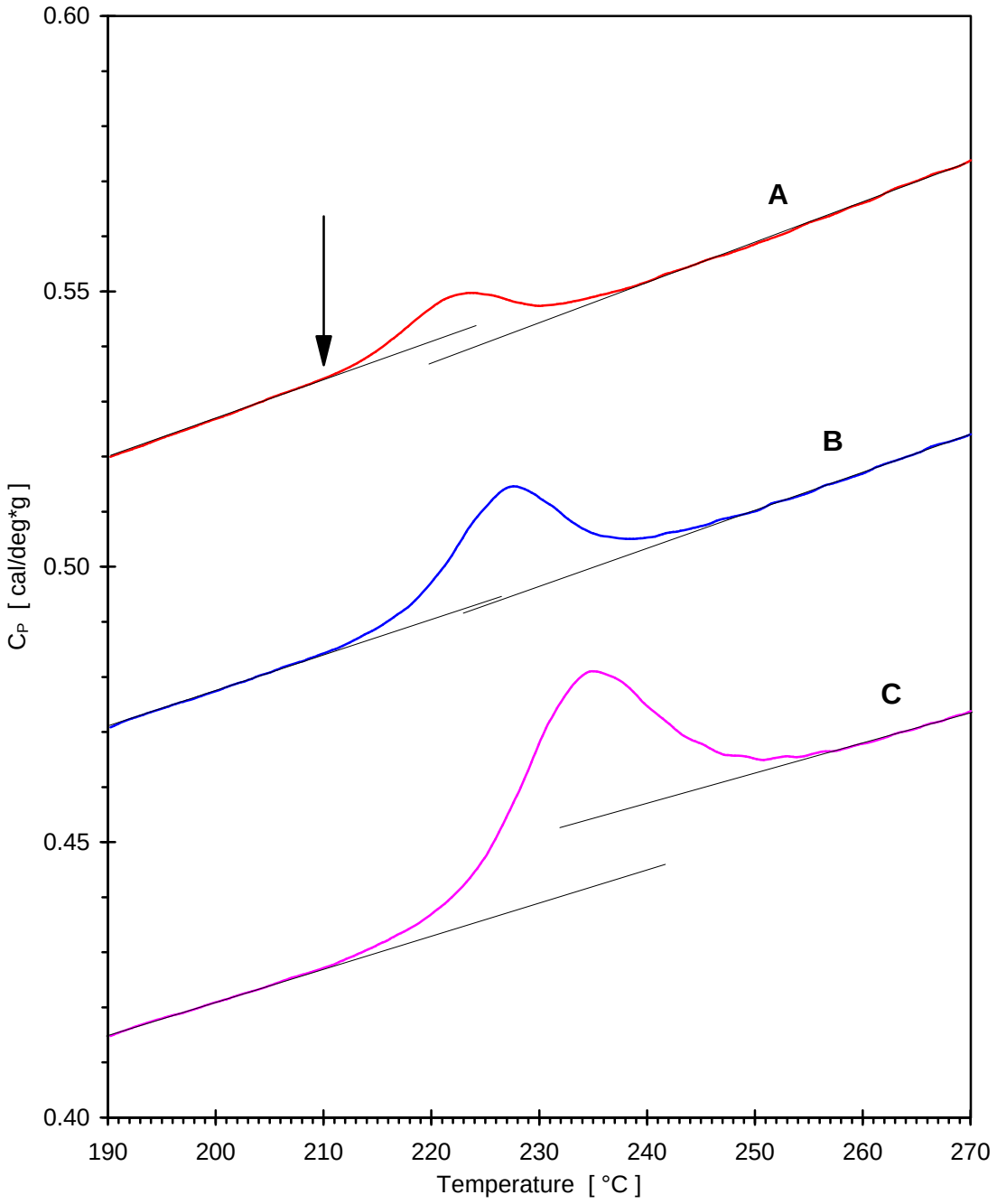


**Figure 4.26** $C_P(T)$ in the vicinity of the low temperature endothermic peak in the melting scans of samples, crystallized for 300 min at 310°C and annealed for short, intermediate, and long times at 210°C. $t_a$ = 4 min (A), 30 min (B), 3843 min (C).

Figure 4.26 shows an expanded view of the scans of selected samples in the 190°C - 270°C temperature range. As can be seen, the $C_P(T)$ traces before and after the peak are linear and to a first approximation have the same slope. This is consistent with the $C_P(T)$ traces expected for a sample, which has a constant crystallinity in this temperature range (i.e. shows very little melting or no melting at all in this range). A clear difference, which is observed between these scans is the vertical shift of the trace after the peak, relative to that before the peak. This shift is different for samples annealed for different times. At short $t_a$ (4 min) the shift is negative, i.e. an exothermic deviation from the trace before the peak, similar to the one observed in cold-crystallized samples, but much smaller in magnitude. At intermediate $t_a$ (30 min) there appears no shift between the extrapolated traces before and after the peak. At long $t_a$ (3843 min) the trace after the peak is shifted significantly upward.

In summary, with increase of annealing time, the relative shift between the linear $C_P(T)$ traces before and after the peak increases in magnitude. At this point we will not comment on the possible reasons for such a shift. We only incorporate this, as an experimental fact, into the quantitative analysis of the low temperature endotherm resulting from annealing at 210°C.

From the observations described above, the following mathematical analysis of the DSC trace in the vicinity of the low temperature annealing endotherm was applied:

The DSC trace in the range of 190°C - 270°C is approximated with the sum of the following functions:

- linear function:

$$f_1(T) = A*T + B \tag{4.4}$$

- symmetrical peak function (see Appendix A at the end of this work):

$$f_2(T) = a * f\left(\frac{T - T_{max}}{b}\right) \tag{4.5}$$

- symmetrical step function, centered at $T_{max}$ (see Appendix B at the end of this work):

$$f_3(T) = a_s * f\left(\frac{T - T_{max}}{b}\right) \quad (4.6)$$

The linear function $f_1(T)$ accounts for the observed linear increase of the $C_P(T)$ before and after the peak.

The symmetrical peak function $f_2(T)$ describes the shape of the peak. It is centered at $T_{max} = T_{max}(low)$, its height at $T_{max}$ is equal to the parameter *a*, and its width is controlled by the parameter *b*. The area of the peak, equal to the its enthalpy $\Delta H_m(low)$ is equal to:

$$\Delta H_m(low) = 2*a*b \quad (4.7)$$

The symmetrical step function $f_3(T)$ is added, in order to account for the relative shift between the linear $C_P(T)$ traces before and after the peak. It is centered at $T_{max}$ and its width is controlled by the same parameter *b* as the peak function $f_2(T)$. In fact the step function is chosen as the derivative of the peak function, scaled by the independent adjustable parameter $a_s$, which controls the magnitude of the relative shift $\Delta C_P(T_{max})$ between the linear $C_P(T)$ traces before and after the peak:

$$\Delta C_P(T_{max}) = 2*a_s*b \quad (4.8)$$

The $C_P(T)$ trace was fitted in the interval 190-270°C (235 datapoints). By variation of the 6 parameters {A, B, *a*, *b*, $T_{max}$, $a_s$} the mean quadratic deviation of the fit from the $C_P(T)$ trace was minimized.

The results from the fitting of the $C_P(T)$ traces of the samples with $t_a$ = 4 min, 30 min, and 3843 min are shown on figure 4.27A-C. The fitted curves are very close to the experimental ones. A good fit was impossible without using a step function with adjustable height of the step. Figure 4.28 shows the annealing time dependence of several of the characteristics of the $C_P(T)$ traces, calculated from the fitted curves: A) $T_{max}(low)$ (left y-axis) and $\Delta H_m(low)$ (right axis), B) peak height and width, and C) the magnitude of the step change $\Delta C_P(T_{max})$.

Samples with the same crystallization history (300 min at 310°C) were annealed also at 240°C and 270°C. The annealing endotherm in their melting scans was analyzed using the same approach as for the samples, annealed at 210°C. The goal of the experiment was to

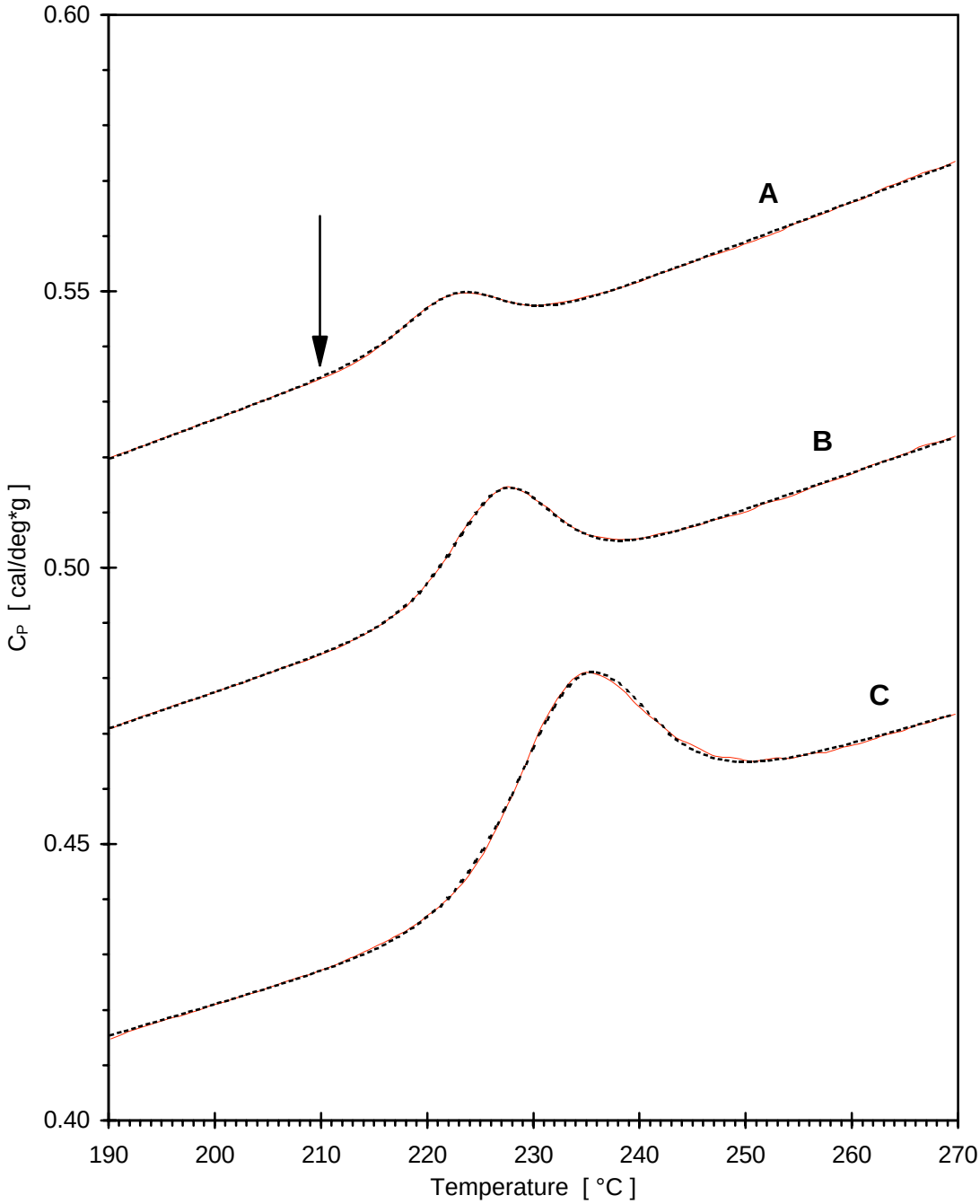


**Figure 4.27** Fitting of the $C_P(T)$ traces in the vicinity of the low temperature peak in the melting scans of samples, crystallized for 300 min at 310°C and annealed at 210°C. Continuous lines - $C_P(T)$, dashed lines - best fit with combination of linear, step, and peak functions. $t_a$ = 4 min (A), 30 min (B), 3843 min (C).

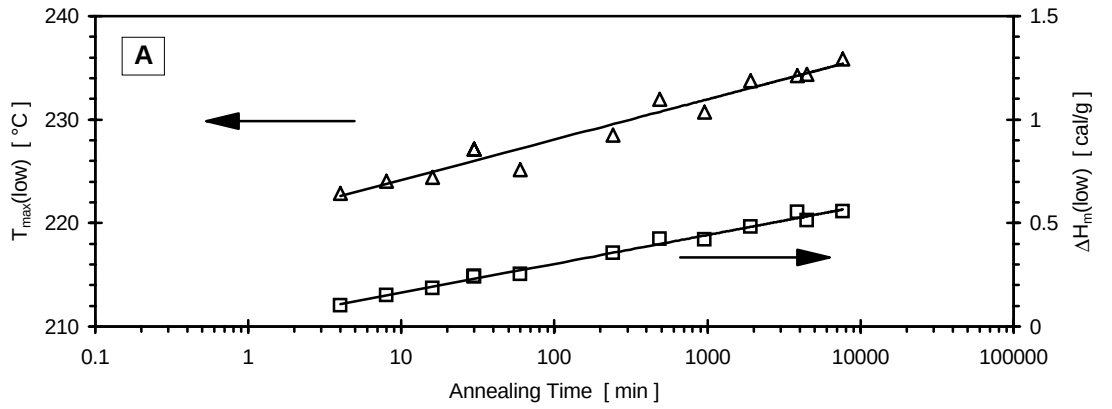


$T_{max}(low) = T_a + 10.3 + 1.6878*Ln(t_a)$ [ °C ]

$\Delta H_m(low) = 0.024 + 0.0606*Ln(t_a)$ [ cal/g ]

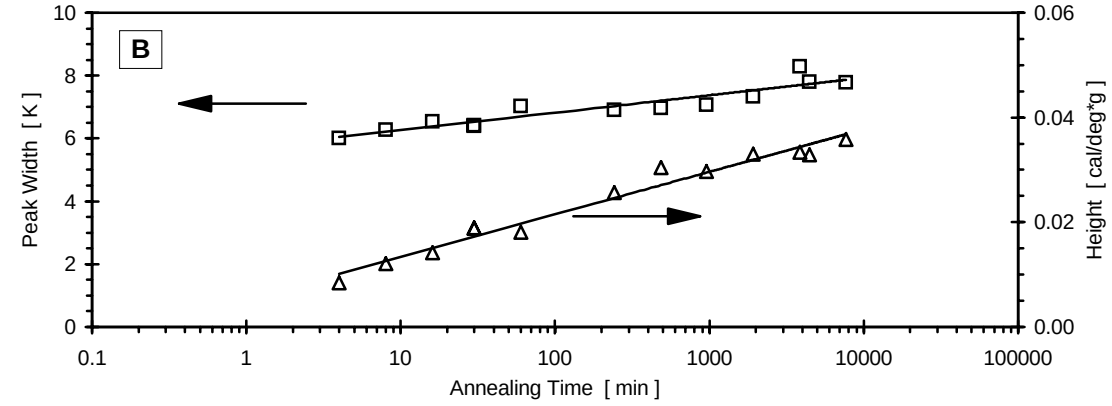


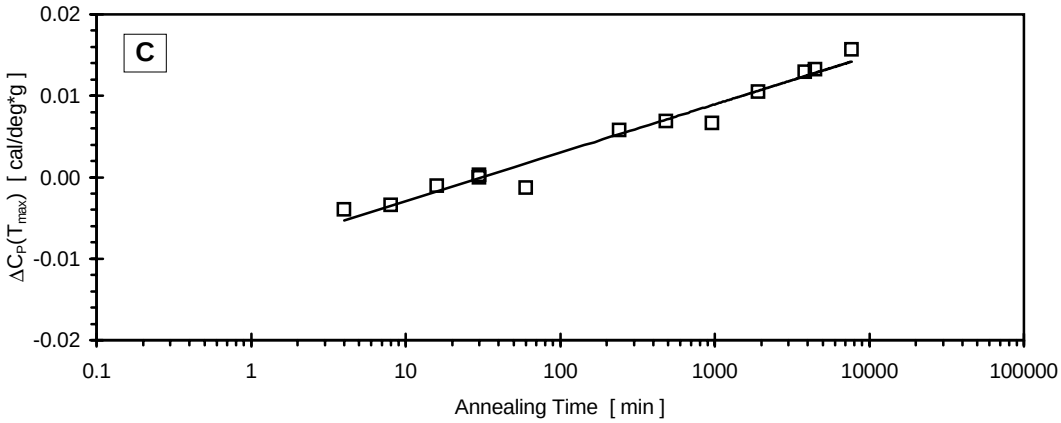


$\Delta C_P(T_{max}) = - 0.0089 + 0.0026*Ln(t_a)$ [ cal/deg*g ]

**Figure 4.28** Annealing time dependence of: A) $T_{max}$(low) and $\Delta H_m$(low), B) peak width and height, C) $\Delta C_P$ change at $T_{max}$(low). Results from fitting the $C_P(T)$ trace of the samples, annealed at 210°C with the sum of linear, step, and peak functions.

look into the dependence of $T_{max}$(low) and $\Delta H_m$(low) on annealing temperature $T_a$ under this particular type of thermal history (figure 3.6).

Figure 4.29 shows the development of the peak parameters with annealing time for the three annealing temperatures. The linear relationship between $T_{max}$(low) and the logarithm of the annealing time is observed under these conditions at all temperatures (figure 4.28-A). The scatter in the datapoints, caused by the fluctuations in $T_a$ in the Carver hot press we mentioned above, does not allow the trend in the changes of the slope and coefficient of the $T_{max}$(low) vs. log($t_a$) relationship to be quantified. The enthalpy of the annealing endotherm $\Delta H_m$(low) also increases linearly with logarithm of the annealing time. The slope of this linear relationship increases with increase of $T_a$. For fixed annealing times, $\Delta H_m$(low) increases with annealing temperature, similarly to the effect of $T_x$ and $T_c$ on $\Delta H_m$(low) (figures 4.14-B and 4.16-B).

The linear increase in the peak height and width with increase in log($t_a$) (figure 4.28-B) is seen at higher annealing temperatures as well. For same annealing times, at higher annealing temperatures the peak is sharper - it becomes narrower and of larger magnitude. The peak height increases (figure 4.29-C) and the peak width decreases (figure 4.29-D) with $T_a$, so that overall the enthalpy $\Delta H_m$(low) increases with $T_a$. The step-change in the baseline is present and changes with increase in log($t_a$) at all annealing temperatures (figure 4.29-E). With increase in $T_a$, $\Delta C_P(T_{max})$ increases and for short annealing times turns from negative to positive values.

The datapoints for annealing times longer than 240 min for the series with $T_a$ = 270°C have been excluded from the plots. The reason for this is the merging of the peak, resulting from annealing at 270°C with the one from the crystallization at 310°C. This

did not allow application of the fitting procedure described above.

The successful fitting of the $C_P(T)$ traces for $T_a$ = 210°C and 240°C with sum of linear, step, and peak functions suggests a model for analyzing the parameters of the low temperature endotherm. This model, although only a phenomenological one at this point, should be applied to the analysis of the low temperature peak under any conditions, if the

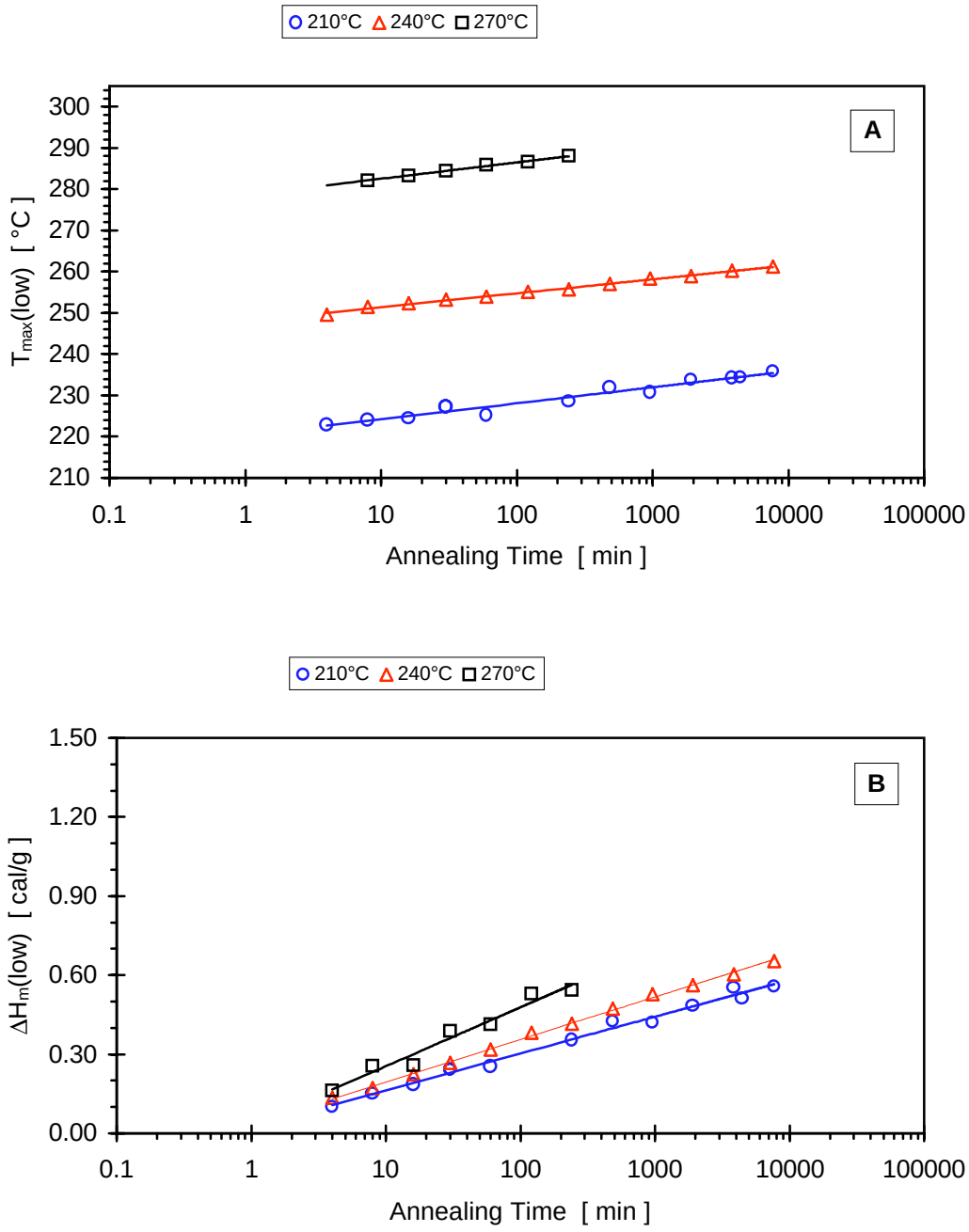


**Figure 4.29** Annealing time dependence of: A) $T_{max}$(low), B) $\Delta H_m$(low), for the samples, crystallized at 310°C for 300 min and annealed at 210°C, 240°C, and 270°C. Results from fitting the $C_P(T)$ trace in the vicinity of the low temperature peak with the sum of linear, step, and peak functions.

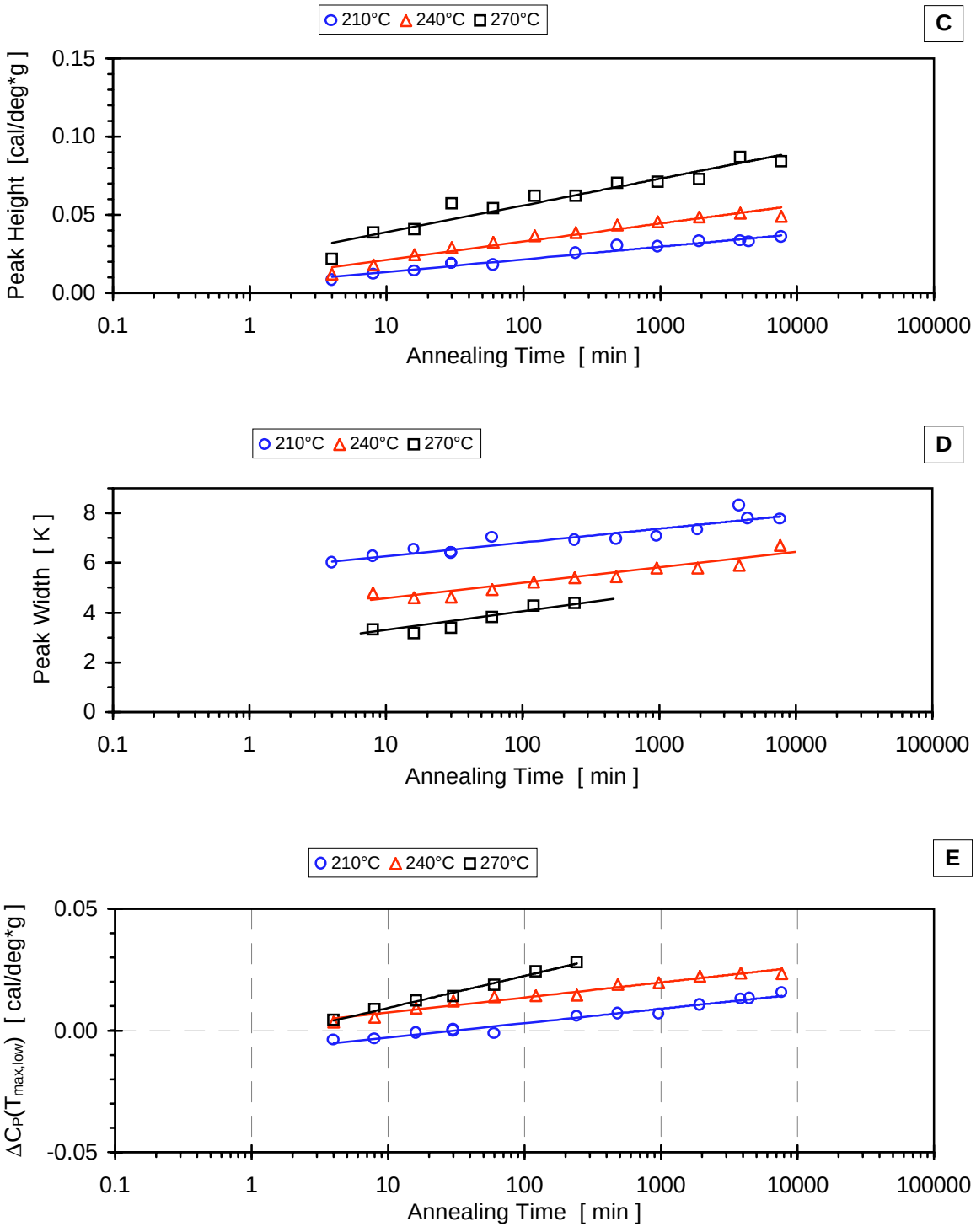


**Figure 4.29**(continued) Annealing time dependence of: C) peak height, D) peak width, and E) $\Delta C_P(T_{max})$ for the samples, crystallized at 310°C for 300 min and annealed at 210°C, 240°C, and 270°C. Results from fitting the $C_P(T)$ trace in the vicinity of the low temperature peak with the sum of linear, step, and peak functions.

correct values for $T_{max}$(low) and $\Delta H_m$(low) are to be derived. Unfortunately, this is difficult to accomplish under most of the experiments described so far. The reason for this is the interference of other phenomena, manifested in the DSC scan of PEEK.

For example, when cold-crystallization or two-step crystallization followed by annealing down is done at temperatures close to $T_g$, the interference of the $C_P(T)$ change at $T_g$ does not allow a good determination of the linear $C_P(T)$ local baseline before the peak. For higher annealing or crystallization temperatures, the peak approaches the beginning of the broad melting range. The peak tail is then superposed to the small endothermic shift of $C_P(T)$ due to melting, which can not be incorporated analytically in the same fashion as in the analysis above. When the crystallization or annealing temperature is above 300°C the peak is superposed on the broad melting endotherm and the entire local baseline can not be resolved analytically.

Thus, depending on the thermal history of the samples, the resulting low temperature endotherm must be analyzed using other, less perfect approaches. One has to eliminate some of the variables of the fitting procedure described above. However, the results above pint out that one characteristic of the analysis must be preserved - the near symmetrical shape of the low temperature endothermic peak. Whenever possible, DSC scans which show low temperature endothermic peak, were analyzed in the manner described above. When this was not feasible, the analysis was done by searching for the best peak function (hyperbolic cosine type function), the subtraction of which from the DSC trace leads to a $C_P(T)$ trace, which behaves smoothly with temperature. The estimate is visual and therefore much less rigorous. The following procedure was used:

We start with a $T_{max}$ value, close to the visually observed and use some starting values for the peak height and width. The calculated values for the peak function are subtracted from the DSC trace. If the peak height is lower or higher than the true peak height, than a characteristic upward or downward deviation of the $C_P(T)$ trace is observed, which disrupts the smooth change of the "local baseline" in the temperature interval, where the peak is observed. To a first approximation, this deviation is a symmetrical peak function. If the peak width is lower or higher than the true peak width, than another type of deviation is observed

after subtraction. By adjusting the peak height and width and "fine tuning" the position of the peak maximum, we try to minimize these deviations in the $C_P(T)$ trace after subtraction of the peak function. The values of $T_{max}(low)$ and $\Delta H_m(low)$, reported in figure 4.16 and the high and low $T_c$ values, reported on figure 4.14 are analyzed with this procedure. In addition to the series annealed at 210°C, 240°C and 270°C, the intermediate $T_c$ values, plotted on figure 4.14 are analyzed by the analytical approach described before.

### *4.2.2 Multiple Melting of Other Polymers*

The results reported in the previous section summarize most of the unique features of the low temperature endothermic peak, observed in PEEK under the various conditions of isothermal crystallization and or annealing we defined in section 3.2.2 (figures 3.3 - 3.7). Even considered alone, these results pose a variety of questions regarding the melting behavior of PEEK.

In the introduction, it was mentioned that a low temperature endothermic peak resulting from long crystallization or annealing is observed in the melting scans of various other polymers. In this section, few examples are provided which examine the time dependence of the low temperature endotherm for other polymers.

After the observation of the peculiar log-time dependence of the parameters of the low temperature endotherm in PEEK, studies in our lab have shown, that the same log-time dependence is observed for the low temperature endothermic peak in cold-crystallized isotactic PS. [50]

Figure 4.30 shows the heating scans of isotactic PS, melt-crystallized in the DSC at 180°C. The melting range of the scan is characterized by the presence of 3 endothermic peaks. The superposition of all $C_P(T)$ traces together shows, that annealing time causes very little or no change at all in the positions and magnitudes of the highest two endothermic peaks. Lemstra et al. [48] have shown, that the presence of these two peaks is due to a melting-recrystallization process during the heating of i-PS. They provide very little information on third peak in the scan - the one, which appears just above the isothermal crystallization

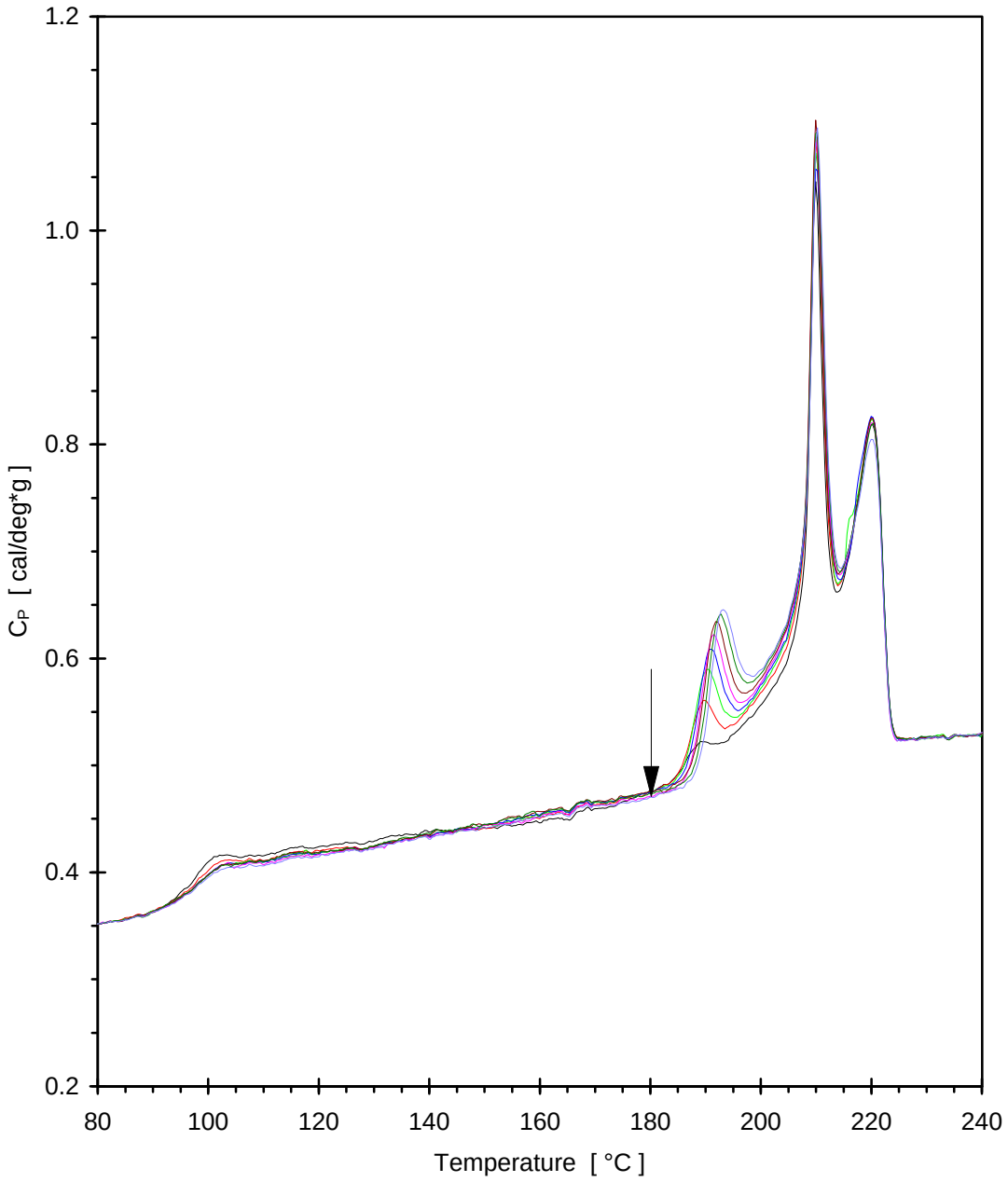


**Figure 4.30** Melting scans of i-PS samples, melt-crystallized in the DSC at 180°C for the following crystallization times: 15 min, 30 min, 60 min, 120 min, 240 min, 484 min, 1010 min, 1920 min. Heating rate 10 K/min.

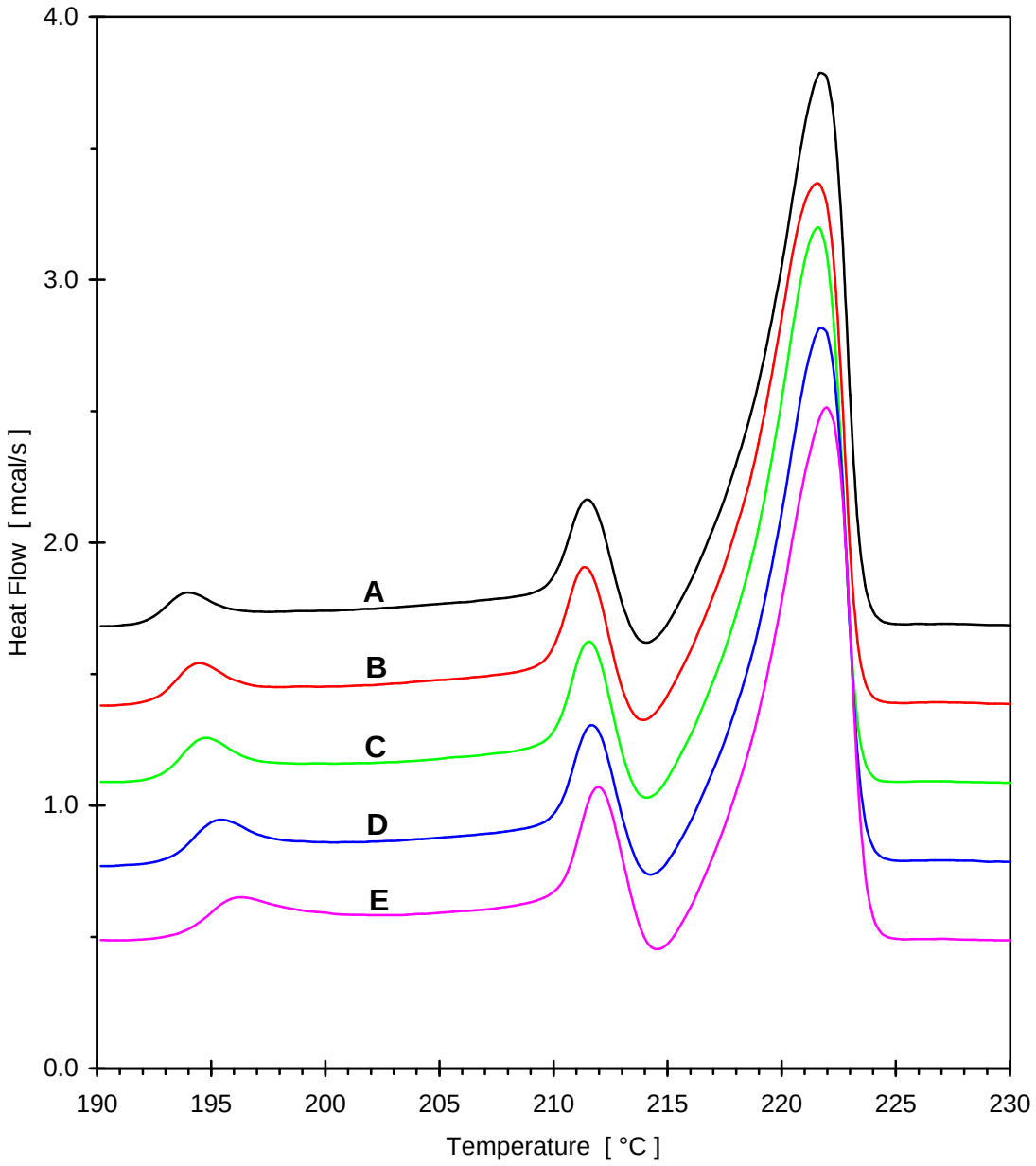


**Figure 4.31** Melting scans of PBT samples, melt-crystallized in the DSC at 190°C for the following crystallization times: A) 4 min, B) 8 min, C) 15 min, D) 30 min, E) 60 min. Heating rate 10 K/min.

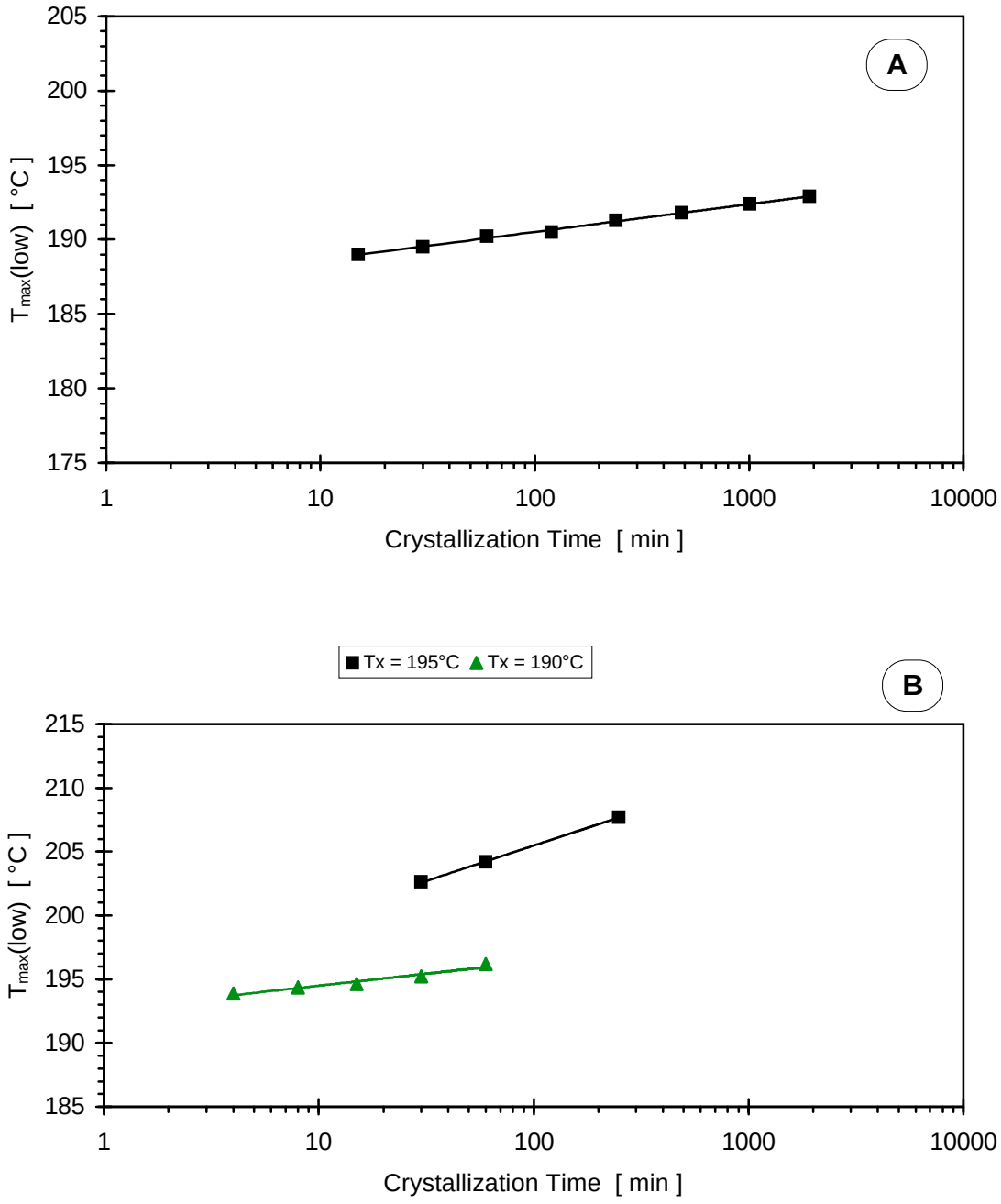


**Figure 4.32** Crystallization time dependence of $T_{max}$(low) in the DSC melting scans of: A) i-PS, melt-crystallized at 180°C, B) PBT, melt-crystallized at 190°C and 195°C.

temperature. Figure 4.30 shows, that this peak steadily increases in magnitude and shifts to higher temperatures as time is increased by a factor of 2.

Figure 4.31 shows the melting scans of PBT, melt-crystallized in the DSC at 190°C. As in the case of i-PS, three endothermic peaks are observed. Those in the range 205°C - 235°C are separated by an exothermic peak, which indicates, that melting-recrystallization takes place. Their positions and magnitudes are not affected by the crystallization time. In the region just above $T_x$ a third endothermic peak is observed, which shows the same characteristic behavior as the low temperature endothermic peak in PEEK and i-PS.

Figure 4.32 shows the dependence of the peak maximum of the low temperature endotherm on crystallization time for i-PS and PBT. A linear relationship between $T_{max}$(low) and log($t_x$) is observed, similarly to the case of PEEK.

Although limited in scope, this investigation of the crystallization time dependence of the low temperature endotherm for i-PS and PBT unequivocally shows the universality of this phenomenon. Currently, a more detailed investigation of two other polymers - i-PP and PET is under way in our laboratory. Preliminary results are similar to the evidence provided in this work.

### *4.2.3 Crystallinity Evaluation*

The results presented in section 4.2.1 show that long crystallization or annealing leads to a significant increase in the enthalpy of the low temperature endothermic transition without significant change of the high temperature melting peak. In view of this observation, we took on the task of studying changes in other physical properties over the same time and temperature scales as the ones, employed for monitoring the low temperature endotherm. In this section we will consider the increase in the crystallinity, associated with the development of the low temperature endotherm.

### *4.2.3a DSC and Uncorrected Density Crystallinities*

The effect of crystallization temperature on the DSC crystallinity of PEEK and in particular on the crystallinity associated with the low temperature melting peak has already

been examined in the literature, but only qualitatively. [16-18, 66, 72] Only one study has attempted to separate the crystallinity associated with the low temperature endotherm from the overall crystallinity. [16] Despite the clear evidence for crystallization temperature dependence of the crystal density $r_c$, [122, 123, 198] there has been no attempt to account for it in the evaluation of crystallinity by the density method. As only few studies have acknowledged the annealing time dependence of the low temperature endotherm and only in a qualitative way, [66, 70, 72, 76] it is understandable that no attempt have been made to study the effect of crystallization time on the crystallinities.

Figure 4.33 shows a semilogarithmic plot of the change of crystallinity with crystallization time $t_x$ for the series of samples, melt-crystallized at $T_x$ = 300°C. The crystallization temperature was chosen as the lowest possible temperature at which crystallization after quenching from the melt proceeds isothermally. The data shows an increase in the DSC crystallinity with time - (A). The magnitude of this increase is on the order of 0.04. This increase in crystallinity is associated with the increase in the enthalpy of the low temperature endotherm - (C). The uncorrected density crystallinity - (B), exhibits a smaller increase in the time range considered - about 0.015.

An attempt to evaluate the WAXS crystallinity of the samples by the method of Hermans and Weidinger was made - equation (3.9). The WAXS diffractograms are shown on figure 4.34 and the crystallinities $c_c^{WAXS}$ on figure 4.33 - (D). The uncertainty of $c_c^{WAXS}$ by the method of Hermans-Weidinger is generally considered to be high as the method is an approximate one. [6] In this case the uncertainty appears to be larger than the overall magnitude of change observed in the DSC and density (uncorrected) crystallinities. Studies are currently undertaken for evaluation of the absolute WAXS crystallinity by the more accurate, but also more demanding, method of Ruland. [125]

The data on figure 4.33 clearly shows a discrepancy between the magnitudes and rates of increase of the DSC and density crystallinities. The semilogarithmic rates of increase of crystallinity from the DSC and density data are respectively 0.016 per decade and 0.008 per decade. The difference between these two values can not be accounted for by their uncertainties (see the equations on figure 4.33). As was mentioned in the experimental

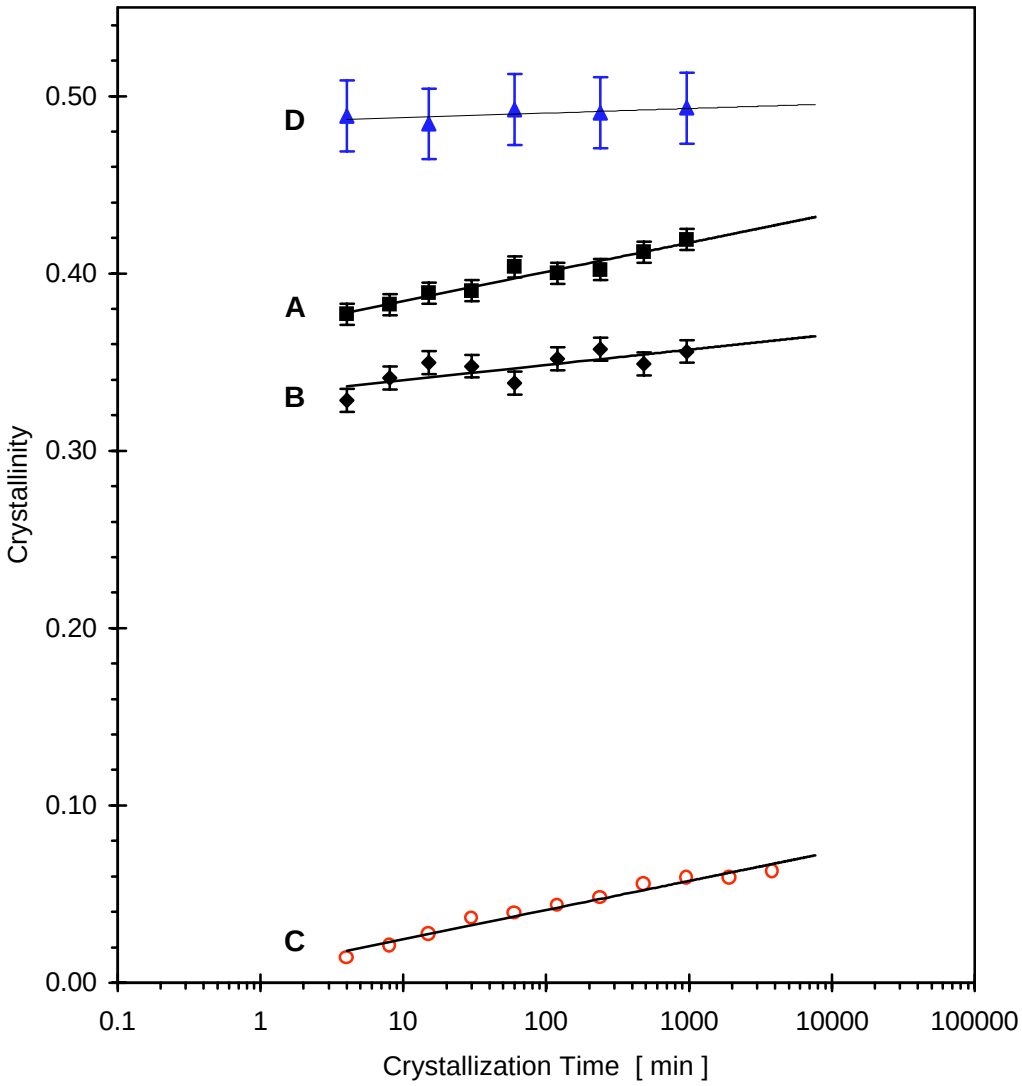


$\chi^{DSC} = 0.3679_{\pm 0.0029} + 0.0165_{\pm 0.0015} * \mathrm{Log}(t_x)$

$\chi^{Dens}$ (uncorrected) $= 0.3312_{\pm 0.0054} + 0.0086_{\pm 0.0028} * \mathrm{Log}(t_x)$

**Figure 4.33** Crystallinities of the samples, melt-crystallized at $T_x$ = 300°C: A) DSC crystallinity; B) uncorrected density crystallinity - equation (2.3); C) crystallinity of the low temperature melting peak; D) WAXS crystallinity (Hermans-Weidinger method).

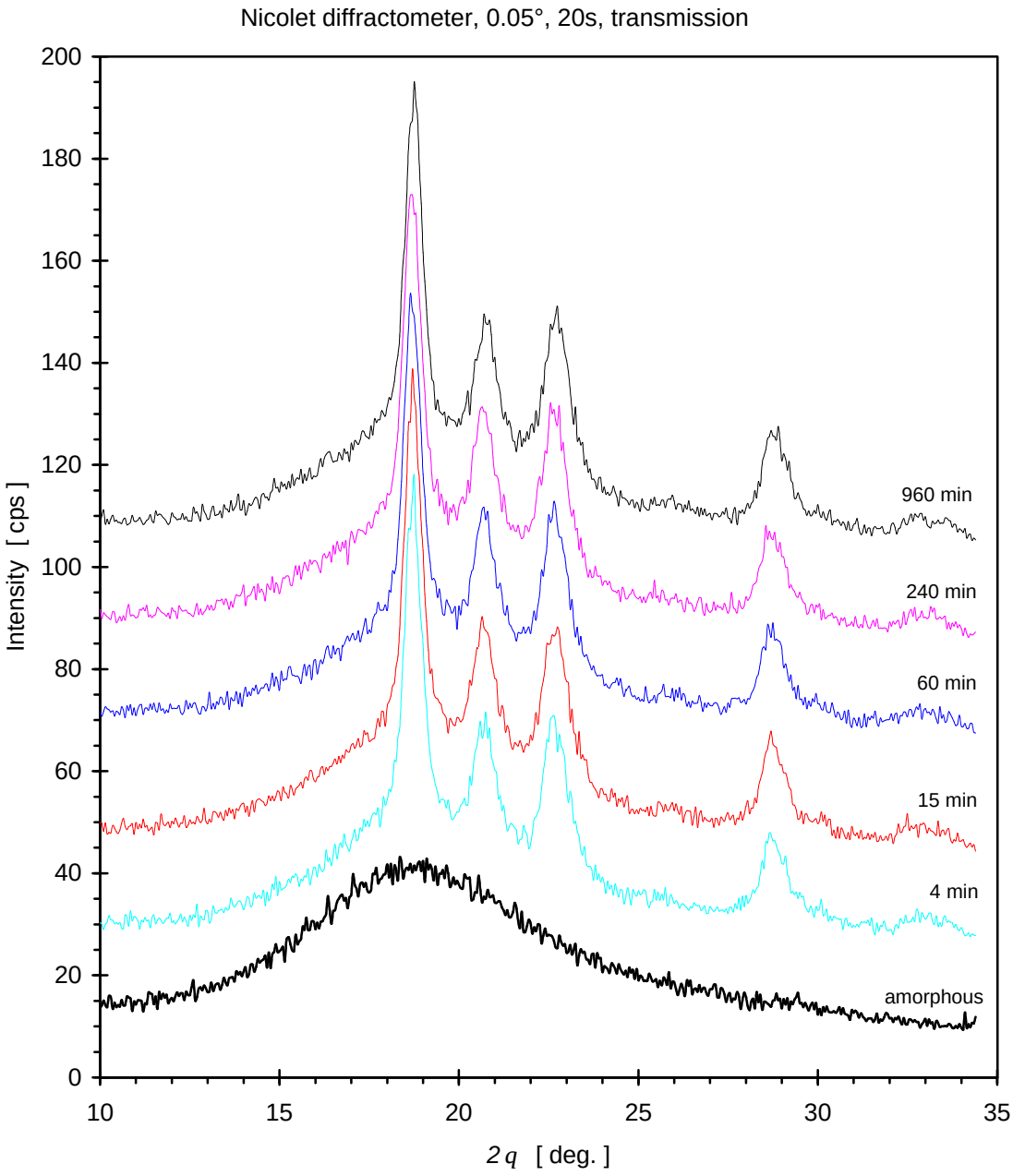


**Figure 4.34** WAXS for crystallinity evaluation of PEEK samples, melt-crystallized at $T_x$ = 300°C for various times $t_x$. Each scan is shifted by 20 cps up from the previous one for clarity.

section there are several problems, which make difficult the calculation of the absolute values of these crystallinities. The absolute values of the reference constants $\Delta H_m^0$, $r_c$, and $r_a$ could differ from these used here ($\Delta H_m^0$ = 31.1 cal/g, $r_c$ = 1.405 g/cm$^3$, and $r_a$ = 1.263 g/cm$^3$; see section 3.2.3). However, such a correction would mostly scale up or down the trends exhibited by the crystallinities and will not affect significantly their time dependencies.

(Note: In section 4.2.3b we will show, that $r_c$ is not a constant in the parametrization of the density crystallinity and determine with sufficient degree of accuracy its variation with annealing time and temperature. This leaves the two lines on figure 4.33 for the DSC and density crystallinities parametrized only by two constants - $\Delta H_m^0$ and $r_a$. In principal it is possible to adjust and make equal the slopes and coefficients of the lines by varying these two parameters. The values, which achieve this, however, are for all practical purposes physically meaningless.)

The results of a single experiment could leave a certain doubt as to whether the discrepancy between $c_c^{DSC}$ and $c_c^{Dens}$ is an artifact due to the particular experimental conditions. As the significant increase in $c_c^{DSC}$ is associated with the increase in the contribution of the low temperature endotherm, a natural choice of an experiment to test whether this is true, is to monitor the development of crystallinity under other conditions, which lead to significant development of the low temperature endothermic peak's enthalpy.

Figure 4.35 shows the change of crystallinity with crystallization temperature $T_c$ for samples, cold-crystallized for $t_c$ = 60 min at various temperatures above $T_g$. Both the DSC crystallinity - (A), and the uncorrected density crystallinity - (B), increase with increase in $T_c$. There is a significant difference between their magnitudes. The rate of increase of $c_c^{DSC}$ with $T_c$ appears to be slightly larger than the rate of change of $c_c^{Dens}$ (uncorrected). The crystallinity contribution of the low temperature endothermic peak increases linearly with increase in $T_c$.

A result similar to figure 4.35 was obtained by taking literature data from DSC and density studies of samples with comparable thermal histories. Uncorrected density

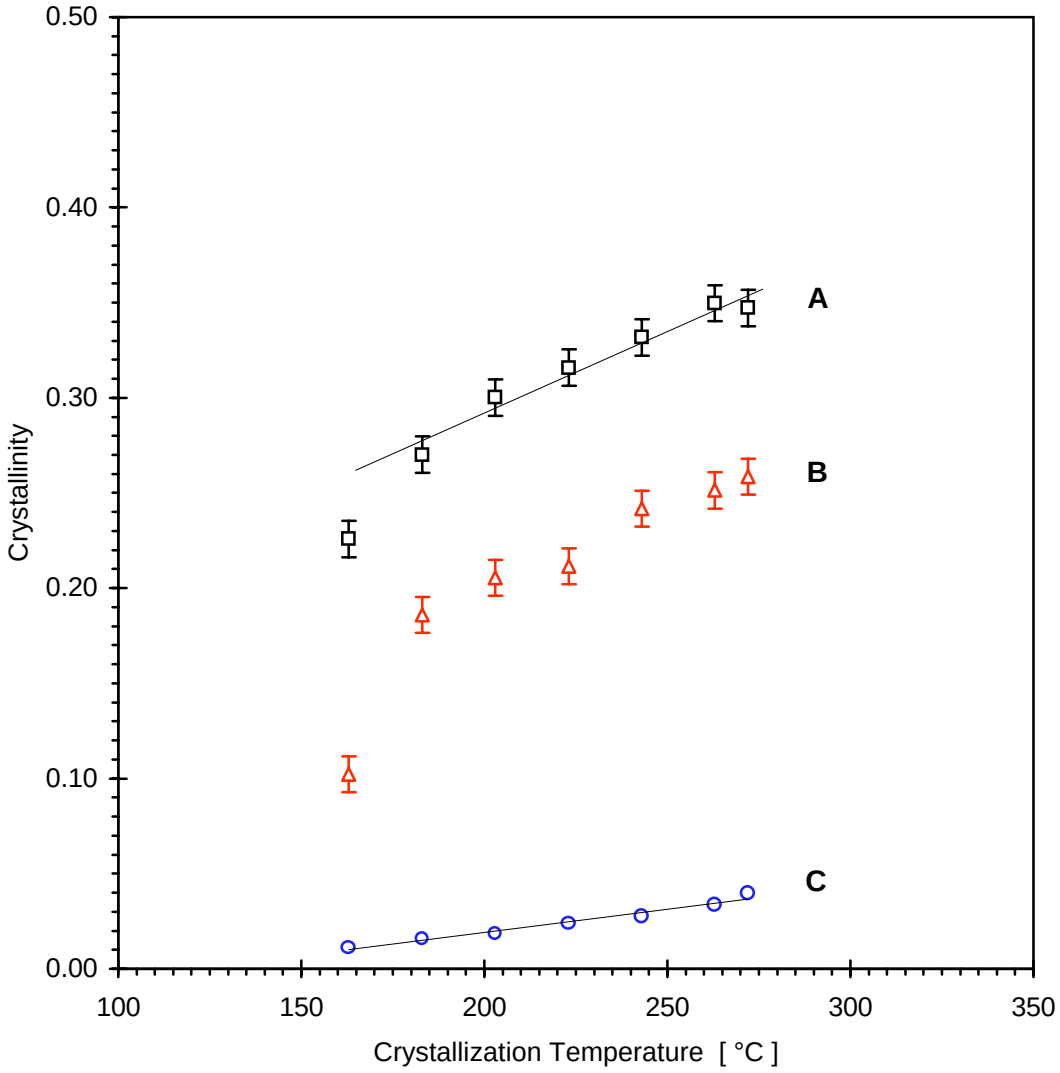


**Figure 4.35** Crystallinities of the samples, cold-crystallized for 60 min at various $T_c$: A) DSC crystallinity; B) uncorrected density crystallinity - equation (2.3); C) crystallinity of the low temperature melting peak.

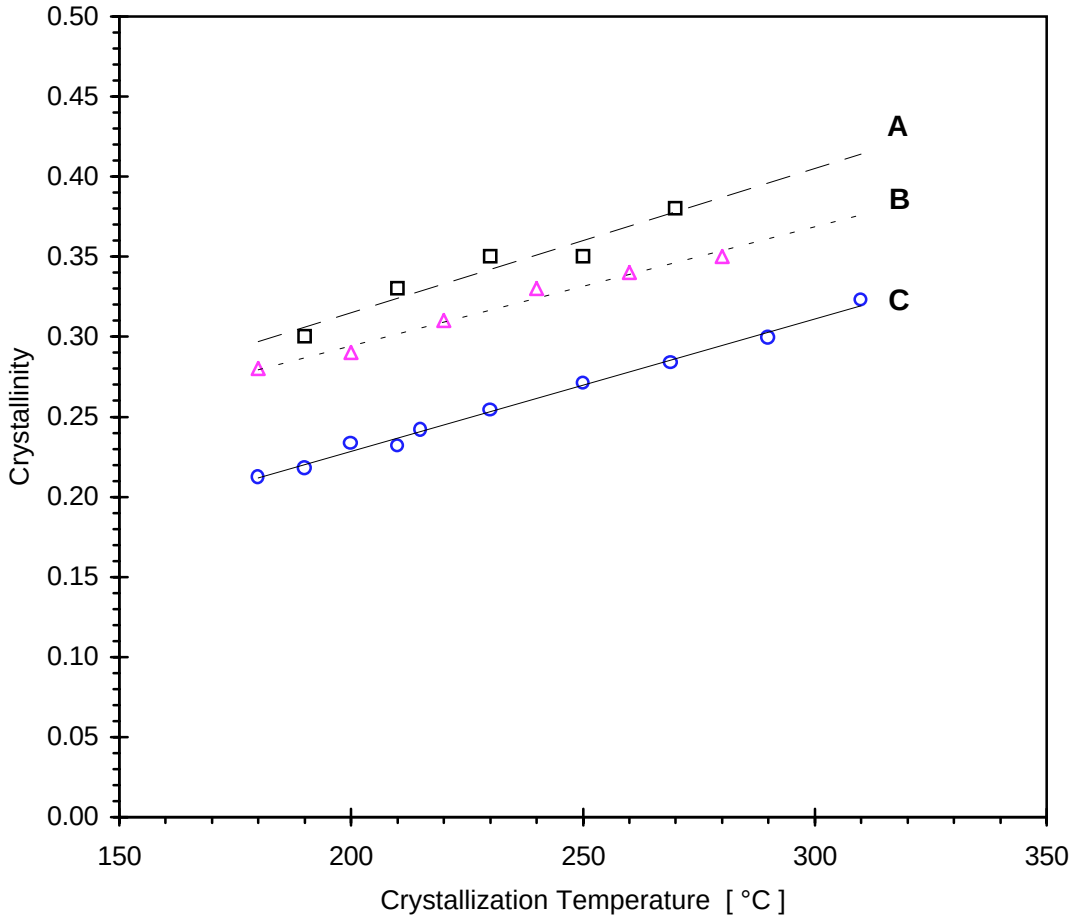


**Figure 4.36** Literature data on crystallinities of PEEK samples, cold-crystallized at various $T_c$: A) DSC crystallinity ($t_c$ = 120 min, Cheng et al. [16]); B) DSC crystallinity ($t_c$ = 60 min, Huo and Cebe [17]); C) uncorrected density crystallinity - equation (2.3), ($t_c$ = 60 min, Lee et al. [65, 66]).

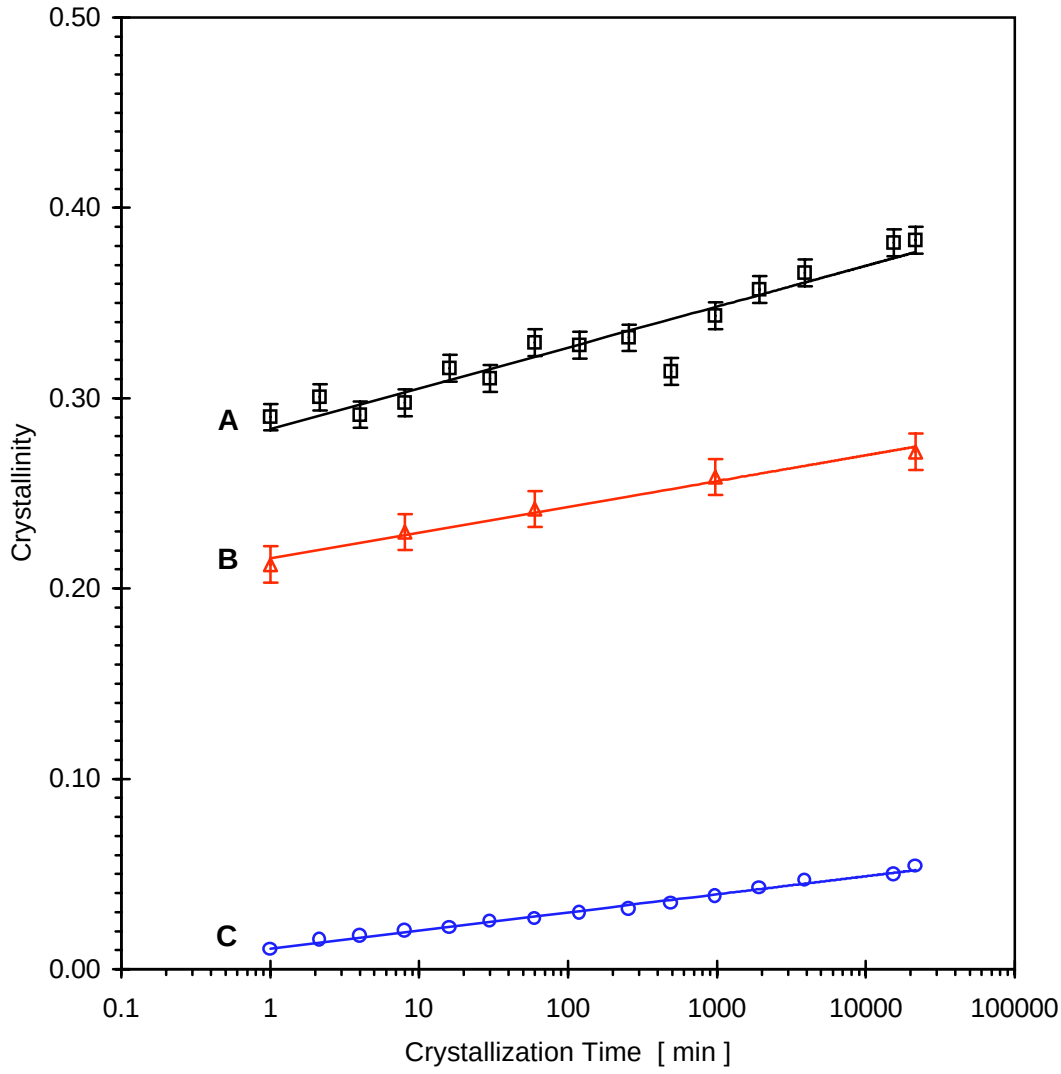


$\chi^{DSC} = 0.2843_{\pm 0.0029} + 0.0221_{\pm 0.0011} * \mathrm{Log}(t_c)$

$\chi^{Dens}$ (uncorrected) $= 0.2158_{\pm 0.0023} + 0.0136_{\pm 0.0009} * \mathrm{Log}(t_c)$

**Figure 4.37** Crystallinities of the samples, cold-crystallized at $T_c$ = 243°C: A) DSC crystallinity; B) uncorrected density crystallinity - equation (2.3); C) crystallinity of the low temperature melting peak.

crystallinity ( $r_c$ = 1.400 g/cm$^3$ and $r_a$ = 1.263 g/cm$^3$) was calculated from the data of Lee et. al. [65, 66] on cold-crystallized samples ($t_c$ = 60 min). DSC crystallinities were taken from the studies of Cheng et al. [16] ($t_c$ = 120 min) and Huo and Cebe [17] ($t_c$ = 60 min). The data is plotted on figure 4.36. It is consistent with the findings of this study.

Figure 4.37 shows a semilogarithmic plot of the crystallinities of samples, cold-crystallized at $T_c$ = 243°C for various crystallization times $t_c$. Again both $c_c^{DSC}$ and $c_c^{Dens}$ (uncorrected) increase with time. The increase of the uncorrected density crystallinity is about 0.06. The magnitude of increase of the DSC crystallinity - (A), over 4.5 decades of time is on the order of 0.09. It is due to the linear increase with log($t_c$) of the contribution of the low temperature endothermic peak - (C). The rates of increase of $c_c^{DSC}$ and $c_c^{Dens}$ (uncorrected) are 0.022 per decade and 0.014 per decade respectively. Therefore, the discrepancy between $c_c^{DSC}$ and $c_c^{Dens}$ (uncorrected) can not be eliminated by rescaling their values through use of different reference constants $\Delta H_m^0$, $r_c$, and $r_a$.

### *4.2.3b WAXS and Crystallinity - Crystal Density from Unit Cell Measurements*

The data presented above already indicates the possibility, that the discrepancy between the DSC and density crystallinities has a fundamental character. This conclusion is enhanced by reevaluation of the density crystallinity. In section 3.2.3b we discussed the origin of this reevaluation - the dependence of the crystallographicaly determined crystal unit cell density on the thermal history of the sample. The dependence of $r_c$ of PEEK on the cold-crystallization temperature $T_c$ has been unequivocally established as a fact by the WAXS studies of Wakelyn [122] and confirmed by Hay et al. [123] and Zimmermann and Konnecke. [198] During the execution of this study, dependence on the crystallization time $t_c$ has been suggested qualitatively by the synchrotron WAXS studies of Jonas et al. [68] In order to be able to apply equation (2.3a) for the corrected density crystallinity, we need to establish quantitatively the rate of "densification" of the crystal unit cell with change of $T_c$ and $t_c$.

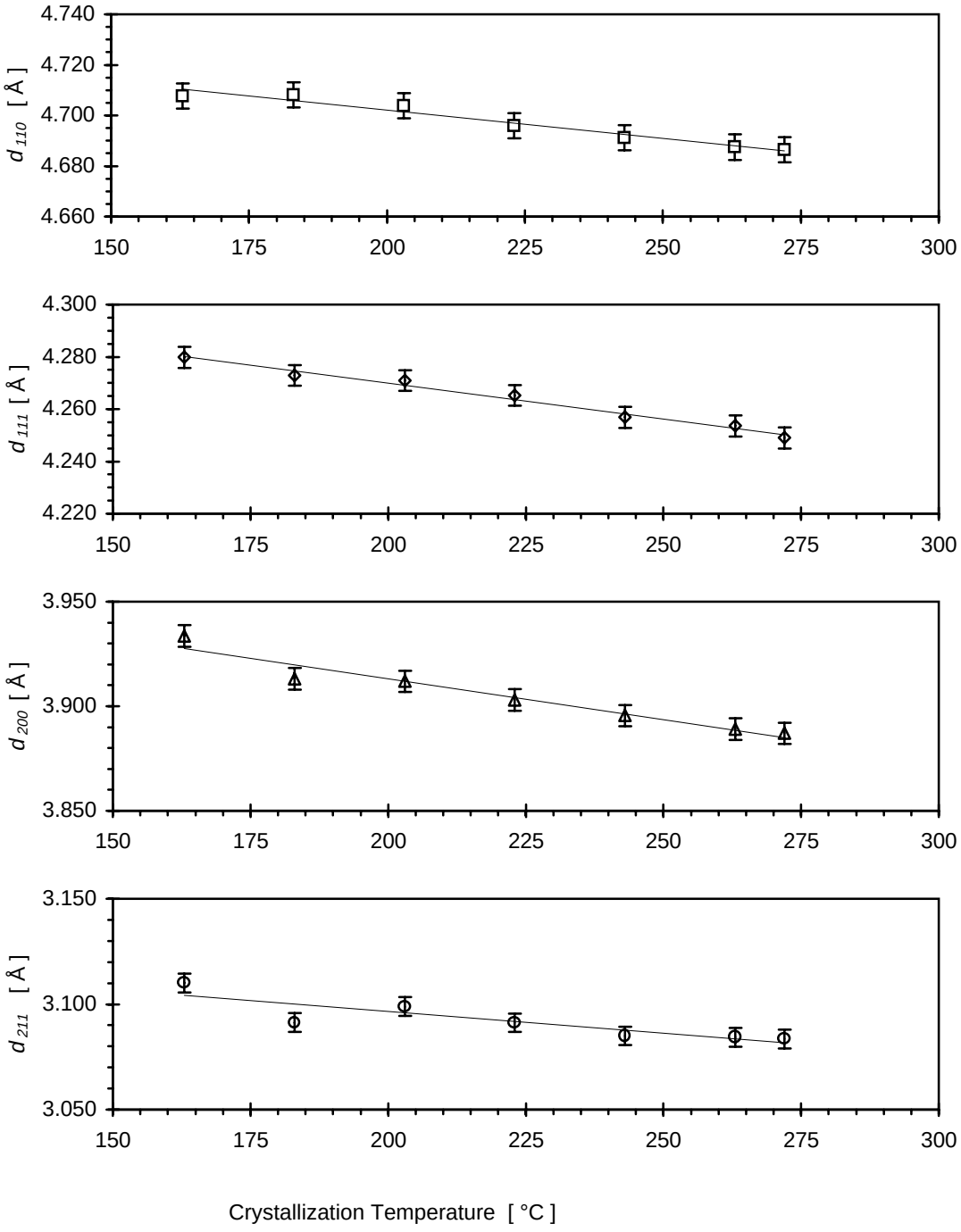


**Figure 4.38** Dependence of the interplanar *d* -spacings on cold-crystallization temperature $T_c$ ($t_c$ = 60 min). From top to bottom: $d_{110}$, $d_{111}$, $d_{200}$, $d_{211}$.

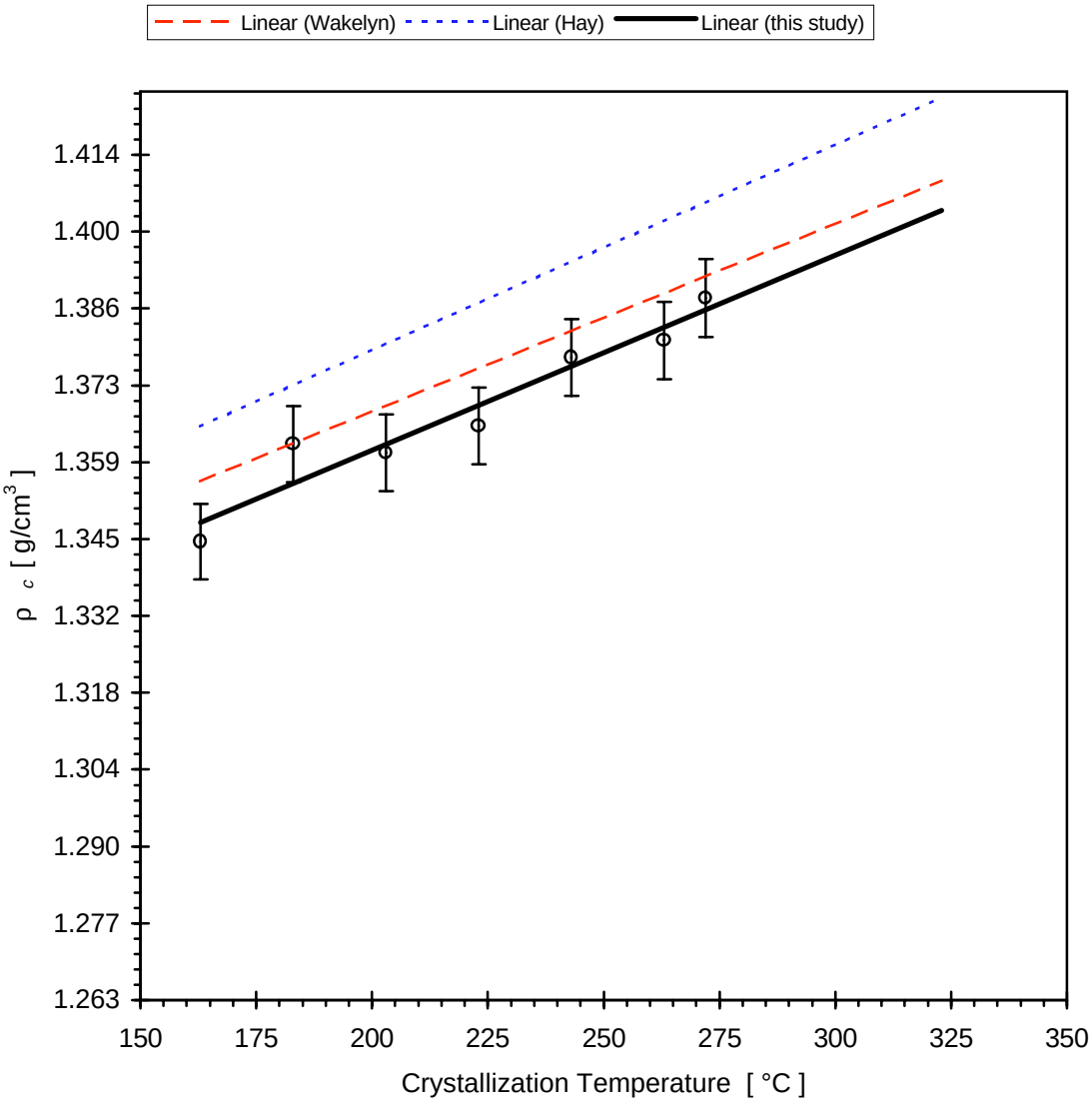


$\rho_c(T_c, t_c=60\text{ min}) = 1.3823_{\pm 0.0123} + 0.00034_{\pm 0.00005}*(T_c - 243)$ - Wakelyn

$\rho_c(T_c, t_c=60\text{ min}) = 1.3760_{\pm 0.0095} + 0.00035_{\pm 0.00004}*(T_c - 243)$ - this study

**Figure 4.39** Dependence of the room temperature crystal unit cell density $\rho_c$ on cold-crystallization temperature $T_c$ ($t_c$ = 60 min). The thin lines represent a linear extrapolation of the results of Wakelyn [122] and Hay et al. [123].

(Note: The term "densification" is used to label the experimentally observed increase of room temperature $r_c$ when $t_c$ and $T_c$ are increased. At this point the question is left open as to whether this is due to a true densification during annealing at $T_c$ or to the post-crystallization relaxation and contraction during quenching.)

In this section a systematic study of the crystallographic density of the crystalline lamellae at ambient conditions is presented for the three different series of samples, characterized in the previous section. It is important to determine accurately the absolute values of $r_c$ for all samples. However, the most important parameter, which we need to know accurately is the rate of "densification", determined from the variation of $r_c$ with $T_c$, $\log(t_c)$, and $\log(t_x)$ within the respective series. This is the parameter, which will determine to a large extent the rate of increase of the true density crystallinity for these series of samples - $c_c^{Dens}$ (corrected), and characterize the true discrepancy between $c_c^{Dens}$ (corrected) and $c_c^{DSC}$.

Figure 4.38 shows the results from the analysis of the WAXS diffractograms of the samples, cold-crystallized for 60 min. The interplanar spacings $d_{hkl}$ decrease with increase in cold-crystallization temperature $T_c$ for all the reflections analyzed - (110), (111), (200), and (211). This confirms the results of Wakelyn, [122] Hay et al., [123] and Zimmermann and Konnecke. [198] The crystallographic density of the unit cell $r_c$ is plotted against $T_c$ on figure 4.39. On the same plot the thin lines represent a linear least squares extrapolation of the results of Wakelyn and Hay et al. The two equations below the plot show, that within the uncertainty of the extrapolation the result is quantitatively the same as Wakelyn's - the "densification" coefficient from both sets of data is determined to be 0.00035 $(g/cm^3)/K$.

Figure 4.40 shows the WAXS diffractograms of two of the samples from the series, cold-crystallized at 243°C. The two scans are slightly shifted along the y-axis for clarity. The results of the analysis are shown in figures 4.41 - 4.43. Figure 4.41 shows the decrease of the interplanar spacings $d_{hkl}$ with increase of cold-crystallization time $t_c$. Figure 4.42 shows the change in the unit cell parameters with $t_c$. According to the results, the "densification" of the unit cell occurs along all crystallographic axes, but mostly along the *a* and *c* crystallographic directions. There is practically no change in the magnitude of the *b* unit cell dimension. The change of the crystallographic density $r_c$ with cold crystallization

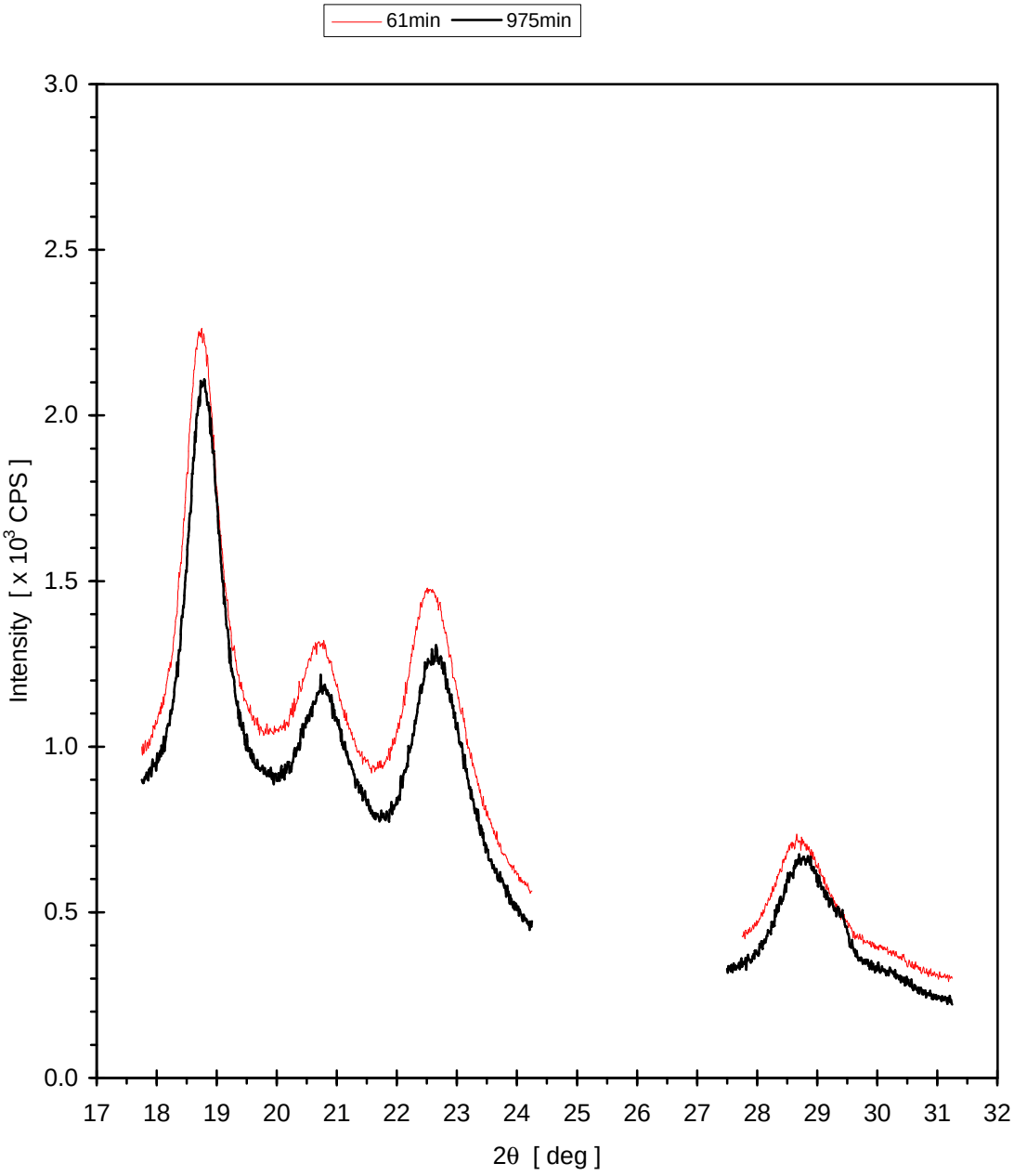


**Figure 4.40** Room temperature WAXS of PEEK samples, cold-crystallized at 243°C for the indicated times. Scintag XDS2000 diffractometer; step scan parameters: step = 0.01°, data collection time = 8 s/step.

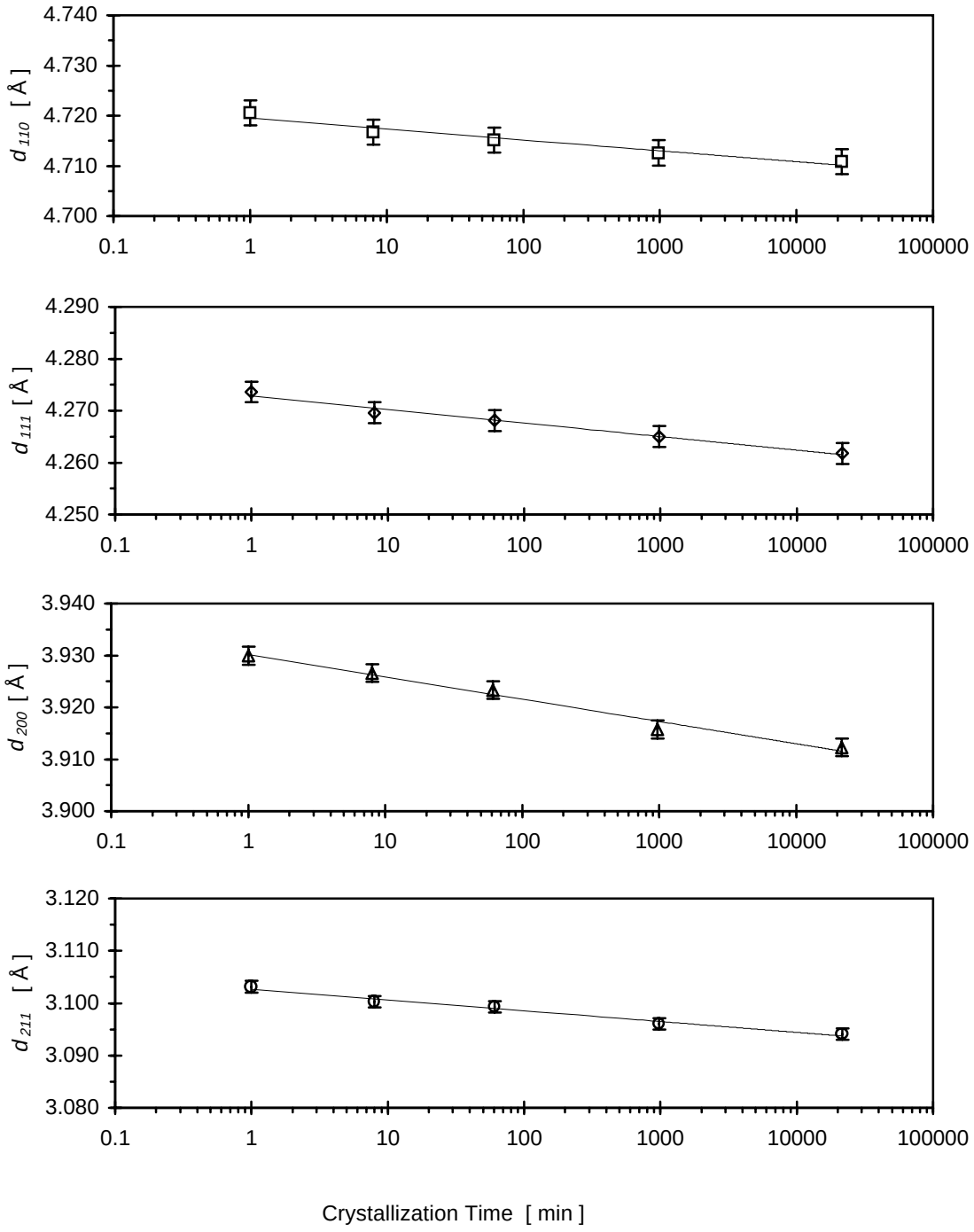


**Figure 4.41** Dependence of the interplanar $d$-spacings on cold-crystallization time $t_c$ at $T_c$ = 243°C. From top to bottom: $d_{110}$, $d_{111}$, $d_{200}$, $d_{211}$.

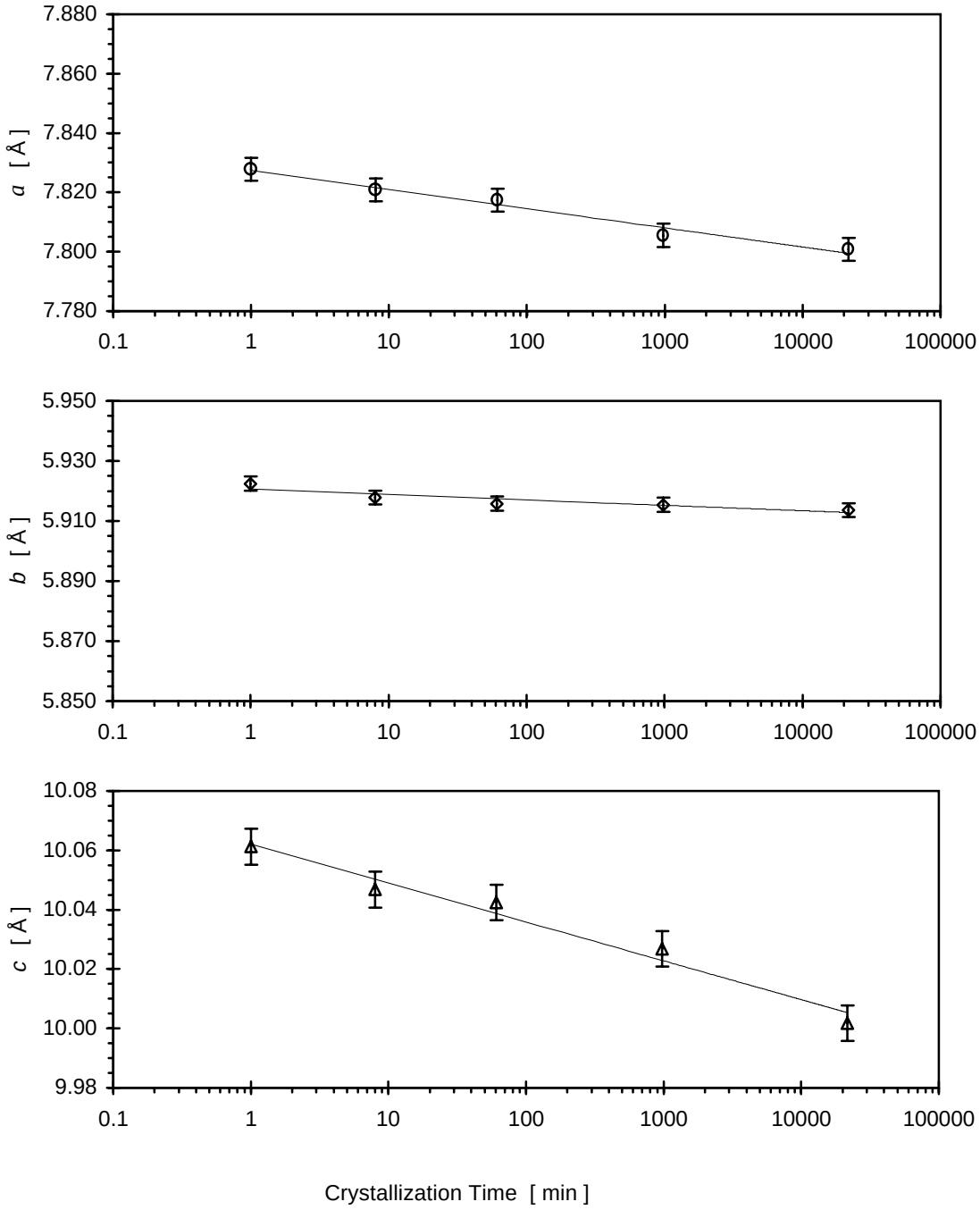


**Figure 4.42** Dependence of the room temperature unit cell parameters on cold-crystallization time $t_c$ at $T_c$ = 243°C. From top to bottom: $a$ , $b$ , $c$ .

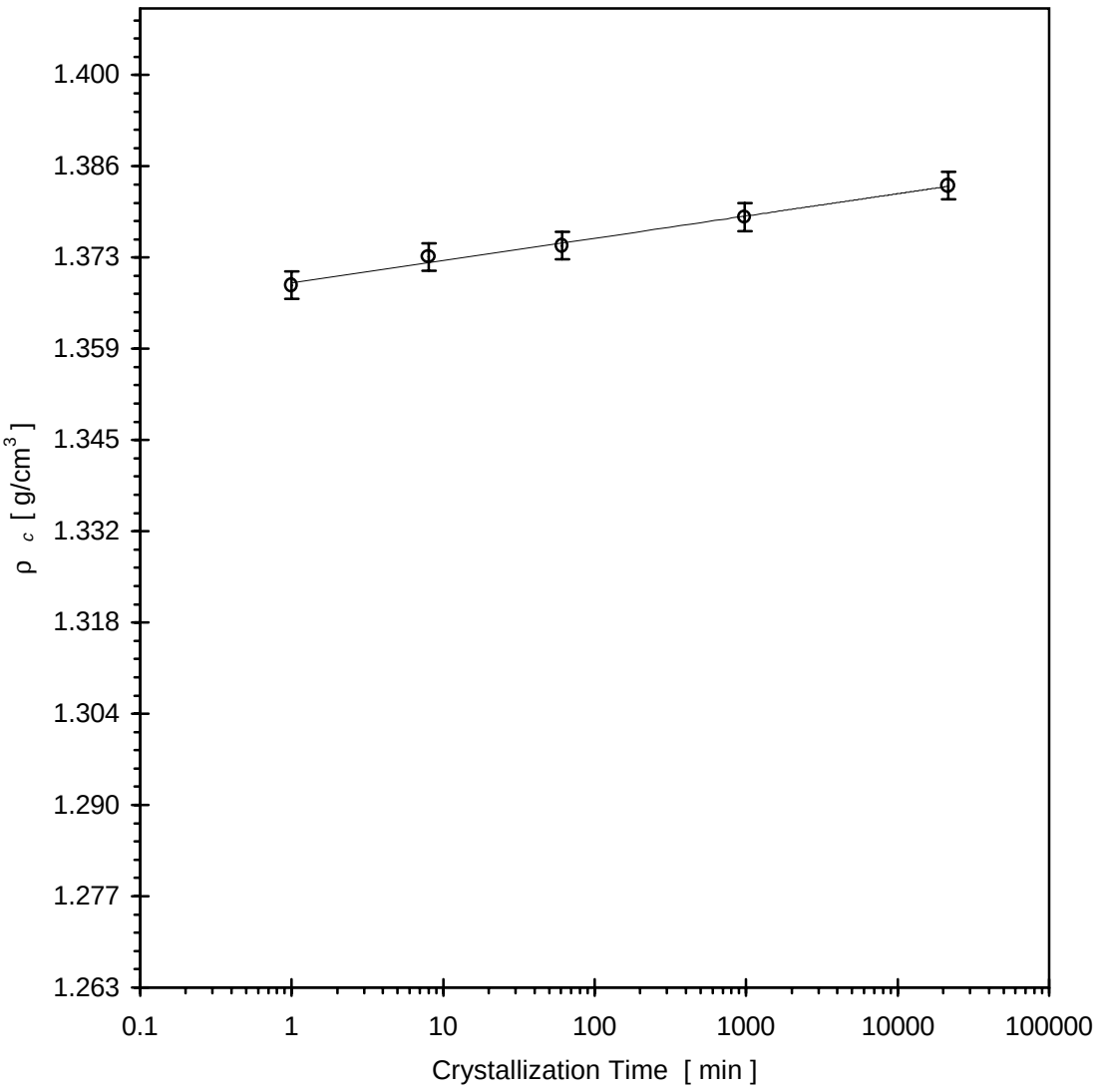


$$\rho_c(t_c, T_c=243°C) = 1.3688_{\pm 0.0004} + 0.00334_{\pm 0.00018} * \log(t_c)$$

**Figure 4.43** Dependence of the room temperature crystal unit cell density $\rho_c$ on cold-crystallization time $t_c$ at $T_c$ = 243°C.

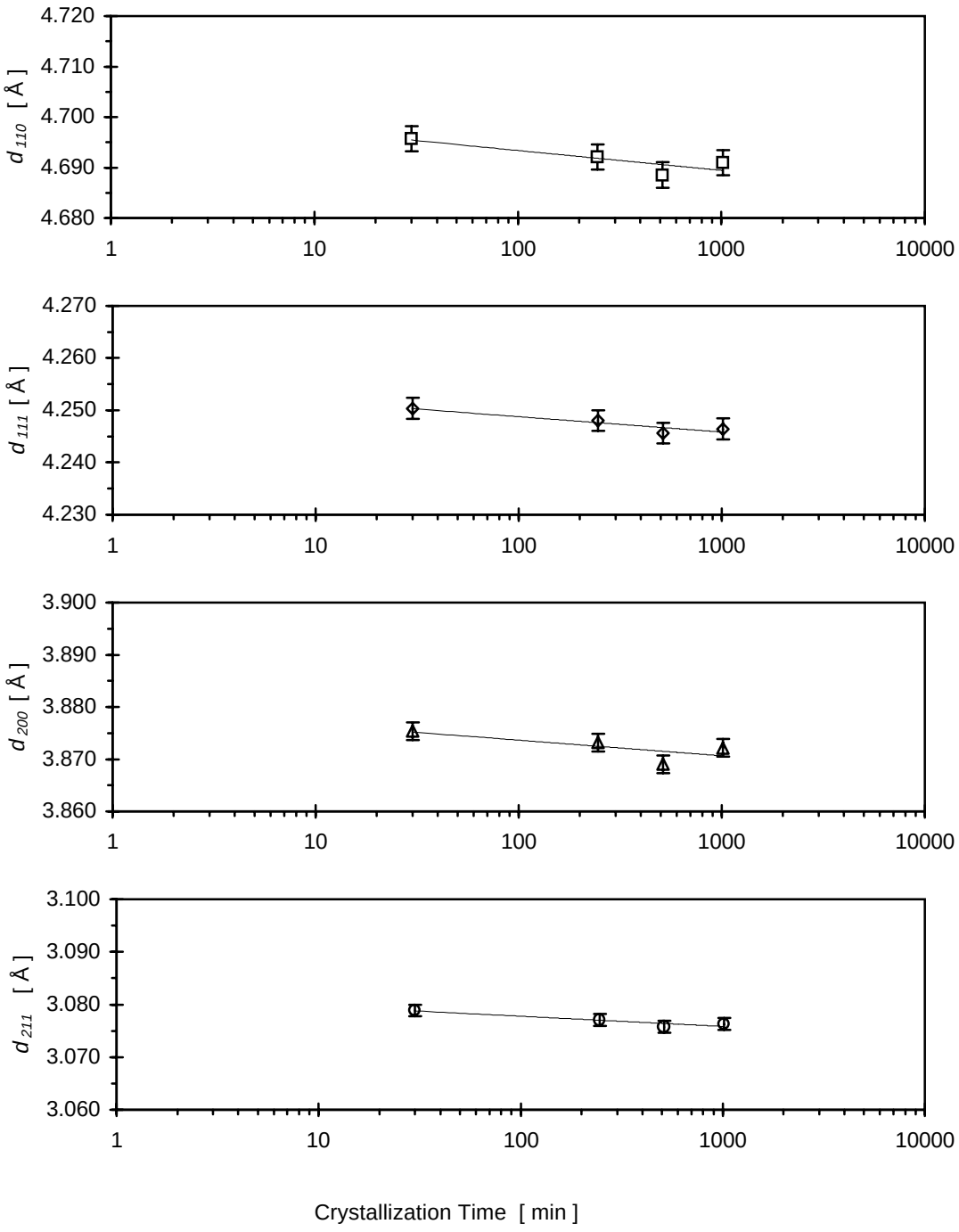


**Figure 4.44** Dependence of the interplanar $d$-spacings on melt-crystallization time $t_x$ at $T_x$ = 310°C. From top to bottom: $d_{110}$, $d_{111}$, $d_{200}$, $d_{211}$.

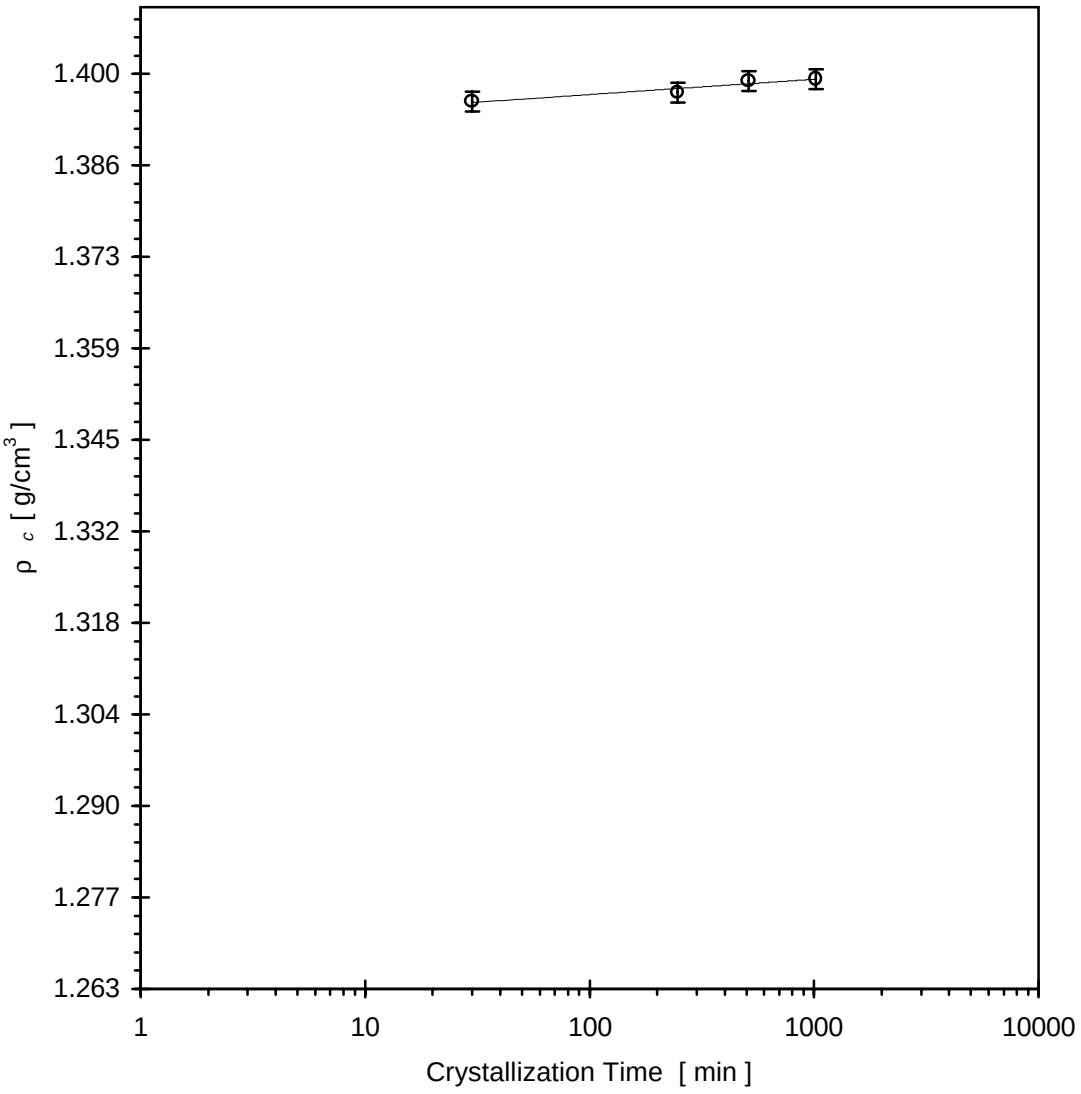


$$\rho_c(t_x, T_x=310°C) = 1.3924_{\pm 0.0011} + 0.0023_{\pm 0.0004} * \log(t_x)$$

**Figure 4.45** Dependence of the room temperature crystal unit cell density $\rho_c$ on melt-crystallization time $t_x$ at $T_x$ = 310°C.

time is presented on a semilogarithmic plot on figure 4.43. A linear least squares extrapolation of the data leads to a value of 0.00334 g/cm$^3$ per decade of time for the "densification" rate at $T_c$ = 243°C. This value is comparable in magnitude with the rate derived from the WAXS data on cold-crystallized PPS at $T_c$ = 245°C - 0.0051 g/cm$^3$ per decade. [124]

The last set of data needed for the reevaluation of the density crystallinities is the variation of the crystal density of the melt-crystallized samples - $r_c(t_x, T_x = 300°C)$. Due to the preparation conditions of these samples, they are too small in size and were not suitable for precise direct evaluation of $r_c$ by WAXS. Investigation was carried out on another set of samples, melt-pressed to a uniform thickness and isothermally crystallized in a Carver hot press at 310°C for various times.

Figure 4.44 shows the dependence of the interplanar *d*-spacings on melt-crystallization time $t_x$ for these samples. The variation of $d_{hkl}$ with log($t_x$) is noticeably smaller than that, observed for the cold-crystallized samples, however the data suggests, that "densification" of the unit cell occurs in the case of melt-crystallized PEEK too - figure 4.45. The linear least squares fit of the $r_c$ vs. log($t_x$) yields a "densification" rate of 0.0023 g/cm$^3$ per decade of time. This value will be used in equation 2.3a for the samples, melt-crystallized at 300°C, with the assumption, that the difference in preparation conditions for the two different sets of samples and the small difference in $T_x$ do not lead to a significant change of the "densification" rate.

### *4.2.3c Corrected Density Crystallinities*

The quantitative evaluation of the dependence of $r_c$ on crystallization time and temperature in the previous section allows the true crystal density to be used for each sample in the three series, according to equation (2.3a) for $c_c^{Dens}$ (corrected):

$$c_c^{Dens}(T_c, t_c) = \frac{r_c(T_c, t_c)}{r(T_c, t_c)} \frac{r(T_c, t_c) - r_a}{r_c(T_c, t_c) - r_a} \qquad (2.3a)$$

Comparison of the trends exhibited by the uncorrected and corrected density crystallinities shows, that the apparent increase of $c_c^{Dens}$ (uncorrected) with $t_x$, $t_c$ or $T_c$ is greatly reduced when the proper crystal density $r_c(t_x)$ or $r_c(t_c, T_c)$ is used.

Figure 4.46 compares the development of $c_c^{Dens}$ (corrected) and $c_c^{DSC}$ with $t_x$ for the melt-crystallized samples. The rate of increase of the density crystallinity is reduced to 0.003 per decade of time and is 5 times smaller than the rate of increase of the DSC crystallinity. The overall increase of $c_c^{Dens}$ (corrected) is less than 0.01, compared with increase of 0.05 for $c_c^{DSC}$. Therefore, after the end of the primary crystallization, the DSC crystallinity increases significantly due to the crystallinity contribution of the low temperature endotherm, while the density crystallinity shows very little change from its initial value or no change at all.

The $T_c$ dependence of $c_c^{Dens}$ (corrected) and $c_c^{DSC}$ for the cold-crystallized samples from this study is shown on figure 4.47 and for the crystallinities calculated from literature data - on figure 4.48. The increase in the density crystallinity with increase in $T_c$ is significantly reduced in magnitude. If we exclude the datapoints for $T_c$ = 163°C (obviously not belonging to the trend), the overall increase of $c_c^{Dens}$ (corrected) is about 0.015 - 0.02, while the increase in $c_c^{DSC}$ is about 0.04 - 0.05. The point at $T_c$ = 163°C is exception from the trend, probably due to the closeness of its crystallization temperature to the glass transition region (the calorimetric $T_g$ of this sample at scanning rate 5 K/min is 156°C and the glass transition region, broadened by the presence of crystallinity, extends from 145°C to 160°C).

Figure 4.49 shows the crystallization time dependence of $c_c^{Dens}$ (corrected) and $c_c^{DSC}$ for the series of samples, cold-crystallized at 243°C. The rate of increase of the density crystallinity is reduced to 0.0083 g/cm$^3$ per decade of time. This is three times lower than the rate of increase of the DSC crystallinity. The absolute increase of $c_c^{Dens}$ (corrected) in the investigated time range (1 min - 21,550 min) is 0.03, while that of $c_c^{DSC}$ is 0.09. The difference between the two crystallinities is matched by the crystallinity contribution of the low temperature endothermic peak.

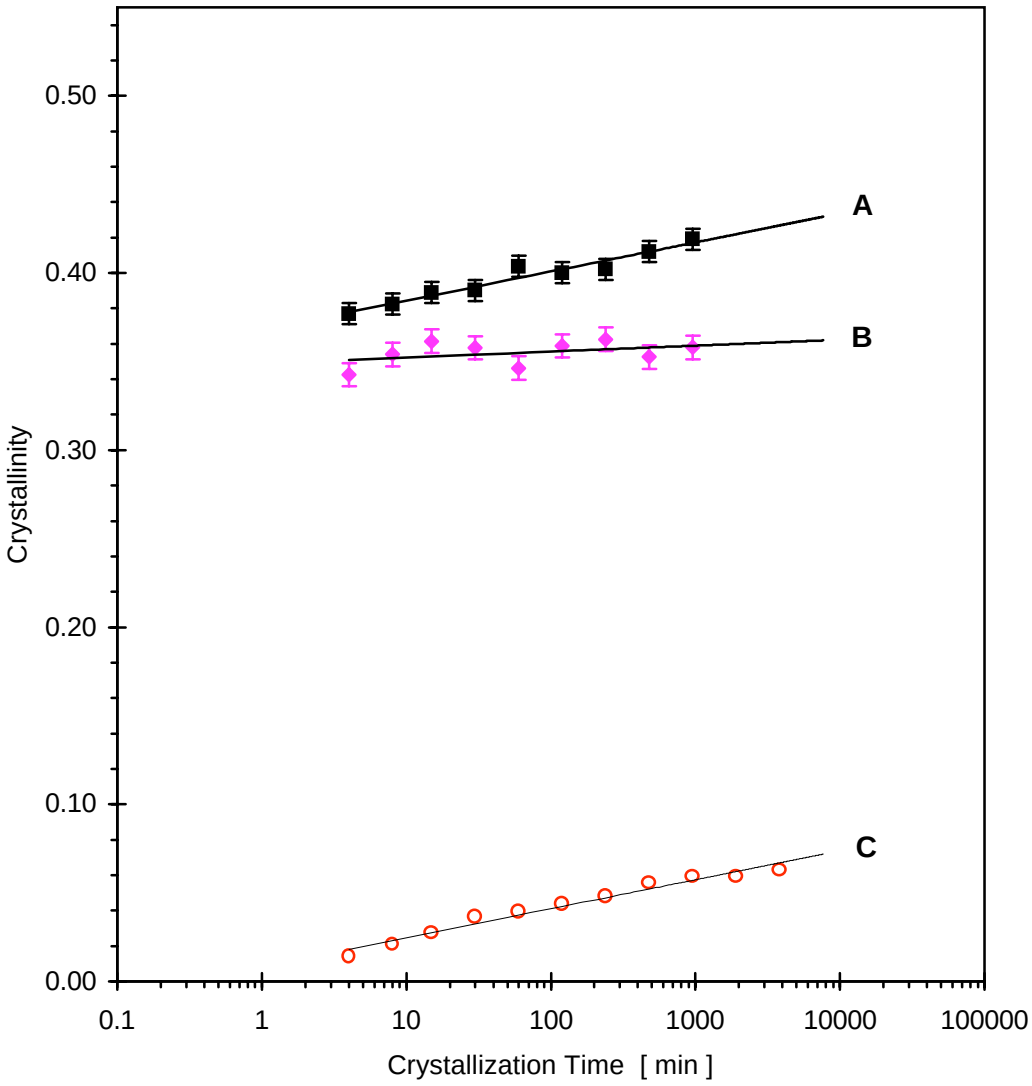


$\chi^{DSC} = 0.3679_{\pm 0.0029} + 0.0165_{\pm 0.0015} * \mathrm{Log}(t_x)$

$\chi^{Dens}$ (corrected) $= 0.3489_{\pm 0.0056} + 0.0033_{\pm 0.0029} * \mathrm{Log}(t_x)$

**Figure 4.46** Crystallinities of the samples, melt-crystallized at $T_x$ = 300°C: A) DSC crystallinity; B) corrected density crystallinity - equation (2.3a), p. 95; C) crystallinity of the low temperature melting peak.

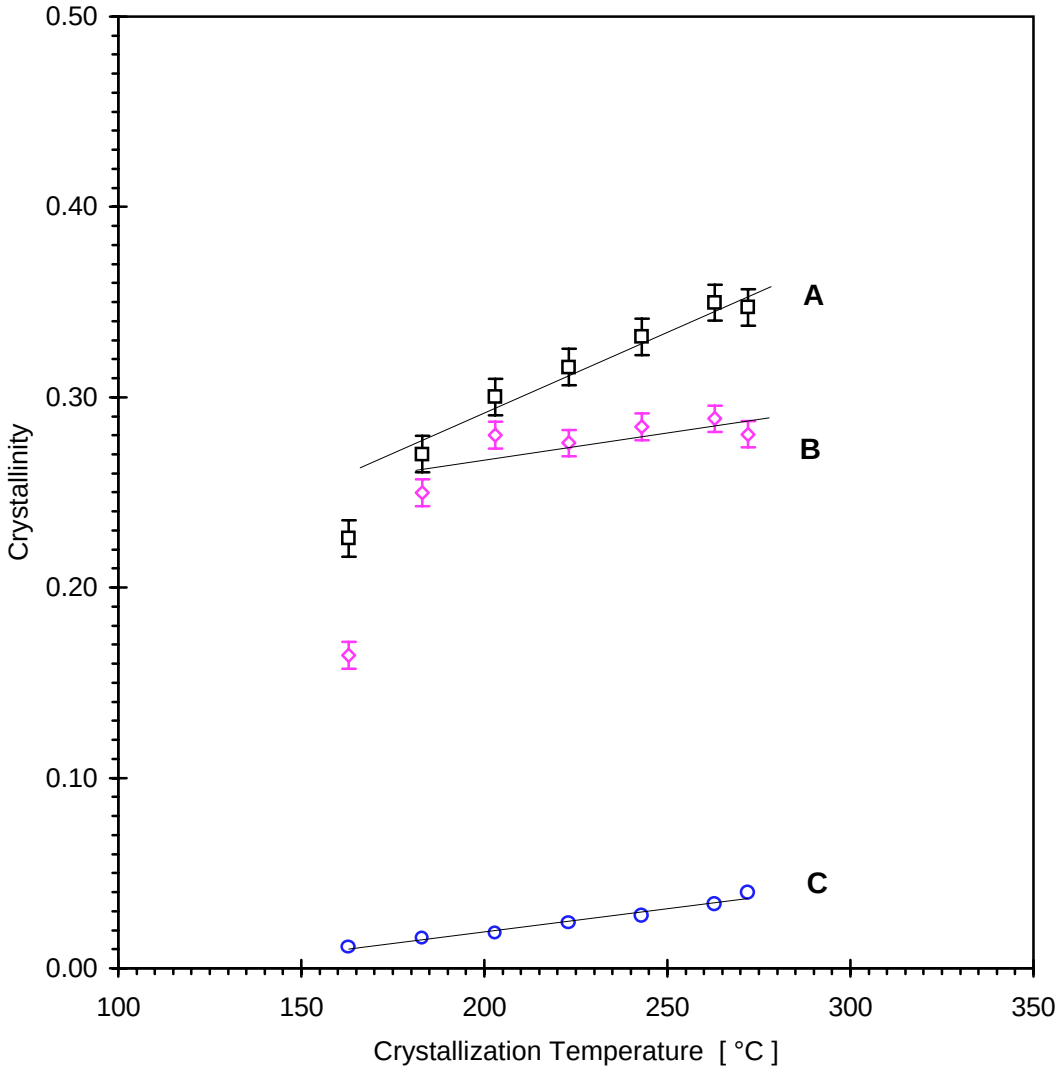


**Figure 4.47** Crystallinities of the samples, cold-crystallized for 60 min at various $T_c$: A) DSC crystallinity; B) corrected density crystallinity - equation (2.3a); C) crystallinity of the low temperature melting peak.

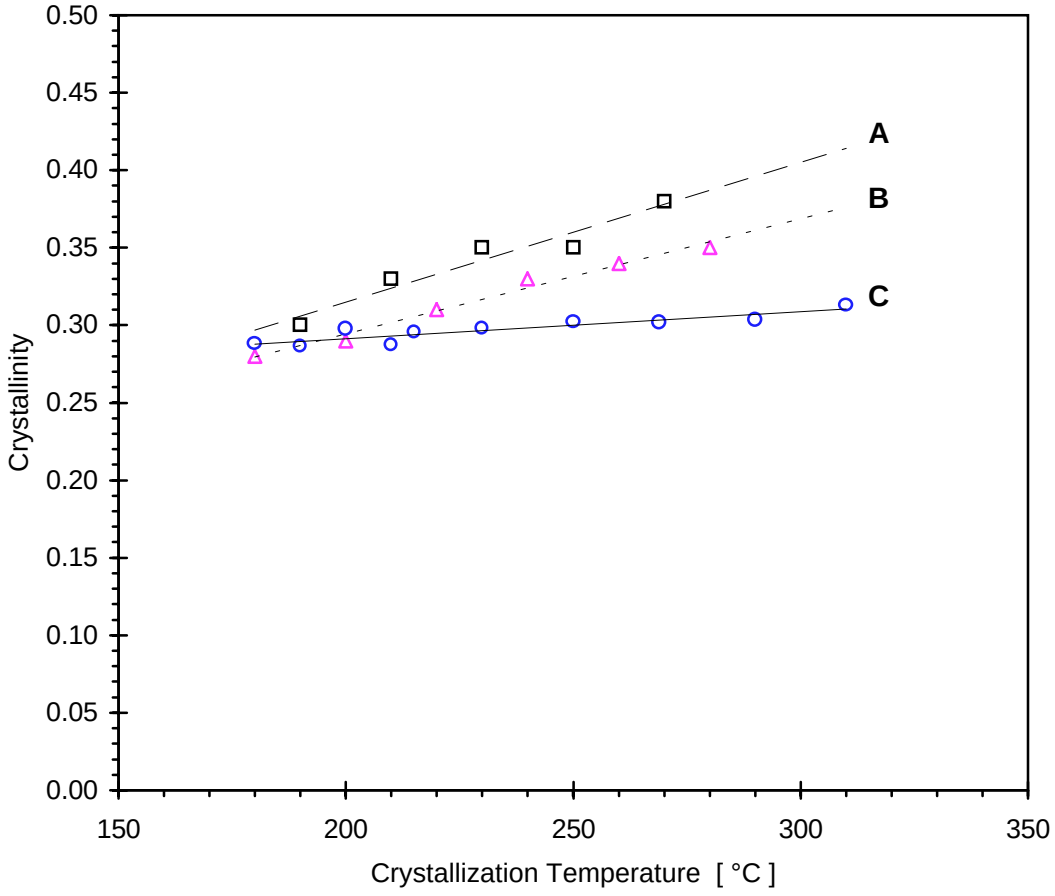


**Figure 4.48** Literature data on crystallinities of PEEK samples, cold-crystallized at various $T_c$: A) DSC crystallinity ($t_c$ = 120 min, Cheng et al. [16]); B) DSC crystallinity ($t_c$ = 60 min, Huo and Cebe [17]); C) corrected density crystallinity - equation (2.3a) (tc = 60 min, density data from Lee et al. [65, 66]).

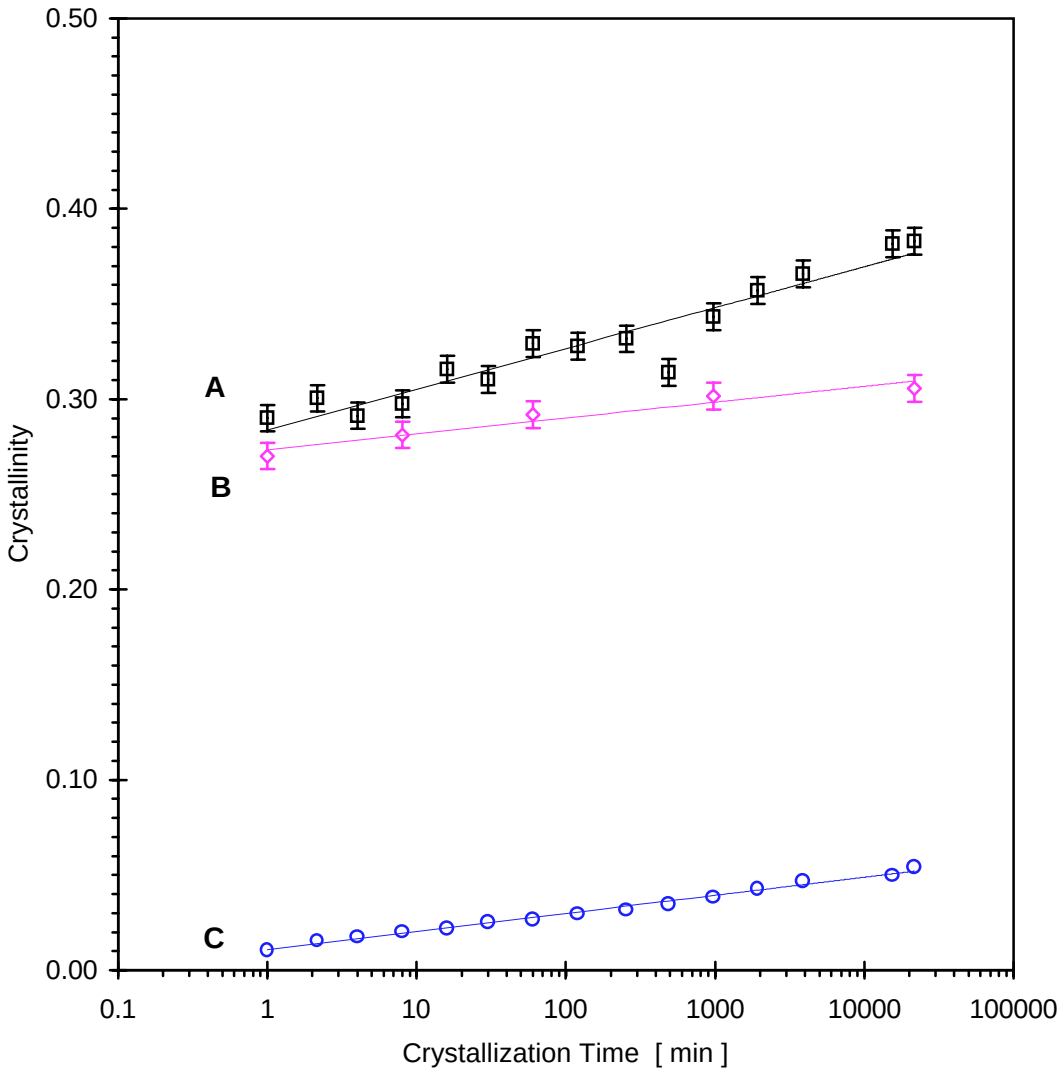


$\chi^{DSC} = 0.2843_{\pm 0.0029} + 0.0221_{\pm 0.0011} * \mathrm{Log}(t_c)$

$\chi^{Dens}$ (corrected) $= 0.2735_{\pm 0.0030} + 0.0083_{\pm 0.0012} * \mathrm{Log}(t_c)$

**Figure 4.49** Crystallinities of the samples, cold-crystallized at $T_c$ = 243°C: A) DSC crystallinity; B) corrected density crystallinity - equation (2.3a); C) crystallinity of the low temperature melting peak.

In summary, the results from the investigation of three different series of PEEK samples and an independent set of literature data on PEEK unequivocally show, that there is a discrepancy between the DSC crystallinity and the "true" (corrected) density crystallinity.

The difference in absolute values, crystallization time dependence, and $T_c$ dependence can not be accounted for by use of different value for the reference constant $\Delta H_m^0$. Using the value of Zoller et al. $\Delta H_m^0$ = 38.5 cal/g, [117] leads to a reduction of the discrepancy between the absolute values of the DSC and density crystallinities, but does not eliminate the difference in their variation with change of $T_c$ and $t_c$. Accounting for the temperature dependence of $\Delta H_m^0$, as suggested by Seguela, [116] makes almost no difference and leads to results, which are practically identical to those presented above. It must be noted, that in all the results and conclusions above, it has been assumed, that the density of the amorphous phase in the semicrystalline polymer is constant and identical to that of purely amorphous PEEK - 1.263 g/cm$^3$. A thorough analysis of this assumption will be presented in the discussion chapter in section 5.3.

### *4.2.4 Small Strain Creep*

The creep compliance *J(t)* for the different aging times at 120°C is plotted as a function of creep time on figure 4.50-A. The changes in *J(t)* with aging time $t_a$ are similar to the characteristic changes in fully amorphous and semicrystalline polymeric glasses below $T_g$. Approximation with the KWW function (equation 2.9a) produces the continuous lines on the plot, which fit very well the experimental data. The shift factors necessary for the superposition of the creep compliance curves at a reference aging time $t_{ar}$ = 18 hrs can be calculated from the parameters of the fit according to the relations in equation (2.11):

$$log\left[a\left(t_a, t_{ar}\right)\right] = log\left[\frac{t\left(t_a\right)}{t\left(t_{ar}\right)}\right] \qquad (4.9)$$

In addition to the horizontal shifts, vertical shifts of:

$$log\left[b\left(t_a, t_{ar}\right)\right] = log\left[\frac{J_0\left(t_a\right)}{J_0\left(t_{ar}\right)}\right] \qquad (4.10)$$

are required in order to superpose the creep compliance curves. The superposition of the creep compliances $J(t)$ from figure 4.50-A is shown on figure 4.50-B. Superposition of the $J(t, t_a)$ creep compliance curves to a master curve in the case of semicrystalline PEEK below $T_g$ has already been reported in the literature. [97, 98] The only difference observed in this study is that vertical shifts, relatively significant in magnitude, are required for the superposition. These arise from the change in the preexponential factor $J_0(t_a)$, which can be interpreted as the effective instantaneous value of the creep compliance at $t = 0$. The nature of these vertical shifts in PEEK will be examined in the discussion part.

The results from the creep test at 160°C are shown on figure 4.51-A. This temperature is about 0-5 K above the calorimetric $T_g$ of the material (at a DSC scanning rate of 5 K/min). The glass transition region is broad, extending from 145°C to about 180°C, therefore the 160°C annealing temperature clearly falls in the glass transition region. The results on figure 4.51 are in line with expectations. At early, as well as at long creep times the creep compliance curves exhibit small curvature which leads to a S-like shape for the curves. The curves are poorly described by the KWW function, especially at short times. Superposition by vertical shifts alone cannot bring them together. The master curve of the compliances at 160°C on figure 4.51-B is obtained from the vertical and horizontal shifts based on the KWW fit as in the case of $T_a$ = 120°C. The shifts are smaller than the ones at 120°C. The horizontal shifts suggest, that at the glass transition region there is still some fraction of the material, which is relaxing slowly and its mobility is affected by the annealing process on the time-scale of the experiment. A similar effect is observed for the test at $T_a$ = 180°C, not shown here.

If the amorphous fraction of PEEK becomes completely relaxed and rubber-like in the 150-180°C range, the horizontal shifts should vanish in that same range. In the absence of horizontal shifts, the vertical shifts (if any) would be due to structural changes causing a depletion of the rubber-like fraction. In the linear viscoelastic region, the dependence of creep compliance on creep time would have to be explained by the viscoelastic response of an entangled and crosslinked network of chains (the crystalline lamellae acting as crosslinks).

The results from the test at $T_a$ = 220°C, however, go in the opposite direction. Instead of converging to a set of analogous or vertically displaced curves, the creep compliance's

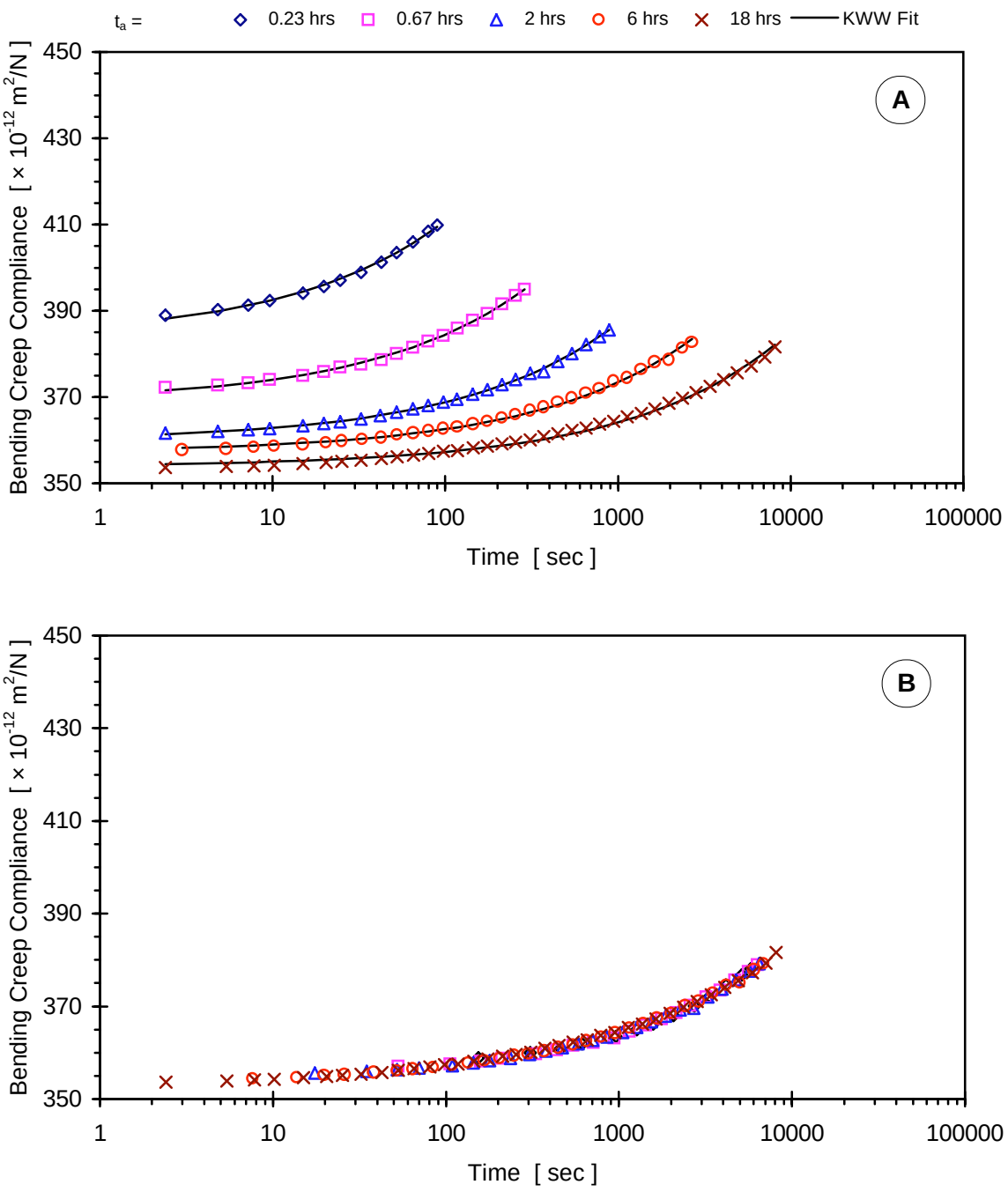


**Figure 4.50** Effect of aging time on the small strain creep of semicrystalline PEEK at $T_a$ = 120°C: A) symbols - raw data, lines - KWW fit (equation 2.9); B) superposition of the data after horizontal and vertical shifts.

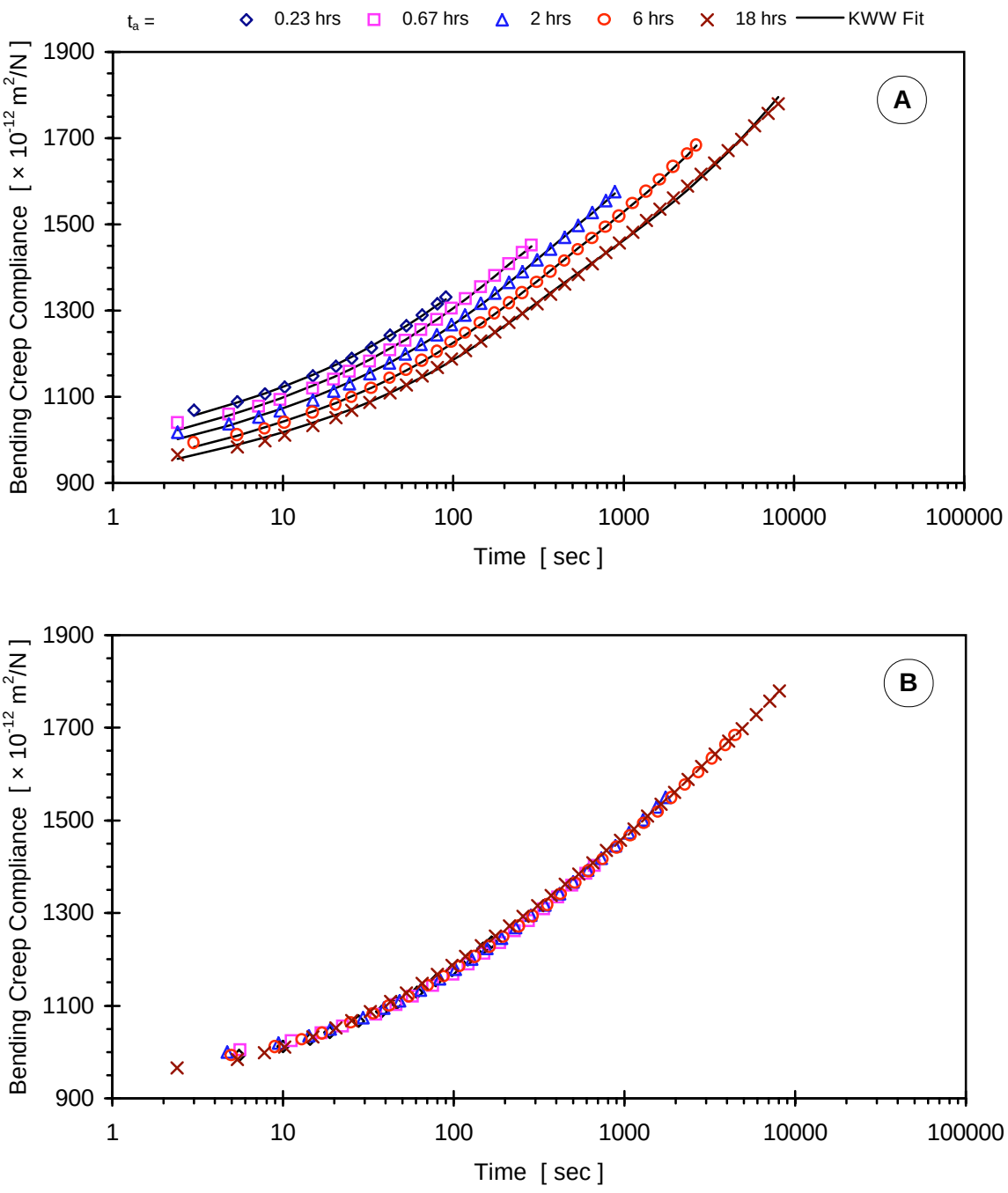


**Figure 4.51** Effect of aging time on the small strain creep of semicrystalline PEEK at $T_a$ = 160°C: A) symbols - raw data, lines - KWW fit (equation 2.9); B) superposition of the data after horizontal and vertical shifts.

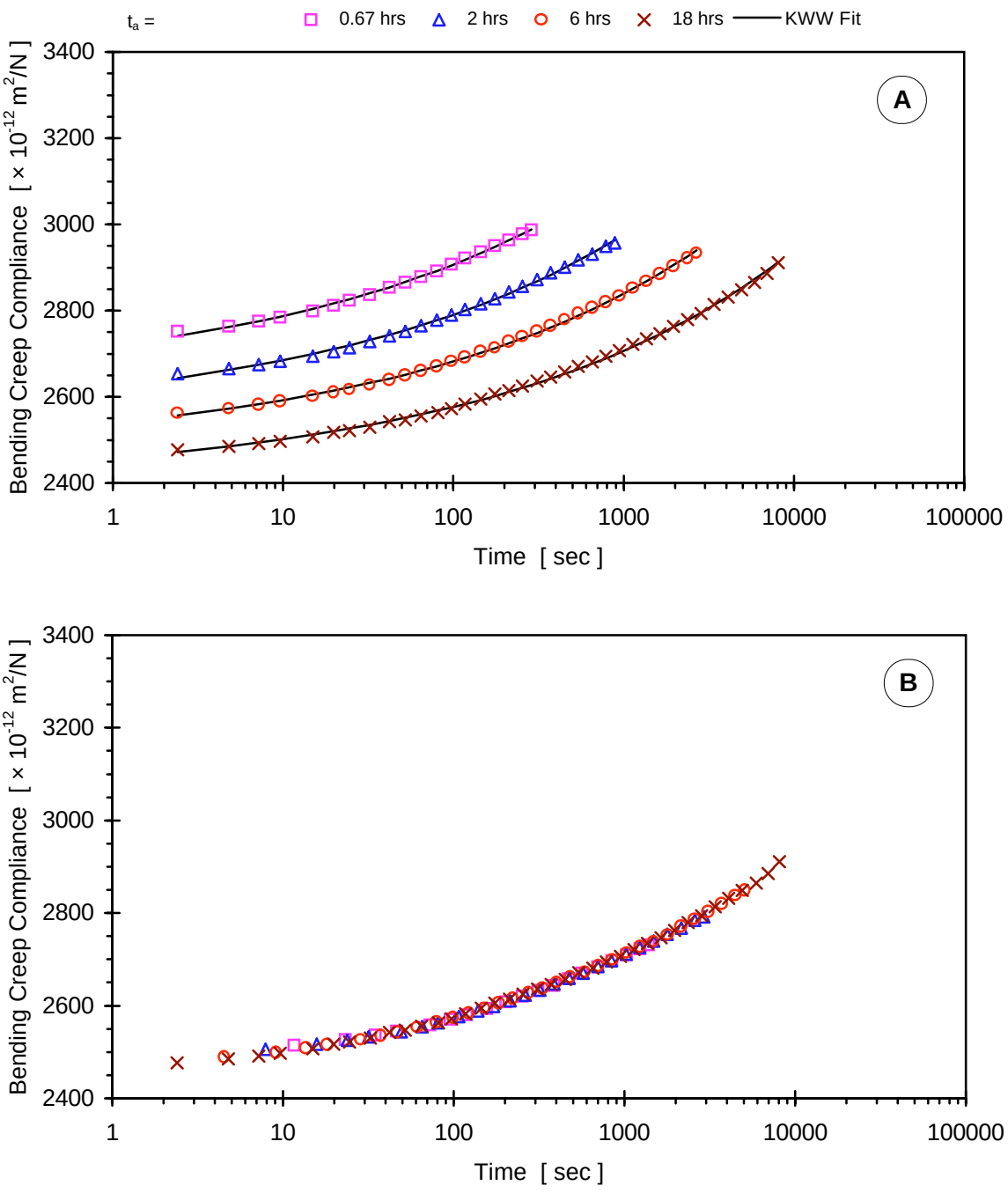


**Figure 4.52** Effect of aging time on the small strain creep of semicrystalline PEEK at $T_a$ = 220°C: A) symbols - raw data, lines - KWW fit (equation 2.9); B) superposition of the data after horizontal and vertical shifts.

dependence on annealing time returns to the behavior observed below $T_g$. The curves on figure 4.52-A have the same characteristic similarity as those below $T_g$. A vertical displacement alone fails to reduce them to a master-curve. The KWW approximation fits the data very well, the parameters suggesting a well correlated set of significant horizontal shifts, combined with vertical shifts. The resulting master curve is displayed on figure 4.52-B.

Figure 4.53 presents the magnitude of the horizontal shifts *log(a)* and their dependence on annealing time at three annealing temperatures. As expected for a polymeric glassy material the dependence of *log(a)* on $log(t_a)$ for $T_a$ = 120°C is linear. The logarithmic horizontal shift rate $m$, defined by equation (2.11), is close to 1. In the glass transition region (160°C) the shifts are much smaller and their dependence on annealing time deviates from the linear trend. Given the possibility of larger uncertainty of the KWW fit in this temperature region we can evaluate only qualitatively the value of the logarithmic horizontal shift rate. The estimated value is about 0.14 - about an order of magnitude less then the value at 120°C. At 220°C the dependence of *log(a)* on $log(t_a)$ returns to linearity and the value of $m$ is intermediate in magnitude - 0.48.

The dependence of $m$ on annealing temperature is plotted on figure 4.54. From a value close to 1 well below $T_g$ it falls to a value close to 0 (or at least a very small value) in the glass transition region. Above $T_g$ the value of $m$ increases and is again close to 1 at the highest $T_a$ investigated.

As was pointed out above, the horizontal shifts alone do not describe completely the similarity of the creep compliances at different aging times. Vertical shifts $log[b(t_a)]$ (equation 4.10) are required for bringing the creep compliances to a master curve. These shifts are well correlated with the aging times $t_a$. For the description of this correlation we define a vertical shift rate $B$ as:

$$B = -\frac{\P\, b(t_a)}{\P\, log(t_a)} \qquad (4.11)$$

(Note: This definition of the vertical shift rate $B$ differs from the one given by Struik. [88] Struik defines the vertical shift rate as:

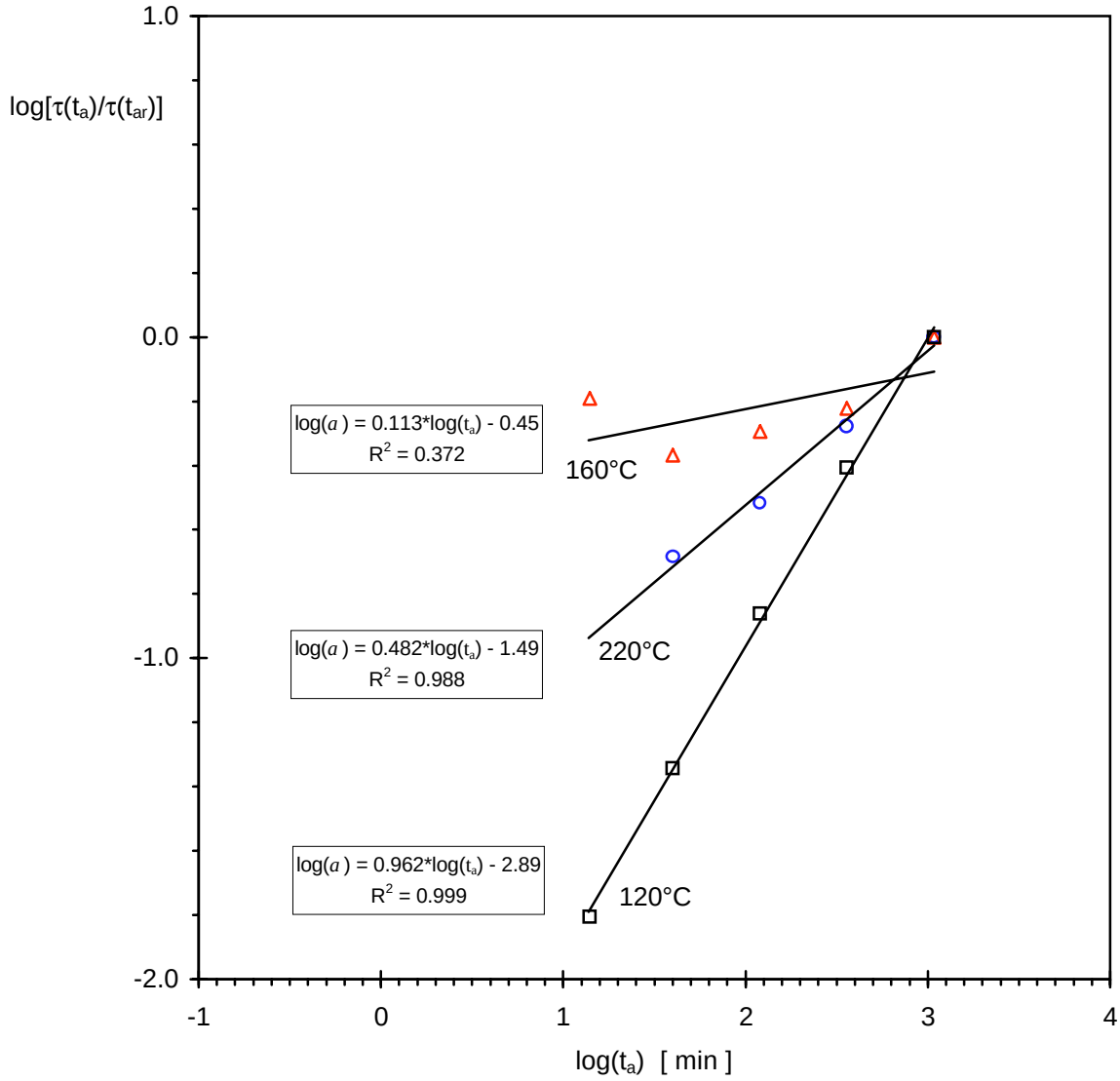


**Figure 4.53** Dependence of the horizontal shifts on aging time in three different temperature ranges: below $T_g$ (120°C), in the glass transition region (160°C), and above $T_g$ (220°C).

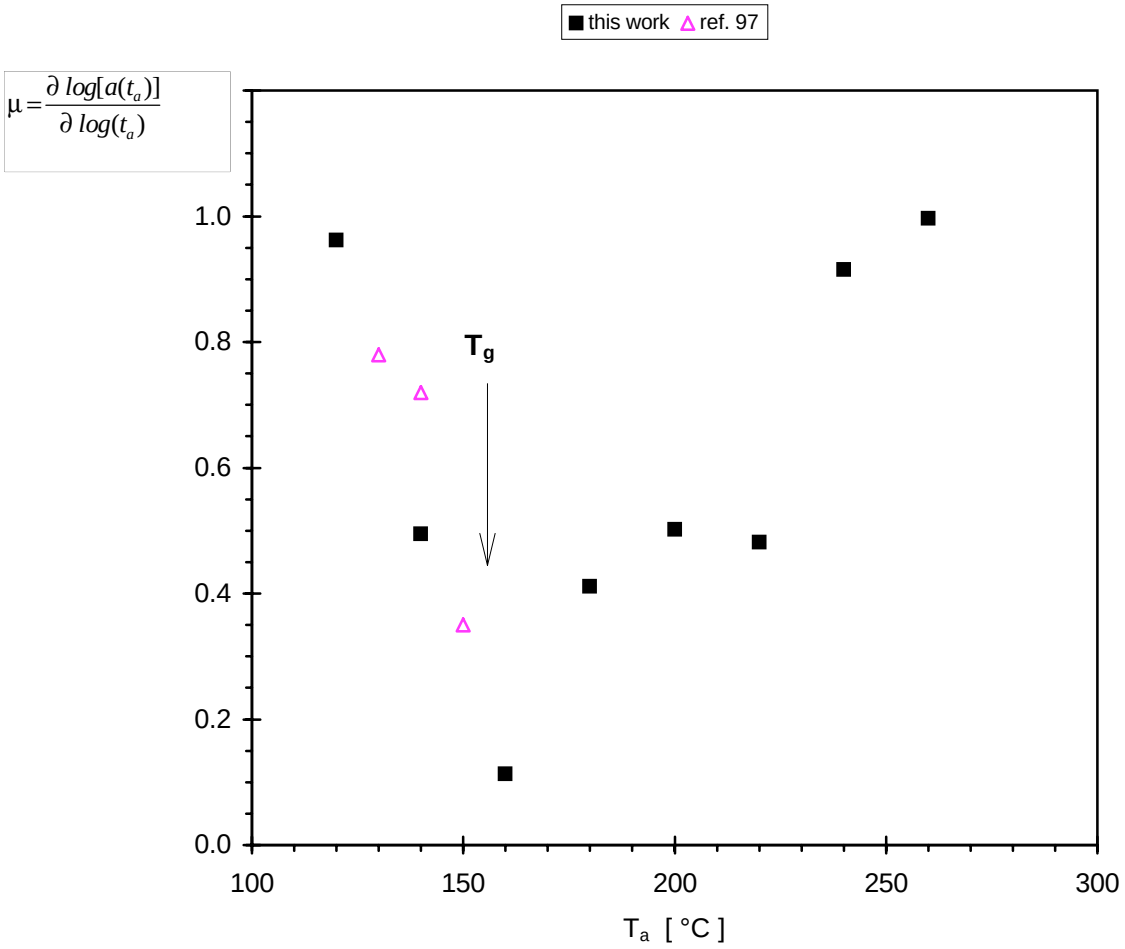


**Figure 4.54** Dependence of the horizontal shift rate μ on annealing temperature $T_a$.

$$B_S = \frac{1}{J(t,t_a)} \frac{\P b}{\P log(t_a)} = \frac{1}{J(t,t_a)} \frac{\P [\Delta J(t,t_a,t_{ar})]}{\P log(t_a)} = \frac{1}{J(t,t_a)} \frac{\P [J(t,t_{ar}) - J(t,t_a)]}{\P log(t_a)}$$

$$\text{or} \quad B_S = -\frac{1}{J(t,t_a)} \frac{\P J(t,t_a)}{\P log(t_a)},$$

where $t$ = 1024 s is chosen as the time at which the vertical shifts are evaluated. This definition of the vertical shifts implies their application as shifts on a normal *J(t)* axis, instead of a logarithmic one. The definition is not rigorous and can not be described analytically. It does not lead to good superposition except at the point of the creep compliance curve, where it is evaluated. In the definition employed in this study, equation (4.11), the vertical shifts arise from rescaling of the pre-exponential factor $J_0(t_a)$. Thus they are evaluated independently from the creep time $t$ and apply to the entire curve. They can be expressed analytically with the parameters of the KWW fit. Equation (4.11) is also consistent with the one given by Buijs and Vroege in reference 135.)

The values of $B$ were calculated from a linear fit of the data on plot of $b(t_a)$ vs. $log(t_a)$. Figure 4.55 shows the dependence of the vertical shift rate on $T_a$. In the entire temperature interval of evaluation the rate has the same sign (positive under this definition - equations 4.10 and 4.11). This comes in contrast with the results of Struik, [88] which show a change in sign of $B$ at $T_g$.

Due to the large uncertainty involved in their evaluation and the presence of only two datapoints below $T_g$, it is not possible to discuss further the nature of the dependence of $B$ on $T_a$. The value of $B$ apparently increases in magnitude with an increase in $T_a$.

The changes in the creep compliance curves with annealing during the "physical aging" tests are accompanied by a change in the thermal properties of the samples. In the previous section we have shown, that annealing of semicrystalline PEEK above $T_g$ causes the observation of a low temperature endothermic peak in the DSC heating scan just above $T_a$. The evolution of the parameters of this peak occurs on a log($t_a$) time scale.

In fact, this observation extends in the temperature region below $T_g$ too. Figure 4.56 shows the DSC heating scans of small amounts of material, taken from the creep test samples after $t_a$ = 1080 min. In scans (B) and (C) ($T_a > T_g$) the low temperature endothermic peak

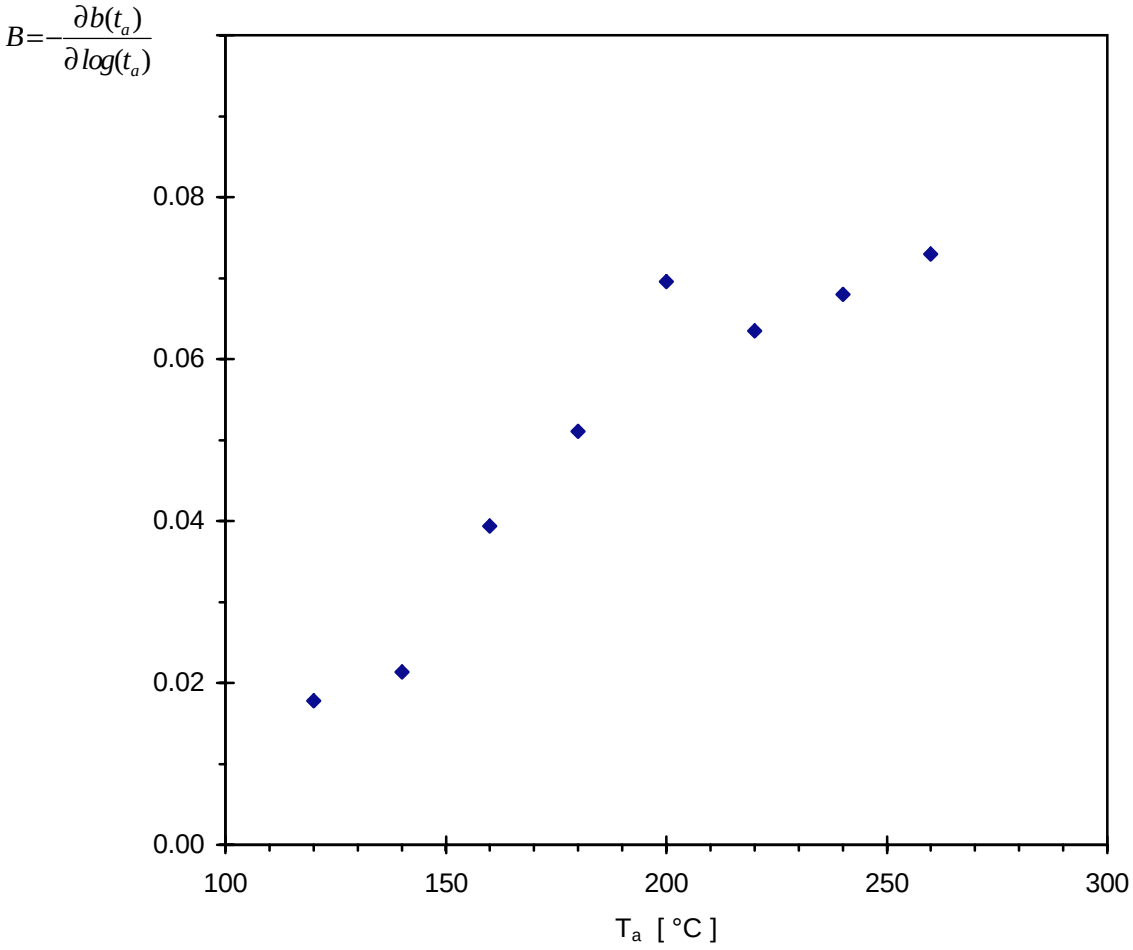


**Figure 4.55** Dependence of the vertical shift rate $B$ on annealing temperature $T_a$.

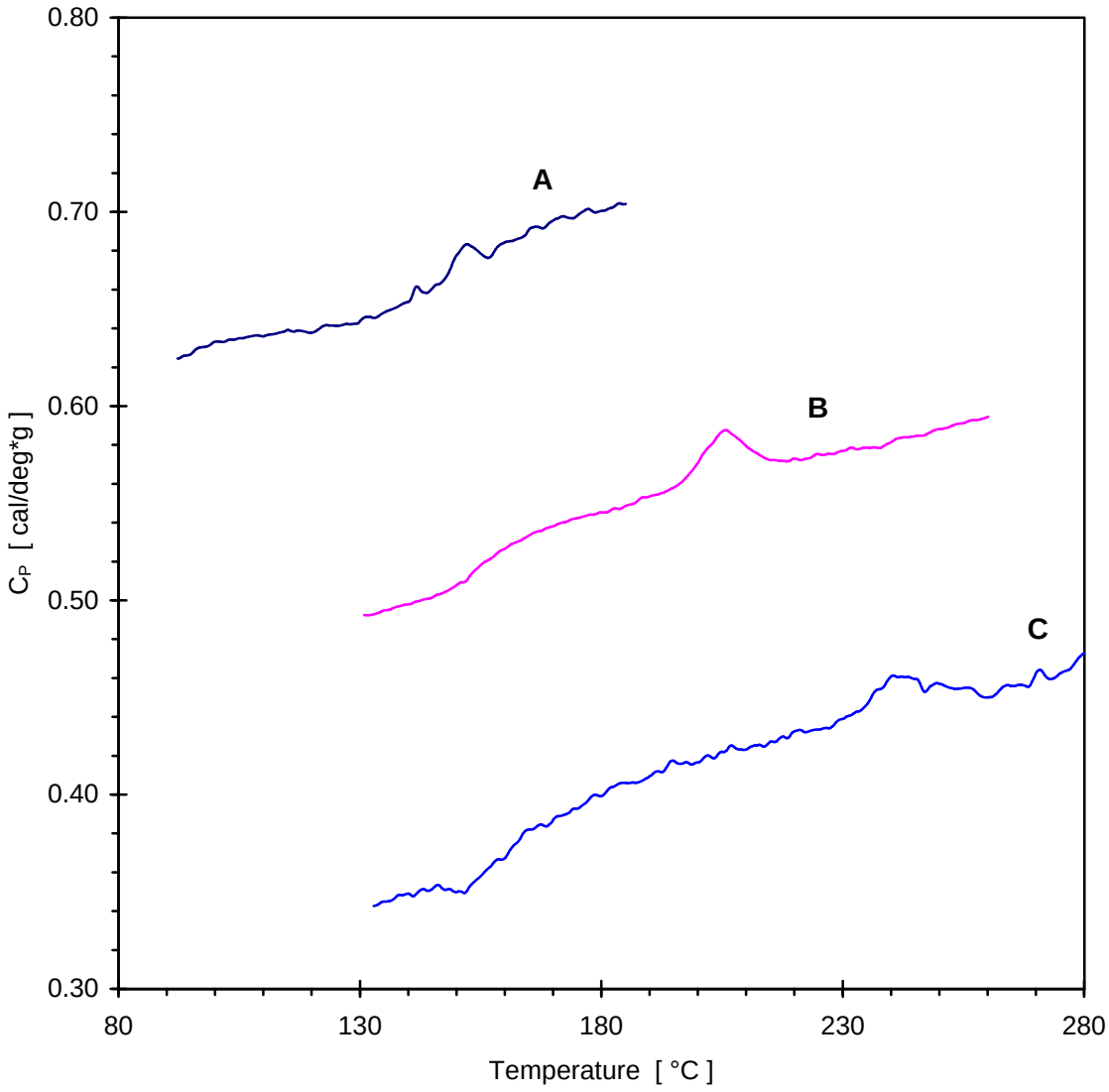


**Figure 4.56** DSC scans of samples from the creep test after $t_a$ = 1080 min at $T_a$ = 120°C (A), 180°C (B), and 220°C (C).

appears just above $T_a$, as expected. In scan (A) ($T_a < T_g$) the endothermic peak appears superposed to the step change in $C_P$ at the glass transition. The use of small amount of material (some of which is stressed by the cutting from the samples) leads to large scatter in the data, especially for scans (A) and (C). Furthermore, the continuous nature of the creep tests does not allow simultaneous monitoring of the evolution of the creep compliance and the thermal properties. The correlation between the results from the creep tests and the DSC investigation of the development of the low temperature endothermic peak will be given in the discussion - section 5.4. A rigorous study of the thermal behavior of samples with the same thermal histories as the creep samples will be presented in section 5.6.3.

### *4.2.5 Calorimetric Glass Transition of Semicrystalline PEEK*

The glass transition of PEEK is another property, related to the relaxation processes, which can be monitored calorimetrically. Cheng et al. [16] have shown a peculiar dependence of $T_g$ on crystallization temperature for melt- and cold-crystallized PEEK samples. $T_g$ of melt crystallized PEEK is rather independent from the crystallization temperature $T_x$ and is only about 5-6 K above the $T_g$ of fully amorphous PEEK (145°C). The glass transition of the cold-crystallized samples is generally higher, but decreases with increase in crystallization temperature $T_c$. Figure 4.57 compares the results from this study with the data of Cheng et al. Our results are slightly higher in magnitude than the data of Cheng et al., but exhibit the same trend with change in $T_c$.

During the execution of the experimental work presented here, preliminary DSC investigations in our group have shown, that the $T_g$ of i-PS depends on crystallization time. [50] Long isothermal crystallization of i-PS leads to an increase in $T_g$ of the polymer, which parallels the development of the low temperature endothermic peak, observed after such thermal history (see also figure 4.30). The next two figures confirm this observation in the case of PEEK.

Figure 4.58 shows the development of $T_g$ with cold-crystallization time $t_c$ for PEEK samples, cold-crystallized at $T_c$ = 243°C. The scatter of the data is relatively significant, compared to the absolute change of $T_g$ within the time interval considered. The line on the

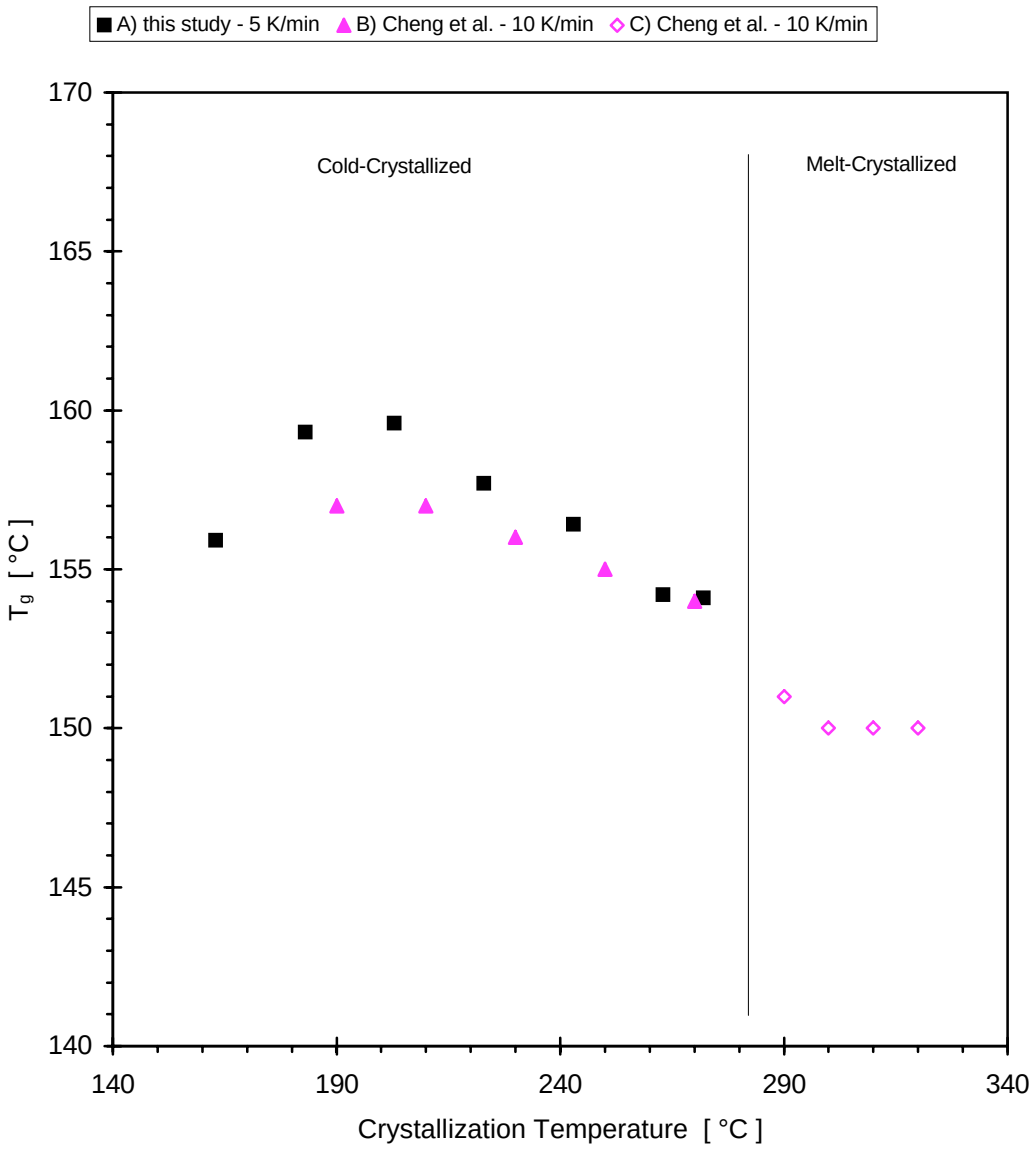


**Figure 4.57** Glass transition temperature of PEEK from DSC: A) this study, $t_c$ = 60 min; B) Cheng et al. [16], $t_c$ = 120 min; C) Cheng et al. [16], $t_x$ = 120 min.

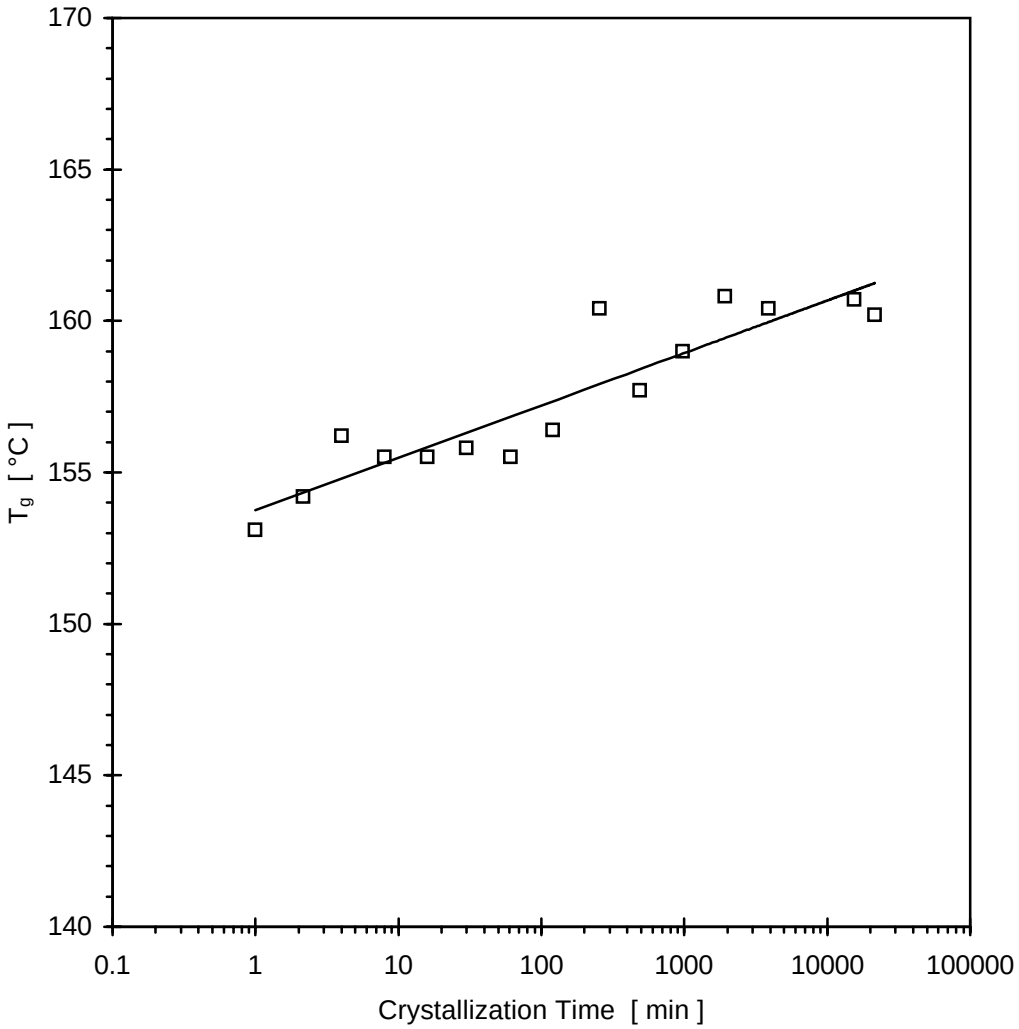


**Figure 4.58** Development of $T_g$ with crystallization time $t_c$ for PEEK, cold-crystallized at $T_c$ = 243°C. DSC heating rate 5 K/min.

plot is to be considered only a guide for the eye, rather than a precise functional dependence of $T_g$ on $t_c$. However, the result unequivocally establishes, that: 1) $T_g$ of PEEK also increases with increase in crystallization time, and 2) the time scale, over which this change is observed is the same as the time scale of development of the low temperature endothermic peak upon long time crystallization from the glass.

Figure 4.59 confirms this observation in the case of another type of thermal history, which leads to the development of a low temperature endothermic peak in the DSC scan of PEEK. The data is from the DSC scans of the samples, melt-crystallized at 310°C for 300 min and annealed below $T_x$ (see figure 4.25 for example). At two different annealing temperatures - 210°C and 240°C, increase in annealing time leads to an increase in $T_g$. The results are fitted to a linear dependence of $T_g$ on $\log(t_a)$ (again rather as a guide for the eye). Although the thermal history of these samples is different from the one for the data shown on figure 4.57, the dependence of $T_g$ on $T_a$ on figure 4.59 is the same as the dependence of $T_g$ on $T_c$ on figure 4.57. $T_g$ decreases as the annealing temperature $T_a$ is raised.

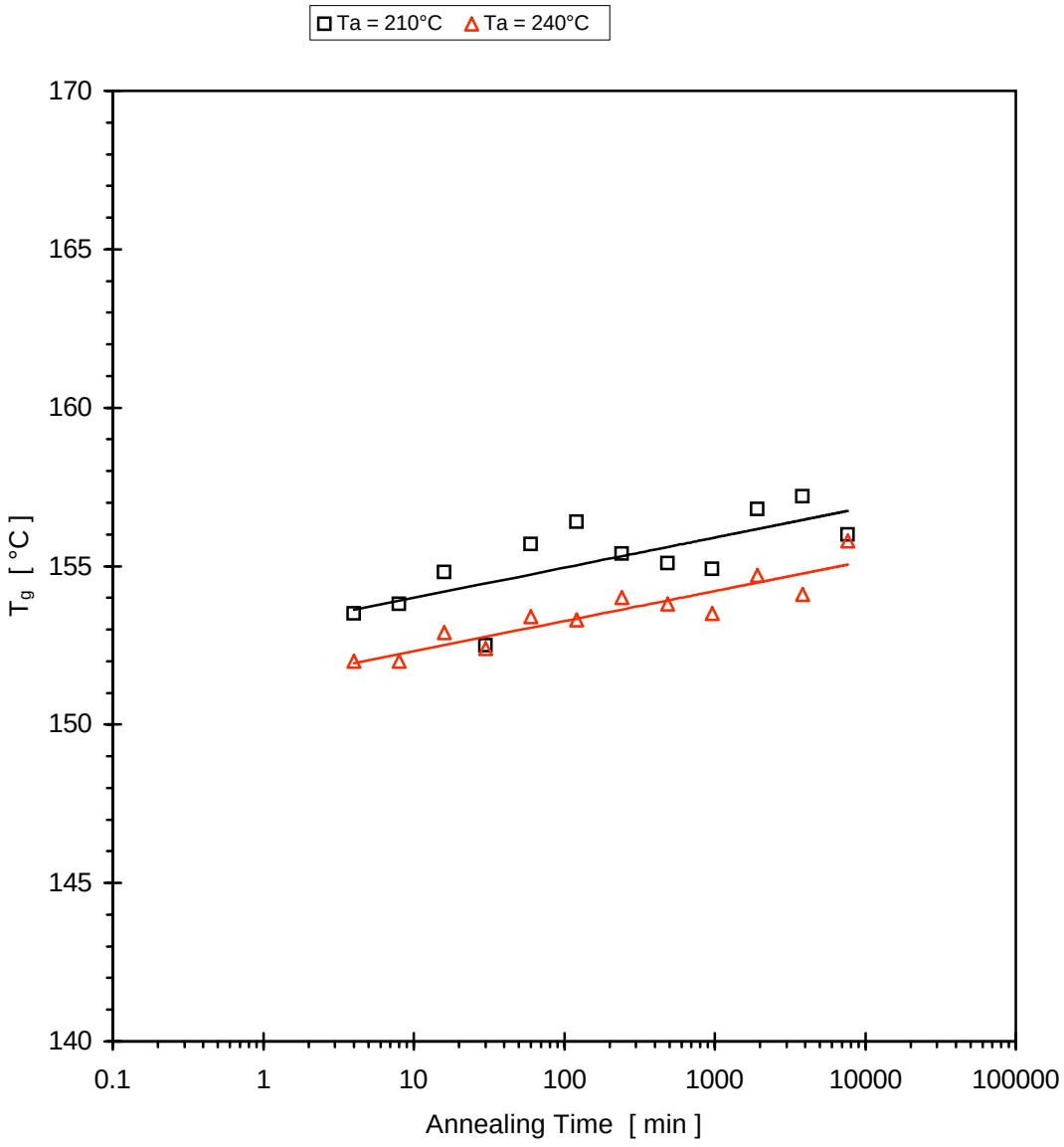


**Figure 4.59** Development of $T_g$ of PEEK with annealing time $t_a$. Samples are melt-crystallized at 310°C for 300 min and subsequently annealed below at the indicated annealing temperatures $T_a$. DSC heating rate 20 K/min.

# CHAPTER 5

# DISCUSSION

The following paragraphs briefly review the main experimental findings of this study. Current models for the dual melting behavior will be reviewed in light of the original results presented here. Some of the results, presented in chapter 4 without discussion or explanation, will be analyzed in light of the results from other experiments. Finally, the results from a few more experiments labeled as "controversial" will be presented. These were labeled as such not because of doubt in the quality of the experimental work or the results, but rather due to the fact that, while complementing the results shown earlier in this study, it is difficult, if not impossible, to accommodate them into any of the currently suggested working models.

## 5.1 Summary of the Effects of Long Crystallization and/or Annealing on the Physical Properties of Semicrystalline PEEK

This experimental study has been undertaken with the specific goal to be the first to focus attention on a set of phenomena, which previously have been either investigated separately and without correlation, or not investigated at all in certain specific cases. While focusing on a single polymer - PEEK, it is transparent that most of these results can be readily obtained on other semicrystalline polymers, if the same systematic investigation is applied.

Discrepancies between crystallinities, determined by various methods, are given in almost every textbook as an example of the limitations of the methods or the inherent uncertainty of this physical variable.

The "dual" or "multiple" melting of many polymers has been investigated since the very early development of polymer thermal analysis and calorimetry. The low temperature melting, which results from long isothermal crystallization and/or annealing, has been identified as a commonly observed phenomenon in a variety of semicrystalline polymers. In fact, a more in-depth reading of some of the oldest papers in the literature on this phenomenon would show to a dedicated reader almost every single detail of the properties of this phenomenon observed in this study.

"Physical aging" of semicrystalline polymers above their nominal $T_g$ is a term which has gained acceptance, at least for describing a number of slow relaxation phenomena observed above $T_g$, if not for providing the true mechanism governing this relaxation.

Finally, the calorimetric determination of $T_m$ and especially of $T_g$ of a polymer is taken as a routine work and often, for practical purpose justifiably, those are quoted as physical constants in reference books and reviews.

Most of the these studies of long annealing effects and/or the low temperature endothermic peak in the DSC scans of polymers have been undertaken with rigor and determination, but remained limited to a single method of investigation, whether DSC or relaxation spectroscopy, for example. Yet there has been no work in the literature until now to point towards the common thread in all these phenomena, which this study has attempted to elucidate.

In summary, these are:

1. Long isothermal crystallization and/or annealing in a wide range of temperatures and under various thermal history profiles between $T_g$ and $T_m^{'}$ of a polymer leads to the development of dual/multiple melting. A low temperature endothermic peak is observed in the DSC scan at temperatures always very close to the original annealing/crystallization temperature(s).

2. The kinetics of development of this low temperature melting peak has been thoroughly characterized for the first time for any polymer. For many of the thermal history profiles employed, several generalizations can be made:

- The peak appears only after the development of primary crystallinity has reached a certain stage. In the initial presence of primary crystallinity, the peak begins to develop almost instantaneously.

- The temperature $T_{max}$(low) at which the peak occurs is determined by the annealing temperature $T_a$ and the annealing time $t_a$. $T_{max}$ increases linearly with $T_a$ and $\log(t_a)$. For the same $T_a$ and $t_a$, $T_{max}$ is practically independent of morphology and previous thermal treatment. (For simplicity, often from here on we will omit the use of the multiple labels {$T_a$,

$t_a\}$, $\{T_x, t_x\}$, and $\{T_c, t_c\}$ for the annealing time and temperature, melt-crystallization time and temperature, and cold-crystallization time and temperature, and will use only $T_a$ and $t_a$.)

- At higher $T_a$ the peak appears closer to the annealing temperature than at lower $T_a$. The rate of increase of $T_{max}$ with $\log(t_a)$ also decreases at higher temperatures.

- The peak increases in height and width with increasing annealing time. Increasing annealing temperature leads to increase in height, but decrease in width.

- The peak is always followed by a step change in the $C_P(T)$ local baseline. This change is initially negative, but with increasing annealing time decreases in magnitude and then becomes positive. The effect is very strong in cold-crystallized samples and less pronounced in melt-crystallized samples annealed below their crystallization temperature.

- After the subtraction of this local step-baseline, the peak appears almost symmetrical in shape.

- The peak enthalpy $\Delta H_m(low)$, evaluated under the step-baseline conditions also increases with increase in $T_a$ and $\log(t_a)$.

- Multiple step annealing down leads to the development of a peak just above each annealing temperature. Multiple annealing up leaves only the peak resulting from the highest annealing temperature, while leaving the high temperature melting peak practically unchanged.

3. The development of a low temperature melting fraction upon long isothermal treatment is paralleled by a slow process of "densification" of the crystal unit cell. It occurs on the same time and temperature scale as the slow secondary crystallization process, reflected in the low temperature melting.

4. The parallel development of these two phenomena results in the absolute necessity for a new approach in evaluating weight fraction crystallinity by density - equation (2.3a).

5. The development of DSC and density crystallinities after reevaluation of the corrected density crystallinity leaves a discrepancy between not only the absolute values, but also the time and temperature dependencies of these two estimates of the same physical

variable. The discrepancy is irreconcilable within the simple two-phase model of the physical state of polymers, already violated by the observation of time-dependence of the value of the "reference constant" $r_c$.

6. The development of secondary crystallinity, the evolution of the thermal stability of the secondary lamellae, and the densification of the unit cell are paralleled by a slowing down of the creep recovery of the polymer during annealing above $T_g$. Under the standard interpretation of such experimental methods, this is assigned to the shift of a broad retardation spectrum to longer retardation times.

7. In addition to the creep recovery results, a calorimetric investigation of the glass transition also reveals that annealing above $T_g$ leads to slowing down of the relaxation processes in a semicrystalline polymer. The glass transition temperature generally decreases when the crystallization/annealing temperature is raised, but increases with $\log(t_a)$ after annealing at any temperature above $T_g$.

8. Preliminary DSC studies of melt-crystallized i-PS and PBT show that the evolution of the low temperature endothermic peak for these two polymers follows the same type of kinetics as that for PEEK, described above.

The linear development of a parameter, when scaled to an arbitrary reference time and/or temperature, is a common feature for many of the variables, describing the phenomena above. $T_{max}$, $\Delta H_m$(low), $\Delta C_P(T_{max})$, $r_c$, $T_g$, $\log(a)$, and $b$ increase with $\log(t_a)$; $T_{max}$, $\Delta H_m$(low), $\Delta C_P(T_{max})$, $r_c$, $T_g$, $m$, and $B$ vary linearly with $T_a$. Results from our group on SAXS studies of PEEK and PET suggest that the long period, lamellar thickness, and amorphous layer thickness also change with $\log(t_a)$ during the time range of secondary crystallization from the melt. [147, 148] These observations seem to be universal and one can expect that many of them can be reproduced for other semicrystalline polymers as well. They reflect a common physical process or several parallel and interconnected processes, which are thermally activated, having a temperature dependence similar to that of segmental relaxation. Their coexistence and correlation must be taken into consideration when the models for the "dual/multiple melting" are reevaluated.

## 5.2 Development of the Low Temperature Melting Endotherm During Crystallization or Annealing

Several of the studies on the melting behavior of PEEK have characterized to a different extent the features of the low temperature melting peak, observed in the DSC melting scan of the polymer after isothermal crystallization or annealing. [16, 63-67, 70, 72, 73] The most comprehensive studies in regard to the low temperature peak so far are the ones by Cheng et al., [16] Lee et al., [65, 66] Bassett et al., [70] and Chang. [72] Valuable qualitative information is available in the works of Blundell et al., [63, 64] Cebe and Hong, [71] and Lattimer et al. [73] Most of the characterization focused on the dependence of the low temperature peak on the isothermal crystallization temperature from the glass or from the melt state at given crystallization or annealing time. In general, in almost all papers, it is quoted that the peak position shifts up in temperature with time. However very few studies provide quantitative data in this aspect. [65, 70, 76]

Based on the original findings of this study, the discussion of the low temperature melting peak could complement the current status of the research in several areas:

- The melting temperature of PEEK, determination of the equilibrium melting point $T_m$, thermal stability of primary vs. secondary lamellae;

- Analysis of the heat capacity of PEEK in the temperature range between $T_g$ and $T_m^{'}$;

- Accurate evaluation of the enthalpy of the melting transition(s) of PEEK and DSC crystallinity; determination of $\Delta H_m^0$;

- Analysis of the physical model(s) for the "dual melting" behavior.

### *5.2.1 Melting Temperatures: $T_{max}$(low) and $T_m^{'}$*

The thermal stability of the crystalline lamellae of PEEK has been analyzed by various authors according to their acceptance of one or the other of the two models of the dual melting of PEEK, reviewed in section 2.4.2: melting-recrystallization mechanism and melting of two different populations of lamellae - primary and secondary. Those authors,

who adhere to the former, reason that the melting temperature associated with the low temperature endothermic peak $T_{max}$(low) is the actual thermodynamic melting point of the existing PEEK lamellae. Those, who adhere to the latter, have taken $T_m^{'}$ of the high temperature final melting as the indicator of the thermodynamic stability of the dominant part of the lamellae - the primary population.

Blundell and Osborn [63] had used $T_{max}$(low) for evaluation of the equilibrium melting temperature $T_m$ of PEEK using the Gibbs-Thomson-Tamman equation. Their approach in using $T_{max}$(low) instead of $T_m^{'}$(high) has been questioned in several publications and alternative ideas and methods have been applied. For example, Lee et al., [65] after realizing that $T_{max}$(low) has a strong heating rate dependence, chose T' = [$T_{max}$(low)+ $T_m^{'}$(high)]/2, extrapolated to infinite heating rate, instead. In their view, this is justified as the limit, when no recrystallization is observed after the initial melting and the low temperature peak reflects the complete, unperturbed melting trace of the PEEK lamellae. The results from DSC melting scans after short crystallization times at low $T_x$ (figure 4.17), as well as from other experiments in the literature [2, 16, 70] clearly demonstrate that $T_{max}$(low) can not possibly be uniquely assigned to the thermodynamic melting point of the primary lamellar population of PEEK.

The following facts support this conclusion:

- The melting of PEEK fractions with low molecular weight shows the presence of a very small low temperature peak. The shape of the melting peak could not be explained as a sum of two melting endotherms, separated by a recrystallization exotherm.

- $T_{max}$(low) is a function of log($t_x$); it does not reach a limiting value at intermediate times as might appear from a $T_{max}$(low) vs. $t_x$ plot. This makes completely arbitrary the choice of $T_{max}$(low) for a given value of $t_x$. $T_{max}$ could be evaluated for any other value of $t_x$ and the extrapolation result for $T_m$ will be completely different.

- $T_{max}$(low) begins to develop in the DSC scans of melt-crystallized PEEK only after the appearance of the high temperature melting peak. This unequivocally establishes the fact

that the lamellae originally formed from the free melt at temperature $T_x$ do not melt just above $T_x$, but at a much higher temperature, generally in the range of 340-355°C.

As a result, most studies of the apparent equilibrium melting temperature of PEEK have applied the Hoffman-Weeks method, utilizing the dependence of $T_m'$(high) on $T_x$ (equation 4.2). [66, 129, 132] These studies consistently point towards a result of $T_m$ = 385±5°C, which is also confirmed by the results on figure 4.2.

Often in the literature on other polymers: PET, [57] Nylon 10,10, [56] i-PP, [44] i-PS, [49] PVC [52] the increase of $T_{max}$(low) with time has been acknowledged, but the data has been analyzed incorrectly by the authors. Plotting $T_{max}$(low) and often $\Delta H_m$(low) against $t_x$ on a linear scale, it appears that soon after the fast increase at short times, the values of $T_{max}$ and $\Delta H_m$(low) level off. It has been clearly shown that this is not correct, as the present extensive data on PEEK and the limited, but very similar in nature, data on other polymers indicates a steady increase of these thermal characteristics with log($t_a$) over the time ranges of investigation. In addition, results in the literature on other polymers indicate the increase in $T_{max}$(low) or $\Delta H_m$(low) with an increase in log($t_a$): PPS,[124] PET,[37, 38, 40, 185] Nylon 6,6, [54,55] i-PP,[45, 46] PVC.[51]

The discussion of the possible origins of the lower thermal stability of the secondary lamellar population will be presented later in this chapter in section 5.5.

### *5.2.2 Heat Capacity of PEEK between $T_g$ and $T_m'$*

The quantitative analysis of carefully recorded heating scans in the vicinity of the low temperature endotherm leads to some new results, which could help the understanding of the complex physical processes involved in the phenomenon of "double melting".

Figure 4.13 showed the melting scans at 20 K/min of PEEK samples cold-crystallized at different temperatures for the same time. Overall the data reproduces the results at 10 K/min on samples with similar thermal history reported by Cheng et al. [16] The most interesting observation from the plot of the different scans together is the fact that the $C_P$(T) values after the low temperature peak are almost the same for all samples in a wide

temperature range. The upper limit of this range is the beginning of the high temperature melting peak, where $C_P(T)$ begins to deviate from its approximately linear increase with temperature. The lower limit is the end of the low temperature peak for each scan. The peculiar result is that these common values of $C_P(T)$ after the low temperature peak are *lower*, than the values before the peak.

The lowering of the $C_P(T)$ trace after the peak has been noticed also by Cebe and Hong [71] and Jonas et al. [68] It can be seen also in the DSC traces of cold-crystallized PEEK, reported by Bassett et al. [70] With the exception of the recent work by Jonas et al., these other papers are in fact the major studies that have provided conclusive evidence against the melting-recrystallization model for the dual melting of PEEK. Yet the nature of the reported deviation from the expected heat flow line is *exothermic* with respect to the trace before the peak! The trivial interpretation of such an exothermic deviation would be a "recrystallization peak". Clearly this is a problem for the dual lamellar population model, which has not received proper attention.

Cebe and Hong [71] reported their observation as an "exothermic peak" after the low temperature melting peak. They interpreted it as a heat of recrystallization of the low melting temperature secondary lamellae, which later melt in the high temperature peak. Such an interpretation would be easily ruled out if the dependence of the low melting peak on time or temperature ($t_a$ or $T_a$) is considered.

(*Note*: A poor resolution in the DSC scan, either due to the use of small amount of sample or to the use of different model calorimeter, has lead the authors to claim, that upon cycling thermal history, there is no low temperature melting peak after annealing at 200°C. They claim, that this only shifts the cold crystallization exotherm to higher temperatures. Then at higher temperature of annealing - 250°C, they observe the low temperature peak just above $T_a$ and claim, that the negative deviation after it is a recrystallization peak. It is obvious, from the results of this study and references 16 and 68, that some of their conclusions are flawed and therefore the descriptions and interpretations of the melting scans in reference 71 should be treated with caution.)

There is no indication, that the exothermic deviation after $T_{max}$(low) is indeed a "*peak*". A more careful collection and analysis of the data (as in figure 4.13 of this study or figure 10 in reference 16) shows that: 1) the $C_P(T)$ deviation *is not a peak*; 2) it is not affected by $T_a$ in a way expected for a "crystallization peak" - the exothermic deviation from $C_P(T)$ is not changed in magnitude by an increase of $T_a$, only its lower limit is shifted.

Nevertheless, Cheng et al. [16] also assigned the negative break in the $C_P(T)$ trace to a manifestation of recrystallization effects. However, probably due to the above mentioned characteristics, their statement is much more cautious. They have also examined an alternative explanation - that the DSC trace after the low temperature peak is the *true* $C_P(T)$ trace of a sample with high content of rigid amorphous fraction. Such an interpretation is plausible for two reasons:

1) The temperature dependence of the trace - $C_P(T)$ after the low temperature peak, is almost linear. Therefore, it could be interpreted as the sum of the specific values of the heat capacities of a mobile amorphous fraction with $C_P(T) = C_{P,Am}(T)$ and a rigid fraction (sum of the crystallinity and the RAF) with $C_P(T) = C_{P,Cr}(T)$.

2) According to their analysis, the RAF content decreases during the scan above $T_g$ until the beginning of the low temperature peak. Therefore, one might intuitively suppose, that the original value of the rigid fraction content could be restored after the peak (for some reason, which is left without discussion).

(*Note*: However, on the basis of the two-phase model, one could argue against the latter argument in the following way: If a certain fraction of the crystalline phase had melted, the $C_P(T)$ value could only be expected to increase, in the absence of recrystallization. Therefore, even if the RAF content is restored, the expected increase in the rigid fraction content would be negated by the decrease in crystallinity due to melting.)

Cheng et al. conclude, that the trace after the peak would correspond to a rigid fraction content much higher, than the one they have calculated from the DSC crystallinity and the rigid fraction content, measured at $T_g$. Based on this, they propose, that the exothermic deviation in $C_P(T)$ after the peak is due to *recrystallization* effects.

Within the context of the characteristics of the low temperature melting peak known by these authors (see also Jonas et al. [68]) and the thermal histories considered by them, their explanation of the relative drop of the magnitude of $C_P(T)$ after the peak is a plausible one. The question about the nature of these effects and how they result into the shape of a trace, which is almost the same for any sample, regardless of $T_a$, has not been raised, however.

The new results on the time dependence of the low temperature endotherm and the $C_P(T)$ trace in its vicinity, presented in this study, illustrate the fact, that the explanation of this phenomenon is not trivial:

1) The analysis of the DSC data clearly demonstrates, that a relative change in the magnitude of the $C_P(T)$ trace after the low temperature peak is observed not only in the case of cold-crystallized samples. The data on figure 4.26 (scan A) show this behavior also in the case of melt-crystallized samples, annealed below their crystallization temperature (thermal history profile of the type shown on figure 3.6).

2) The change in $C_P(T)$ after the low temperature peak is affected by the annealing time (figure 4.26). The kinetics of this change is similar to that, characteristic for the other parameters of the peak - $T_{max}(low)$ and $\Delta H_m(low)$. With increase in $\log(t_a)$ $\Delta C_P(T_{max,low})$ changes from negative to positive in linear fashion (figure 4.28-C).

3) The annealing temperature dependence of the change in $C_P(T)$ after the low temperature peak is approximately the same as the one described by Cheng et al. [16] for cold-crystallized samples. In addition, for given $t_a$ $\Delta C_P(T_{max,low})$ decreases with increase in $T_a$ and turns to positive, however, the $\log(t_a)$ dependence of $\Delta C_P(T_{max,low})$ is present at any annealing temperature (figure 4.29-E).

Within the trivial assignments of changes in heat flow during heating and the models for the "double melting", these new characteristics of the $\Delta C_P(T)$ change at $T_{max}(low)$ can not be explained.

The relatively large exothermic deviation in the heat flow after the peak during heating of cold-crystallized samples above $T_c$ (figure 4.13) can be qualitatively assigned to the structural reorganization in the material above $T_c$. There is indisputable evidence, that the

density of the crystalline phase undergoes changes with increase in the cold-crystallization temperature [68, 122, 123, 198] and time (figures 4.40-4.43 and references 68 and 155). Jonas et al.[68] have shown by time resolved and temperature dependent WAXD and SAXS, that irreversible changes in the structure and morphology of the samples are observed above $T_c$ during heating/cooling cycles. Qualitatively, one could assign the integrated heat from the exothermic deviation of the heat flow above $T_{max}$(low) to the latent heat of reorganization. In the case of samples, melt-crystallized and annealed below $T_x$ for short times, the negative change in $C_P(T)$ is very small. This correlates with the small degree of reorganization, expected in a sample, which has been well crystallized from the melt at temperature, much higher than the annealing temperature.

An expansion of this idea is possible, based on the knowledge of the kinetics of development of the low temperature endotherm. It is reasonable to expect, that the released heat during the reorganization will follow the same kinetics as $\Delta H_m$(low), namely - a log($t_a$) dependence. One can superpose this log($t_a$) dependence to the linear increase of temperature during heating in the DSC and assume for a moment, that no further melting occurs during the scan (expected $T_{max}$(low) is higher than the temperatures during heating).

From these assumptions it can be deduced, that a large release of heat $\Delta H_r(t_1)$ will be expected initially during heating through an interval $\Delta T = q^*\Delta t = q^*t_1$. This would lead to a relatively large negative deviation in $C_P(T)$. Continuous heating through the next interval with the same width $\Delta T = q^*\Delta t = q^*(t_2-t_1)$ would lead to less heat release as the enthalpy increases logarithmically with increase of time and therefore - temperature in the scan above $T_{max}$(low). Thus the released heat would be expected to be less and less at higher temperatures and the heat capacity should quickly return to a value, very close to the true $C_P(T)$ expected at this temperature.

Bringing the dependence of $T_{max}$(low) on time and temperature, however, changes this conclusion. $T_{max}$(low) expected for a sample, annealed for a short time just above the previous low temperature endotherm would be very close to $T_a$. Thus the process of annealing during heating will soon be interrupted by melting. The resulting $C_P(T)$ will depend on the balance of the heat of reorganization (annealing) during heating and melting of

material annealed just below the current temperature in the scan. This balance will probably depend on heating rate, initial $\Delta H_m$(low) (resulting from the annealing at $T_a$) and overall thermal history and morphology. The drop in the heat flow at $T_{max}$(low) would be due to the imbalance between the heat of reorganization and the heat of melting at $T_{max}$(low), when the low temperature melting enthalpy is added at this temperature.

Such an idea has been intuitively proposed by Busfield and Blake [44] in the case of i-PP. The idea is similar to the original melting-recrystallization model for the "double melting" behavior, [39, 63, 64] but applied only to the secondary lamellar population, melting at the low temperature endotherm. Furthermore, it complies with the known kinetics of development of the low temperature endotherm. A critical test of this idea would be a study of the dependence of $\Delta C_P(T_{max,low})$ on the heating rate (e.g. on the "annealing time" during heating), which at the present time does not exist. Further elaboration of this idea would be highly speculative without the support of additional experimental evidence.

This point of view, however, is still confronted by the observation of a positive deviation in $C_P(T)$ above $T_{max}$(low) for long annealed samples in the cold-crystallized and two-step annealed series of samples.

As mentioned above, application of the two-phase model to the heat capacity gives the following result: melting of a small fraction of secondary lamellae at the low temperature endothermic peak would actually lead to an increase in the heat capacity after the peak. For a sample, cold-crystallized for 60 min at 240°C, this increase is equal to approximately +0.001 cal/deg*g (this is based on extrapolated solid and liquid heat capacities and the melting enthalpy of the low temperature endotherm - figure 4.14). For a sample, melt-crystallized and annealed below $T_x$ at 240°C the same type of estimate (see figure 4.29 for melting enthalpy data) leads to an expected increase in $C_P(T)$ by +0.0003 cal/deg*g. The observed values of the $\Delta C_P(T_{max,low})$ increase for these and longer times are much higher (see figure 4.29-E). In general, they exceed the projected values by almost an order of magnitude. One reason for this could be the fact, that for the estimate of the liquid and solid heat capacities extrapolation is made from the data in temperature ranges, which are far away from the range of study. There is no better alternative, however. Due to a variety of technical as well as

theoretical difficulties stemming from the kinetics of development of the low temperature peak and the failure of the standard two-phase model, it is practically impossible to determine the heat capacity of the crystalline phase between $T_g$ and $T_m^{'}$ on the basis of the two phase model. Therefore, the nature of the turn from negative to positive changes in the heat flow above $T_{max}$(low) remains unclear.

A model for the peculiar changes in $C_P(T)$ above $T_{max}$(low) would have to rely on quantitative information about how relative changes in $C_P(T)$ depend on the evolution of other physical characteristics under similar thermal history. Such a model can not be constructed based on the currently available results. More dedicated studies are needed, in order to get a better understanding of the dependence of the observed changes in the heat flow on changes in the structure and morphology during crystallization and on thermal history in general.

For example, the study by Jonas et al. [68] mentioned above in connection with the latent heat of reorganization idea suggested that reversible heating below $T_c$ leads to reversible changes in the parameters of the structure (unit cell volume, apparent crystallinity, long period etc.), governed by thermal expansion only. The detailed knowledge of the effect of thermal history on the development of the low temperature melting transition suggests that this might not be true. Dynamic studies at a constant rate of heating in the synchrotron would allow observation only of the early stages of the processes, which occur during annealing. The log(time) rate of development of the low endotherm in cold crystallized samples, is relatively large, as is the rate of change in the structural parameters (density for example). The magnitude and rate of the effect under two-step annealing below $T_x$ (or $T_c$ for that matter) is very small, but still noticeable by calorimetry.

One can speculate, that further changes in the structure during annealing of cold-crystallized samples below $T_c$ could occur at a magnitude and rate, which are small enough, that previous WAXD and SAXS studies have been unable to resolve them. However, if their existence is proven, then the hypothesis about the reversibility of structural changes upon heating and cooling below the highest annealing temperature [68] will have to be revised. All the currently available data on thermal expansion of PEEK, which is based on methods with

slow data collection (i.e. scattering methods with weak radiation sources), will have to be reconsidered as well. A test of this hypothesis would require a dedicated study of the long time annealing effect at temperatures below $T_c$, which does not exist at this time in the literature.

To end the discussion of the heat capacity, it should be mentioned, that the change in $C_P(T)$ at $T_{max}(low)$ is another phenomenon, which is universally observed under any thermal history, leading to the development of a low temperature melting endotherm. Furthermore, this change can be also seen in the case of cold-crystallization and/or annealing of other polymers between their respective $T_g$ and $T_m^{'}$: PET, [189] PBT, [14, 58, 189] PPS. [15] On this basis, it could be expected that a detailed study of the annealing time and temperature evolution of the DSC trace in the vicinity of the low temperature endotherm for these polymers will find analogous features of the $C_P(T)$ change at $T_{max}(low)$.

### *5.2.3 Enthalpy of the Melting Transition(s) of PEEK: $DH_m(low)$, $DH_m(total)$, $DH_m^0$*

The technical details of the evaluation of the heat of fusion and DSC crystallinity were already discussed in the experimental section - 3.2.3a. In this section we focus on possible problems in the evaluation of the melting enthalpy, arising from the general features of the "double melting" scan of PEEK, presented in this study.

#### *Evaluation of $DH_m(low)$*

For the analysis of the effect of thermal history on crystallinity, associated with the low temperature melting endotherm, and the overall DSC crystallinity, an accurate evaluation of $\Delta H_m(low)$ is needed.

As was mentioned in the previous section, several literature studies [16, 68, 71] have shown, that the local baseline in the vicinity of the low temperature endothermic peak exhibits significant changes with temperature during the DSC scan and is different for different initial morphologies before the scan (cold- vs. melt-crystallization). None of the

previous studies gave a detailed description of how exactly the $\Delta H_m$(low) is evaluated under such widely different local baseline conditions. The results of this study, summarized and discussed in the previous sections, provide additional information, which suggests that a careful selection of the local baseline is needed as it changes with annealing time, temperature and type of thermal history.

Previous studies of the double melting of PEEK and other polymers often have concentrated on two particular types of thermal histories: melt-crystallized samples at relatively high crystallization temperatures and samples, cold-crystallized from the amorphous glassy state. In the DSC scans of the former, the low temperature endothermic peak merges with the beginning of the high temperature final melting peak. This makes difficult the separation of the two and the assignment of their respective transition enthalpies. In the DSC scans of the latter, the low temperature peak is followed by a significant drop in the local baseline, already discussed in the previous section.

Thus in both cases the evaluation of the contribution of the low temperature melting peak is hindered by the difficult assignment of a local baseline. Furthermore, there appeared to be no correlation between the possible baselines in these two cases, although the nature of the phenomenon is the same - low temperature melting. No conclusion could be drawn about the shape of the peak either, as in the former case it has a steep front and a wider and less steep tail, while in the latter case the situation appears to be reversed - a small rise, followed by a steep drop.

The systematic probe into the shape of the low temperature peak and the local baseline in its vicinity was driven by the initial observation, that in quite a few special cases, where the peak is strong, it appears to be symmetrical in shape (see for example the scans for high $T_c$ in figure 4.13 and the long annealing times on figure 4.21). Further investigation in few special cases (presented later in this chapter), where the unique thermal history produces a low temperature annealing peak, which dominates the DSC scan, confirmed this observation.

As a result, it was shown, that in the vicinity of a well resolved low temperature endothermic peak, $C_P(T)$ can be successfully fitted with the combination of a linear function

of temperature - the "true" heat capacity before the melting peak, a symmetrical step-function - the change in $C_P$ at the peak, and a peak-function - the melting peak (see section 4.2.1, p. 168-180).

With adjustment of some of the parameters of the fit, a very good fit is produced in the cases DSC scans of cold-crystallized samples and melt-crystallized samples, annealed below $T_x$. Interestingly, in the case of melt-crystallized samples, the attempts to resolve the low temperature peak by subtraction of a peak function alone did not produce satisfactory results. The residual scan (which should represent the high temperature melting peak) showed fluctuations in the range of the low temperature peak, which could not be minimized by adjustments in the parameters of the subtracted peak. A smooth line for the residual scan was obtained only when a combination of a peak and a step function (reflecting positive change in $C_P$) was subtracted. This observation allows the same model to be applied under various thermal histories, which leads to the correct separation of the melting enthalpy of the low temperature endothermic peak from local baseline changes, regardless of what their origin might be.

***Evaluation of $DH_m$(total)***

The discussion of the evaluation of $\Delta H_m$(total) comes naturally as an extension of the discussion of the heat capacity between $T_g$ and $T_m^{'}$ in the previous section. It was shown, that a change in $C_P(T)$ is observed at the low temperature endothermic peak. This change is always observed, when the thermal history of the sample includes annealing and leads to a low temperature endothermic peak. The two possible explanations for the $\Delta C_P(T_{max})$ change in the heat capacity lead to two very different approaches in evaluating the total enthalpy of melting and therefore, ultimately - in the evaluation of the DSC crystallinity:

1) If one accepts the view, that the change in $C_P(T)$ is a manifestation of a shift in the balance between melting and recrystallization of the secondary (low melting) lamellae, then the total melting enthalpy must include all endothermic and exothermic contributions, roughly between the lowest $T_a$ and the end of melting. This is the approach described in the experimental section - 3.2.3a.

2) If on the other hand one accepts the idea, that the $C_P(T)$ values above the low temperature peak represent the true heat capacity of the sample at these temperatures, then obviously a different procedure for evaluation of the total melting enthalpy must be applied.

For example, in the case of cold-crystallized PEEK, it was shown, that changes in the time and temperature of annealing do not affect the high temperature peak and lead only to changes in the low temperature peak's melting enthalpy. The total melting enthalpy will be the sum of the enthalpies of the high temperature peak and the low temperature one. The changes in $\Delta H_m(low)$, the evaluation of which was discussed at the beginning of this section, will determine the relative changes in $\Delta H_m(total)$. The accurate evaluation of $\Delta H_m(low)$ will be critical for the evaluation of the changes in $c_c^{DSC}$.

The evaluation of the total melting enthalpy and DSC crystallinity is based on the assumption stated in 1) above and is described in the experimental section. Adherence to the other assumption will change the technique of evaluation of the melting enthalpy and lead to different values of the DSC crystallinities. A rigorous evaluation of the DSC crystallinities under this method would be meaningless until further studies clarify the physical origin of the change in $C_P(T)$ above $T_{max}(low)$ with time, temperature and conditions of annealing. From the known time and temperature dependence of $\Delta C_P(T_{max,low})$ one can qualitatively estimate the effect on the results, presented in section 4.2.3.

The discrepancy between DSC and density crystallinities will remain for all series of samples. The time-dependent series of samples will be affected very little as the small change in $\Delta C_P(T_{max,low})$ with $\log(t_a)$ would produce an almost constant correction. The series affected the most would be the temperature-dependent series of cold-crystallized samples, due to the change in the width of the interval between $T_{max}(low)$ and $T_{onset}(high)$ (see figure 4.13). Qualitatively, the slope of the overall DSC crystallinity (see figures 4.35 and 4.47) would be the same as the slope of the contribution of the low temperature endotherm.

(*Note*: In reference 16, Cheng et al. state that melting in the DSC scan of PEEK can be detected shortly after the glass transition region. Thus Cheng et al. propose, that evaluation of the melting enthalpy must be done over a wide temperature range, roughly between 180°C and 360°C. However, the results of this study suggest that this observation is not universal.

It was probably due to the specific thermal history employed by Cheng et al. All of their samples were cooled very slowly - at a rate of -0.31 K/min, from the crystallization temperature to room temperature. Such thermal history results in cooling times to reach $T_g$ on the order of up to 300 min. If one approximates the continuous cooling with step-wise regime of cooling, based on the knowledge of the effect of annealing on the melting scan of PEEK, it can be predicted that such thermal history will produce significant low temperature melting fraction. Its melting upon heating from the glass will be spread through the entire interval between $T_g$ and $T_a$. In this study, on the other hand, the samples were always pre-crystallized for long time and then fast-cooled. With times to reach $T_g$ on the order of seconds, very little additional crystallization upon cooling will be expected. Indeed, the first indication of melting is observed at approximately $T_a$ and above for cold-crystallized samples, and at about 260-300°C for melt-crystallized samples, depending on the time and temperature of crystallization.)

The problems, discussed above, if found legitimate, point towards the possibility that the enthalpy of fusion for a 100 % crystalline PEEK, evaluated by Blundell and Osborn [63] on the basis of a correlation between $\Delta H_m$(total) and WAXS crystallinity, is not correct. We will continue using its value, on the assumption, that a relative change of $\Delta H_m^0$ only scales up or down the DSC crystallinities, but does not affect significantly their rate of change with $T_a$ and $\log(t_a)$.

In summary, the analysis of the discrepancy between DSC and density crystallinities will be based on the assumption, that the total heat flow between the beginning of melting (low temperature melting) and the end of melting (the $C_P$ of the melt) reflects the total melting enthalpy of the transition.

## 5.3 Discrepancy between DSC and Density Crystallinities and the Physical State of the Amorphous Fraction

In section 4.2.3 it was demonstrated that a discrepancy exists between the values of the DSC crystallinity $c_c^{DSC}$ and the density crystallinity $c_c^{Dens}$ of PEEK. The discrepancy is

observed not only in the results of this study, but in literature data on DSC and density crystallinities as well.

The discrepancy between $c_c^{DSC}$ and $c_c^{Dens}$ is not only observed in their absolute magnitude for any given sample, but also in their dependence on the time and temperature of crystallization. The difference in the time- and temperature-dependence of these two quantities is associated with the large increase in the DSC crystallinity. The latter is due to the linear increase of the low temperature peak's melting enthalpy with $T_a$ and $\log(t_a)$.

This claim is further substantiated by a similar observation by Chung et al. [124] in the case of PPS. After applying the correct values for the crystal density of PPS, which take account of the densification of the unit cell with increase of $t_c$ and $T_c$, they arrive at a discrepancy between the values of the DSC and density crystallinities of PPS. In their analysis of this observation, however, they make contradictory conclusions.

On the one hand they propose that the density of the amorphous phase might vary with crystallization and annealing conditions just as the crystal density does. This is suggested as an explanation for the discrepancy of the DSC and density crystallinities' values and trends.

On the other hand, while acknowledging this fact and the presence of a large rigid amorphous fraction in their polymer, they still make the claim that the two-phase model is valid for the calculation of the density crystallinities.

In the following, this controversy will be analyzed with the data from this study (section 4.2.3), as well as the literature data on PEEK [16, 17, 65, 66] and the PPS data of Chung et al. [124]

If the two-phase model of crystallinity is to be still valid, then the DSC and density crystallinity values and trends must be brought together by examining the possible sources for deviation from their expected values.

One such source is the value of the melting enthalpy of a fully crystalline polymer $\Delta H_m^0$. If its value has not been properly determined, then the DSC crystallinity values could be under- or overestimated. As was mentioned earlier, correcting for that error will only

scale up or down in magnitude the values of $c_c^{DSC}$, but will not correct for the significant difference in the dependence of $c_c^{DSC}$ and $c_c^{Dens}$ on crystallization temperature and time.

Another possible source of error in determining the DSC crystallinities is the use of the same value of $\Delta H_m^0$ for calculating the crystallinity from both melting peaks, which can be positioned quite far apart on the temperature scale. In general $\Delta H_m^0$ reflects the melting enthalpy of a fully crystalline PEEK in the temperature range of 330-350°C. The melting enthalpy of a fully crystalline PEEK at much lower temperature (as is the case with cold-crystallization of PEEK just above $T_g$) will be reduced. [116] This will lead to a temperature dependent correction to the DSC crystallinity attributed to the low temperature endotherm and an overall increase in the DSC crystallinities. The magnitude of this increase, however, is very small and does not compensate for the discrepancy between $c_c^{DSC}$ and $c_c^{Dens}$. Furthermore, as the increase in $T_{max}$(low) with increase in crystallization time is small compared to its distance from the main melting region, this type of correction will not affect the discrepancy in the magnitude of change of the DSC and density crystallinities with crystallization time.

The other possible source of the difference between $c_c^{DSC}$ and $c_c^{Dens}$ is the value of the amorphous density $r_a$ or, put in more general terms, the nature of the amorphous phase in the semicrystalline polymer. The value of $r_a$ is used in equation (2.3a) as a physical constant for the polymer, the same as that for a completely amorphous PEEK.

If the two-phase model is to be valid (i.e. the DSC and density crystallinity values and trends are to be reconciled), then one could use equation (2.3a) for calculating the value $r_a^{calc}$ (the amorphous density) must take in order for the DSC and density crystallinities to be equal. For this purpose $c_c^{Dens}$ is substituted in the equation with $c_c^{DSC}$ and the values of $r_c(t_c, T_c)$ and $r$ are used as in the calculation of the corrected density crystallinity. Then the amorphous density is calculated according to the equation:

$$r_a^{calc}(T_c, t_c) = \frac{1 - c_c^{DSC}}{\frac{1}{r(T_c, t_c)} - \frac{c_c^{DSC}}{r_c(T_c, t_c)}} \qquad (5.1)$$

Figure 5.1 compares the parameters involved in this calculation and presents the result in the case of the samples cold-crystallized at 243°C. Plotted are the values of $r_c$, $r$, and $r_a^{calc}$. The value of $r_a$ for the purely amorphous PEEK is represented by the dotted line. The calculated amorphous density must decrease with increase of crystallization time $t_c$.

Figure 5.2 presents the same result for the temperature dependent series of cold-crystallized samples. For $r$ (A) and $r_a^{calc}$ (C) the symbols represent the results from this study, whereas the continuous lines - the literature data, plotted in figure 4.48. The results of this study are practically identical with the results from the literature data - the calculated amorphous density decreases with increase in cold-crystallization temperature.

Figure 5.3 shows the results for the series of melt-crystallized samples. The decrease of $r_a^{calc}$ with crystallization time appears less than in figures 5.1 and 5.2 but is still present.

Analysis of the data of Chung et al. [124] (on PPS samples, cold-crystallized at $T_c$ = 245°C) leads to the same result - figure 5.4. The amorphous density of semicrystalline PPS, calculated with equation (5.1), decreases significantly with increase in $\log(t_c)$.

The conclusion from this exercise is that in order for the crystallization temperature and time dependencies of the DSC and density crystallinities to be reconciled, the density of the amorphous phase must decrease with crystallization time during the secondary crystallization process. The departure of $r_a^{calc}$ from the equilibrium value is higher for samples cold-crystallized at higher temperatures and somewhat less for melt-crystallized samples.

(*Note*: As was noted in section 4.2.3 for the observed crystal density, here one must again emphasize, that this is an *apparent* decrease of $r_a^{calc}$ with crystallization time and temperature. The quantity in question is the density of the amorphous phase at room temperature. The question whether $r_a$ actually decreases in real time during the secondary crystallization remains to be answered. Some recent investigations by real time WAXS of melting and isothermal crystallization of PEEK have suggested, that the average amorphous density at $T_c$ actually increases during the secondary crystallization process. [149] This conclusion, however, is derived indirectly - from the shape and position of the amorphous

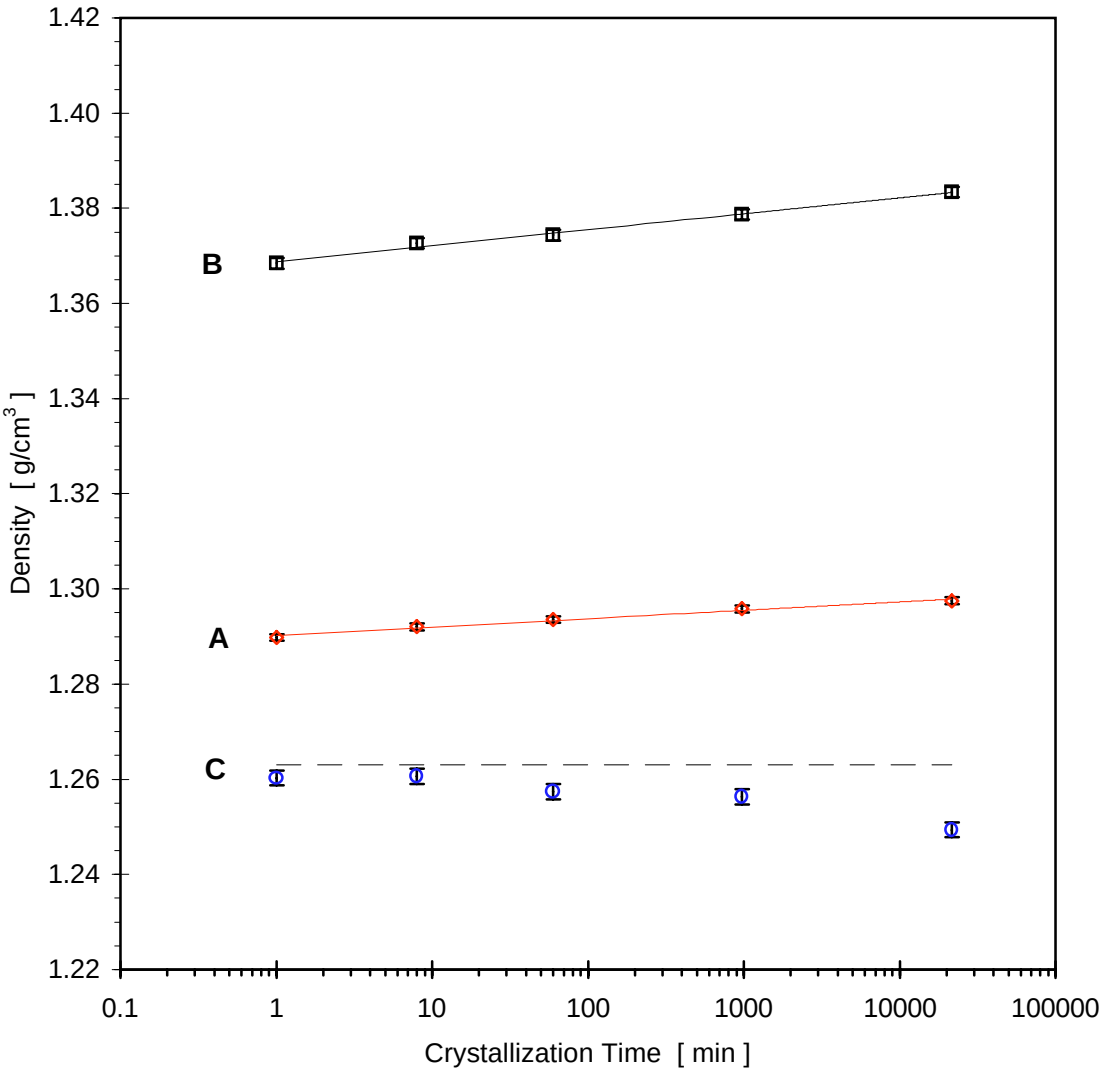


**Figure 5.1** Dependence of the room temperature densities on crystallization time $t_c$ for the samples, cold-crystallized at $T_c$ = 243°C: A) bulk density, B) crystal unit cell density, C) density of the amorphous phase, calculated according to the two-phase model assumption of equivalence of DSC and density crystallinities - equation (5.1). Dashed line reperesents the density of fully amorphous PEEK.

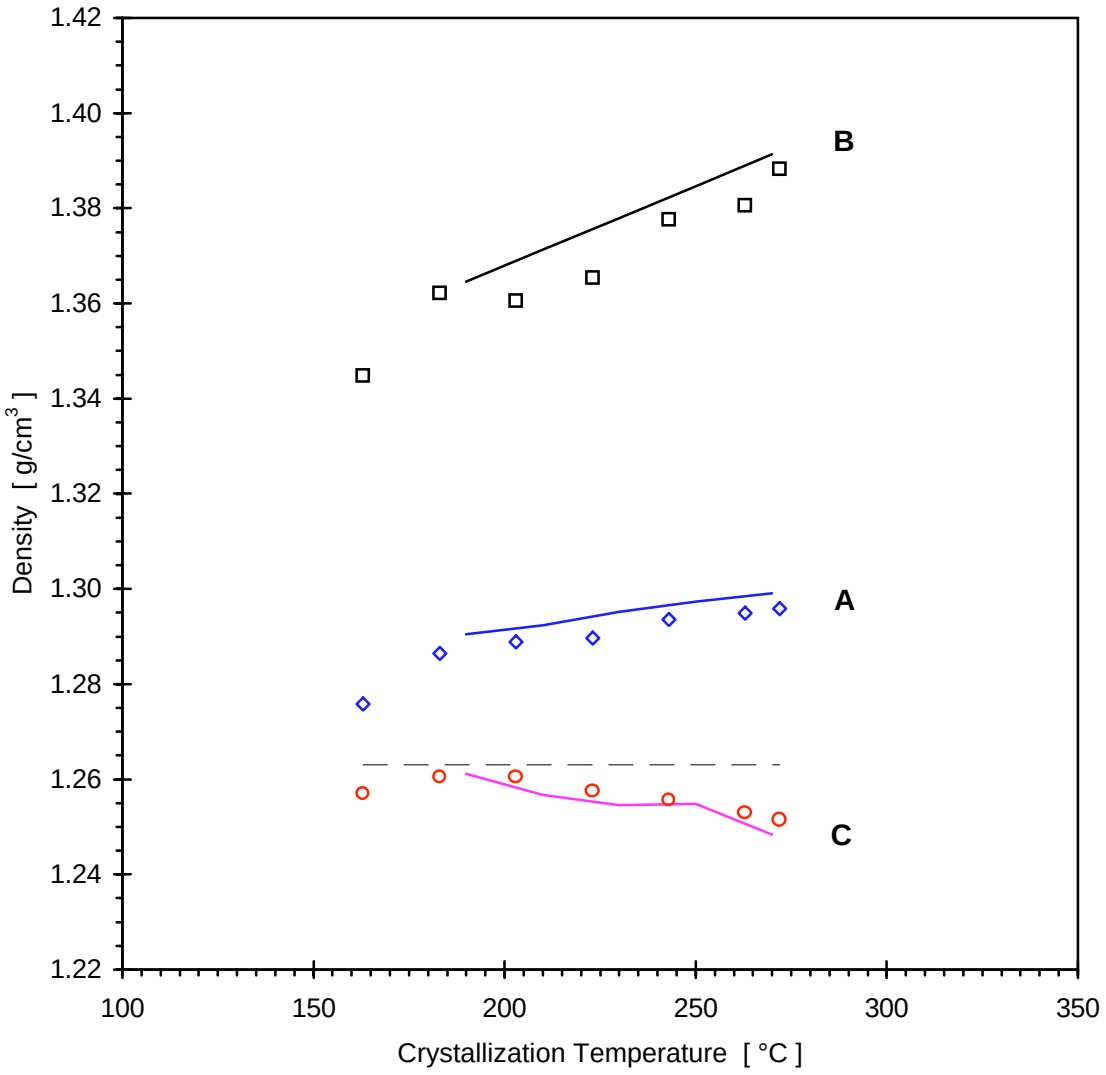


**Figure 5.2** Dependence of the room temperature densities on $T_c$ for the samples, cold-crystallized for 60 min at various temperatures: A) bulk density, B) crystal unit cell density, C) density of the amorphous phase, calculated according to the two-phase model assumption of equivalence of DSC and density crystallinities - equation (5.1). Dashed line reperesents the density of fully amorphous PEEK. Symbols - the results of this study; continuous lines - results from the literature data on figure 4.48.

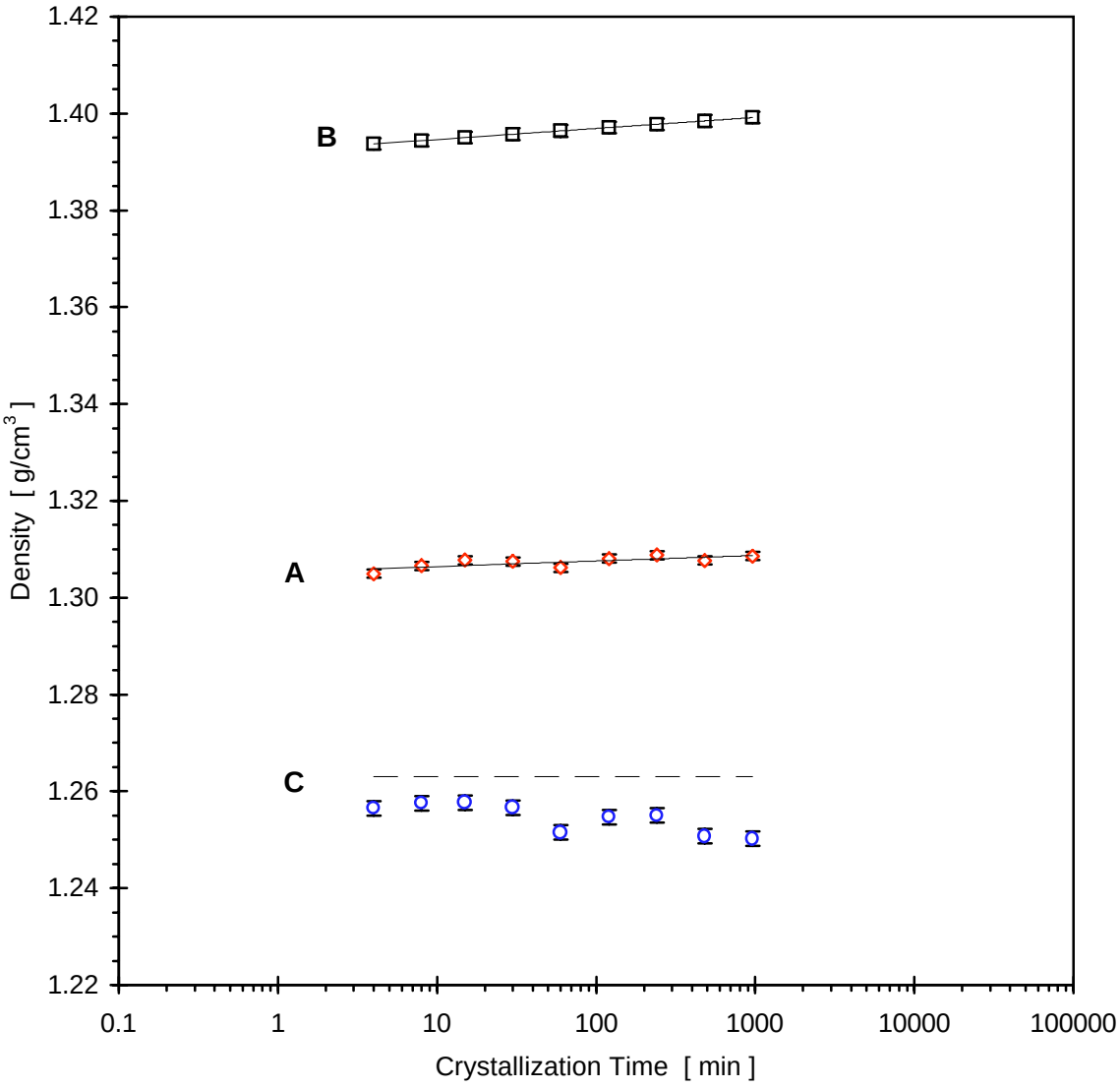


**Figure 5.3** Dependence of the room temperature densities on crystallization time $t_x$ for the samples, melt-crystallized at $T_x$ = 300°C: A) bulk density, B) crystal unit cell density, C) density of the amorphous phase, calculated according to the two-phase model assumption of equivalence of DSC and density crystallinities - equation (5.1). Dashed line represents the density of fully amorphous PEEK.

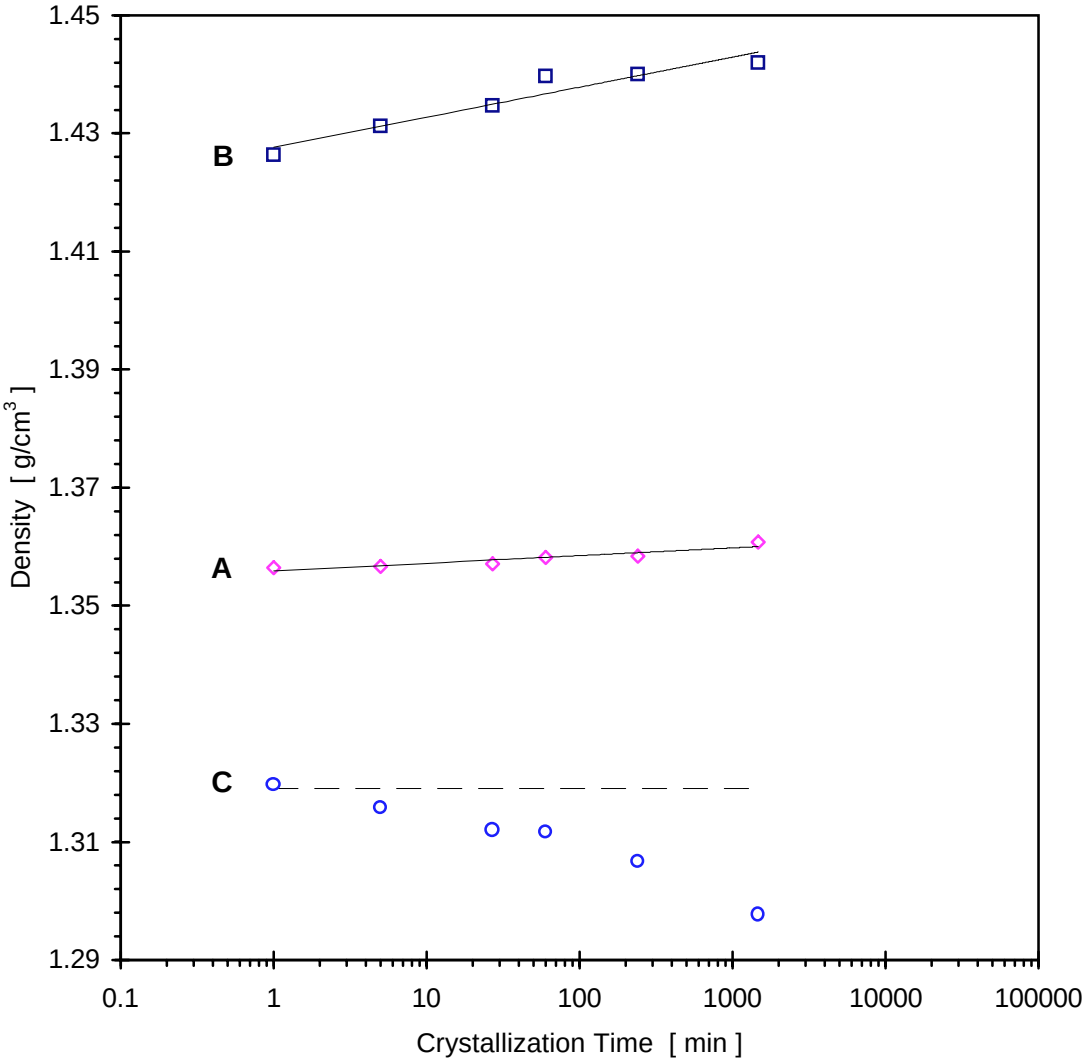


**Figure 5.4** Dependence of the room temperature densities on crystallization time $t_c$ for PPS samples, cold-crystallized at $T_c$ = 245°C: A) bulk density, B) crystal unit cell density, C) density of the amorphous phase, calculated according to the two-phase model assumption of equivalence of DSC and density crystallinities - equation (5.1). Dashed line represents the density of fully amorphous PPS. Data from the study of Chung et al. [124]

halo after separation of the crystalline reflections. Whether this is an artifact of the separation procedure or an indication of true physical change remains unclear.)

However, the analysis clearly demonstrates that application of the two-phase model for the physical state of a semicrystalline polymer consistently leads to ambiguous results for the crystallinity:

- The standard equation for calculation of density crystallinity - equation (2.3), is inapplicable due to the fact, that the room temperature crystal unit cell density is a function of crystallization time and temperature. Figure 5.5 illustrates the change of $r_c$ with $T_c$ (along the horizontal axis) and $t_c$ (along the vertical axis at 243°C) for PEEK (A) and PPS (B). The nature of this change is similar for both polymers. One can speculate that this might be another universally observed phenomenon for semi-flexible chain polymers with medium degrees of crystallinity.

- The corrected equation for the density crystallinity - equation (2.3a), leads to significant correction of the crystallization temperature and time trends of $c_c^{Dens}$. One significant practical implication of equation (2.3a), which illustrates the inapplicability of the standard two-phase model is the fact, there is *no one-to-one correspondence between bulk density and crystallinity*. Two samples with the same bulk density can have different values of $r_c$ (due to different thermal histories) and therefore - will be characterized by different values of $c_c^{Dens}$.

- There is a difference between the absolute magnitude and the rates of increase of density and DSC crystallinities with crystallization time and temperature. This difference further implies: either a significant change occurs in another parameter - $r_a^{calc}$, considered a physical constant by the two-phase model, or possibly the evaluation of DSC crystallinity from the total enthalpy of the melting transitions needs to be reexamined. The evaluation of $\Delta H_m$(total) and $\Delta H_m$(low) was examined in detail in earlier sections. Several aspects of a question not consider so far - whether $\Delta H_m$(low) truly represents the enthalpy of a melting transition of secondary lamellae, will be presented later in section 5.6 under the title of *controversial results*.

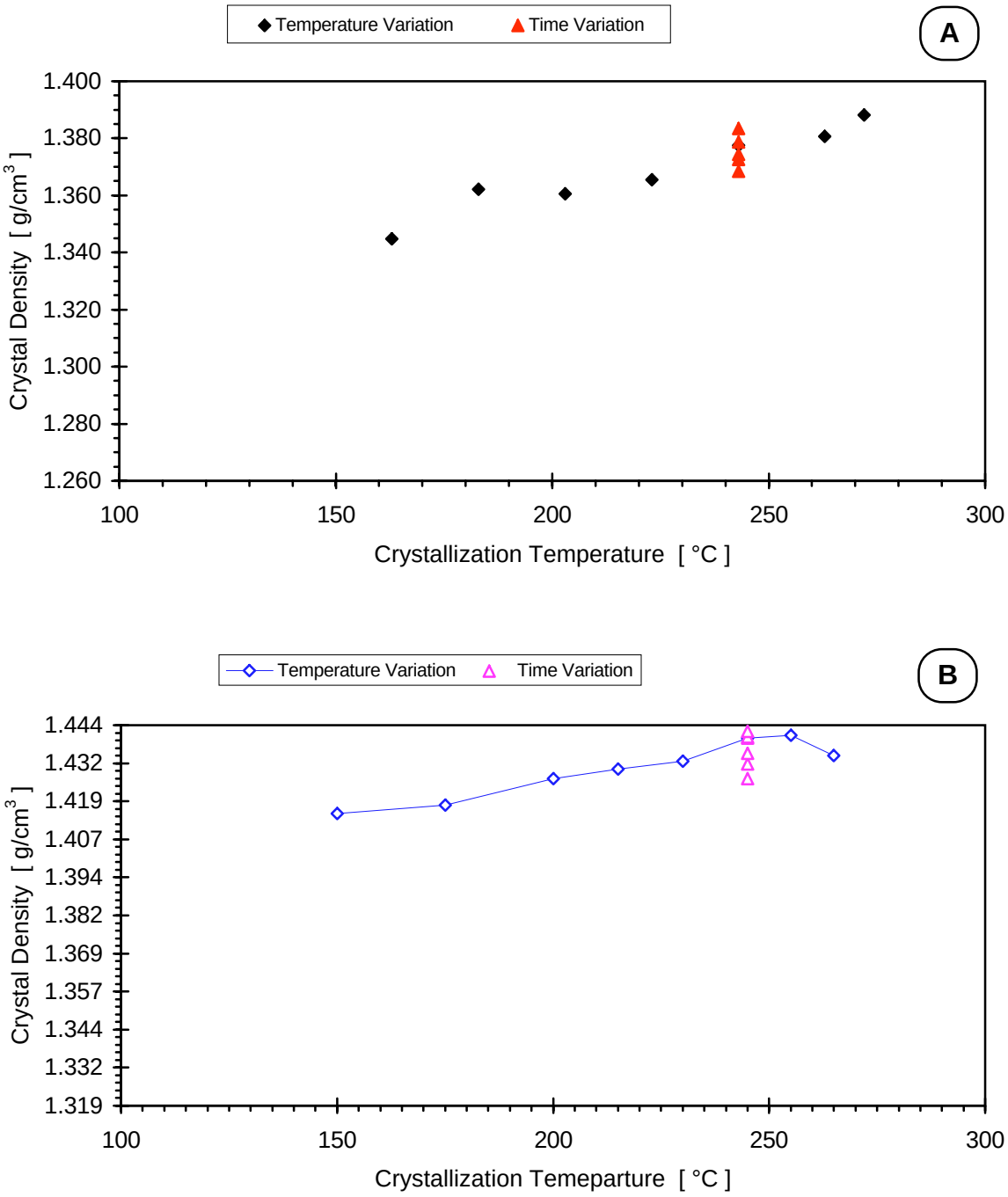


**Figure 5.5** Dependence of the room temperature crystal unit cell density $\rho_c$ on $T_c$ and $t_c$ for: A) cold-crystallized PEEK and B) PPS. Data on PPS is from reference 124.

In summary, this section analyzed the increase of the low temperature endothermic peak and the overall increase in crystallinity associated with it. Considered within the frame of an ongoing (secondary) crystallization process, the results certainly strike as non-trivial.

The primary crystallization is a process of densification of an undercooled metastable polymer liquid. The driving force under the large undercoolings in these experiments is large enough to allow for fast transition towards the more stable crystalline phase. The equilibrium state of the polymer is the fully crystalline state and not the semicrystalline state achieved under the chain folding crystallization mechanism. Therefore at any point during the secondary crystallization process (i.e. the later stage of long crystallization and/or subsequent annealing) a driving force towards continuation of the crystallization should exist. The global result of this driving force should be densification of the polymer.

The crystallinity data confirms that the secondary crystallization proceeds under a mechanism which is different from and much slower than the primary one. However, the density data, considered within the simple two-phase model, suggests also that overall *the amorphous phase is departing from equilibrium* by dilating, instead of densifying. This result cannot be justified and understood in the simplistic framework of the standard two-phase model.

Various other aspects of the failure of the standard two phase model are addressed in greater detail in a series of experimental studies and literature reviews by several groups currently working in the field. [82, 147-149, 151, 152, 154-156] Some of the ideas, outlined in these sources, will be presented later in section 5.5. They will be analyzed mainly in connection with the current model for the "double melting" behavior of PEEK and the other effects of long annealing between $T_g$ and $T_m^{'}$, presented in this study.

## 5.4 Analysis of the Small Strain Creep Results

Section 4.2.4 presented the results from the small strain creep studies of the effect of long annealing below and above $T_g$. Even without further elaboration, these results present new and original findings, which should generate interest for future studies. The phenomenon of "physical aging" above the nominal $T_g$ has been extensively demonstrated for

the first time for a polymer other than the high crystallinity polyolefins - PE and i-PP.[46,47,87-93] Only one other study has examined the physical aging of a partially crystalline polymer both below and above the nominal $T_g$ - a recent paper by Buijs and Vroege on creep studies of liquid-crystalline copolyester. [135]

### *5.4.1 Summary*

The results from the momentary creep studies in both temperature ranges, below and above $T_g$, are similar to those found by Struik and others for PE and i-PP. [45, 46, 85-96] The form of the creep compliance curves for different aging times at all temperatures is characteristic of a "short time response" in the sense discussed in section 2.5.2. With the exception of the creep compliance curves measured at 160°C (note that $T_g$ = 155°C by DSC at 10 K/min), all other plots of J(t) vs. log(t) exhibit the following characteristic response:

- The J(t) curves below $T_g$ exhibit time dependence without an indication of approach to equilibrium.

- The J(t) curves above $T_g$ exhibit time dependence on a time scale significantly in excess of the characteristic time scale of the glass transition. No change in shape, indicative of an approach to equilibrium, is observed.

- No change to a constant slope is observed at "long" times for $T_a > T_g$. The latter has been predicted by Struik and related to a creep response characteristic of chains which are just entering the glass transition region. [88] Struik claims that this type of response dominates the creep compliance in the temperature range for $T_g^L < T_a < T_g^U$ ("Region 3").

Analysis was done with the reduced KWW analytical form, used by Struik, and is therefore subject to the constraints discussed in section 2.5.2. It leads to an analytical procedure for building an effective "master curve" with a shape similar to the shape of the individual curves.

In addition to the characteristic dependence of the small strain creep compliance on annealing time and temperature below $T_g$, this study has shown, that the same type of response is generated upon annealing above $T_g$:

- The creep compliance's functional dependence on creep time is described by the KWW function, equation (2.9a). It represents the fact, that the creep recovery process is governed by a broad spectrum of retardation times. Significant deviations from the KWW functional dependence are observed only for aging temperatures in the nominal glass transition range.

- The creep compliance curves for different aging times can be superposed by applying a combination of horizontal and vertical shifts.

- The shifting is characterized numerically by the relations between appropriate parameters of the KWW function: the horizontal shifting is characterized by the relative increase of the logarithm of the average retardation time (equation 2.11); the vertical shifting - by the relative change of the "instantaneous" value of the creep compliance - $J_0$ (equation 4.10).

- The rate of aging is characterized by the horizontal shift rate $m$ (equation 2.12). Its value is small far below $T_g$, increases to 1 at temperatures not too close to $T_g$, and decreases sharply in the glass transition region. At temperatures above the glass transition the horizontal shift rate is still finite and increases to 1 with increase in $T_a$.

The horizontal shift rate has generally the same temperature dependence as the one derived by Struik for i-PP and PE with the same analytical approach. [88-91] The discontinuity of $m(T_a)$ at $T_g$ (figure 4.54) has two equally possible origins:

- It could be considered an indication of the breakdown of the specific analysis and technique employed due to the thermorheological complexity of the viscoelastic response in a "Region 3" temperature range as discussed by Struik [88] and in the review (section 2.5.4). For example, the dependence of the shifts on $\log(t_a)$ at 160°C is nonlinear (figure 4.53) and the value of $m$ given is only a linear estimate of the overall change observed.

- A low value of $m$, approaching zero, is expected as $T_a$ approaches $T_g$ ($T_g^L$). This behavior is expected for the "aging" amorphous fraction regardless of the "physical aging" model used.

The vertical shift rate is significantly different from the one described by Struik only in the immediate vicinity of $T_g$, where Struik predicts and observes change in the sign of the vertical shifts (i.e. from positive to negative or vise versa, depending on the definition of a vertical shift). At present it is impossible to conclude which of the following possible reasons accounts for this difference:

- erroneous analysis (the breakdown of the method as discussed above),

- extremely limited number of datapoints on the temperature scale - practically only one temperature, 160°C, shows an indication of closeness to $T_g$,

- the temperature range near $T_g$ is a range of overlap of and transition between two *different* active relaxation mechanisms, occurring in physically different locations of the amorphous phase. If true, the main consequence would be that comparison of the apparent vertical shift rates below and above the nominal $T_g$ is physically meaningless as they reflect different relaxation mechanisms.

### *5.4.2 Critical Analysis of Struik's Model for Physical Aging Above $T_g$*

Struik's model for the physical aging of PE and i-PP, which was discussed in section 2.5.4, proposed the existence of an extended glass transition in these two polymers. It is based on two assumptions [88]: 1) the response of the crystalline phase is elastic; 2) the crystallinity is constant throughout the experiment. The model is effectively the same as the model for the viscoelastic behavior of filled rubbers. [88] The crystalline lamellae are assumed to be acting as inert rigid fillers in the amorphous phase.

The observation of exceedingly high retardation times above the nominal glass transition of these polymers ($T_g = T_\beta$) is explained by the model through the restricted mobility of the amorphous chains in the crystal-amorphous interphase. The relaxation times of tie-chains, long folds, and short folds (see figure 2.2) are higher than the relaxation times for cilia or free unattached chains in amorphous regions of the semicrystalline material. Segmental mobility is affected the most in the immediate vicinity of the crystalline lamellae, whereas at large distances away from them the mobility approaches that of a bulk amorphous polymer.

Thus, above $T_g$ some parts of the amorphous fraction of the polymer have relaxation times characteristic of a glass, other parts are rubber-like and others are just passing through their glass transition. [88] Increase in temperature above $T_g$ leads to a shift of the relaxation spectrum towards short relaxation times, but at any temperature below the crystalline $\alpha$-relaxation a significant part of the amorphous phase has sufficiently low mobility to lead to a glass-like response. Above the $\alpha$-relaxation temperature $T_\alpha$ the crystal-amorphous interphase is able to relax through the increased ability of the chains to undergo motion within the crystalline lamellae. [136-138] Between the nominal $T_g$ ($T_\beta$) and $T_\alpha$, the fraction of the amorphous phase which has high relaxation times is able to undergo physical aging.

The strength of Struik's model lies in its ability through an unified mechanism to rationalize complex experimental results for a variety of polymers. [91] The concept of the extended glass transition explains horizontal and vertical shifting through time-temperature changes in the mobility of a non-homogeneous amorphous phase. It is a significant departure from the standard two-phase model of semicrystalline polymers. [91]

Several of the critiques of Struik's ideas have suggested, that different mechanisms might account for the complex manifestation of “physical aging” in semicrystalline i-PP and PE. [46, 47, 92-95] To the extent, that they suggest alternative physical models for the phenomenon of physical aging, these models either directly involve secondary crystallization, [46, 92] or propose changes in the strengths of the $\beta$-relaxation ($T_g$) or $\alpha$-relaxation ($T_\alpha$), which could originate from ongoing secondary crystallization during aging. [47, 93-95]

The most comprehensive analysis of this alternative idea is given in one of Struik's original papers. [91] He acknowledges, that secondary crystallization is a feasible optional mechanism, which in an extended two-phase model of the semicrystalline state could account for the stiffening changes above $T_g$ simply through an increase of crystallinity. His arguments against secondary crystallization (based on i-PP and PE data) are as follows [91]:

1) Physical aging mainly results in changes in mobility (horizontal shift) - a shift of the retardation spectrum to higher retardation times. [46, 88-93] The primary effect of secondary crystallization is an overall change in the material property, e.g. a vertical shift. Even

allowing for changes in mobility with increase of crystallinity, one has to explain how the second-order effect (mobility) overshadows the first order effect (stiffening).

2) The experimental data suggest a continuity of the mechanism of physical aging across the nominal glass transition range ($T_\beta$). If aging above the nominal $T_g$ is assumed to occur through crystallization, this cannot be the sole mechanism of physical aging at all temperatures. Physical aging below $T_g$ is similar in semicrystalline and in fully amorphous polymers. Thus, crystallization must be ruled out as a source of the aging effects below $T_g$ as there is no physical ground and no experimental evidence for crystallization below the nominal $T_g$ of these polymers (and for any polymer in general). Therefore, a different model must account for aging effects in semicrystalline and amorphous glasses below $T_g$. If crystallization is considered the sole cause of aging above $T_g$, the model does not possess the continuity at $T_g$, which the data from mechanical studies strongly points toward.

(*Note*: It is important to note for future reference, that Struik's model proposes a change in aging mechanism at $T_g^U$ (= $T_\alpha$) - the upper limit of the extended glass transition range. Above this temperature, Struik attributes the effects of "aging" (understood in a broader sense as time-evolution of properties [86, 169]) to secondary crystallization. [91] A large amount of experimental evidence exists in support of *lamellar thickening* as the mechanism for secondary crystallization in i-PP and PE above their α-relaxation temperatures. [3, 21-30] There appears to be no correlation between these studies and the studies of secondary crystallization/physical aging below $T_\alpha$, which were reviewed earlier. Only Struik's work makes a connection between the two ideas, by suggesting that a change in the aging mechanism occurs at $T_\alpha$, above which thickening, e.g. secondary crystallization, becomes possible.)

3) The experimental evidence by Wunderlich et al. [10] for the existence of a rigid (e.g. glass-like) amorphous fraction in semicrystalline polymers above their calorimetric $T_g$, suggests that this fraction would not be able to crystallize above $T_g$, but should be able to physically age below its respective $T_g^U$.

4) During aging above $T_g$, the change in the modulus with change in density is much higher than the change induced by different crystallinity values - table 3 in reference 91.

Even though the first three arguments are only qualitative, they raise problems which are indeed important and must be dealt with. It is possible to resolve these apparent contradictions in an enhanced version of the secondary crystallization model for physical aging above $T_g$. Furthermore, the evidence for physical aging above $T_g$ in PEEK presented in this study and in a liquid crystalline polymer [135] suggest that in order to be consistent, Struik's requirement for an universal model for the physical aging below and above $T_g$ must apply to those and other polymers as well. This presents a challenge to Struik's model, as the crystallinity investigation presented in this study and the morphological studies by other authors [70, 73, 74] lead to the conclusion that crystallinity of PEEK increases during aging above $T_g$ ($T_g^U$). In the case of i-PP, Struik has acknowledged that the literature data is contradictory - evidence for as well as against increase of crystallinity during aging had been presented. [91]

The last of the arguments above, together with the somewhat ambiguous conclusions about crystallinity change during aging, are the only strong quantitative objections against the secondary crystallization model for physical aging above $T_g$ presented by Struik. That last argument, however, is somewhat misleading. For example, in the case of i-PP (table 3 in reference 91), Struik claims, that 0.1 % change in density during aging above $T_g$ results in 18-25% change in stiffness. The ratio of the latter to the former, equal to 180-225, represents the sensitivity of the compliance to densification during aging. This value is compared against a value of 35-45, obtained from crystallization of PP samples with different tacticity (e.g. different densities, crystallinities and compliance values).

The comparison can hardly be justified for two reasons. First, a change in the compliance due to the chemical modification itself (different tacticity) might complement the change due to differences in crystallinity. Second, the "sensitivity ratio" calculated by Struik should be analyzed from a crystallinity stand point as well. In a semicrystalline i-PP with initial crystallinity 0.6, 0.1% change in density during aging is approximately equivalent to increase in crystallinity by 0.011 ($r_a$ = 0.854 g/cm$^3$; $r_c$ = 0.936 g/cm$^3$ [139]). Such an increase in crystallinity during aging, *if observed and confirmed by other methods*, could be compatible with a decrease in compliance by 18-25% (note, that the total change in

compliance with crystallinity between crystallinity values of 0 and 1 is usually on the order of 100,000 %).

In the case of PEEK the experimental vertical shift rate, determined from a plot of $b = J_0(t_a)/J_0(t_{ar})$ vs. $\log(t_a/t_{ar})$, can be compared with the theoretical prediction, based on crystallinity change. The latter can be determined from the DSC and density log(t)-rates of secondary crystallization, which have been studied extensively (section 4.2.3).

For the theoretical prediction, one needs an equation which relates the compliance of the semicrystalline composite matrix to the crystallinity $c_c$ (volume fraction) and the specific values of the compliance for the crystalline and amorphous phases $J_a$ and $J_c$. Several different approaches to the choice and justification of such an equation exist in the literature. In addition, the limiting values $J_a$ and $J_c$ can not always be determined directly. A detailed review of these problems can be found in the literature. [136, 140-142] This discussion will focus only on investigating the possibility that the change in the pre-exponential factor of the bending creep compliance $J_0$, defined by equations (2.9a), (4.10), and (4.11), is due to the increase in the volume fraction crystallinity during secondary crystallization. This, of course, would be limited only to the physical aging results above the nominal glass transition.

The two extreme models for the mechanical properties of a two phase system are the Reuss series model and the Voight parallel model - figure 5.6-A. The series model represents the case of an uniform stress field throughout the two phases and additivity of strains. The compliance is the harmonic mean of the compliances of the two phases and is dominated by the term, which represents the phase with the lower compliance. Thus the Reuss series model leads to the extreme lower bound estimate for the compliance of the two-phase semicrystalline composite.

The parallel model represents the case of an uniform strain field throughout the two phases and additivity of forces. The compliance is the arithmetic mean of the compliances of the two phases and is dominated by the term, which represents the phase with the higher compliance. The Voight parallel model leads to the extreme upper bound estimate for the compliance of the two-phase semicrystalline composite.

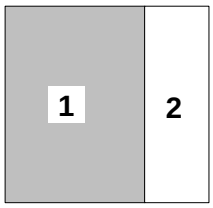


Voight Model

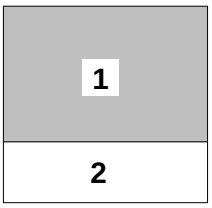


Reuss Model

A

$$\frac{1}{J} = \frac{j_1}{J_1} + \frac{j_2}{J_2}$$

$$J = j_1 * J_1 + j_2 * J_2$$

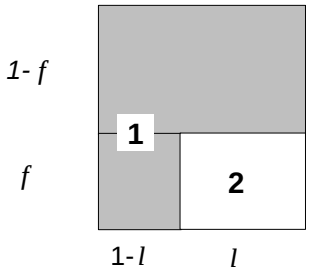


Takayanagi's Model

B

$$J = (1-f) * J_1 + \frac{f}{\frac{1-l}{J_1} + \frac{l}{J_2}}$$

**Figure 5.6** Models for calculating the mechanical properties of a two phase semicrystalline polymer: (A) extreme bound estimates - Voight and Reuss models, (B) combination of the two extreme bounds - Takayanagi's model.

Neither of the two models is correct, due to the fact, that the assumption of uniform stress or strain fields throughout the material is a gross oversimplification. Under uniform stress field, discontinuities in the strain will exist at the interface between the matrix and the dispersed phase. Under uniform strain field assumption, large gradients will exist in the force field at the interface.

A model, named after Takayanagi, presents a slightly more realistic approach, intermediate between the Voight and Reuss models [140, 141, 143, 144] - figure 5.6-B. In the case of homogeneously dispersed inclusions of phase 2 in a matrix of phase 1, some of the matrix material is considered to be under constant stress, while the rest of the matrix, interconnected with the inclusions, is considered to be under constant strain. Thus the model is a combination of the series (Reuss) and parallel (Voight) models. The state of mixing of the two models is represented by the parameters $l$ and $f$, which represent, respectively, the effective series and parallel fractions. Their product is equal to the volume fraction of the dispersed phase. The equation for the compliance is as follows:

$$J = (1-f) * J_1 + \frac{f}{\frac{1-l}{J_1} + \frac{l}{J_2}} \qquad (5.2)$$

When the dispersed phase is in the form of spherical inclusions, according to Takayanagi, [143] the solution of Kerner's equations [145] for the moduli of multiphase systems, leads to the following expressions for $l$ and $f$ through the volume fraction of the dispersed phase:

$$l = \frac{2+3*j_2}{5} \qquad (5.3)$$

$$f = \frac{5*j_2}{2+3*j_2} \qquad (5.4)$$

To complete the Takayanagi model for semicrystalline polymers, one needs to specify which phase acts as the matrix and which one is the dispersed phase. Takayanagi suggested[143] that in the case of polyethylene resins, the dispersed phase is the amorphous

phase. This assumption has been questioned by Matsuoka. [144] Nevertheless, Takayanagi has shown, that equations (5.2) ÷ (5.4) with $j_2 = 1 - c_c^{vol}$ are suitable for the description of the mechanical properties of various polyethylene resins. [143]

An alternative approach to calculation of the mechanical properties of semicrystalline polymers has recently been presented in a study by Janzen. [142] Janzen's approach presents an unified treatment of the problem, which illustrates the common features of most of the models of the mechanical properties of semicrystalline polymers as two phase composites. The starting point of Janzen's review is the idea, that the solutions of the problem for any mechanical property (moduli or compliances) under different mechanical models can be expressed in a generalized form, analogous to the Clausius-Mosotti equation:

$$\frac{Y-1}{Y+A} = j_1\left(\frac{Y_1-1}{Y_1+A}\right) + j_2\left(\frac{Y_2-1}{Y_2+A}\right) \qquad (5.5a)$$

where $Y$ is the property in question, $Y_1$ and $Y_2$ are the pure phase properties, $j_1$ and $j_2$ are their volume fractions, such that $j_1 + j_2 = 1$, and $A$ is a function of the geometry of mixing and the type of property under consideration. The equation can be rearranged into a more symmetrical form:

$$Y = \frac{Y_1Y_2 + A(j_1Y_1 + j_2Y_2)}{A + j_2Y_1 + j_1Y_2} \qquad (5.5b)$$

At the two limits - when $A$ approaches zero or infinity, the above equation reproduces the two extreme bounds - the Voight (parallel) or Reuss (series) equations.

Substitution of $A$ with other expressions reproduces various other models as well. For example, for compliances and $A = (2/3)*J_1$ equation (5.5b) is equivalent to the Takayanagi model with phase 1 chosen as the matrix phase. Similarly, substitution with $(2/3)*J_2$, leads to the Takayanagi model with phase 2 being the matrix. (Note: These statements are true in the case of compliances; for moduli the reverse of the numerical coefficients in the expressions for $A$ must be taken.)

Janzen points out, that substitutions of the kind $A = \xi * Y_i$ (i = 1, 2) are equivalent to the upper or lower bound estimates, for certain models. In addition to the Takayanagi model,

the results of other models are reproduced, as well. In particular, Hashin-Shtrikman bounds on the shear compliance [142] are reproduced for:

$$A = Y_i \frac{8 - 10n_i}{7 - 5n_i} \qquad i = 1,2 \tag{5.6}$$

where $n_i$ is the Poisson's ratio for the respective phase. When $n_i$ = 0.5 these bounds are equivalent to the Takayanagi results (with *i* being the matrix phase in the model).

Therefore, Takayanagi's model with an amorphous matrix can be considered as giving an exact Hashin-Shtrikman upper bound of the compliance, as $n_a$ = 0.5 is a safe assumption. For the model with a crystalline matrix the Takayanagi result is equivalent to the assumption $n_c$ = 0.5, which is generally not correct. With proper rearrangement of the result it can be shown, that if $J_c << J_a$, for most crystallinity values (except the extreme limits) the result is very close to the Hashin-Shtrikman lower bound estimate for the values of the compliance.

The coincidence of these results is due to the fact, that their treatments are generally confined to state of mixing with high symmetry (i.e. isotropic spherical inclusions in an isotropic matrix). The Halpin-Tsai model [142, 146] is equivalent to substituting $A = \xi * Y_m$ in equation (5.5b), where *m* stands for the matrix phase. The parameter $\xi$ is a shape dependent "geometric factor", [146] function of the geometry of the inclusions. It is interesting to note, that with an increase in the anisometry (aspect ratios) of the inclusions, which results in a decrease in $\xi$ (in the case of compliances), the properties of the composite become closer and closer to the properties of the inclusions, even at relatively low fractional volumes of the latter. That leads to the peculiar fact (see figure 5.7 for example) that, in a certain range of crystallinity values, the mechanical property values of a semicrystalline polymer could be described successfully by both - a Takayanagi model with a crystalline matrix and spherical amorphous inclusions (as in reference 143), and a Halpin-Tsai model with an amorphous matrix and highly anisometric crystalline lamellae! [146] This suggests, that despite being quantitatively successful, the Takayanagi model's assignments of the matrix and inclusions might not have direct physical meaning in the case of semicrystalline polymers.

In summary, the Voight and Reuss models provide the extreme bounds for the mechanical properties of a semicrystalline polymer; the Takayanagi model (resp. the Hashin-

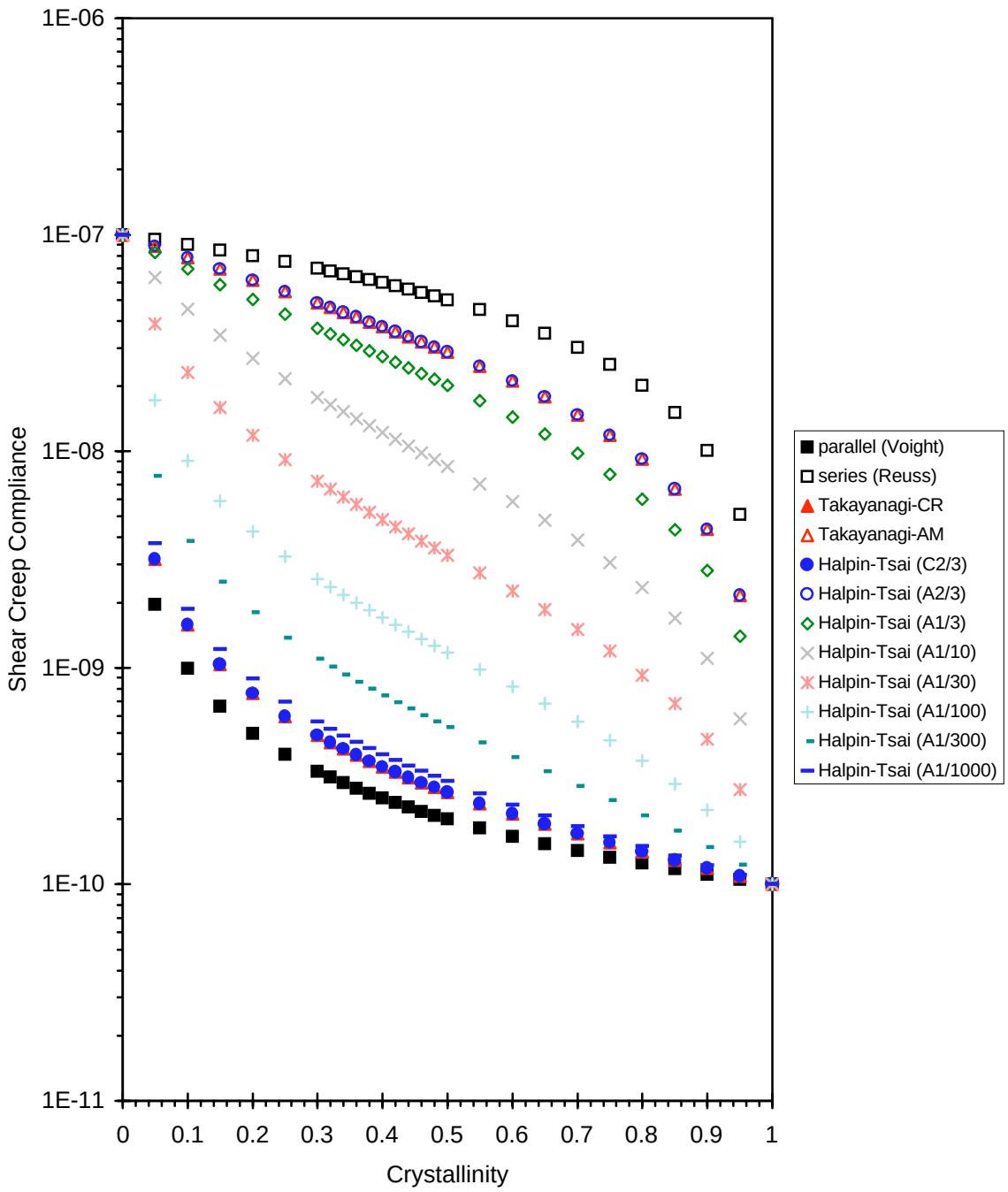


**Figure 5.7** Predictions for the dependence of shear creep compliance on volume fraction crystallinity from various mechanical models: series (Reuss), parallel (Voight), Takayanagi (amorphous and crystalline matrix), and Halpin-Tsai (A and C indicate amorphous or crystalline matrix; the number is the ξ-value).

Shtrikman estimates) provides tighter bounds (function of the somewhat artificial choice of the "matrix phase"), and the Halpin-Tsai model could lead to an even closer estimate, if the microstructure (the aspect ratios of the crystalline lamellae) can be successfully assessed - figure 5.7.

For the purpose of this discussion, however, the important values are not only the property values themselves, but their sensitivity to change in crystallinity. It is important to note, that in the crystallinity range we are generally interested in (0.3 ÷ 0.5, as in PEEK, i-PS, PET, and PBT, for example), both Reuss and Voight models provide estimates of the variation of compliance with crystallinity, which are closer to the lower bound. A higher sensitivity to crystallinity change is predicted by (in order of increasing sensitivity): Reuss (series) model, Takayanagi model with amorphous matrix (and its equivalents), Voight (parallel) model, Takayanagi model with crystalline matrix (and its equivalents), Halpin-Tsai models with very small and very high lamellar aspect ratios, Halpin-Tsai models with intermediate lamellar aspect ratios. This can be qualitatively assessed by looking at the slopes of the various curves on figure 5.7.

For the comparison of the experimental data (figures 4.50 - 4.52) with the theoretical predictions, the Takayanagi model will be employed, with the crystalline phase as the "matrix phase". The reasons for this choice are: its simple mathematical expression (equation 5.2), the relatively small change in $J_0$ with temperature across the glass transition region (from $300\times10^{-12}$ $m^2/N$ to $3000\times10^{-12}$ $m^2/N$), suggesting that values of $J_0$ above $T_g$ are closer to the values of $J_c$, and the intermediate sensitivity to crystallinity changes for crystallinities in the range of 0.32 - 0.4 (figure 5.7).

Substitution of equations (5.3) and (5.4) in equation 5.2 leads to the following dependence of $J_0$ on crystallinity $c_c$ (volume fraction):

$$J_0 = J_c \frac{2c_c J_c + (5-2c_c)J_a}{(5-3c_c)J_c + 3c_c J_a} \qquad (5.7a)$$

As $J_c << J_a$, by dropping the terms, containing $J_c$ from the numerator and denominator, this expression can be reduced to:

$$J_0 \quad = \quad J_c \quad \frac{(5-2c_c)}{3c_c} \tag{5.7b}$$

The theoretical prediction for the vertical shift *b* becomes (see equation 4.10):

$$b(t_a, t_{ar}) = \frac{J_0(t_a)}{J_0(t_{ar})} = \frac{J_c(t_a)}{J_c(t_{ar})} \times \frac{[5-2c_c(t_a)]}{[5-2c_c(t_{ar})]} \times \frac{c_c(t_{ar})}{c_c(t_a)} \tag{5.8a}$$

The first term is approximately unity, assuming that during aging either there are no changes in the crystalline compliance or these changes are very small and an order of magnitude smaller than the crystallinity induced changes. During secondary crystallization (see figure 4.37)

$$c_c(t_a) = c_c(t_{ar}) + \mathrm{b} \times log\left(t_a / t_{ar}\right) \tag{5.9}$$

From the data on figure 4.37 for $t_{ar}$ = 40 min it follows that $c_c(t_{ar})$ is about 0.3. The log-time rate of secondary crystallization (for volume fraction crystallinity) by DSC at 243°C is $\mathrm{b}_{DSC}$ = 0.02 (decade)$^{-1}$ and by density - $\mathrm{b}_{Dens}$ = 0.007 (decade)$^{-1}$. As $\mathrm{b} \times log\left(t_a / t_{ar}\right)$ is much smaller than $c_c(t_{ar})$, equation (5.8a) can be expanded in series. If only the first order term is kept, equation (5.8a) becomes:

$$\frac{J_0(t_a)}{J_0(t_{ar})} \approx \quad 1 - \frac{\mathrm{b} \times log\left(t_a / t_{ar}\right)}{c_c(t_{ar})\left[1 - \frac{2}{5} c_c(t_{ar})\right]} \tag{5.8b}$$

Equation (5.8b) allows for a direct comparison between the theoretical prediction for the linear decrease of compliance with log($t_a$) during aging and the experimental vertical shift rate, plotted on figure 4.55.

The result of the comparison for $T_a$ = 240°C is plotted on figure 5.8. It is clear, that the change in compliance predicted by the Takayanagi model from the increase of density crystallinity - curve (C), is much smaller than the experimentally observed one. Even if a model which predicts a stronger dependence of the compliance on crystallinity is used, the theoretical prediction from density crystallinity can not be brought close to the experimental result. The use of DSC crystallinity in equation (5.8b) leads to a prediction, which is close to

the experimental data. These results should be viewed with caution, however, for the following reasons:

1) The justification for using the Takayanagi model is not rigorous. In order for the choice of a particular model to be fully justified, it would have to predict correctly the observed values of the compliances as well. In the present study this could not be verified as the exact values of the pure phase compliances $J_a$ and $J_c$ at $T_a$ are unknown.

2) If another mechanical model for the properties of the semicrystalline polymer is chosen, it would likely have to be of the Halpin-Tsai type, with a relatively high lamellar aspect ratio. This, according to the review of the models above (see figure 5.7), will lead to a stronger sensitivity of the compliance to crystallinity changes.

3) The log-time secondary crystallization rates used for the theoretical predictions on figure 5.8 are too high and should be viewed as an upper bound estimate. This is due to the fact, that the thermal history of the samples on figure 4.37 (cold-crystallization from the amorphous glassy state) is not exactly the same as the history of the creep samples (annealing below $T_c$ after initial cold-crystallization).

The corrections for the last two effects, would separately tend to shift the theoretical curves on figure 5.8 in opposite directions. A Halpin-Tsai model with high anisometry will increase the negative slope of curves (B) and (C). Lower values of the log-time secondary crystallization rates will decrease the negative slope of the curves. One can not predict whether these corrections will be of the same order of magnitude. Most likely, the result will appear qualitatively similar to that, presented on figure 5.8.

In conclusion, the observed vertical shift in the compliance during isothermal aging above $T_g$ appears compatible in magnitude with an increase of crystallinity during the secondary crystallization stage, as measured by DSC. The prediction, based on density crystallinity, can not account for the stiffening of the polymer during aging.

With respect to the origin of the relationship between the parallel observations of "physical aging" and secondary crystallization, an alternative model is currently being explored. [216] It expands on the idea proposed by Chai and McCrum [94, 95] that the observation of "physical aging" above $T_g$ is due to changes in the relaxation strength, rather than the

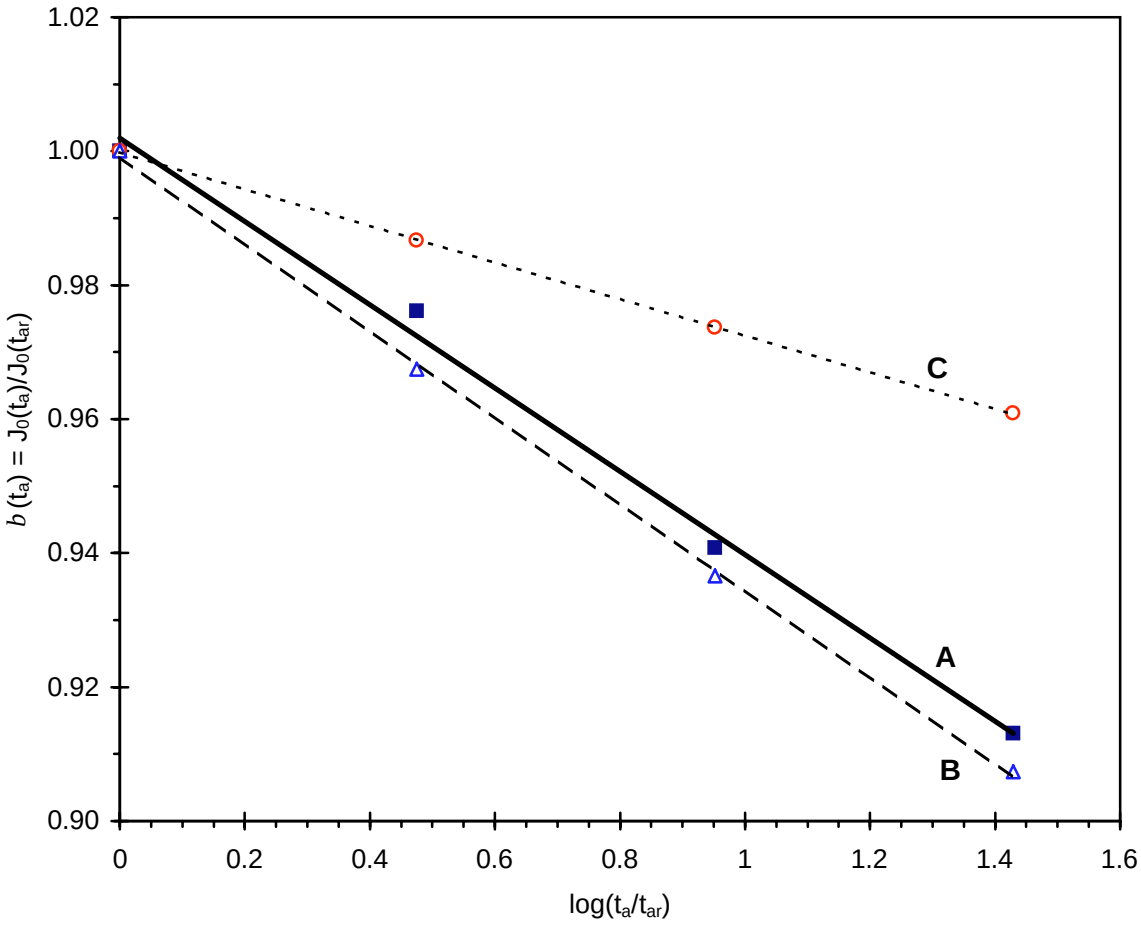


**Figure 5.8** Comparison of the experimental (A) annealing time dependence of the vertical shift at 240°C with the theoretical predictions based on the log-time increase of DSC (B) and density (C) crystallinities. Predictions are based on Takayanagi's model for the crystallinity dependence of the mechanical properties of semicrystalline polymers.

relaxation spectrum. Its main operative proposal is that upon annealing above $T_g$ the fractional conversion from a relaxed phase (amorphous) to unrelaxed and/or relaxing phase (crystalline and constrained/"rigid" amorphous) is the sole origin of the "physical aging" phenomenon. This fractional conversion occurs through secondary crystallization, therefore, the kinetics of "physical aging" is governed by the kinetics of the secondary crystallization process.

These new ideas originate from a conceptually different interpretation of the experimental observation which had lead to the proposed existence of "rigid amorphous fraction" (RAF) in a semicrystalline polymer above the calorimetric $T_g$. [10, 12-19] The result in question is the abnormal crystallinity dependence of the heat capacity - the failure of the two-phase analysis of the heat capacity above $T_g$ (which was reviewed in section 2.3.2). This analysis relies on the use of the "pure phase" properties of the crystalline and amorphous components. The formation of a network-like semicrystalline structure from the homogeneous isotropic relaxed amorphous melt invokes the possibility that certain *specific properties* of the amorphous fraction in a semicrystalline polymer could be significantly different from these of a totally amorphous liquid at the same temperature. This would result in a somewhat different interpretation of the "RAF" and, quite possibly, lead to significant reevaluation of the magnitude of the "RAF" content assigned in several studies in the literature. [10, 12-19]

Linear amorphous polymers fall in the class of "fragile liquids" [199, 203] characterized by strongly non-Arrhenius behavior above $T_g$, inherent ability for reorganization, and large heat capacity changes at $T_g$. "Strong liquids" are mainly open network glasses. They exhibit low heat capacity change at $T_g$ and show resistance to structural change. Intuitively it seems attractive to borrow the idea and apply it to the structural differences between the fully amorphous polymer and the inhomogeneous amorphous fraction in a semicrystalline polymer with varying degrees of microscopic constraint. Based on the characteristic features of the two classes of liquids, an amorphous network linked by crystalline lamellae, as illustrated in figures 2.2 - 2.4 would be expected to behave as a "strong liquid", as opposed to the homogeneous unconstrained supercooled melt which is a "fragile liquid". The formation of a

network-like semicrystalline structure during crystallization would lead to a transition of the amorphous chains from "fragile" to "strong" behavior. [199] This idea provides a slightly different, molecular interpretation of the experimental data, which had originated the "rigid amorphous fraction" concept. The lower than predicted heat capacity values in semicrystalline polymers above $T_g$ would be the result of a lowered specific heat of the entire amorphous fraction or at least a part of it.

In view of these considerations, a more cautious approach is taken towards the definition of a "rigid amorphous fraction". In the following section, the terms "*rigid amorphous fraction*" and "*constrained amorphous fraction*" will be used interchangeably to the extend that they reflect certain change in the properties of the amorphous fraction above $T_g$. However, the concept of "rigidity" above $T_g$ would be replaced by the characteristic features of "strong" liquids: different specific values for certain intensive properties and resistance to structural reorganization with change in temperature. The latter includes, for example, the possibility that the retardation spectrum of the constrained/"rigid" amorphous fraction above the calorimetric $T_g$ is characterized by retardation times which are longer than those expected at and above the glass transition of a linear amorphous polymer.

## 5.5 Secondary Crystallization, RAF, Physical Aging and the Two-Phase Model in the Case of Semicrystalline PEEK

The review sections of this study (2.3 - 2.5) discussed experimental evidence for some deficiencies of the simple ("static") two-phase model of the physical state of semicrystalline polymers. The results of this study present further evidence for the failure of the simple two-phase model to describe the physical state of a semicrystalline polymer in the case of PEEK. This includes (but might not be limited to) the inability of the simple two-phase model to account for:

- the inherent instability of the semicrystalline state, manifested in the existence of the secondary crystallization process;

- the nonequilibrium nature of the two phases, manifested in the fact, that the densities of the two phases depend on the crystallization/annealing conditions above $T_g$,

- the inherent heterogeneity of the amorphous phase, examples of which are the detection of a constrained/"rigid" amorphous fraction and the existence of a distribution of large relaxation times above the nominal glass transition of the polymer.

In the following, a model will be discussed which accounts for the above mentioned deficiencies of the two-phase model. As most of the experimental work in this study was focused on the phenomenon of "double melting" in PEEK (its time-temperature evolution) and the effects which parallel its manifestation, the new ideas will be presented as a revised and extended model for the "multiple melting" of PEEK and the phenomena which parallel it.

The review section (2.4.2) presented some of the arguments against the melting-recrystallization model for the double melting of PEEK which was proposed by Blundell and Osborn [63, 64] and further discussed by Lee and Porter [65, 66] and Jonas et al. [67, 68] The strongest argument against the melting-recrystallization model appears to be the direct morphological observation of secondary lamellae by Bassett et al. [70] and their low temperature melting and recrystallization (that is, the melting and recrystallization of the secondary lamellae *alone*), observed by Lattimer et al. [73] However, the most important argument for the current discussion is related to the development of the melting peaks during isothermal crystallization. The results of Cheng et al., [16] Bassett et al., [70] Marand and Prasad, [2] and this study (figure 4.17) leave no doubt, that the lamellae, which form first and are the dominant population, melt in the temperature range of the high temperature melting peak, whereas the melting of the lamellae, which develop later, is represented by the low temperature endothermic peak. This sequence of events, together with the extensive characterization of the time-temperature dependence of other phenomena, allows the identification of the primary and the secondary crystallization stage at the level of lamellar morphology formation.

The fact that, upon fast crystallization from the amorphous glassy state or the free melt, practically no low temperature melting is observed until the high temperature melting peak almost reaches its maximum intensity (figure 4.17), allows us to link the beginning of the secondary crystallization stage with an advanced stage of the development of the sperulitic superstructure. The fact that, upon slow crystallization from the melt, there is low temperature melting even when significant part of the polymer has not crystallized (figure

4.21 - curve B), allows to locate the secondary lamellar growth behind the advancing spherulitic growth front.

(*Note*: The results, discussed later in section 5.6.2, further confirm, that upon high temperature annealing the growth of the secondary lamellae occurs within the boundaries of unmelted spherulites or between unmelted clusters of lamellae within the spherulites.)

With this in mind, the results of this study agree with the ideas of the dual lamellar population model of the "double melting" of PEEK. The model explains the low melting point of the secondary lamellae as arising from their small size, which is the result of the constraining effect of the already present primary lamellae on their growth and stability at any given crystallization temperature. [70] Yet, as was pointed out in the review section, the model in its original form [16, 70, 71] remains vague about the mechanism of the secondary lamellar growth. Furthermore, it does not even address the origin of the time-dependence of the melting enthalpy and the thermal stability of the secondary lamellae (the $\log(t_a)$ dependence of $T_{max}$(low)). One should note, that the first quantitative studies of the low temperature endotherm [78-80] appeared after this model was put forth.

The dual lamellar population model of Bassett et al. [70] which proposed a secondary lamellar growth by insertion between primary lamellae, has been revised in recent years. A new model has been proposed and discussed, based on the heterogeneous lamellar stack morphology. [82, 147, 151, 152, 154, 155] The ideas, which play central role in the development of a more detailed morphological model and mechanism of secondary lamellar growth, are inseparable from the discussion in recent years of the morphological features of the primary crystallization at the lamellar level.

The analysis of the SAXS profile of semicrystalline polymers in the solid state, which results from the electron density variations on the scale of the interlamellar distance, results in the determination of two characteristic average lengths $l_1$ and $l_2$ ($l_1 < l_2$). One of them is the average lamellar thickness $l_c$, the other - the average thickness of the amorphous layer $l_a$. In polymers with intermediate crystallinity values (less than 0.5), the standard approach has been to identify the smaller length with the average thickness of the crystalline layer ($l_1 = l_c$). Thus local (linear) crystallinity at the lamellar level is assumed to be close to the global

(bulk) crystallinity (by volume), as measured by independent methods. This approach has been applied to the SAXS studies of PEEK by Blundell and Osborn, [63] Jonas et al., [68, 157] Lee et al., [66] and Wang et al. [85] This is not the only possible interpretation, however, as scattering techniques can not distinguish between the more and less dense parts of the scattering medium (Babinet's Reciprocity Principle).

In a SAXS study of PET, Santa Cruz et al. [153] argued for the adoption of the larger characteristic length as the crystalline thickness. Similarly, in later studies of PEEK, Hsiao et al., [84, 155] Sauer et al., [154] and Verma et al. [82, 147] argued for identifying $l_2$ with $l_c$. The main reasons for this assignment are the following:

1) Crystallinity estimates by other methods (DSC, WAXS, density) lead to volume fraction crystallinity of "fully crystallized" PEEK (after long crystallization from the melt or the amorphous glass) of about 0.3-0.4. A reverse identification of the two characteristic lengths on the other hand leads often to linear (local) crystallinity of about 0.2, which is too low and violates the requirement, that local crystallinity must be equal to or larger than the bulk crystallinity. [82, 155]

2) An estimate of the lamellar thickness from the line broadening of WAXS peaks results in a lower limit for $l_c$ of about 60-80 Å. [82, 155] This is consistent only with the identification of $l_c$ with the larger characteristic length by SAXS.

3) The assignment of $l_c$ to the smaller characteristic length $l_1$ often leads to a value of 20-40 Å for the thickness of the crystalline lamellae. [63, 66, 68, 85, 157] That value is equivalent to 2-4 unit cells in the c- crystallographic direction and 1.5-2.5 repeat units being in crystallographic order. This would be physically unreasonable [155] and, therefore, the alternative assignment must be adopted.

The assignment of the higher characteristic length to the crystalline lamellar thickness leads to the conclusion, that the local (linear) crystallinity within the immediate surroundings of the lamellae is larger than the volume (bulk) crystallinity. This discrepancy can be accounted for by assuming that part of the morphology consists of homogeneous amorphous regions (interfibrillar or interstack "amorphous gaps", [154] "liquid pockets"/"amorphous pockets" [151, 155]), which are large enough not to be detected by the SAXS method and

contribute to the SAXS scattering profile only through local density fluctuations. [82, 155] The rest of the morphology consists of stacks of crystalline lamellae, separated by narrow amorphous interlamellar gaps. [82, 84, 153-155] Typical characteristic lengths of the lamellar stack morphology of PEEK are: long spacing - $L$ = 150-180 Å, [82, 84, 63, 66, 155] crystalline lamellar thickness - $l_c$ = 90-120 Å, [82, 84, 154, 155] thickness of the amorphous interlamellar layer - $l_a$ = 40-50 Å. [82, 84, 154, 155]

The lamellar stack morphology is consistent with the electron microscopy (TEM) studies of Lovinger et al. [83] Electron micrographs of melt-crystallized PEEK show a coarse spherulitic morphology, consisting of stacks of crystalline lamellae, arranged into fibrils, and large interfibrillar amorphous gaps. The size of these gaps is estimated to be about 800-1000 Å [83] which is consistent with the assumption, that the density fluctuations caused by them can not be resolved in typical SAXS experiments. [82]

The lamellar stack morphology provides some insights on the possible origin and location of the rigid amorphous fraction (RAF) of PEEK. It is generally agreed, that the detection of a RAF above $T_g$ of the polymer results from the constraining effect of the crystalline lamellae on the adjacent amorphous regions. [16-18, 157] Some authors claim, that the "interphase" between the crystalline lamellae and the amorphous phase is the physical location of the rigid amorphous fraction. [17, 157] Sauer and Hsiao [154, 156] have made an interesting observation, that for PEEK, PET, and N-TPI (new thermoplastic polyimide) the rigid fraction by DSC and dielectric spectroscopy ( $f_r^{DSC}$ and $f_r^{DS}$ ) is approximately equal to the total volume fraction of the material within the stacks ( $j_{st} = f_r^{SAXS}$ ). While SAXS is not sensitive to the mobility of the species in the scattering medium, this interesting correlation between the rigid fraction from relaxation studies and a characteristic of the heterogeneous semicrystalline morphology suggests a model for the correspondence between the different parts of the morphology and their mobility.

(Note: The statement about insensitivity of SAXS to the mobility of the species in the scattering medium would be generally incorrect. As SAXS measures the density difference between the medium - amorphous phase, and dispersed phase - crystalline lamellae, temperature-dependent SAXS would be able, in principle, to detect thermal transitions

through the effect they have on the temperature dependence of the density of *one* of the phases. Thus a change in the temperature slope of the invariant in semicrystalline PEEK would be an indication of the glass transition region. At first it appears, that the above mentioned model is completely incompatible with this characteristic break in the linear change of the SAXS-invariant with temperature. However, one must note, that the interpretation of temperature-dependent SAXS data alone is not always straightforward and should be used with caution, especially when attempting quantitative analysis as in references 74 and 147. The SAXS invariant measures the *density difference* between the crystalline and the amorphous, e.g. "rigid"/"constrained" amorphous, fractions in the stacks. Thus it is assumed that any peculiar changes in the temperature profile of the invariant are attributed entirely to changes in the interlamellar amorphous phase. One objection to such a simplistic approach immediately comes to mind: experimentally it has been observed by WAXS, that the thermal expansion coefficient of the PEEK crystalline lamellae shows a step-change at the glass transition. [68] This observation precludes quantitative derivation of thermal expansion from the temperature dependence of the SAXS invariant, unless crystal density is monitored and evaluated with a reasonable degree of certainty simultaneously. Furthermore, if the glass transition has an effect on the crystalline lamellae, it is obviously due not to thermal expansion, but to relaxation effects. The latter would have a temperature-dependent rate and its effect on the "apparent" thermal expansion by SAXS must be taken into account. In conclusion, direct evidence for or against a "rigid" interlamellar amorphous fraction cannot be derived based on simplistic interpretation of the temperature dependence of the SAXS invariant alone.)

According to this model, [150, 154, 156] the mobile amorphous fraction (MAF) in PEEK is the amorphous material in the interstack regions ("liquid pockets"). The amount of material in the liquid pockets determines the relaxation strength of the glass transition. Its mobility is affected only mildly by the presence of semicrystalline lamellar stacks. Therefore, its glass transition range is slightly broadened and shifted a few degrees above the glass transition of a purely amorphous PEEK. [150] This is confirmed by the observations made in section 4.2.5 and by literature sources. [16, 17, 157]

The RAF in PEEK, is part of the interlamellar amorphous layer or, possibly, the entire interlamellar amorphous layer. Certainly, if the thickness of this layer is about 20-50 Å, the mobility of the folds and tie-chains of a semi-rigid chain polymer would be greatly reduced. Sauer suggests, that the small size of the interlamellar gap, combined with the chain microstructure, leads to the effective immobilization of the entire interlamellar layer at the low equivalent relaxation frequency of a DSC experiment (~$10^{-2}$ Hz for glass transitions). [150]

The ideas presented above lead to the following model for the correlated phenomena observed upon long time crystallization and/or annealing of PEEK (multiple melting, physical aging, densification of crystals, crystallinity discrepancy):

1. With the effective end of the primary crystallization stage locally (i.e. behind the advancing growth front of the spherulites) or both locally and globally (when the primary crystallization is fast), a *lamellar stack morphology* is established.

2. The lamellar stacks consist of crystalline lamellae and interlamellar amorphous layers. The latter represent practically the entire constrained crystal-amorphous interphase - the so called *rigid amorphous fraction* of PEEK. The interstack (or interfibrillar) amorphous regions are relatively large regions of almost unconstrained mobile amorphous material - the *mobile amorphous fraction.*

3. The interconnected lamellar stacks form the fibrillar matrix of the spherulitic superstructure. The interstack regions of mobile amorphous phase are effectively confined between the fibrils - "*liquid pockets*".

4. Within the spherulites' boundaries the instantaneous volume changes in response to temperature change (thermal expansion) and transient changes due to unrelaxed interfacial tensions (stresses with thermal origin) are governed by the response of the interconnected lamellar stacks.

5. Due to the low crystallinity, at any time after the completion of the primary crystallization stage a thermodynamic driving force toward further crystallization will be present. The crystallization proceeds through the *secondary crystallization* stage.

6. Secondary crystallization occurs within the "liquid pockets". The mobile amorphous phase has sufficient mobility for the realization of three dimensional order within the pockets.

7. The mass transfer due to the formation of new more dense regions within the pockets (new crystalline lamellae) leads to a depletion of the remaining part of the pockets. In order to restore the density of the remaining amorphous fraction in the pockets to its equilibrium value, the volume of the liquid pockets must contract.

8. The volume contraction of the liquid pockets is controlled by the overall volume contraction of the spherulite e.g. the volume contraction of the matrix of lamellar stacks. The later is governed by the slow relaxation of the interlamellar amorphous fraction which also enables the slow densification of the primary crystalline lamellae.

9. Secondary crystallization is the result of the balance of the two processes: thermodynamically driven crystallization within the liquid pockets, which results in lower density of the surroundings of the lamellae (e.g. "negative pressure", dilatational forces), and contraction of the volume, governed by the long relaxation times of the RAF within the primary lamellar stacks, which relieves the "negative pressure".

This main framework of the revised dual lamellar population model results in the explanation of certain phenomena without the need to specify further details of the model:

***physical aging***

The "physical aging" of semicrystalline PEEK above the nominal glass transition is the result of both - secondary crystallization and the relaxation of the constrained amorphous fraction. The long retardation times characterize the response of the "rigid"/"constrained" amorphous fraction. The horizontal shift of the creep compliance curves is due to the self-retardation of the secondary crystallization process, governed by the extent of relaxation of the RAF during secondary crystallization. The vertical shift is mostly the result of increase in crystallinity due to the formation of new, secondary lamellae. The apparent continuity in the change of the vertical shift rate across the nominal glass transition could be the result of the fact, that although through different mechanisms, slow volume relaxation governs the

isothermal decrease of the creep compliance below $T_g$ (through densification of the amorphous glassy pockets) as well as above $T_g$ (through RAF controlled relaxation during secondary crystallization within the pockets).

***glass transition***

The increase in crystallinity during annealing above $T_g$ can account for the log-time increase in $T_g$ after aging (figures 4.58 and 4.59). An increase in crystallinity within the liquid pockets by 0.01-0.02 during secondary crystallization (for the samples on figures 4.46 and 4.25-4.29) would not affect significantly the relaxation strength (by DSC) and might even not be detectable due to the fact, that the uncertainty of the $f_{RAF}^{DSC}$ values is about ±0.05 (compounded from the relative uncertainty of the $C_P(T)$ values, estimated by Cheng et al. to be at best ±2% [16]). A slightly larger increase in crystallinity during the secondary crystallization (as for the cold-crystallized samples - figures 4.47-4.49) might result in a change in relaxation strength (see $C_P(T)$ change above the glass transition between the scans on figure 4.13). Irrespective of the change in relaxation strength, however, in both cases the insertion of new lamellae or lamellar stacks in the liquid pockets must affect the mobility of the remaining amorphous fraction. Generally, the effect should be similar to that due to the primary lamellae. Therefore, during the development of secondary crystallinity an increase in $T_g$ would be expected. This explains the observation of the log-time increase in $T_g$ during the secondary crystallization stage for samples with otherwise completely different initial morphologies - figures 4.58 and 4.59.

Less straightforward is the explanation of the peculiar decrease in $T_g$ with an increase in $T_c$ (figure 4.57) and $T_a$ (figure 4.59). Cheng et al. claim that this is due to the morphological features of crystallization at low vs. high temperatures. [16] At high temperatures, crystallization results in larger lamellae (or lamellar stacks) and at low temperatures - smaller and less perfect lamellae. They suggests, that this difference in morphology results in larger crystal-amorphous interphase and higher constraints (larger residual strain at the interphase) and therefore - higher $T_g$ for the samples with lower crystallization temperature. In the context of the finite lamellar stack model, such an interpretation is consistent with the direct morphological observations (by TEM) of Lovinger

et al. [83] With a decrease in crystallization temperature, they observed, that the coarseness of the spherulites decreases. A smaller size of the interstack gaps at lower crystallization temperature would result in a larger influence of the adjacent lamellar stacks on the relaxation of the MAF and higher $T_g$.

However, if these ideas are applied to the case of cold-crystallized samples (figure 4.57 and references quoted there) and melt-crystallized samples, annealed below $T_x$ (figure 4.59), such an interpretation is inconsistent with the major assumptions of these authors and the present study (namely, the adoption of a dual lamellar population model of the thermal stability of the lamellar microstructure).

The lamellar stack morphology and the spherulitic superstructure are formed during the primary crystallization stage. In the case of the cold-crystallized samples, primary crystallization upon heating occurs in the 165-190°C range. The argument about the effect of crystallization temperature on $T_g$ will apply only if one assumes that the morphology of the primary lamellae changes with increase in $T_c$, that is, after the end of the primary crystallization. This amounts to assuming a continuous melting and recrystallization of the entire lamellar population during heating to the cold-crystallization temperature (e.g. the melting-recrystallization model for the multiple melting of PEEK). As was discussed above, that model has been shown to be inconsistent with other experimental evidence, including that obtained by DSC.

In the case of the melt-crystallized samples annealed *below* $T_x$ (figure 4.59), the annealing will produce no change in the primary lamellar morphology. The above mentioned explanation could apply only to the secondary lamellar population and its environment. However, instead of dense vs. coarse superstructure, the interpretation would be rather as more constrained (low $T_a$) vs. less constrained (high $T_a$) environment of the newly formed secondary lamellae.

An alternative explanation is suggested by Jonas and Legras. [157] The decrease in $T_g$ is explained in terms of a change in the loss of conformational entropy of the amorphous regions upon crystallization. Crystallization and/or annealing at lower temperatures results in kinetic trapping of some of the accessible conformations and their exclusion from the regions

of phase space, which can be explored through large scale segmental motions by the chains in the amorphous regions. The loss of degrees of freedom results in higher activation energy and therefore higher $T_g$.

***multiple melting and secondary crystallization***

The model proposes that the physical location of the secondary crystallization process is outside the existing semicrystalline primary lamellar stack morphology - in the amorphous gaps between primary lamellar stacks. It explains qualitatively the slow rate of secondary crystallization through the limiting effect of the slow relaxation of the constrained amorphous fraction (RAF), necessary for the continuation of secondary crystallization. The temperature dependence of the secondary crystallization rate can be explained through the increased mobility of the so called RAF with increase in crystallization or annealing temperature.

However, the model does not answer unambiguously some of the questions related to the melting of the secondary lamellae - the origin of their lower thermal stability and the time-temperature dependence of the melting temperature $T_{max}$(low), which was examined in section 4.2.1:

The original dual lamellar population model suggests, that the lowering of the melting temperature of the secondary lamellae is due to their smaller size (i.e. thinner lamellae inserted between thicker primary lamellae). [16, 70, 71] This idea is kept by some authors in the revised dual lamellar population model as well. [82, 84, 155] An immediate consequence of this idea is the conclusion, that the extremely broad range of melting temperatures of the secondary lamellae (170-340°C) observed in this study and literature sources [16, 72, 73] must correspond to a very broad distribution of secondary lamellar sizes, which must be smaller than the observed sizes of the primary lamellae. A further illustration of this conclusion is the observed apparent sequential crystallization of secondary lamellae with progressively smaller and smaller sizes (reflected in "multiple melting" DSC scans with up to 12 peaks) upon stepwise annealing at successively lower temperatures after melt-crystallization. [72, 73] While the effect of size on thermal stability of polymer lamellar crystals is very intuitive and well understood, [42, 113] until a direct morphological evidence from a carefully designed

experiment connects the low temperature melting of secondary lamellae to their smaller sizes, this remains only a good operative idea.

(*Note*: The above critique is based on the fact, that so far direct morphological evidence for different lamellar sizes (electron microscopy) only suggests, that the smaller lamellae are the ones, which melt at the low temperature endotherm. [70] In semicrystalline polymers, the broad high temperature melting peak alone is usually associated with the melting of a distribution of lamellar sizes. [42, 113] There is no direct evidence from the morphological studies, that the different lamellar sizes they display do not belong to the primary lamellar population. An intriguing exception is a description, given by Lattimer et al., [73] of a sequence of events, observed within a coarse spherulitic superstructure during stepwise heating. The authors report (without providing evidence) time resolved observation at high temperatures in the electron microscope of the crystallization, melting, immediate recrystallization and growth upon annealing of a separate population of PEEK lamellae, while the primary lamellae, which form the coarse spherulitic superstructure, remained unchanged during the experiment.)

One can speculate, that in addition to the small size of the secondary lamellae, residual dilatational forces acting on them ("negative pressure", interfacial tension) could affect their thermal stability. [151] The discrepancy between DSC and density crystallinity, discussed earlier in this chapter (section 5.3), provides an argument in support of the existence of such forces and their possible effect on the thermal stability of the secondary lamellae. The higher DSC crystallinity values (and WAXS crystallinity values [125]) imply, that the calculated average density of the amorphous phase at ambient conditions, measured at different extents of secondary crystallization, is lower than the equilibrium value (figures 5.1-5.4). The resulting "negative pressure" (dilatational stresses) would lead to a depression of the melting point of the secondary lamellae, embedded in the "liquid pockets". This idea provides a viable explanation for the time-dependence of the melting point of the secondary lamellae.

In the context of the idea that smaller size alone determines the lower thermal stability of the secondary lamellae, the time-dependence of $T_{max}$(low) leads to physically meaningless

conclusions. The increase in $T_{max}$(low) with log($t_a$) would correspond to increase in crystal thickness on the order of an angstrom or less (that is, a small fraction of the unit cell and repeat unit lengths). Such small effect could be interpreted only as "perfection" of the lamellae. The time-temperature evolution of $T_{max}$(low) can not be interpreted as resulting from the effect of "size" or "perfection" alone.

The concept of "negative pressure" (and the physical changes associated with its formation) provides a reasonable explanation of the increase in thermal stability of the secondary lamellae with increase in log($t_a$). With increase in log($t_a$), the volume of a "liquid pocket" decreases, while the volume fraction of (secondary) crystalline lamellae formed within it increases. Upon heating these lamellae melt just above $T_a$ due to a large melting point depression, caused by the dilatational stress ("negative pressure") exercised on them. With the beginning of melting, the "negative pressure" is partially relieved due to the transformation of the lamellae into a less dense amorphous material within a constrained volume. Therefore, the longer the annealing time, the higher the mass fraction, which transforms upon melting and the larger the reduction of the "negative pressure" at the time of melting. This effective reduction leads to an increase in the observed melting temperature of the secondary lamellae with increase in log($t_a$).

The revised dual lamellar population model of the semicrystalline state presented above provides a reasonable explanation for a number of the time-dependent phenomena observed beyond the primary crystallization stage in PEEK.

At this stage the new model addresses the time-dependent phenomena above $T_g$ ("physical aging", multiple melting, RAF etc.) only in PEEK. As was pointed out in the review (chapter 2), these phenomena are universal for many crystalline polymers. A classification scheme for chain-folding semicrystalline polymers, based on the presence or absence of a crystalline $\alpha$-relaxation, [152] is a first step in achieving a universal model for the time-dependent structural relaxation in semicrystalline polymers above $T_g$. Table 5.1 summarizes the various observations, incompatible with the simple two-phase model, for several semicrystalline polymers.

**Table 5.1** List of polymers for which experimental data suggest violations of the standard two-phase model of the physical state of semicrystalline polymers.

**Failures of the Two-Phase Model of Crystallinity**

| Polymer | | Low Endotherm and "Physical Aging" | | RAF - $\Delta C_P(T_g)$ anomaly | $c_c^{DSC}$ - $c_c^{Dens}$ anomaly |
|---|---|---|---|---|---|
| Material | $\alpha$ Relaxation | $T_g$-$T_\alpha$ | $T_g$-$T_m$ | | |
| **HDPE** | 50°C | ✓✓ | ** | 11 | 168 |
| **i-PP** | 100°C | ✓✓ | ** | 13 | - |
| **PPS** | no | | ✓✓ | 15 | 124 |
| **PEEK** | no | | ✓✓ | 16 | this study |
| **i-PS** | no | | ✓✓ | 206 | * |
| **PBT** | no | | ✓✓ | 14 | * |
| **PET** | no | | ✓✓ | 113, 170 | 40, * |

* - currently under investigation - Marand et al.

** - annealing above $T_\alpha$ and/or close to $T_m^{'}$ also leads to a log($t_a$)-dependent (low temperature) melting endotherm [27, 29, 158, 161, 173, 174], however, its molecular origin is expected to be different - "surface melting"; thickening

To finish this discussion, several alternative ideas will be mentioned *without elaborate analysis*. Some of them are compatible with the current model, others are not. These include:

- growth of single secondary lamellae between the primary ones (Bassett et al. [70]) vs. growth of stacks of secondary lamellae within the mobile amorphous phase (in the "liquid pockets");

- growth at the crystal-amorphous interface - small new crystals or "surface crystallization" and "surface melting";

(*Note*: This idea would require a major revision of the ideas about the "rigidity" of the interphase - RAF and its role. It is quoted here because surface crystallization and surface melting had been extensively explored [29, 158] as a model for the isothermal structural reorganization and thermal stability upon heating-cooling cycles of PE at high temperatures i.e. *above the crystalline α-relaxation temperature*. Hutchinson and Kriesten effectively suggest the same idea for explaining the low temperature endothermic peak and the "physical aging" of i-PP below the α-relaxation as well. [45, 46])

- growth of different, possibly - fringed-micellar type of crystals during the secondary crystallization stage;

(*Note*: This idea is based on the similarity between the "double melting" phenomenon and melting after isothermal annealing of PVC [51-53] which is believed to form crystals of fringed-micellar type. See also related results and comments at the end of section 5.6.3.)

- effect of conformational entropy change in the amorphous regions and/or the crystal-amorphous interphase upon crystallization;

(*Note*: This idea has already been mentioned above in connection with the explanation of the dependence of $T_g$ on crystallization temperature, which is provided in reference 157. For additional reference see Wunderlich's discussion of polymer melting in reference 42 and section 4.7 of reference 113.)

- a transition of the amorphous chains from "fragile" to "strong" behavior [199] upon formation of a network-like semicrystalline structure.

(Note: As was mentioned at the end of section 5.4, the main operative value of this idea currently lies in the possible explanation of the abnormal crystallinity dependence of the heat capacity reflected in the concept of a "rigid amorphous fraction" above $T_g$. [10] The concept of "rigidity" above $T_g$ would be replaced by the characteristic features of "strong" liquids. The transformation from a "mobile"/"fragile" amorphous polymer to "rigid"/"strong" liquid could also explain the change in the ability for structural reorganization from fast primary crystallization to slow secondary crystallization. The former is characteristic of the ease of structural reorganization in the "mobile"/"fragile" linear amorphous polymer, the latter is similar to the resistance to structural reorganization in "strong" liquids. The heat capacity of the semicrystalline polymer above $T_g$ would be lower than predicted from the simple two-phase model due to the fact that the heat capacity of the constrained amorphous phase is lower, than that of the pure amorphous phase. Inherent to the "strong"/"fragile" classification of liquids is the analysis of the complex "topology" of the potential energy hypersurface in configurational space. The density and distribution of local minima, their barriers and organization in "megabasins" of minima play an important role in identifying the differences between the two classes of liquids, but are at this point of development of the physics of semicrystalline polymers and glasses a visualization tool, rather than characteristics rigorously derived on the basis of statistical mechanics.)

- an alternative model for the origin of the "physical aging" phenomenon. [216]

(Note: The model, already briefly discussed at the end of section 5.4, is a significant departure from Struik's extended glass transition model. While it acknowledges the existence of a "constrained" amorphous fraction above $T_g$ characterized by large retardation times, it examines the possibility that changes in the relaxation strength alone are the sole origin of the "physical aging".)

## 5.6 Some Controversial Results

The preceding sections of this chapter discussed the majority of the results presented in chapter 4. Some new ideas for the explanation of original, as well as literature data, were explored and a revised version of the dual lamellar population model of semicrystalline

PEEK was presented in its relation to time dependent phenomena above $T_g$ ("multiple melting" and "physical aging").

This section presents additional original results from studies of the "multiple melting" of PEEK. Despite the fact, that some of the effects had already been studied in the literature, they have not been given enough consideration within the dual lamellar population model. These include:

1. The heating rate dependence of the low temperature melting endotherm - section 5.6.1.

The effects observed in heating rate studies of the melting of PEEK [63, 65, 66, 70] in general have extensively discussed and explained only within the melting-recrystallization model of the multiple melting of PEEK. [63, 65, 66] Authors who support the dual lamellar population model have either not addressed the relation of the heating rate dependence to the model [16, 70] or did not study it at all. [71, 82, 84, 155]

2. Melting of semicrystalline PEEK, annealed above its initial crystallization temperature at very high annealing temperatures - section 5.6.2.

Results of such annealing experiments are presented in the study of Chang [72] and Bassett et al. [70] Some of the morphological evidence presented by Bassett et al. [70] and by Lattimer et al. [73] appears directly related to these experiments, rather than to any other DSC investigation of the multiple melting of PEEK. The significance of this high temperature annealing, however, has not been given enough consideration. The results presented in section 5.6.2 suggest a new set of morphological experiments (for example, WAXS, SAXS, TEM). These appear to require a demanding setup, but ultimately should be able to provide more conclusive evidence for the structural changes during annealing and subsequent melting of PEEK, than the current evidence in support of the dual lamellar population model.[70,82,84,155]

3. DSC studies of the effect of annealing in the immediate vicinity of the calorimetric glass transition of semicrystalline PEEK (enthalpy relaxation below $T_g$ and low temperature melting above $T_g$) - section 5.6.3.

The experiments examine the validity of several statements made [51, 46, 159] that the magnitude and the rate of increase of the enthalpy of the low temperature endothermic peak above $T_g$ are much higher than the characteristic values, known for the enthalpy relaxation of amorphous polymeric glasses below $T_g$.

The last two experiments can be characterized as exploring the phenomenon of the low temperature endotherm at the boundaries of the temperature range, where it is observed - between $T_g$ and $T_m'$. This is in contrast to the literature studies and the results reported in chapter 4, in which characterization of the multiple melting phenomenon in PEEK has been done at intermediate crystallization and/or annealing temperatures. After the extensive characterization at intermediate temperatures has lead to a good knowledge of the thermal behavior of PEEK, this new approach can provide valuable information about the nature of the physical changes, which occur upon annealing of PEEK above $T_g$.

### *5.6.1 Heating Rate Dependence of the Low Temperature Melting Peak of PEEK*

Several heating rate studies of the double melting behavior of PEEK [65, 66, 69, 70] have established the following characteristics:

- The temperature of the maximum of the main (high temperature) melting peak decreases with an increase in the heating rate $q$. [65, 66, 69, 70]

- The peak maximum of the low temperature melting peak increases with an increase in $q$. [65, 66, 69, 70] The increase appears approximately linear with $\log(q)$. [65, 66]

- The enthalpy of the low temperature peak increases linearly with an increase in $\log(q)$. [16]

These results have been interpreted in terms of a balance between two competing processes melting and recrystallization. Lee and Porter [65, 66] and Ostberg and Seferis [69] propose, that the observations are due to the melting and recrystallization of the entire population of polymer lamellae (e.g. melting-recrystallization model). Ostberg and Seferis draw an analogy with a similar interpretation of the heating rate studies of PET by Fakirov et

al. [40] Cheng et al. [16] suggest, that the low melting temperature population of lamellae might recrystallize after melting and melt again at the high temperature endotherm. The balance between the melting and the recrystallization of these secondary lamellae leads to the apparent "conversion" [16] between the two melting peaks - a linear increase in $\Delta H_m$(low) with log($q$) and a constant total melting enthalpy. According to Lee and Porter, however, the total melting enthalpy decreases with increase in log($q$). [66] Bassett et al. [70] propose, that the changes in the high and low temperature melting peaks with heating rate suggest only a modest reorganization during scanning of the lamellar population, which melts at high temperatures. This conclusion is based on the fact, that the double melting character of the scan of PEEK, crystallized at 310°C, is retained even at heating rates of 80 K/min. This suggests, that recrystallization would have to be extremely fast in the temperature range above the low melting peak (~ 320°C). Studies of the crystallization rates of PEEK in this range do not support such statement. [70]

The next few paragraphs present data which illustrates the experimental observations listed above as well as some original results. The studies were performed on melt-crystallized PEEK in order to minimize the melting range of the polymer in the DSC. This minimizes scanning time and leads to better reproducibility of the baseline and temperature calibration of the DSC.

Figure 5.9 shows the melting scans of PEEK, crystallized from the melt in the DSC at 308°C for 60 min. The scans were recorded at intermediate heating rates - 2.5 K/min, 5 K/min, 10 K/min, and 20 K/min. Correction with the appropriate baseline was applied.

No temperature calibration of the heating scans and the melting peak parameters was initially applied (figures 5.9 - 5.11). This was done in order to compare the heating rate dependence of the two different melting peaks of PEEK with the heating rate dependence of the melting peak of the lead standard.

The "modest reorganization" of the high temperature melting peak is evident in the decrease of the temperature of its maximum with increase in heating rate. The temperature calibration correction would have to account for the thermal lag in the sample. Therefore, it will shift the high heating rate scans to lower temperatures and only increase the apparent

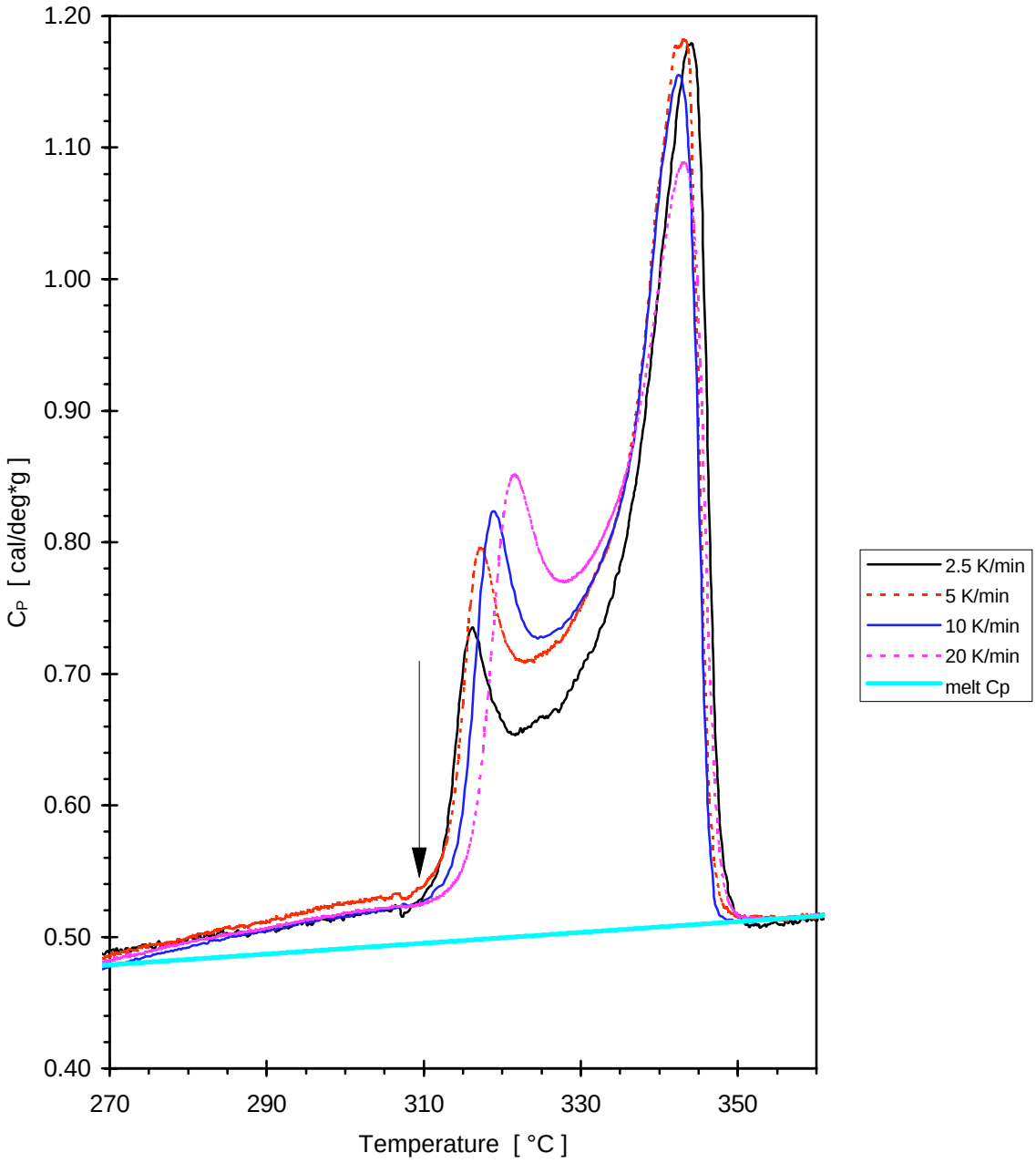


**Figure 5.9** DSC heating scans of PEEK, melt-crystallized at $T_x$ = 310°C for 60 min, recorded at heating rates: 2.5 K/min, 5 K/min, 10 K/min, and 20 K/min.

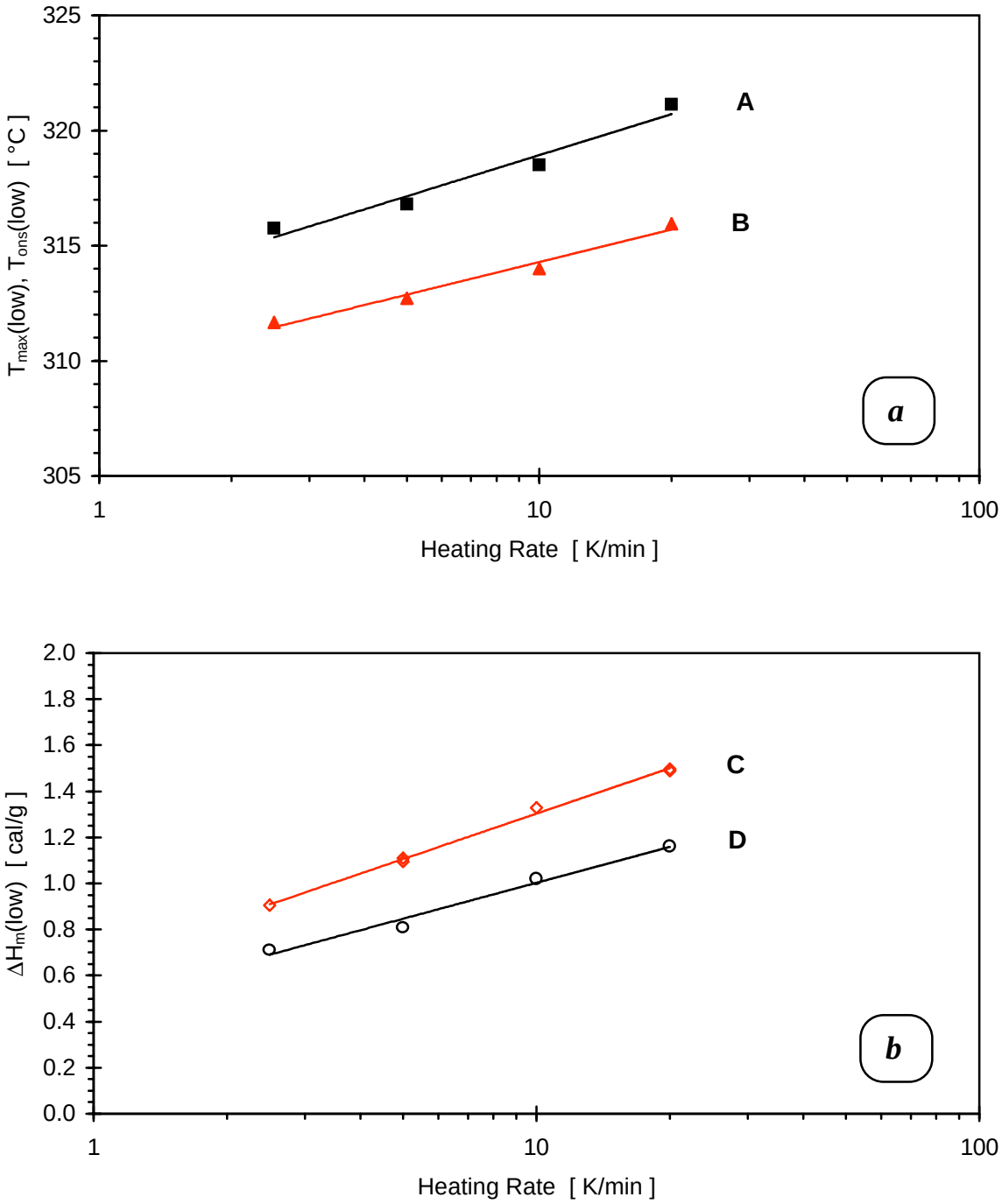


**Figure 5.10** Dependence of $T_{max}$(low) and $\Delta H_m$(low) on heating rate in the DSC for the melting scans shown on figure 5.9: A) - peak maximum $T_{max}$(low) and B) - peak onset $T_{ons}$(low); $\Delta H_m$(low) from calculations with: C) linear baseline and D) step baseline.

drop of the maximum of the high temperature peak. Its reorganization is further pointed out by the decrease in height of the high temperature peak with increase in heating rate. The magnitude of this decrease and the parallel increase in $\Delta H_m$(low) are modest indeed.

Figure 5.10-*a* shows the increase in the temperature of the peak maximum - $T_{max}$(low), and peak onset - $T_{onset}$(low), of the low temperature peak with an increase in log(*q*). Without temperature calibration, their dependence on log(*q*) slightly deviates from linear.

The melting enthalpy of the low temperature peak is shown on figure 5.10-*b*. Its evaluation is subject to the uncertainty, associated with resolving the local baseline of the low temperature endothermic peak, discussed at the end of section 4.2.1. Evaluation with a linear local baseline (C) leads to larger values for $\Delta H_m$(low) than evaluation with a continuous "step baseline" (D). Both sets of data, irrespective of the evaluation method, show an approximately linear increase in $\Delta H_m$(low) with an increase in log(*q*).

Another set of experiments was performed, for the purpose of investigating the dependence of the corrected characteristic temperatures of the melting scan of PEEK on heating rate. The sample in this study is a thin film (~0.15 mm), pressed and isothermally crystallized from the melt in the Pasadena SP210C hot press for 90 min at temperature 310°C. As was discussed earlier in section 4.2.1, the true isothermal crystallization temperature of the press is several degrees lower and was determined to be about 305°C. All samples were prepared at the same time, were chosen from a small area of the film (i.e. with no significant gradient in $T_x$) and therefore have the same thermal history. Melting scans were collected at heating rates ranging from 0.62 K/min to 80 K/min. The sample weight was kept small and the same for all heating rates (~ 2 mg) in order to ensure small steady state temperature gradient within the sample. This was probably true at slow heating rates, while for the highest heating rates a significant temperature gradient (and a thermal lag of the melting transition, associated with it) is expected. [113] For this purpose the melting scans of a lead standard were collected as well. The PEEK melting scans were compared with them under the assumption, that the thermal lag of the sample is approximately the same as the

thermal lag of the lead standard, which would allow temperature calibration of the PEEK melting transitions and reveal their inherent heating rate dependence.

The melting scans of the lead standard were collected at the same heating rates as the PEEK samples. The melting temperature of lead is 327.5°C - about midway between the low and high temperature melting peaks of the PEEK samples investigated.

Due to the small sample mass the stability of the baseline for the eight different heating rates used was not sufficient for a more rigorous evaluation of the melting peaks with the use of a local step-baseline (as described at the end of section 4.2.1). The melting peaks of lead and PEEK were analyzed with the help of the $MC^2$ software package for thermal analysis. The results are shown on figures 5.11 and 5.12.

Figure 5.11-*a* shows the heating rate dependence of $T_{max}$(lead) and $T_{onset}$(lead) - the temperatures of the peak maximum and peak onset for the melting peak of the lead standard; $T_{max}$(high) - the temperature of the maximum of the high melting peak, $T_{max}$(low) and $T_{onset}$(low) - the peak maximum and onset temperatures of the low temperature peak of PEEK. Figure 5.11-*b* shows the same parameters, plotted against a logarithmic heating rate axis.

$T_{onset}$(lead) increases linearly with an increase in the heating rate $q$. $T_{max}$(lead) increases faster with increase in $q$, but when extrapolated to infinitely slow heating rate, the two temperatures approach the equilibrium melting temperature of lead.

The uncorrected melting temperature of the high temperature melting peak of PEEK - $T_{max}$(high), initially decreases with an increase in $q$. This decrease is opposite to the trend observed in $T_{max}$(lead) and is due to the reorganization of the PEEK lamellae during the melting scan. Lamellae, which melt at 310°C, for example, would be dynamically annealed for 8 min, 16 min, and 32 min during the scan from 310°C to 320°C at heating rates 1.25 K/min, 0.62 K/min, and 0.31 K/min respectively. Such times are sufficient for the *recrystallization* of these lamellae and subsequent melting at higher temperatures. With increase in heating rate the amount of material, which recrystallizes and the temperature of recrystallization decrease, leading to the decrease in $T_{max}$(high) of PEEK.

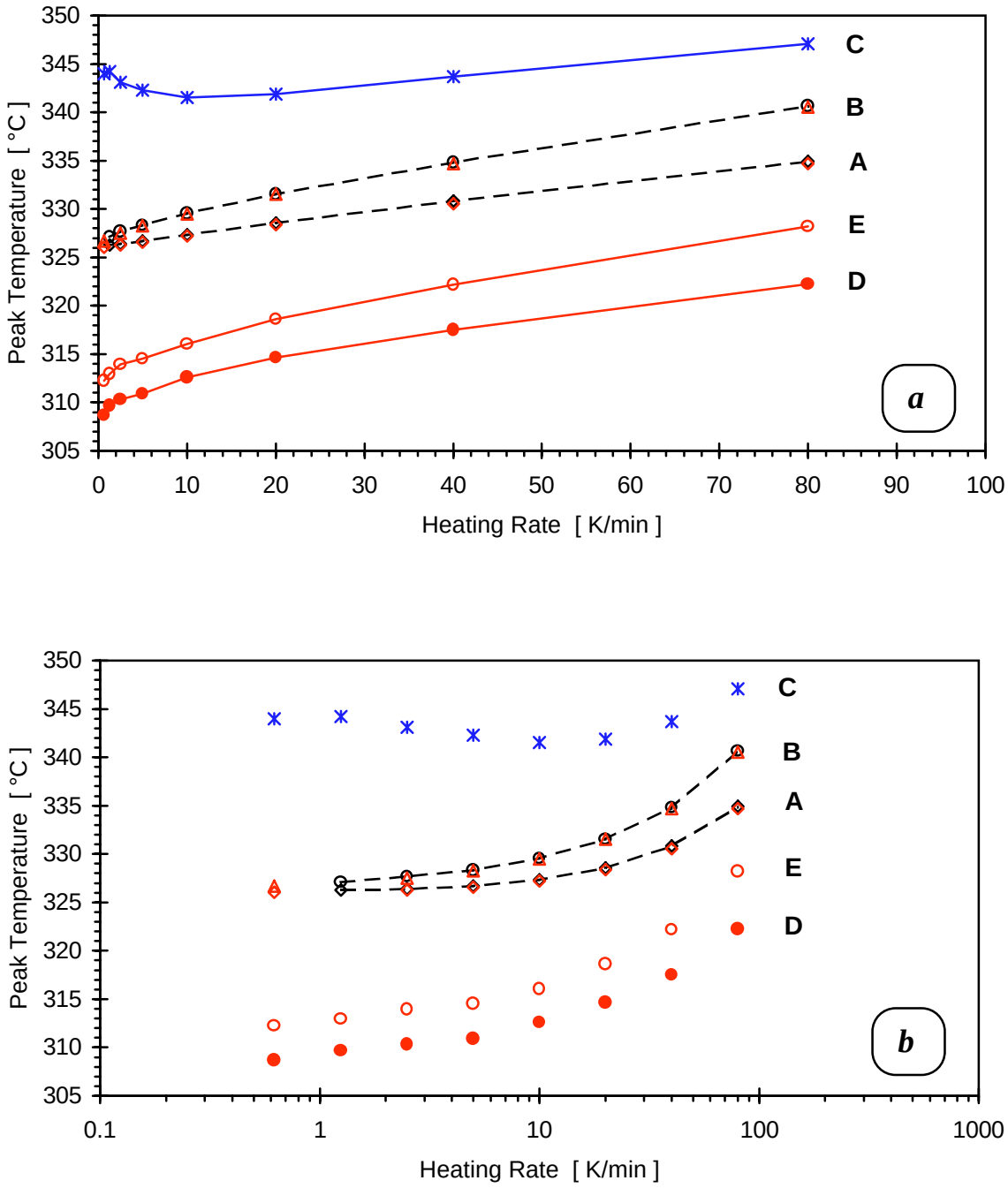


**Figure 5.11** Dependence of the peak temperature on the DSC heating rate (***a*** - linear plot, ***b*** - semilogarithmic plot): A) peak onset temperature and B) peak maximum temperature of a lead standard; C) peak maximum of the high temperature melting peak of PEEK; D) peak onset and E) peak maximum of the low temperature melting peak. PEEK samples were crystallized for 90 min at 305°C in a hot press.

At higher heating rate $T_{max}$(high) increases with increase in *q*. This change in the trend is expected to be due to the thermal lag effect, which offsets the partial reorganization (at these heating rates the recorded peak maximum temperature of lead $T_{max}$(lead) is increasingly larger than the true melting temperature of lead). Due to the highly asymmetric shape of the high temperature melting peak of PEEK, evaluation of its onset temperature and comparison with the onset temperature for lead is not appropriate and was not done.

In contrast, the low temperature melting peak of PEEK is highly symmetric. It is broader than the melting peak of lead, but much narrower than the high temperature melting peak of PEEK. The symmetry of the peak and its relatively narrow shape (for this crystallization temperature) justify a comparison of its peak onset and maximum with those of the lead standard.

The plot with the linear heating rate axis (figure 5.11-*a*) shows, that at high heating rates the behavior of $T_{max}$(low) and $T_{onset}$(low) appears similar to the behavior of $T_{max}$(lead) and $T_{onset}$(lead). With a decrease in heating rate, however, these parameters for PEEK decrease at a faster rate than in the case of lead and the dependence of $T_{onset}$(low) on *q* is not linear. This difference is better illustrated on the plot with the logarithmic heating rate axis (figure 5.11-*b*). With decrease in log(*q*), the difference between $T_{max}$(low) and $T_{onset}$(low) does not approach zero, as for lead, but appears to retain a constant value. The results from figure 5.11 are replotted on figure 5.12 in a such a way as to emphasize the difference between the melting of PEEK and lead.

Figure 5.12-*a* shows the difference between same type characteristics for the different peaks:

A) [$T_{max}$(high) - $T_{max}$(lead)] - curve A.

Subtraction of $T_{max}$(lead) from $T_{max}$(high) is equivalent to subtraction of the thermal lag contribution to $T_{max}$(high), under the assumption, that the effect has same magnitude and trend with log(*q*) for both - semicrystalline PEEK and crystalline lead. With an increase in log(*q*), this parameter decreases linearly throughout the entire range of heating rates. This indicates, that the slowing down of reorganization effects continues to manifest itself throughout the entire range of heating rates applied.

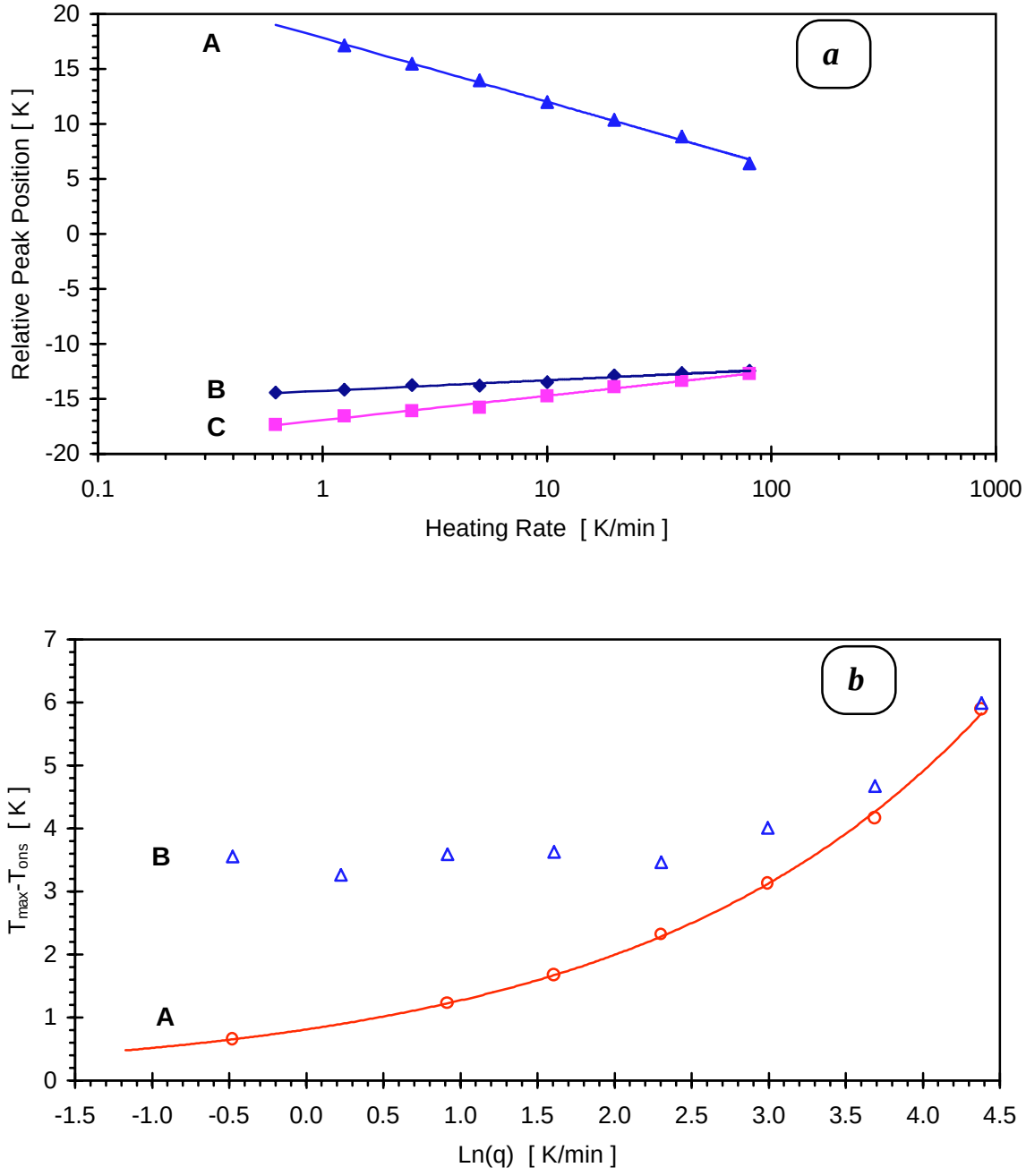


**Figure 5.12** (***a***) - Relative position of the melting temperatures of the high and low melting peaks of PEEK: A) $T_{max}$(high)-$T_{max}$(lead), B) $T_{max}$(low)-$T_{max}$(lead), C) $T_{onset}$(low)-$T_{onset}$(lead). (***b***) - Heating rate dependence of the difference between peak maximum and peak onset temperatures for: A) lead standard, B) the low temperature melting peak of PEEK. Calculated from data on figure 5.11.

B) [$T_{max}$(low) - $T_{max}$(lead)] - curve B, and [$T_{onset}$(low) - $T_{onset}$(lead)] - curve C.

The two curves merge at high heating rates. This indicates, that at very high heating rates the thermal lag effect dominates the shape and position of the low temperature endotherm of PEEK. However, at low heating rates other mechanisms, perhaps inherent to the kinetic nature of the low temperature endothermic peak, dominate the shape and position of the peak.

Figure 5.12-*b* characterizes the heating rate dependence of the width of the low temperature endotherm of PEEK by comparing the difference [$T_{max}$-$T_{onset}$] for lead and PEEK. In the case of lead - curve A, with decrease in log(*q*) the difference approaches zero, following an exponential dependence. For the low temperature endotherm of PEEK - curve B, the difference merges with the result for lead at high heating rates. At low heating rates it appears to attain a constant value of about 3.5 K. This peculiar observation could also be inherent to the kinetic nature of the low temperature endotherm.

At last, one must note the fact that some of the results on the characteristics of the low temperature endotherm could have been affected by the method of analysis of the DSC scans. The new findings reported here must be reexamined with an experiment, in which the thermal history is favorable to a rigorous evaluation of all characteristics of the DSC heating trace in the vicinity of the low temperature endothermic peak, according to the local step-baseline method presented at the end of section 4.2.1. With this, a more definitive conclusion about the effect of heating rate on the melting enthalpy could be obtained.

In summary, the heating rate studies of the melting of PEEK show, that:

- melting and recrystallization during the heating scan have significant effect on the high temperature melting peak of PEEK even for melt-crystallized samples.

- after calibration with a lead standard, the low temperature melting peak in the scan of PEEK increases in magnitude and position linearly with increase in logarithm of the heating rate.

- although the peak of the low temperature endothermic transition is relatively sharp and symmetrical (see section 5.6.2), at slow heating rates its width does not follow the

heating rate dependence of the sharp melting peak of lead. The observed behavior appears to be due to the nature of the transition, rather than to thermal lag effects.

### *5.6.2 Annealing of Almost Fully Melted PEEK near $T_m'$*

The study of Bassett et al. [70] contains some experiments, in which originally amorphous PEEK has been heated up from the glassy state, crystallized upon heating and annealed at very high temperatures, close to the melting range in the continuous heating scan of amorphous PEEK. These experiments are equivalent to the thermal history profile shown in figure 3.4 for annealing temperatures $T_a$ ($T_c$ in the notation of figure 3.4) in the 320°C - 345°C range. The following experiments by Bassett et al. are closely related to the data presented later in this section:

- Short time annealing ($t_a$ = 10 min) at progressively higher temperatures - $T_a$ = 310°C - 340°C, and scanning after cooling down below $T_g$.

- Isothermal annealing for different times at a relatively high annealing temperature - $T_a$ = 320°C.

The first set of these experiments (different $T_a$'s, same $t_a$) shows at low annealing temperatures a low temperature endothermic peak, which appears as a small shoulder at the beginning of the main melting peak. With increase in $T_a$ more of the material which melts in the main melting peak is melted before the start of the annealing. The low temperature peak increases in magnitude and for the given annealing time at certain annealing temperature (between 320°C and 330°C) merges with the main melting peak. At the highest annealing temperature ($T_a$ = 340°C) a small sharp peak is observed on the high side of a broad melting curve, which resembles the melting curve of the original unannealed polymer. The former is identified with the melting of a *self-seeded* polymer, melted and recrystallized at 340°C, the latter - with the melting of the polymer, recrystallized on cooling. Results similar to these are shown also in the study of Chang. [72]

The results presented in the following paragraphs will help illustrate the difference between the melting of the high and low melting populations of lamellae when the annealing temperature is very high and in the melting range of the primary lamellae. They extend the

observations of Bassett et al. [70] and Chang [72] by monitoring the annealing time dependence of the low and high temperature melting peaks at several different annealing temperatures along the melting trace of a fully amorphous PEEK, heated from the glass.

The samples were heated fast in the DSC (at the fastest rate possible - 320 K/min) to the annealing temperature $T_a$. The several annealing temperatures used: 325°C, 334°C, 340°C, 343°C, and 345°C, span approximately the part of the scan of an amorphous PEEK, in which melting proceeds from about 30% to 90-95% of the total melting enthalpy (see figures 3.1 and 4.13). After annealing for various lengths of time at $T_a$, the melting scans were recorded without quenching (at most $T_a$s except 340°C). The scans were recorded at heating rate 10 K/min after quick drop in temperature to ($T_a$ - 5) - ($T_a$ -10) K for about 10 - 15 s. The latter step was done to allow for the collection of a longer baseline before the beginning of the melting peak(s) and to increase the accuracy of the melting enthalpy evaluation.

Figure 5.13 shows the melting scans of samples annealed for various lengths of time at $T_a$ = 325°C (scans B-G) and $T_a$ = 334°C (scans H-N). At $T_a$ = 325°C the annealing results in the development of a low temperature melting peak, which appears as a shoulder at the beginning of the main high temperature broad melting peak. The low temperature endotherm progressively increases in magnitude and shifts up in temperature with increase in log($t_a$). The high temperature peak remains unchanged and is practically identical with the remaining unmelted part of the melting scan of initially amorphous PEEK heated up from the glassy state - scan A. The results of the annealing at 325°C are qualitatively similar to the annealing up of melt-crystallized PEEK, shown on figure 4.21.

Scan H shows the melting of a sample, annealed at 334°C for a very short time - heated up to 334°C and immediately cooled down, denoted as $t_a$ = 0.1 min on the plot. This scan is practically identical with the remaining unmelted part of the scan of an initially amorphous PEEK. The tail parts of scans A and H, superposed on the lower part of figure 5.13, coincide. For short annealing times at 334°C, the low temperature peak first appears as a small narrow low temperature shoulder of the main melting peak. With increase in $t_a$, the low temperature peak increases sharply in magnitude and shifts up in temperature, while the

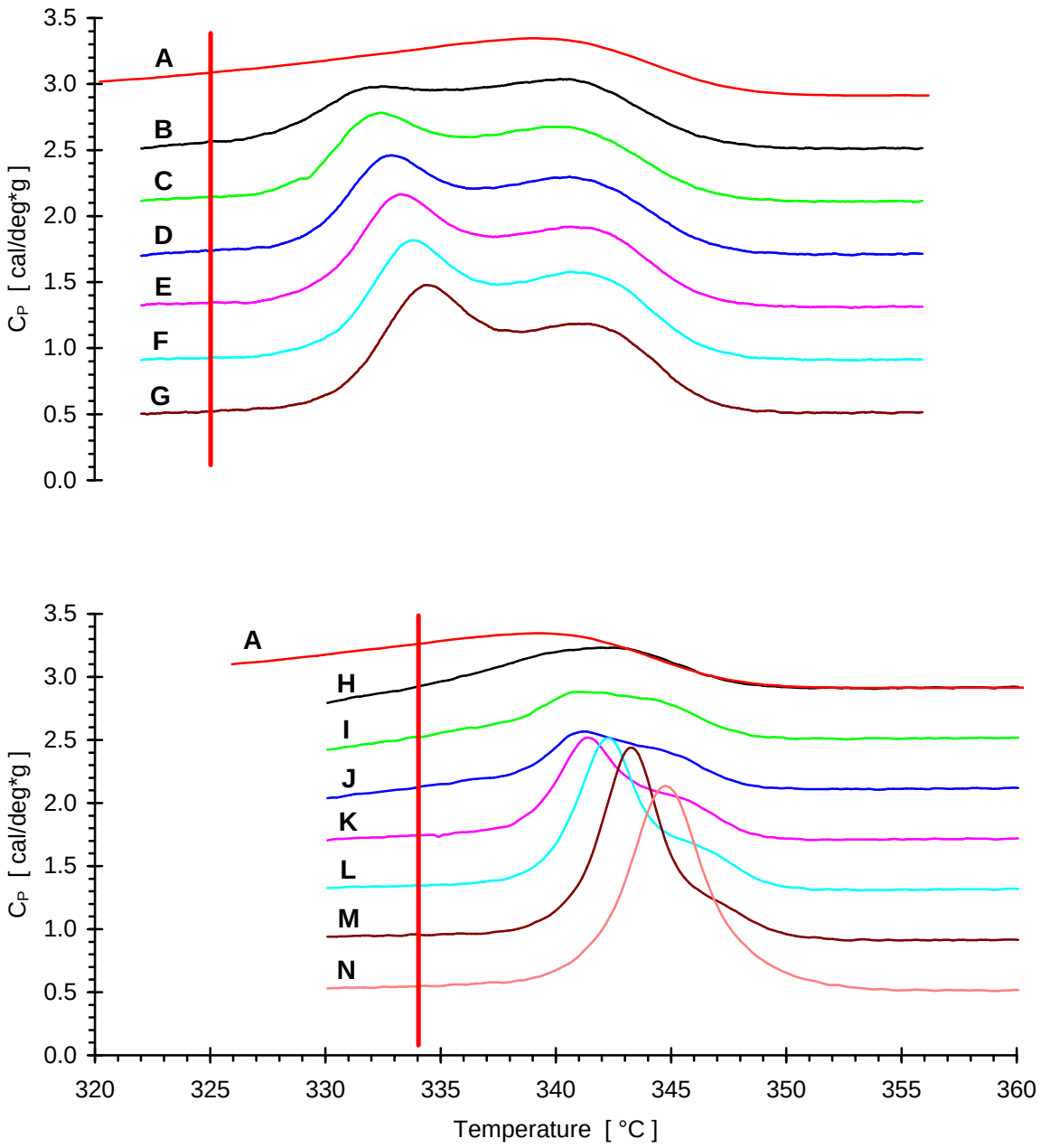


**Figure 5.13** DSC melting scans of PEEK samples, annealed up in the melting range after cold-crystallization during heating up from the amorphous glassy state. Scan **A** - heating scan of an initially amorphous sample; scans **B - G** - annealing at $T_a$ = 325°C for 2 min, 8 min, 16 min, 33 min, 60 min, and 120 min; scans **H - N** - annealing at $T_a$ = 334°C for 0.1 min, 1 min, 2 min, 8 min, 30 min, 123 min, and 483 min. Heating rate is 10K/min. Vertical lines mark the two annealing temperatures.

high temperature peak shifts slightly up, but shows very little increase in area. At 334°C for the times used in figure 5.13, the induction time for crystallization is high and very little primary crystallization from the free melt occurs due to the decrease of nucleation density with increase in temperature (extrapolation of the results shown on figures 4.15 and 4.19). However, in the presence of unmelted primary lamellar morphology, primary crystallization could still occur at a slow rate within the melted parts of the superstructure (consider the self-seeding technique of crystallization at high temperatures, widely used in microscopy and described in reference 160).

For long annealing times the two peaks overlap. Their separation (for the evaluation of the enthalpy of the low temperature peak's contribution) is done according to the method described at the end of section 4.2.1, under the assumption, that the trend in the development of the high temperature peak with $\log(t_a)$ is continuous at all times.

The scans after annealing at $T_a$ = 340°C are shown on figure 5.14. At 340°C a significant part of the polymer is melted (note, that there is a difference of about 1-2 K between the isothermal annealing temperature in the DSC and the recorded temperature in the DSC scan at 10 K/min due to thermal lag). Yet due to the presence of still unmelted primary lamellae, even short annealing times as low as 1 min cause the appearance of a low temperature melting peak. In the visual absence of a large high temperature broad melting peak in the scans the peak is denoted as "low temperature melting" for consistency with the results of the other crystallization and/or annealing experiments on PEEK.

It is clear, that the increase in magnitude and shift up in temperature with annealing time at $T_a$ = 340°C is similar to the observations at lower annealing temperatures, where the high temperature melting peak's contribution to the melting enthalpy is larger. Therefore, the melting peak on figure 5.14, which evolves with annealing time, must represent the melting of secondary lamellae, formed at 340°C under the constraining effect of the small fraction of primary lamellae, which had not melted. The slight asymmetry of the peak at shorter crystallization times, which becomes stronger for the sample with $t_a$ = 3834 min (G), is an indication of the presence and evolution of a "high temperature" melting peak in the scans. It reflects the melting of the primary lamellae, unmelted at 340°C, as well as the very slow primary crystallization at 340°C.

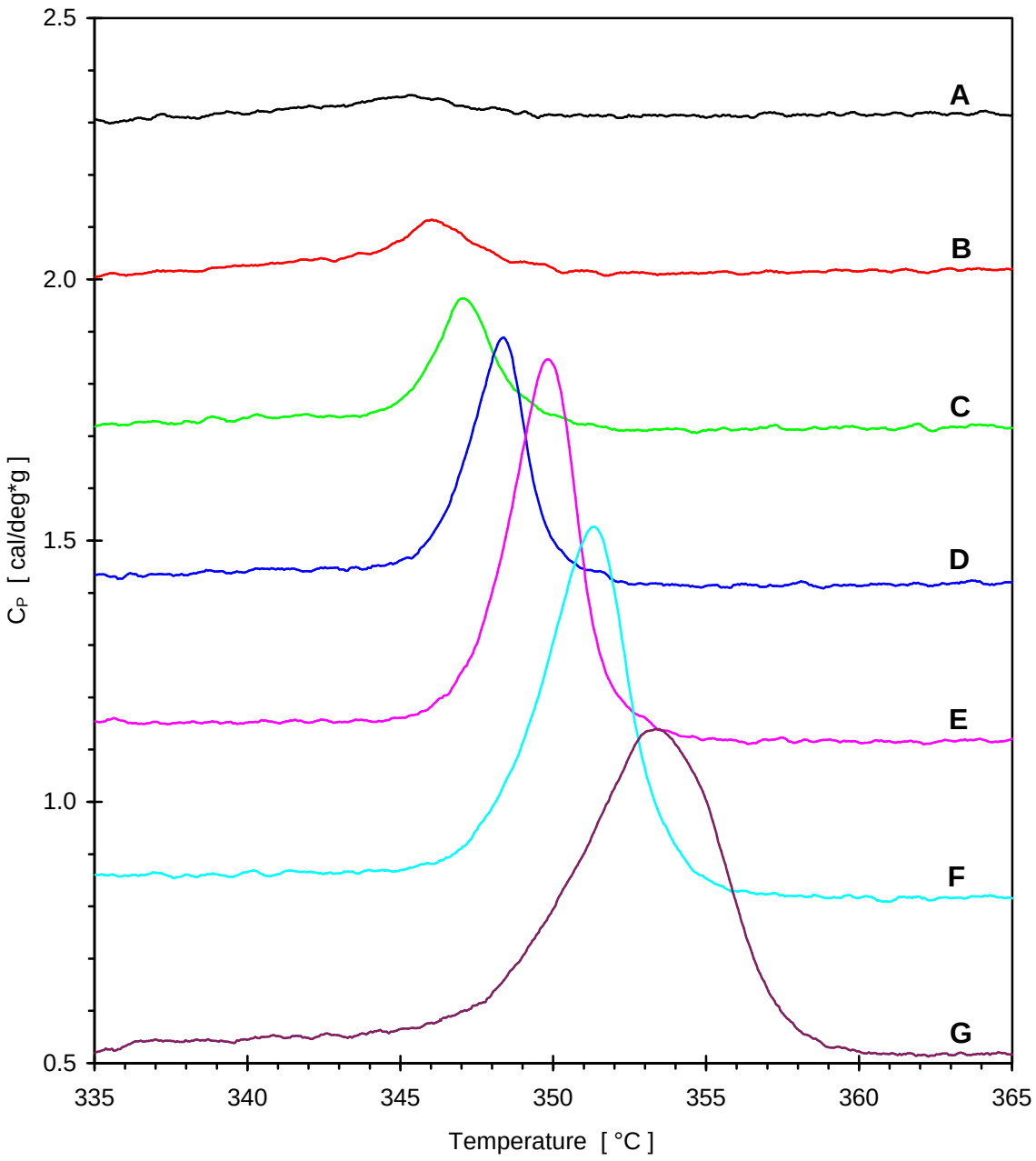


**Figure 5.14** DSC melting scans of PEEK samples, with the same thermal history as the ones in figure 5.13, but annealed at the end of the melting range at $T_a$ = 340°C for the following annealing times: A) 1 min, B) 4 min, C) 16 min, D) 60 min, E) 240 min, F) 965 min, G) 3834 min. Heating rate is 10 K/min.

Figure 5.15 is a replotting of the melting scans of the samples annealed at 334°C (from figure 5.13) without the displacement along the vertical axis. It illustrates the presence and evolution of the two different components of the melting scan - the low temperature sharp symmetric peak, which evolves linearly with logarithm of annealing time, and the broad high temperature peak - the fraction of the original primary lamellae, which remains unmelted at $T_a$ and slowly reorganizes upon annealing.

With increase in the annealing temperature, the fraction of lamellae, which melt completely at $T_a$ increases. Irrespective of the annealing temperature or time and the presence or absence of unmelted primary lamellae at $T_a$, upon cooling down the amorphous material will crystallize. Upon fast cooling small primary lamellae will fill the remaining volume of the sample, unoccupied by the primary lamellae, which did not melt at $T_a$, and the secondary lamellae, which develop in their presence at $T_a$.

On figure 5.16 the melting scans of the samples annealed at $T_a$ = 340°C and scanned without further crystallization or annealing (those, taken from figure 5.14), are superposed with the scans of samples, which were annealed for the same times and at the same annealing temperature, but *quenched and scanned from below $T_g$*. The samples, which were scanned without quenching show the evolution with increase in $\log(t_a)$ of the sharp low temperature melting peak. A small broad high temperature peak component cab be resolved only from the asymmetry of the sharp annealing peak, as observed in figure 5.14, and from the trend observed in figures 5.13 - 5.15 as the annealing temperature increases.

The original goal of the experiment was after annealing at 340°C to quench down and freeze the samples' crystallinities (by DSC) as shown on figure 5.14 (see also figure 5.17 later). The melting enthalpy of the samples on figure 5.14 is dominated by the contribution of the sharp symmetric peak which is the same as the low temperature melting peak, studied at lower $T_a$'s in chapter 4. Therefore, successful quenching of the morphology, which develops upon annealing at 340°C, would have allowed to evaluate crystallinity and morphology dominated by the contribution of secondary lamellae and to monitor their evolution with time. Although the samples scanned from below $T_g$ were quenched in liquid $N_2$, this did not prevent them from crystallizing upon cooling down.

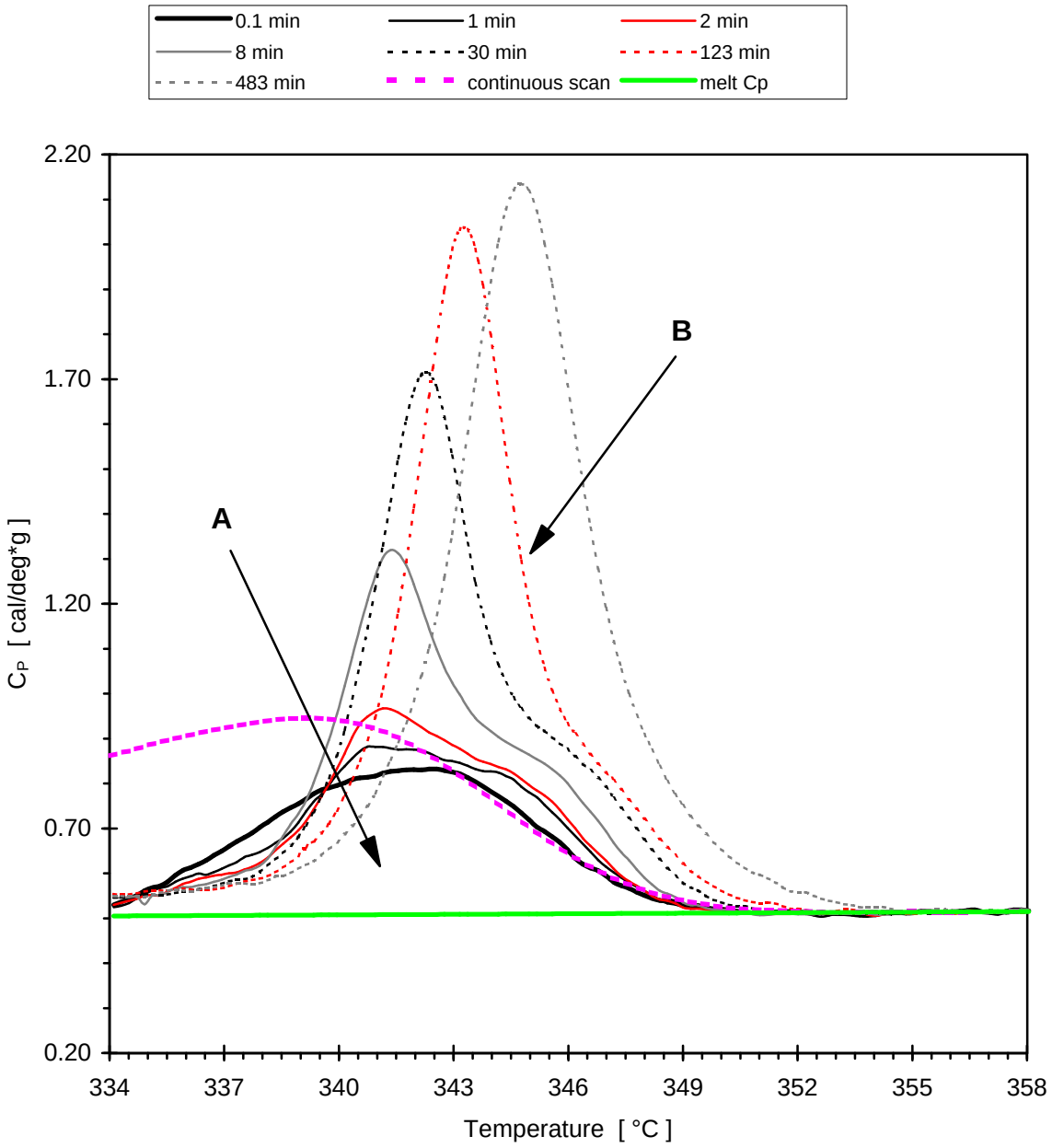


**Figure 5.15** Plot without vertical displacement of the DSC melting scans of the samples, annealed at 334°C (from figure 5.13). The remaining unmelted part (A) of the original high temperature melting peak (the scan of an initially amorphous sample) reorganizes slowly - moves up in temperature, but little in intensity. The sharp symmetric peak (B) is a low temperature shoulder of the main melting peak at short times, then increases in intensity and moves up in temperature.

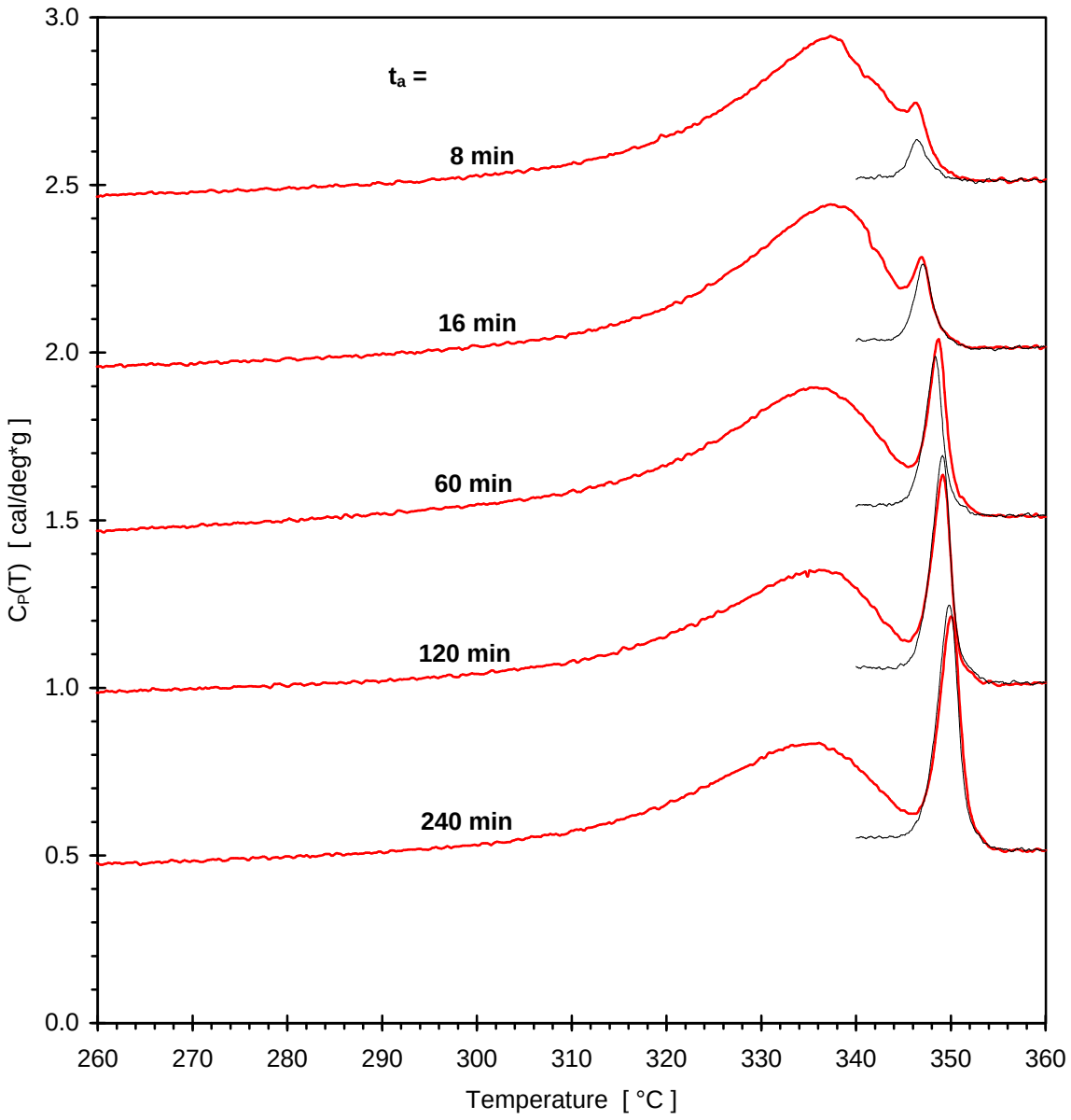


**Figure 5.16** Comparison of the melting scans of PEEK samples, annealed up from the amorphous glassy state at $T_a$ = 340°C and scanned without quenching (from figure 5.14) and after quenching below $T_g$. The peak which results from annealing (i.e. the "low temperature" melting peak) is the same in position, shape and magnitude for both types of post-annealing thermal history. The fast quenching (in liquid $N_2$) does not prevent the samples from crystallizing upon cooling. Their scans show the main (i.e. "high temperature") melting peak, typical for PEEK, crystallized at high undercooling. Heating rate is 10 K/min.

The broad melting peak between 290°C and 350°C in the melting scans of the samples scanned from below $T_g$ is typical for the melting of primary lamellae, formed upon fast crystallization during cooling down from the melt. [70, 72] In addition, a sharp symmetric peak appears at the high temperature end of the broad one. This peak reproduces with remarkable precision the position and magnitude of the melting scan of PEEK, annealed for the same time, but scanned without quenching. Therefore, the thermal stability of the secondary lamellae, formed upon annealing in the melting range of PEEK at 340°C, appears unaffected by the subsequent primary crystallization upon cooling down. Thus, although it is impossible to quench the secondary lamellae alone, by variation of the annealing time at 340°C and subsequent controlled crystallization upon cooling one could obtain samples with various fractions of secondary lamellae. From scans shown on figure 5.16 one can estimate, that an increase in $\log(t_a)$ by only 1.5 decades between 8 min and 240 min results in increase in secondary crystallinity by DSC from 0.01 to 0.07 i.e. from about 3% of the total crystallinity to about 20%. Given the relatively short annealing times on the order of only few hours, this could allow even direct observation of secondary crystallization in real time experiments such as high temperature hot stage electron microscopy or WAXS and/or SAXS studies with synchrotron radiation sources.

With the advances in the last decade in the fields of electron microscopy and especially in real time WAXS/SAXS studies with synchrotron radiation, the most demanding part of such an experiment appears to be the selection of the thermal history profile of the sample: choice and maintenance of the annealing temperature, which would optimize the above experiment. The next two figures provide quantitative data, which could help the choice of thermal history for the experiment.

Figure 5.17-A shows the linear increase in $T_{max}(low)$ with increase in $\log(t_a)$ for several annealing temperatures in the melting range of PEEK. Figure 5.17-B shows the evolution with increase in $\log(t_a)$ of the melting enthalpy of the low temperature (annealing) peak, expressed as DSC crystallinity. Figure 5.18 shows the annealing temperature dependence of the parameters of the linear fit of data shown in figure 5.17:

$$\Delta H_m(low) = a + b*\log(t_a) \qquad (5.10)$$

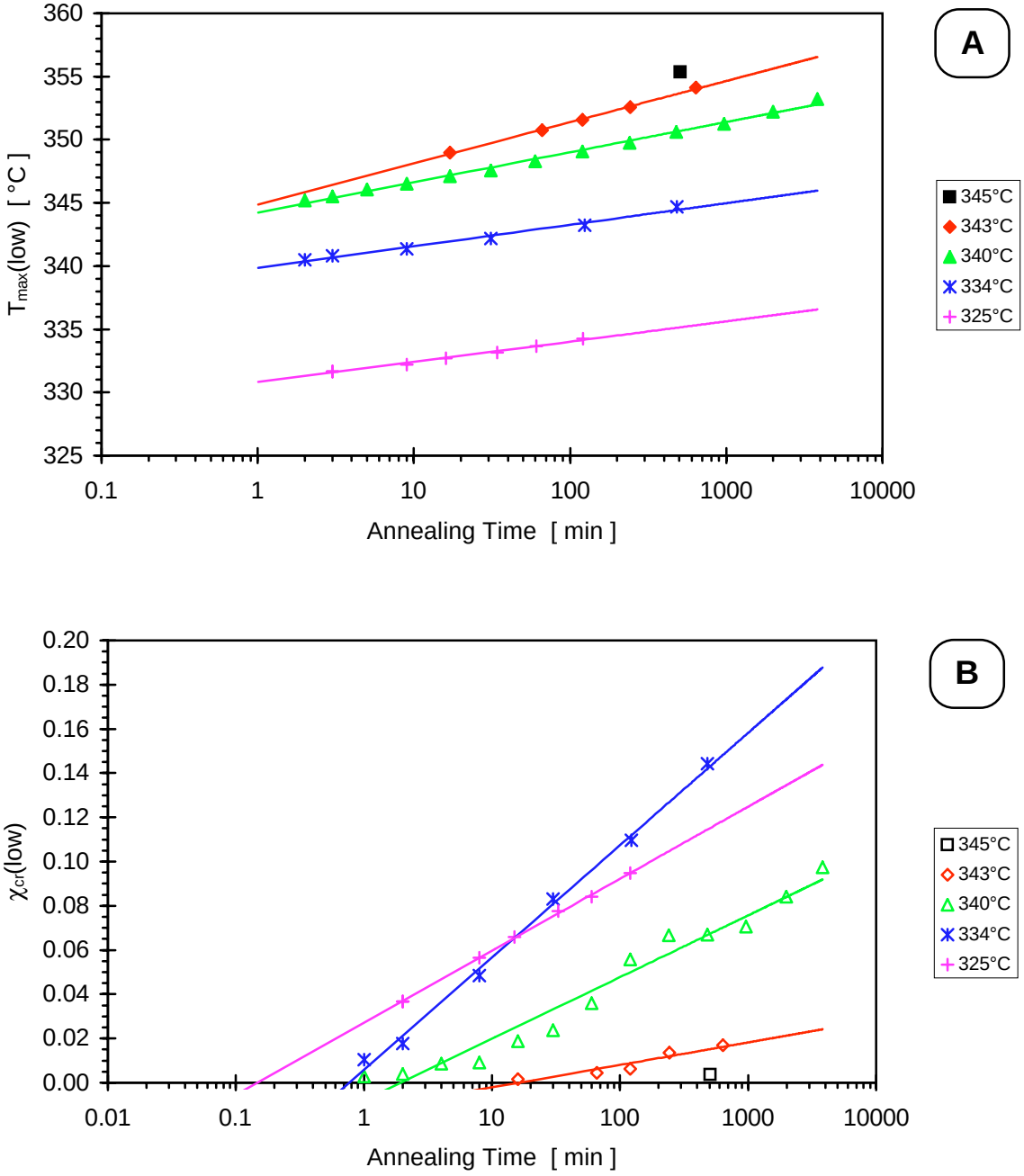


**Figure 5.17** Dependence of: A) $T_{max}$(low) and B) $\chi_{cr}$(low) on annealing time for PEEK samples, heated fast from the amorphous glassy state and annealed at several temperatures in the melting range of a cold-crystallized PEEK (see figures 5.13-5.15).

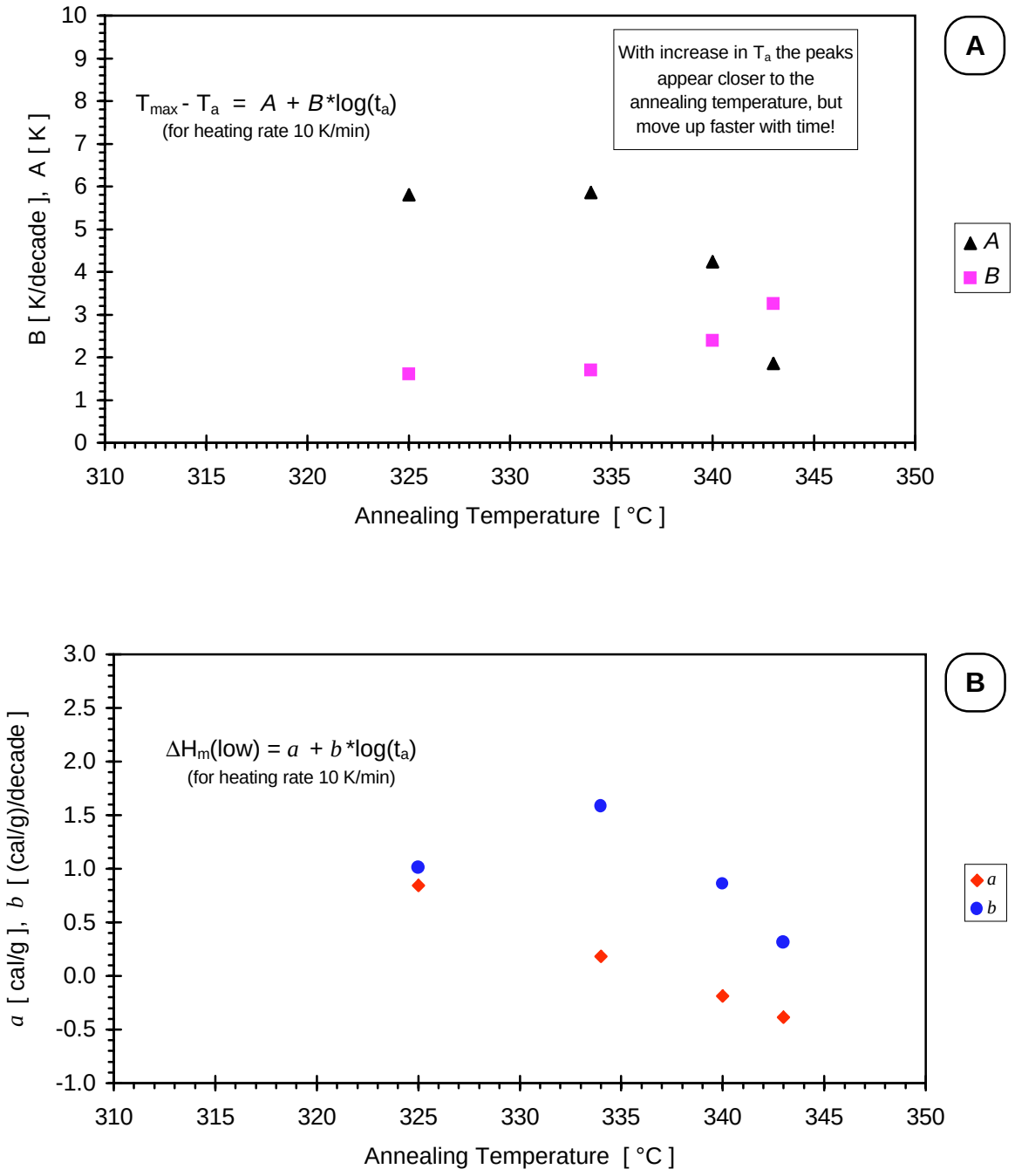


**Figure 5.18** Parameters of the linear dependence on $\log(t_a)$ for: A) $T_{max}$(low) and B) $\Delta H_m$(low). Calculated from linear fitting of the data on figure 5.17.

$$T_{max}(low) = T_a + A + B*\log(t_a) \quad (5.11)$$

where $A = A(T_a)$, $B = B(T_a)$, $a = a(T_a)$, and $b = b(T_a)$.

At any of the annealing temperatures, the nature of the peak, which results from annealing, does not change - its shape, position, and evolution with time and temperature are the same as the low temperature melting peak resulting from the thermal histories employed in the experiments of chapter 4. For short annealing times at higher annealing temperatures the peak appears closer to $T_a$ ($A$ decreases with an increase in $T_a$).

The only dramatic difference is in the magnitude of the melting enthalpy of the low temperature peak and its rate of increase. Annealing of semicrystalline PEEK at these high temperatures leads to the largest observed melting enthalpies of the low temperature endothermic peak (compare figure 5.16-B with figures 4.33, 4.35, and 4.37). This observation initially follows the general trend of increase in $\Delta H_m(low)$ with increase in $T_a$ observed under other types of thermal histories (figures 4.14, 4.16, and 4.29). At the highest annealing temperatures, however, the trend is reversed. Between 334°C and 345°C the overall magnitude (figure 5.17-B) and rate of increase (figure 5.18-B) of $\Delta H_m(low)$ continuously decrease. Based on the current knowledge of the evolution of the low temperature melting peak, the following explanation of the rates and magnitudes observed in figure 5.17-B and 5.18-B appears most plausible:

Increasing $T_a$ leads to an increase in the log-time rate of secondary crystallization in the constrained environment of primary lamellae which do not melt (see also figure 4.29). At low annealing temperatures in the melting range of PEEK only a small fraction of the primary lamellae melts and the macroscopic superstructure is largely left unchanged. Upon annealing this fraction might recrystallize into larger and/or more perfect primary lamellae if the existing superstructure and/or the rate of primary crystallization allow this to occur within the annealing times employed. If these amorphous gaps in the largely unchanged superstructure, which are created by the melting of the primary lamellae at $T_a$, are not favorable for the creation of thicker lamellae, the amorphous material in them will contribute to secondary crystallization at $T_a$. As long as the fraction of primary lamellae, which melt at $T_a$, is relatively small and uniformly dispersed, their melting leads to an increase of the constrained

amorphous fraction at $T_a$, which is the starting material for secondary crystallization. The increase in the coarseness of the superstructure by partial (local) melting leads to larger $\Delta H_m$(low) values. As long as no large volumes of completely melted primary lamellae are created, annealing at $T_a$ most likely leads to secondary crystallization.

With a further increase in $T_a$ more primary lamellae melt and large volumes of completely melted amorphous material would appear in the superstructure. At the same time at higher $T_a$ the primary crystallization rate is lower and primary crystallinity will develop only after very long annealing. In the absence of primary crystalline lamellae, no secondary crystallization would occur in the large homogeneous regions of amorphous melt either. Secondary crystallinity develops only in the constrained amorphous regions of the superstructure between primary lamellae (or stacks of lamellae), which have not melted. With increase in $T_a$ the relative fraction of these constrained amorphous regions decreases due to the progressive increase in the fraction of melted primary lamellae. This explains the absolute decrease in the magnitude of the melting enthalpy of the low temperature melting peak between $T_a$ = 334°C and $T_a$ = 345°C observed in figure 5.17-B as well as the decrease in its rate of change - the parameter *b* in equation (5.10), shown in figure 5.18-B.

As long as there are clusters of primary lamellae, unmelted at $T_a$, secondary crystallization proceeds in the constrained gaps between the lamellae (or the stacks of lamellae). Even at $T_a$ = 345°C, long annealing of the amorphous material between the few primary lamellae left produces secondary lamellae, the melting of which can be detected.

One might propose, that fractional crystallization occurs at the high annealing temperatures employed in the experiments described above. This would attribute the observed melting behavior to the melting of narrow fractions with different thermal stability, which separate during annealing. Studies of the PEEK fractions (described in sections 3.1.1, 3.2.1 and 4.1) were not done on the scale of the experiments presented in this section due to the limited amount of material available. Preliminary studies of fraction PEEK4-5 ($M_w$ = 18,200 g/mol, *PDR* = 1.2) show, that under similar experimental conditions (annealing at high $T_a$ in the melting range) its melting behavior is the same as that of the commercial PEEK, described in this section. Thus until more extensive studies of the multiple melting

behavior of the fractionated material, the idea of fractional crystallization at high annealing temperatures can not serve as an explanation for the melting behavior characterized in this section.

In conclusion, the results presented in this section provide clear evidence, that optimum experimental conditions for the studies of secondary crystallization and the melting of secondary lamellae are realized upon annealing of initially semicrystalline PEEK in the melting range of the distribution of primary lamellae. In real time studies of secondary crystallization in this temperature range and subsequent melting, more than 50% of the crystallinity of the sample (by DSC) might form during the secondary (annealing) stage and should be easily detectable by scattering techniques or hot stage microscopy. With careful selection and accurate maintenance of the quite demanding setup for such experiments morphological evidence in support of one or another model for the secondary crystallization stage and the multiple melting phenomenon should be readily obtainable. The results would be far more convincing than any other evidence presented earlier. Previous studies had usually relied on data from experiments in which crystallinity change due to secondary crystallization (the low temperature melting peak contribution) is a small fraction of the overall crystallinity. [63, 64, 66-68, 70, 71, 74, 82, 85, 155]

In relation to the hypothesis about the universal nature of the secondary crystallization process in various semicrystalline polymers, it must be pointed out that annealing in the melting range of an initially semicrystalline sample leads to similar observations in other polymers as well: i-PP, [161] i-PS, [49] and Nylon 10,10. [56] In the field of microscopy, the experiments investigated above are well known as the crystallization and melting of a "self-seeded" polymer. [160]

### *5.6.3 "Enthalpy Recovery" Below and Above $T_g$* [217]

This section presents the results of an investigation by differential scanning calorimetry (DSC) of two mobility controlled processes in the amorphous phase of semicrystalline PEEK - enthalpy relaxation below the glass transition ($T_g$) and secondary crystallization above $T_g$. Both result in the observation of an endothermic peak just above the

annealing temperature in the DSC scan of the polymer - the enthalpy recovery peak and the low temperature melting peak, respectively. An earlier study of melt-crystallized PEEK [78] pointed out the striking similarity in the time and temperature dependence of the endothermic peak for these two processes. In studies of annealing effects below and above $T_g$ Illers [51] claimed, that in the case of crystalline PVC the enthalpy recovery peak below $T_g$ is an order of magnitude smaller than the melting peak above $T_g$, which is similar in nature to the low temperature melting peak of PEEK and other semicrystalline polymers. Hutchinson and Kriesten [46] compared the enthalpy relaxation rate in atactic PS below $T_g$ - 0.9 (J/g)/decade at 85°C, with the rate of increase of $\Delta H_m$(low) with increase in log($t_a$) for semicrystalline i-PP at room temperature - 0.9 (J/g)/decade for a sample with crystallinity 0.60. They concluded, that the rate of enthalpy loss on aging of the constrained RAF of i-PP is much higher than a typical enthalpy relaxation rate. Wunderlich [159] has made a similar comment with respect to earlier ideas from our group that the low temperature endothermic peak in the heating scan of isothermally melt-crystallized PEEK is recovery of the enthalpy, lost upon enthalpy relaxation of the rigid amorphous fraction of PEEK above the nominal $T_g$. [78-80]

All the above arguments are based on the "dual" or "extended" glass transition concept (see the discussion in sections 2.5.4 and 5.4 and references therein). If the low temperature melting peak, observed upon annealing between the nominal $T_g$ and $T_m'$, is the enthalpy recovery peak of the RAF below its respective glass transition, then it is assumed that its kinetics must be similar to the enthalpy recovery of an amorphous glassy polymer below $T_g$.

This section examines the effect of annealing in the immediate vicinity of the calorimetric $T_g$ of initially semicrystalline PEEK. This subject is of particular interest given the peculiar results from the small strain creep studies of "physical aging" of semicrystalline PEEK below and above $T_g$ (reference 81 and sections 4.2.4, 5.4, and 5.5). Literature reports on the enthalpy relaxation of semicrystalline PEEK are somewhat limited [96, 102] and do not allow direct comparison with the studies of multiple melting of PEEK above $T_g$. A report on the aging of semicrystalline PEEK below $T_g$ has even made an inaccurate statement that no enthalpy recovery peak is observed. [97] Furthermore, no other studies in the literature have

examined directly the similarity between the enthalpy recovery peak at or below $T_g$ and the low temperature endothermic (annealing) peak above $T_g$ except the studies on PVC by Illers[51] and Bair and Warren. [53] More recent references on studies of enthalpy recovery in other semicrystalline polymers include: PET, [162-165, 170, 201] PEN. [162] On the general subject of "physical aging" (including enthalpy relaxation) of amorphous and semicrystalline polymers several review papers have appeared recently. [166, 169, 197, 200, 201]

Initially amorphous PEEK samples were annealed under nitrogen for 35 min at 300°C in a BlueM mechanical convection oven, model MO1420SA. This initial treatment, common for all samples, produces a semicrystalline material with crystallinity by DSC of 37%. The samples were subsequently annealed in the oven for various times in a wide temperature range, encompassing the glass transition: 100°C, 120°C, 130°C, 140°C, 150°C, 160°C, 180°C, 200°C, and then quenched to room temperature.

DSC scans of these samples were collected from 75°C to the end of melting at a heating rate of 20 K/min. The heat flow output was corrected by baseline subtraction and calibrated with a sapphire standard. The enthalpy recovery peaks and the low temperature melting peaks were resolved from the total heat flow by subtraction of the DSC scan of a sample, subjected only to the initial crystallization at 300°C, common for all annealed samples.

$T_{max}$ and $\Delta H_a$ denote respectively the temperature of the peak maximum and the transition enthalpy of both types of endothermic peaks observed - the enthalpy recovery peak below $T_g$ and the low temperature melting peak above $T_g$ ($T_g$ = 155°C by DSC at a heating rate of 20 K/min). Distinction between the two different peaks can be made by observing the labels for the annealing temperature $T_a$.

Figure 5.19 shows the DSC scans of samples, annealed at 100°C - approximately 50 K below $T_g$. The enthalpy recovery peak appears as a sub-$T_g$ small and broad peak even for the longest annealing times employed. Although the initial state of the samples at $T_a$ = 100°C is far removed from equilibrium, the decrease in the excess enthalpy, measured by $\Delta H_a$, is very small due to the very long relaxation times, expected at this temperature.

At $T_a$ = 120°C - figure 5.20, the peak begins as a small and broad sub-$T_g$ enthalpy recovery peak, then increases substantially in magnitude and shifts up in temperature into the glass transition region. With further increase in annealing temperature - at $T_a$ = 130°C (figure 5.21) the enthalpy recovery peak is superposed to the glass transition. Its magnitude continues to increase with increase in $T_a$ and log($t_a$). This trend is not reversed even for annealing at 140°C (figure 5.22) - at the lower end of the glass transition range. At $T_a$ = 140°C the enthalpy recovery peaks are still very strong, well resolved and superposed on the glass transition. The larger enthalpies can be attributed to the acceleration of the aging process as relaxation times decrease with increase in $T_a$. No leveling off in the dependence of $\Delta H_a$ on log($t_a$), typical for enthalpy recovery of amorphous polymeric glasses, [96, 166, 167, 198, 200] is observed.

Figure 5.23 shows the DSC scans of the samples annealed at 160°C - at the upper end of the glass transition; figure 5.24 - the samples annealed at 180°C and figure 5.25 - those, annealed at 200°C - well above $T_g$. At these temperatures, according to the standard two phase model of semicrystalline polymers, the amorphous fraction, although somewhat constrained by the crystalline lamellae, is liquid-like and should be in equilibrium. Therefore, no enthalpy relaxation and subsequent recovery should be observed.

The scans for $T_a$ = 160°C show the appearance of an endothermic peak just above the annealing temperature - the well known low temperature melting peak in the melting scan of PEEK, annealed above $T_g$. With increase in annealing time the peak increases in magnitude and shifts up in temperature. At the higher annealing temperatures above $T_g$ - 180°C and 200°C, the peak evolution has the same characteristics, but appears stronger and more clearly resolved.

As was have discussed earlier (sections 2.4.2 and 5.5), calorimetric and morphological studies of the "double melting" of PEEK suggest that the origin of this peak is the melting of a population of crystalline lamellae with low thermal stability (lower than the stability of the primary lamellae, which melt at higher temperatures). Their development is associated with the process of secondary crystallization in PEEK, which develops upon isothermal crystallization and/or annealing above $T_g$. [70, 71, 151]

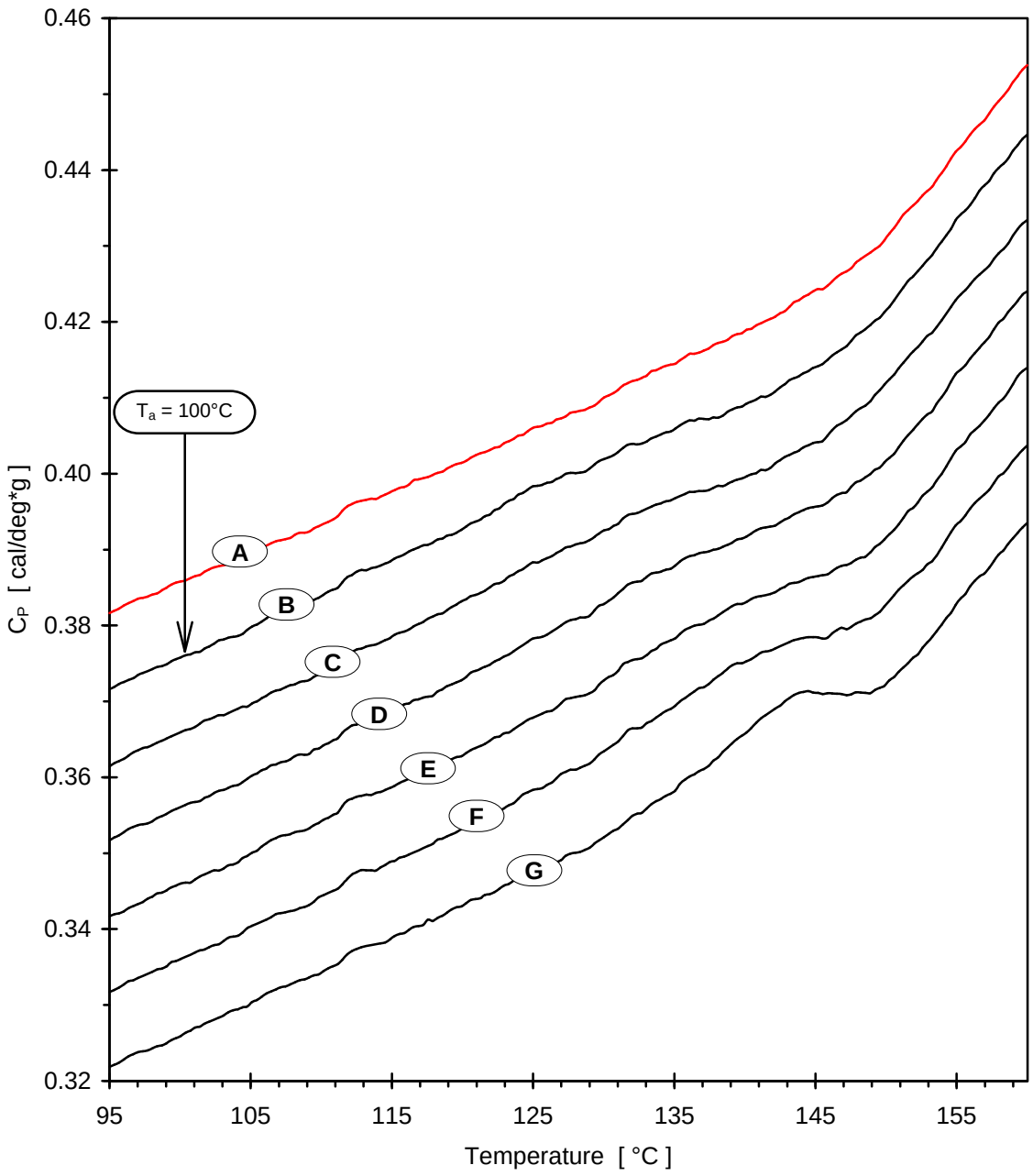


**Figure 5.19** DSC heating scans of PEEK samples, cold-crystallized at $T_c$ = 300°C for $t_c$ = 35 min and subsequently annealed at $T_a$ = 100°C for: A) 0 min, B) 14 min, C) 41 min, D) 122 min, E) 377 min, F) 1080 min, G) 3253 min.

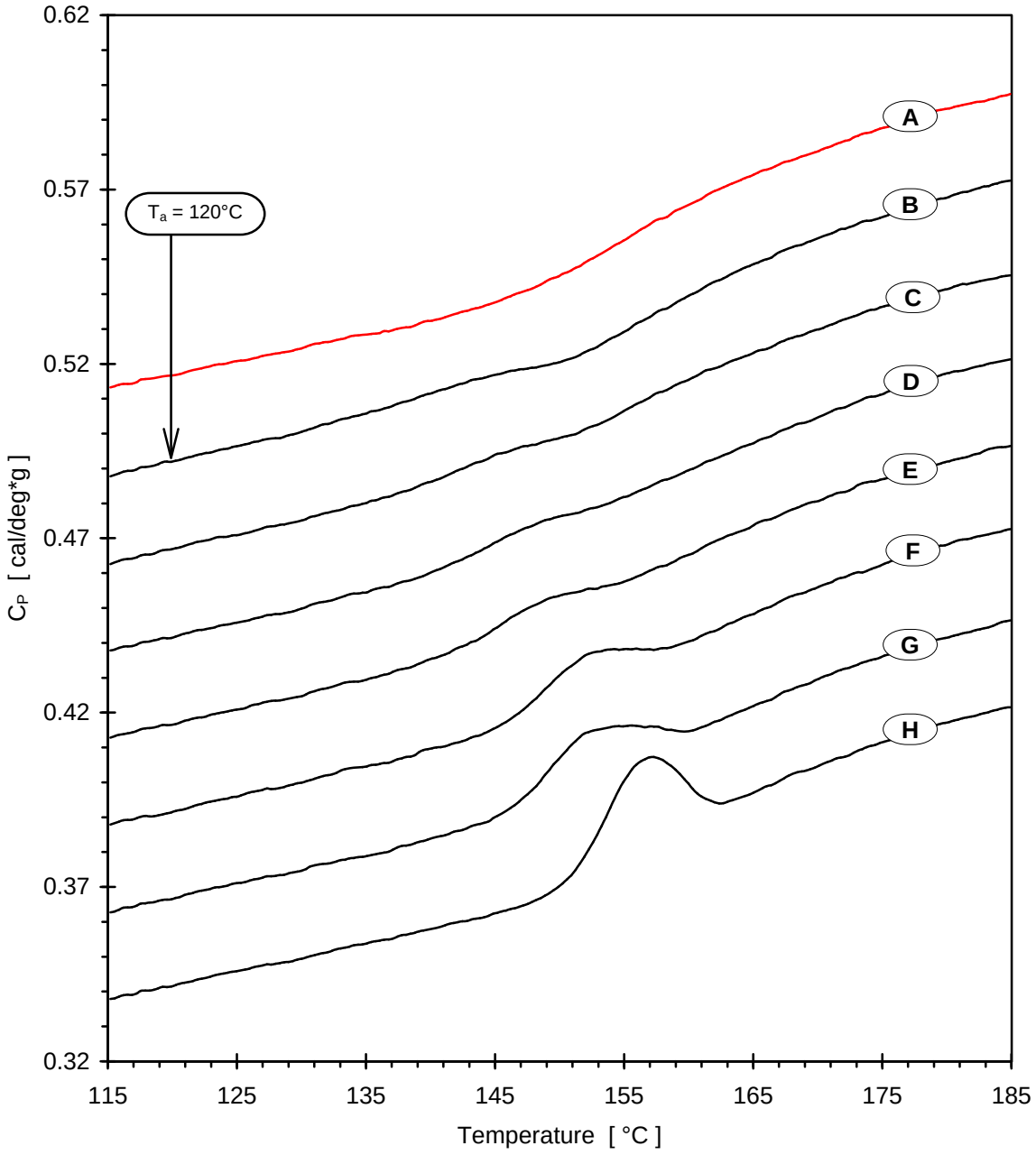


**Figure 5.20** DSC heating scans of PEEK samples, cold-crystallized at $T_c$ = 300°C for $t_c$ = 35 min and subsequently annealed at $T_a$ = 120°C for: A) 0 min, B) 14 min, C) 41 min, D) 140 min, E) 360 min, F) 1080 min, G) 3360 min, H) 9881 min.

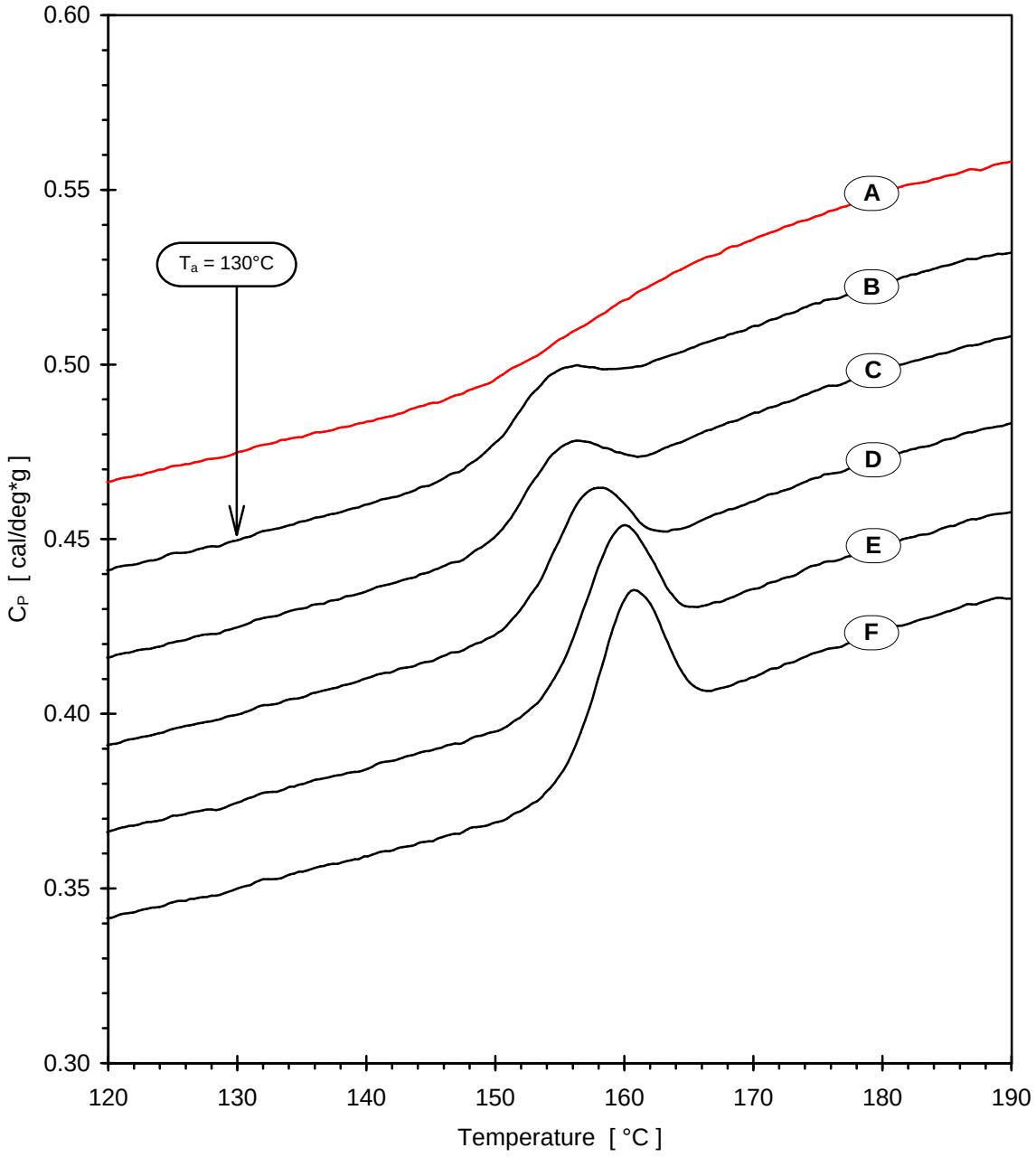


**Figure 5.21** DSC heating scans of PEEK samples, cold-crystallized at $T_c$ = 300°C for $t_c$ = 35 min and subsequently annealed at $T_a$ = 130°C for: A) 0 min, B) 120 min, C) 364 min, D) 1083 min, E) 3493 min, F) 9925 min.

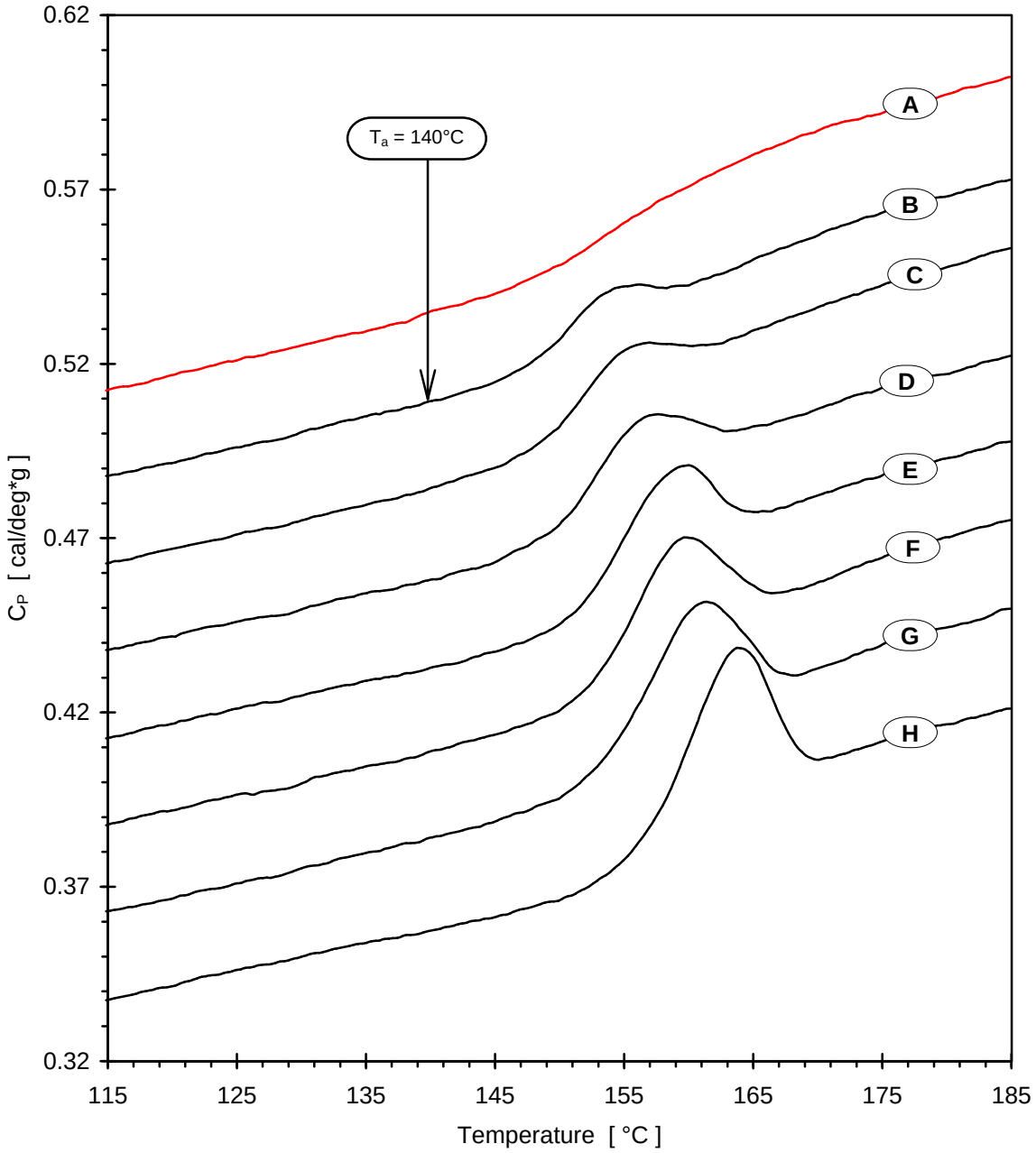


**Figure 5.22** DSC heating scans of PEEK samples, cold-crystallized at $T_c$ = 300°C for $t_c$ = 35 min and subsequently annealed at $T_a$ = 140°C for: A) 0 min, B) 14 min, C) 41 min, D) 120 min, E) 360 min, F) 1080 min, G) 3253 min, H) 9930 min.

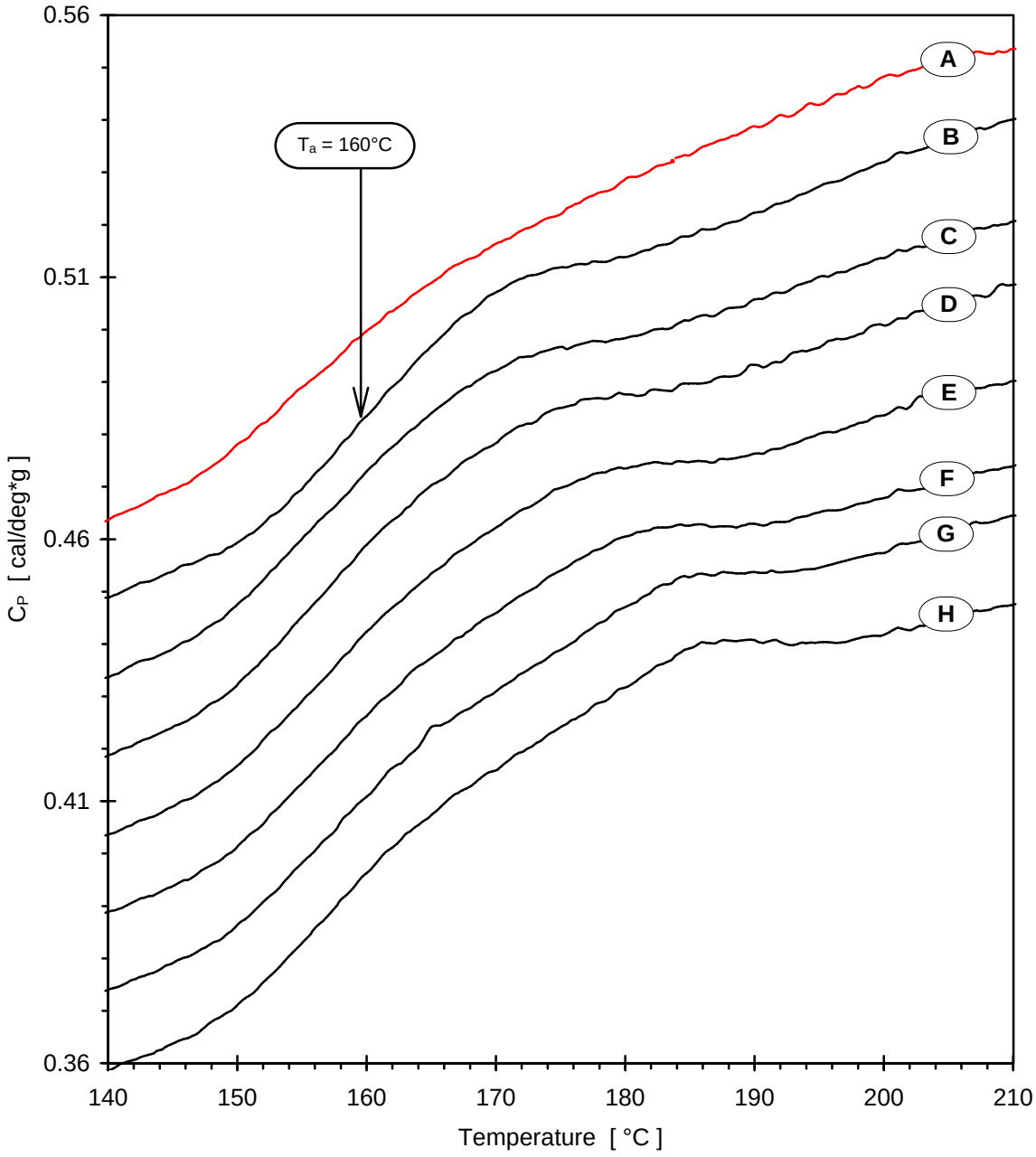


**Figure 5.23** DSC heating scans of PEEK samples, cold-crystallized at $T_c$ = 300°C for $t_c$ = 35 min and subsequently annealed at $T_a$ = 160°C for: A) 0 min, B) 14 min, C) 41 min, D) 135 min, D) 360 min, E) 1091 min, F) 3260 min, G) 6324 min.

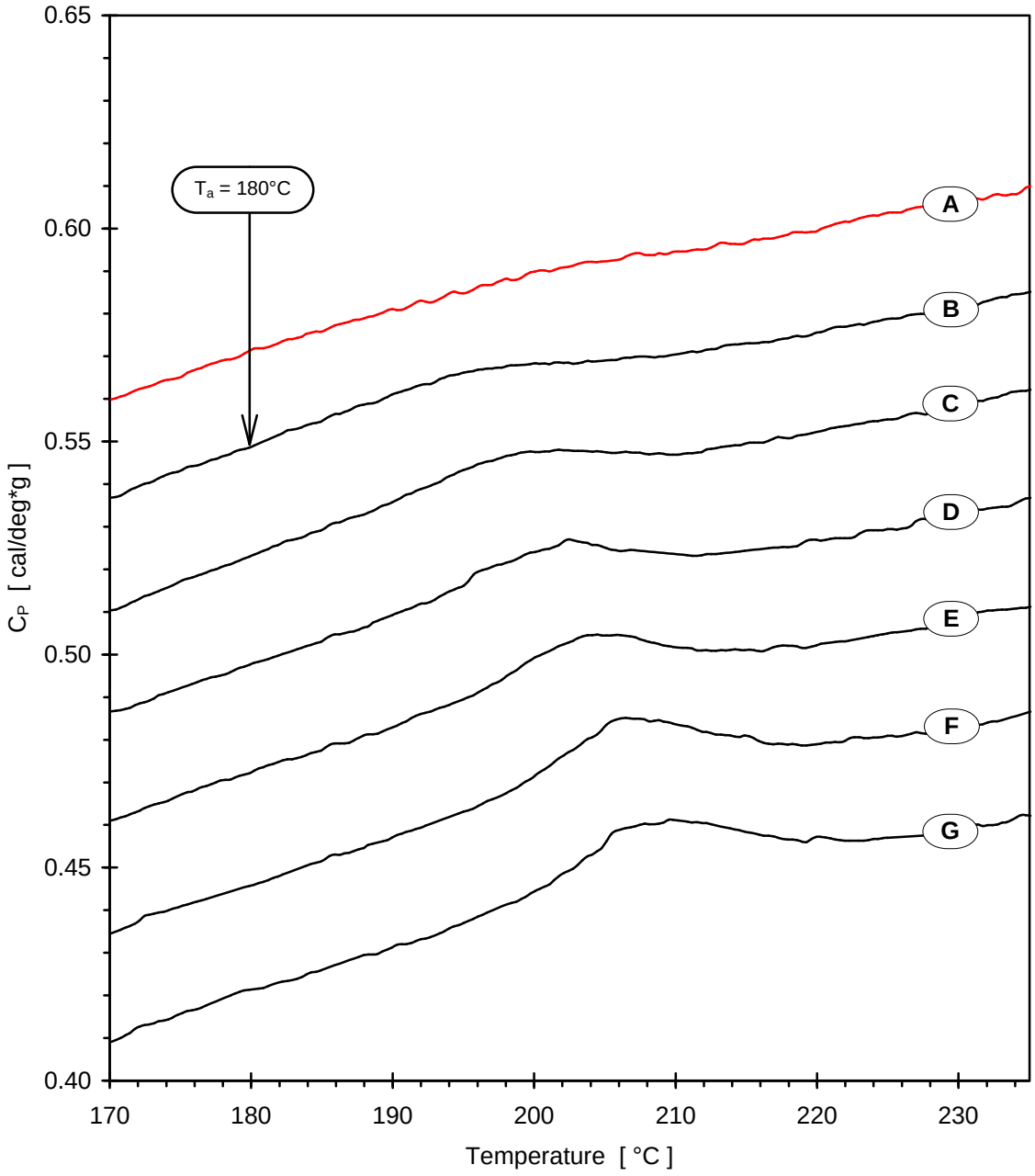


**Figure 5.24** DSC heating scans of PEEK samples, cold-crystallized at $T_c$ = 300°C for $t_c$ = 35 min and subsequently annealed at $T_a$ = 180°C for: A) 0 min, B) 14 min, C) 41 min, D) 120 min, E) 382 min, F) 1085 min, G) 3243 min.

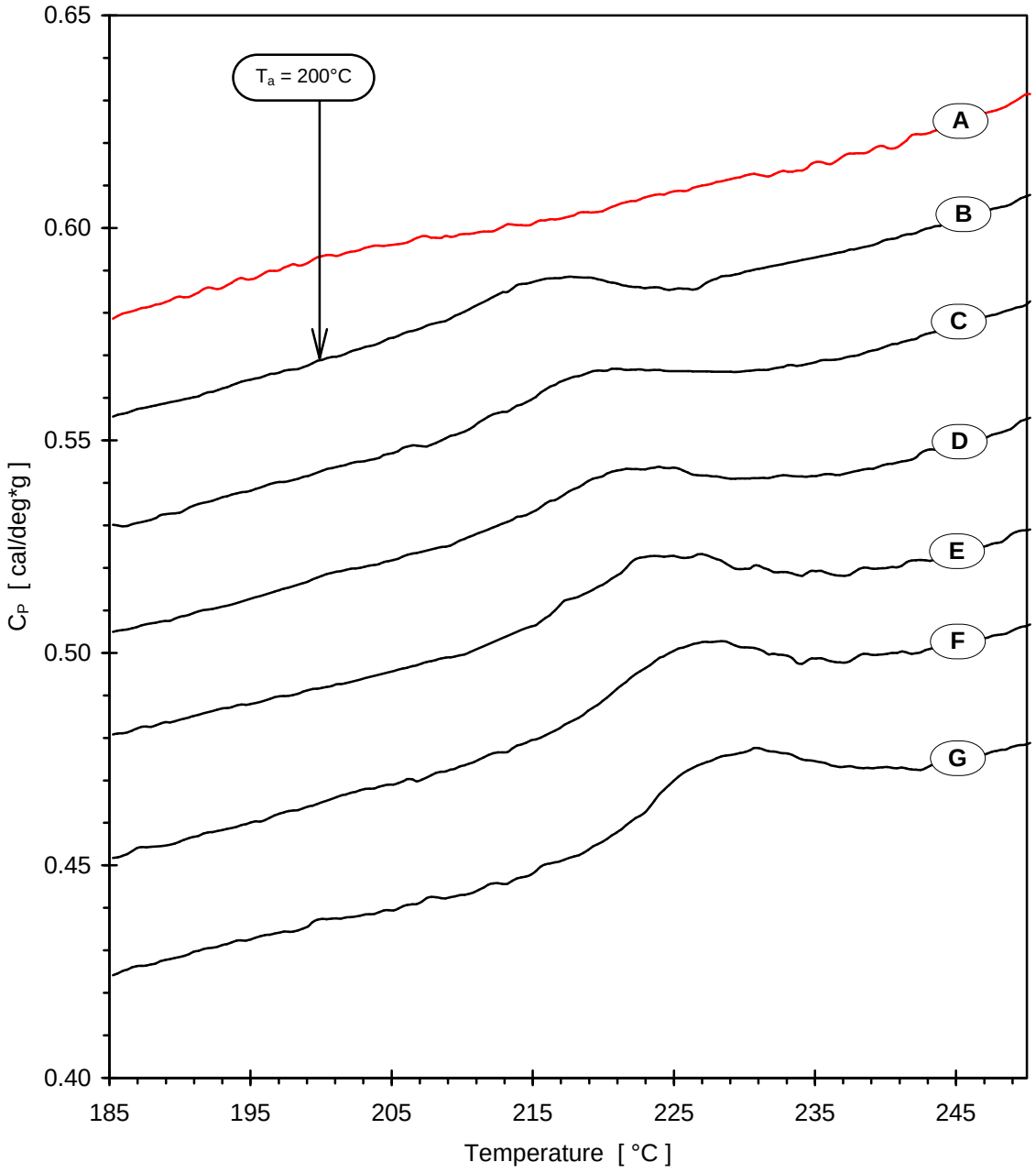


**Figure 5.25** DSC heating scans of PEEK samples, cold-crystallized at $T_c$ = 300°C for $t_c$ = 35 min and subsequently annealed at $T_a$ = 200°C for: A) 0 min, B) 14 min, C) 41 min, D) 120 min, E) 360 min, F) 1115 min, G) 3240 min.

Recent results from our group have shown [78-80] that the double melting phenomenon in melt-crystallized PEEK exhibits characteristics similar to the enthalpy recovery process in amorphous glasses below $T_g$ [166, 167]: the peak maximum temperature $T_{max}$(low) and the associated transition enthalpy $\Delta H_m$(low) increase linearly with log($t_a$), and $T_{max}$(low) and $\Delta H_m$(low) increase with increase in $T_a$. The results presented in section 4.2 show, that the same characteristic behavior describes the low temperature endothermic peak in the melting scan of PEEK under any crystallization and or annealing thermal history profile, which involves isothermal annealing above $T_g$.

With the experiment presented in this section, the scans on figures 5.19 - 5.25 are direct evidence of the similarity between the endothermic peaks which appear as a result of annealing below and above $T_g$, respectively. This opens at least two important questions about the observations displayed in figures 5.19 - 5.25:

First, are there more common characteristics for the enthalpy relaxation below $T_g$ and the secondary crystallization above $T_g$, other than the apparent similarity in the endothermic peaks they result in upon subsequent heating? Second, what is the origin of the similarity between the enthalpy recovery and the low temperature melting peaks?

One answer to the first question comes straight from examining the annealing time dependence of $\Delta H_a$ and $T_{max}$. The plot of $\Delta H_a$ vs. log($t_a$) for the enthalpy recovery peaks ($T_a < T_g$) is shown on figure 5.26-B and for the low temperature melting peaks ($T_a > T_g$) - on figure 5.26-A. On both plots an approximately linear increase in $\Delta H_a$ with log($t_a$) is observed at any given $T_a$. For a fixed log($t_a$) value, $\Delta H_a$ increases with increase in $T_a$ for the low temperature melting peak (figure 5.26-A), as well as for the enthalpy recovery peak (figure 5.26-B). Note that the latter is somewhat unexpected. For annealing temperatures very close to $T_g$ (as is the case with $T_a$ = 140°C and the single point for $T_a$ = 150°C), $\Delta H_a$ must decrease with increase in $T_a$ [102, 166, 167] due to the decrease in the excess frozen enthalpy, which is the limiting value of $\Delta H_a$.

Figure 5.27 shows the evolution of $T_{max}$ with annealing time. Within the time range studied, $T_{max}$ increases linearly with log($t_a$) for all annealing temperatures. The change in the trend in the middle of the plot indicates the glass transition region, which separates the

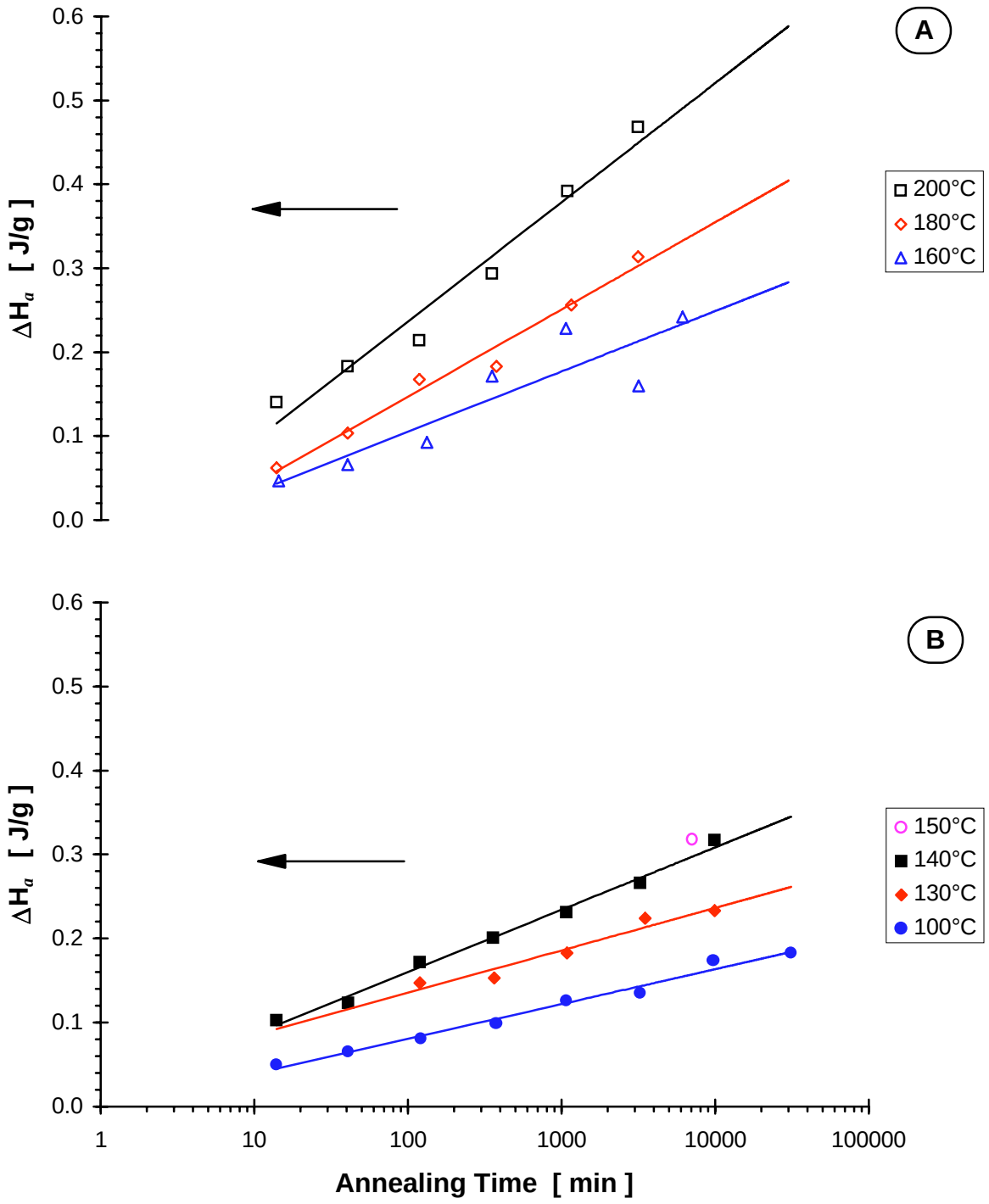


**Figure 5.26** Development of the transition enthalpy $\Delta H_a$ with annealing time: A) low temperature melting peak data, B) enthalpy recovery peak data.

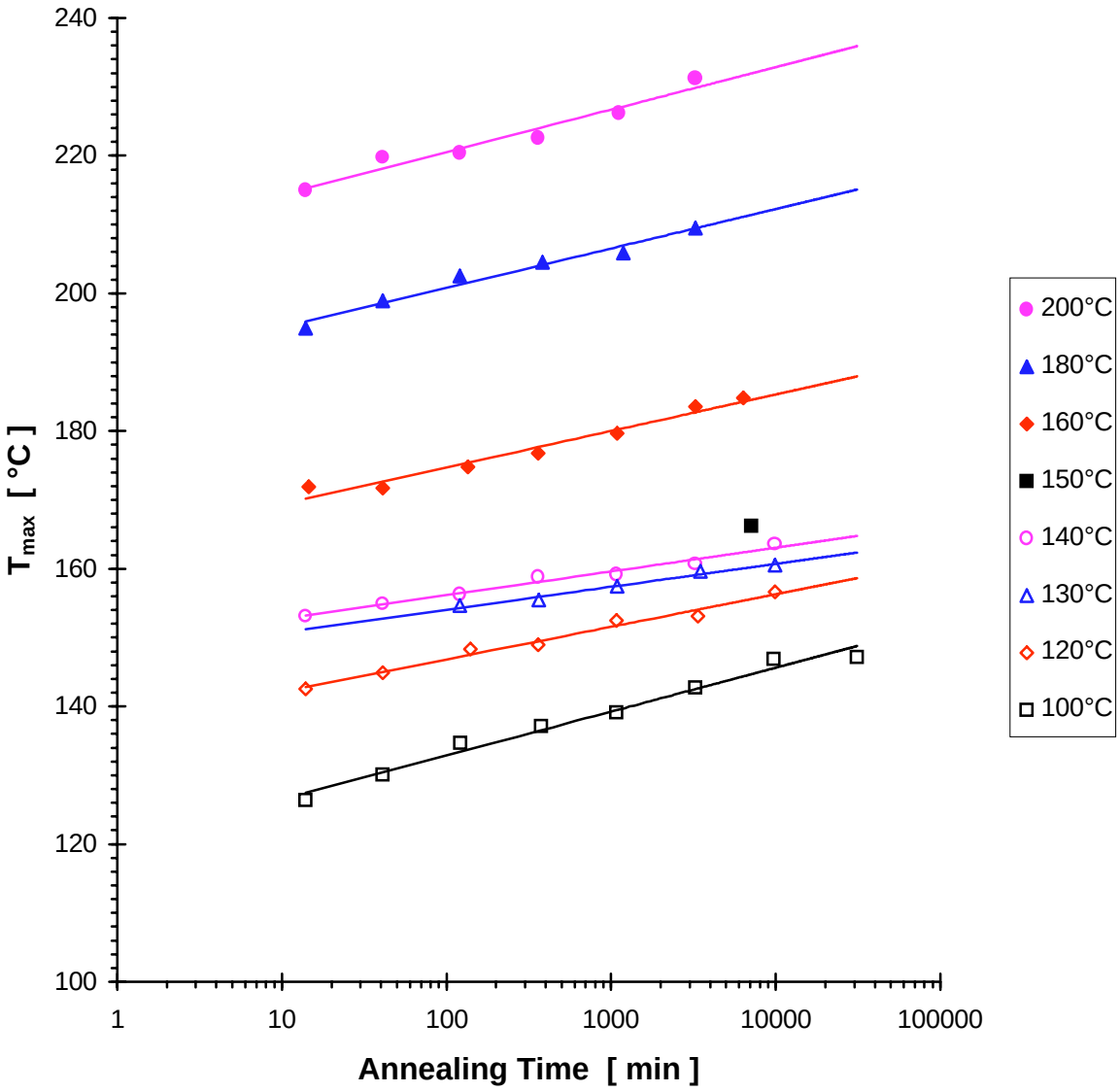


**Figure 5.27** Annealing time dependence of the peak maximum $T_{max}$ for different annealing temperatures below and above $T_g$.

enthalpy recovery data (lower part of the plot) from the low temperature melting data (upper part of the plot).

The next step in examining the similarity between the enthalpy recovery and the low temperature endotherm is to analyze the trends shown in figures 5.26 and 5.27. For this purpose, the data were fitted with linear functions of $\log(t_a)$ as shown in equations(5.10) and (5.11), used earlier in the previous section:

$$\Delta H_m(\text{low}) = a + b*\log(t_a) \qquad (5.10)$$

$$T_{max}(\text{low}) = T_a + A + B*\log(t_a) \qquad (5.11)$$

Below $T_g$ the parameter *A* in equation (5.11) is the difference between the peak maximum and annealing temperatures, for a reference aging time of 1 min. The choice of a fixed reference time of 1 min for all aging temperatures is somewhat ambiguous as it does not reflect the change in the relaxation times with change in $T_a$. However, while keeping in mind this ambiguity, one can still relate *A* to the initial mobility of the amorphous chains at $T_a$. Above $T_g$ *A* reflects the relative thermal stability of the secondary lamellae, extrapolated to short annealing times i.e. to the early stages of the secondary crystallization at $T_a$. One can speculate, that this thermal stability might be also determined by kinetic factors such as the mobility of the amorphous chains above $T_g$, reduced by the presence of crystalline lamellae.

The quantity *b* in equation (5.10) is physically interpreted as: 1) the rate of increase of secondary crystallinity as represented by the melting enthalpy of the secondary lamellae (for $T_a > T_g$), and 2) the rate of enthalpy relaxation (for $T_a < T_g$). In essence, both processes describe a slow approach to equilibrium. Therefore, regardless of the particular physical nature of the process, *b* is a measure of the rate of approach to equilibrium.

The annealing temperature dependence of the parameters *b* and *A* is plotted on figure 5.28-A. Below $T_g$ the value of *A* decreases with increase in $T_a$. This is in line with the well known behavior of the enthalpy recovery peak in amorphous polymeric glasses - as the annealing temperature approaches the glass transition, the peak appears closer and closer to $T_a$ until enthalpy relaxation ceases at $T_g$. [166, 167] In the glass transition region the value of *A* shows a significant drop. At the upper end of the glass transition region, *A* rises sharply

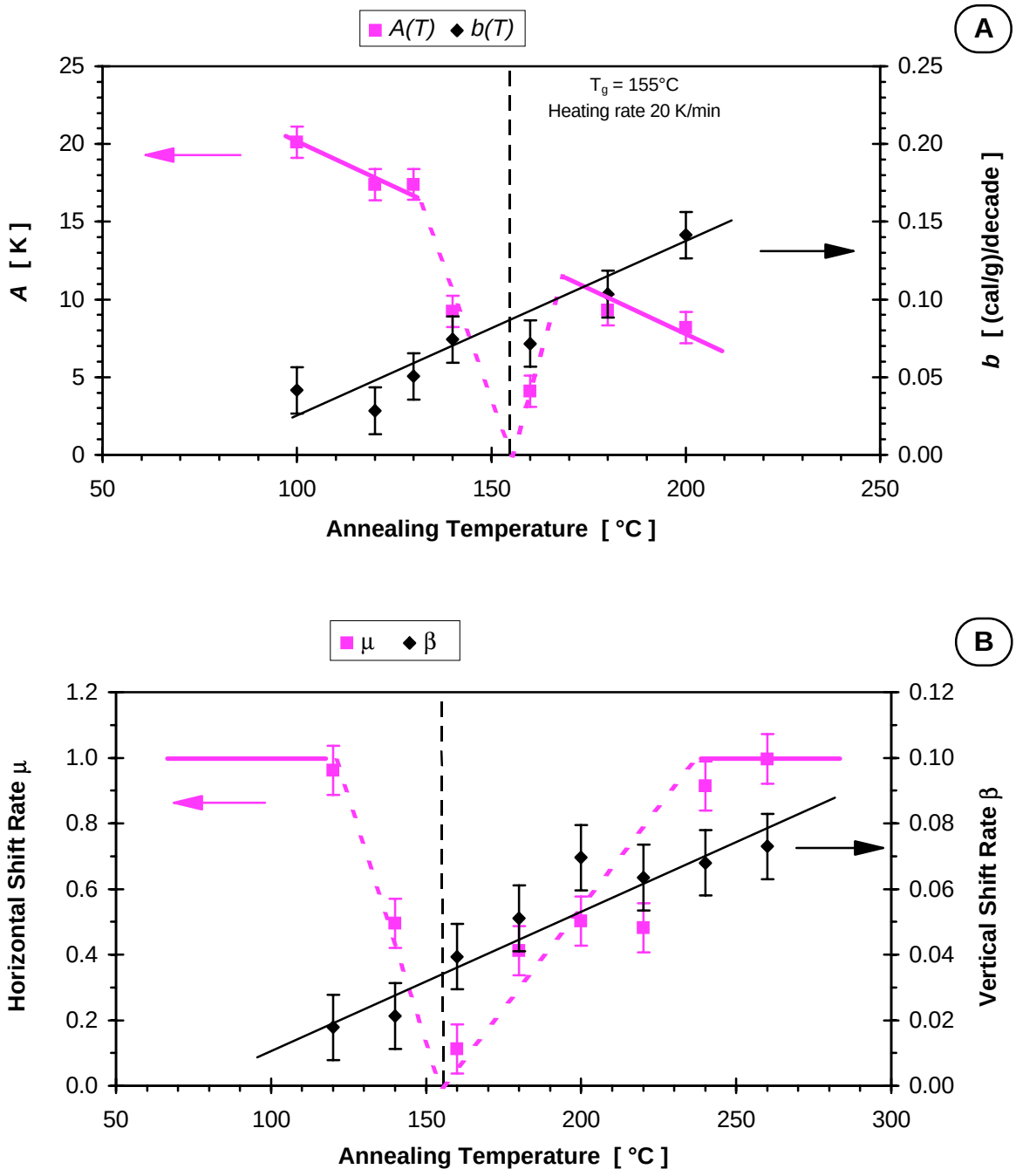


**Figure 5.28** Annealing temperature dependence of: (**A**) the parameters of the linear dependence of $T_{max}$ and $\Delta H_a$ on $\log(t_a)$: $A(T_a)$ - equation (5.11), $b\,(T_a)$ - equation (5.10); (**B**) the horizontal and the vertical shift rate from the studies of physical aging of semicrystalline PEEK below and above $T_g$ by momentary small strain creep compliance measurements (section 4.2.4).

again. Far above $T_g$ it decreases with increase in $T_a$, which is similar to the trend found in PEEK, crystallized or annealed under various other thermal histories above $T_g$ (figures 4.20 and 5.18). If the two points in the glass transition region($T_a$ = 140°C and 160°C) are excluded, the rest of the data for *A* follows the same linear trend with $T_a$, regardless of the fact, that they characterize two different processes below and above $T_g$. Even more peculiar is the fact, that the parameter *b* (equation 5.10) shows a trend of continuous increase throughout the entire temperature interval studied, including the glass transition range.

Despite these striking similarities in the evolution of the endothermic peak in the heat capacity, resulting from annealing below and above $T_g$, one could be tempted to judge them as purely accidental. Indeed, such a conclusion had been drawn in the case of partially crystalline PVC. [51, 53] Two independent studies observed, that the enthalpy recovery peak, resulting from annealing below $T_g$, is very similar to the melting peak just above $T_a$, resulting from annealing above $T_g$. Both studies claimed that such a similarity in the evolution of these two processes is accidental. Such a conclusion might have been rather hasty. At least in the case of PEEK, additional data exists, which clearly indicates a similarity between the structural relaxation below $T_g$ and the slow approach to equilibrium above $T_g$.

A study by small strain creep recovery (reported and analyzed in section 4.2.4 and reference 81), observed "physical aging" of semicrystalline PEEK below as well as above the nominal (calorimetric) glass transition. Following the method of Struik, [87, 88, 135] the transient creep compliance curves $J(t)$ for different annealing times $t_a$ were reduced to master curves by a combination of horizontal and vertical shifts. The susceptibility of the material to "physical aging" is characterized by the horizontal shift rate $m(T_a)$ - equation (2.11), and the vertical shift rate $b(T_a)$ - equation (4.11).

These two functions are plotted together against $T_a$ on figure 5.28-B. The dependence of *m* on $T_a$, typical of semicrystalline polymers, [88] is very similar to the dependence of the parameter *A* on $T_a$ from figure 5.28-A. In the case of the enthalpy relaxation process below $T_g$, both parameters are related to the temperature dependence of relaxation times. The vertical shift rate *b* shows the same type of annealing temperature dependence as the rate of approach to equilibrium - the parameter *b* on figure 5.28-A. In the case of the secondary

crystallization process above $T_g$, both $b$ and $b$ characterize the secondary crystallization rate, as was demonstrated earlier in section 5.4.

In summary, the kinetics describing "physical aging" of PEEK below and above $T_g$, as observed by creep recovery studies, is similar to the kinetics of enthalpy relaxation and secondary crystallization of semicrystalline PEEK, as observed by DSC. The correlation of the results from two independent methods - DSC and small strain creep recovery, leads to the conclusion that the similarity between the effects of structural relaxation below $T_g$ and secondary crystallization above $T_g$ is probably not accidental. Independent studies of the two processes have established already the fact, that both are mobility controlled phenomena. The polymeric glass with frozen excess enthalpy below $T_g$ and the partially crystalline polymer with crystallinity less than unity above $T_g$, are away from their respective equilibrium states. Therefore, both processes are also a manifestation of the slow approach to equilibrium. The correlation between the two phenomena might originate from the similar nature of the molecular motions required en route to the final equilibrium state.

A full answer to the second question posed above would need a more solid experimental and theoretical investigation of the kinetics and molecular nature of structural relaxation below $T_g$ and secondary crystallization above $T_g$. In addition to PEEK, other semicrystalline polymers should be examined as well. The best candidates would be polymers with intermediate crystallinity values and readily accessible temperature ranges of enthalpy relaxation and secondary crystallization, in which crystallinity has a small influence on $T_g$, for example, PET and i-PS. Further studies of the effect of initial crystallinity on the magnitude of these phenomena will be very helpful in clarifying the nature of their apparent similarity.

# CHAPTER 6

# CONCLUSIONS

The effect of long annealing above the glass transition of PEEK on the evolution of several characteristics of the physical state of the polymer was studied by differential scanning calorimetry, wide angle x-ray diffraction and small strain creep measurements. Isothermal annealing of PEEK above $T_g$ beyond the end of the primary crystallization stage results in the observation of a low temperature endothermic peak in the heat capacity just above the annealing temperature. According to the dual lamellar population model, this peak reflects the melting of crystalline lamellae with low thermal stability, formed at the annealing temperature and stable just up to a few degrees (~ 5 - 30 K) above it. Preliminary investigations of the development of the low temperature melting peak suggested that the evolution of the low melting temperature population of lamellae occurs on a time-scale different from that of the initial fast crystallization. This study concentrated on the time and temperature dependence of the structural reorganization which occurs in semicrystalline PEEK upon annealing at temperatures between the nominal (e.g. calorimetric) glass transition and the melting range.

As a result of these investigations, the following conclusions can be drawn:

1. Beyond the fast (primary) crystallization process, the evolution of the inherently nonequilibrium semicrystalline state is manifested in several interrelated phenomena: slow (secondary) crystallization, structural reorganization of the crystalline lamellae, and slowing down of the relaxation of a constrained amorphous phase.

2. Secondary crystallization is manifested in the evolution of a (secondary) lamellar population with lower thermal stability and in the increase in crystallinity determined by several methods, of which DSC and density crystallinity are studied in this work.

3. The evolution of the thermal stability of the low melting temperature (secondary) lamellae and the kinetics of secondary crystallization were studied extensively by investigating the dependence of the characteristics of the low temperature melting peak, $T_{max}$(low) and $\Delta H_m$(low), on annealing time and temperature under various thermal histories.

The dependence of these two parameters on log(time) and temperature is similar to that characteristic for structural relaxation of amorphous polymeric glasses below $T_g$.

4. The structural reorganization of the crystalline phase upon annealing during the secondary crystallization stage is manifested in the densification of the crystalline lamellae with time and the dependence of the crystal density on annealing temperature. The annealing time-temperature evolution of the room temperature crystal density parallels the evolution of crystallinity.

5. Crystal density at ambient conditions is not a physical constant and therefore, there is no one-to-one correspondence between bulk density and crystallinity. The standard definition of density crystallinity is invalid and a corrected definition is suggested.

6. During secondary crystallization, DSC and density crystallinities increase linearly with $\log(t_a)$ and $T_a$. There is a discrepancy between the crystallinity values determined by the two independent methods. The observed dependence of the crystal density on annealing conditions (time and temperature of annealing) necessitates the use of a corrected equation for the density crystallinity. The latter further increases the discrepancy between DSC and density crystallinities.

7. "Physical aging" of PEEK above the nominal $T_g$, observed for the first time in this work, is the result of both - slow relaxation of a constrained amorphous phase and secondary crystallization. The slow relaxation is manifested in the high retardation times observed above $T_g$ and the shift of the retardation spectrum towards higher retardation times upon annealing. Secondary crystallization appears a likely candidate for the stiffening of the polymer with annealing time - the vertical shifts in the superposition of the creep compliance curves observed in the "physical aging" experiments.

8. The simple two phase model does not describe adequately the physical state of semicrystalline polymers. It fails to address the slow approach to equilibrium through secondary crystallization, the dynamic changes in the physical properties of the "pure" phases (crystal and amorphous density dependence on annealing conditions), and the possible heterogeneity of two phases - the presence of two different crystalline lamellar populations and amorphous fractions with different levels of constraint.

The current study of the effects of long annealing above the glass transition on the physical state of a polymer has been restricted to a single polymer - PEEK, with a limited review on other semicrystalline polymers (in the case of RAF, "multiple melting" and "physical aging" - respectively in sections 2.3, 2.4 and 2.5) and few examples on other polymers in sections 4.2.2, 5.6.2, and 5.6.3. Some of the ideas presented in recent reviews on the subjects of secondary crystallization [151, 152] and dielectric relaxation [150] in semicrystalline polymers suggest that the implications of the results of this study could be much broader. For one, by applying a systematic approach - investigation of the time-temperature dependence and evolution of a variety of properties of a semicrystalline polymer, this study unequivocally established that a common thread exists between the above listed phenomena. From a theoretical point of view this suggests that a significant number of independent experimental studies and models for their explanation might have to be reviewed and reexamined as necessarily interrelated (i.e. "physical aging" vs. secondary crystallization, lamellar thickening vs. growth by lamellar inclusion, crystallinity evaluation vs. structural changes in the pure phases, to name a few).

From the point of view of applied polymer science - this study provides a link between independently observed variations of physical and material properties with processing and/or exploitation conditions. Thus it can serve as a guiding methodology in investigations of certain applied properties of semicrystalline thermoplastic materials (for example, their tailoring by small variations in processing conditions - time-temperature effect on morphology). It provides the fundamental background needed for examining the stability and deterioration of material properties upon planned or accidental, short or prolonged exposure above the glass transition range of semicrystalline polymers. For example, the methodology of this study could be extended into the field of prediction of "aging"/secondary crystallization induced long term increase in moduli and embrittlement during exposure above $T_g$ and development of strategies for reduction of such undesired changes. [202]

The importance of the latter has been recognized for polyolefins at least 30 years ago and has lead to intensive and focused research in the field, [205, 31-35, 45-47, 86-95] due to the natural occurrence of annealing/"aging" during processing and the lifetime of a product. On the

other hand, for high temperature semicrystalline polymers (i.e. high $T_g$/high $T_m$) such as i-PS, PET, PBT, and nylons, experimental studies and results are limited and often uncorrelated. The relatively undemanding conditions for most applications of some of these polymers (small packaging and fibers, exploitation well below $T_g$) has lead to reduced interest in investigation of "high-temperature aging" (with the exception of the fiber applications, for which the effect of high temperature annealing on the thermal stability and morphology, naturally occurring during heat-setting and exploitation, has been studied with a somewhat higher degree of consistency).

In a new class of materials - high temperature thermoplastics, such as PEEK, with potential for application in advanced high temperature composites, there is a substantial ground for renewed interest in "aging" above $T_g$. It involves both optimization of quite demanding processing conditions (high temperature melt processing and/or solidification through high temperature crystallization) and planned exposure above $T_g$, which depends on the rating for thermal/thermomechanical/thermodiffusional stability of the particular polymer or composite. [204]

# CHAPTER 7

# FUTURE WORK

Based on this study, the following suggestions for future work are made:

***on the PEEK fractions***

- To perform SAXS studies of narrow molecular weight fractions, prepared in sufficient amount by batch fractionation, according to the procedure outlined in section 3.1. The purpose of this study will be to determine the equilibrium melting temperature $T_m$ from the relationship between observed melting temperature and lamellar thickness (Gibbs-Thomson-Tamman equation [42]). The results will be compared with the molecular weight dependence of $T_m$ derived by the Hoffman-Weeks method in this study (section 4.1.1).

- To investigate the dependence of $T_m^{'}$ on $T_x$ by the Hoffman-Weeks method at several heating rates in the DSC in order to determine whether reorganization during the melting scan might be the origin of the observed dependence of the equilibrium melting temperature on MW (figure 4.5).

***on isothermal annealing and the low temperature endothermic transition***

- To continue the studies of the heating rate dependence of the low temperature endothermic peak's parameters for different thermal histories (see section 5.6.1). This study will focus on evaluation of the effect of heating rate on the dependence of $T_{max}$(low) and $\Delta H_m$(low) on log($t_a$).

- To continue the WAXS studies of the crystallization/annealing temperature dependence of the densification rate of the crystalline lamellae in situ and at room temperature (e.g. after quenching below $T_g$). (*currently under progress*)

- To evaluate the crystallinity during the secondary crystallization stage "in situ" by dilatometry and by WAXS and compare it with the DSC crystallinity. (*currently under progress*)

The last two investigations must determine whether the discrepancy between DSC

and density crystallinities is an intrinsic characteristic of the secondary crystallization process or a result of thermally generated stresses during quenching which are due to the difference in thermal expansion coefficients of the crystalline lamellae and the amorphous fraction.

## BIBLIOGRAPHY

[1]DePorter J. K., Baird D. G., Wilkes G. L., J. Macromol. Sci. - Rev. Macromol. Chem. Phys., C33(1) , 1 (1993)

[2]Marand H., Prasad A., Macromolecules, 25, 1731 (1992)

[3]Schultz J., "*Polymer Materials Science*", Prentice-Hall: Englewood Cliffs, NJ (1974)

[4]Hoffman J. D., Davis C. T., Lauritzen J. I., "*Treatise on Solid State Chemistry"*, ed. Haney E. B., vol. 3, 497-613 (1976)

[5]Magill J. H., "Morphogenesis of Solid Polymer Microstructures", in "*Treatise on Materials Science and Technology, Volume 10, Properties of Solid Polymeric Materials, Part A*," ed. Schultz J. M., Academic Press: New York (1977)

[6]Runt J. P., "Crystallinity Determination", in "*Encyclopedia of Polymer Science and Engineerin*g", ed. Kroschwitz J. I., Wiley: New York, 2nd ed., 482 (1984-1990)

[7]Boyer R. F., J. Polym. Sci. Polym. Symp. Ed., 50, 189 (1975)

[8]Flory P. J., "*Principles of Polymer Chemistry*", Cornell Univ. Press: Ithaca, NY (1953)

[9]Mandelkern L., "The Crystalline State", in "*Physical Properties of Polymers*", ed. Mark J. E., ACS Washington D.C. (1984)

[10]Wunderlich B., "Glass Transition in Partially ordered Molecules", in "*Progress in Colloid and Polymer Science*", ed. Killian H.-G. and Pietrala M., Springer: New York, vol. 96, 22 (1994)

[11]Beatty C. L., Karasz F. E., J. Macromol. Sci. - Rev. Macromol. Chem., C17, 37 (1979)

[12]Suzuki H., Grebowicz J., Wunderlich B., Brittish Polym. J., 17, 11 (1985)

[13]Grebowicz J., Lau S.-F., Wunderlich B., J. Polym. Sci.: Polym. Symp., 71, 19 (1984)

[14]Cheng S. Z. D., Pan R., Wunderlich B., Macromol. Chem., 189, 2443 (1988)

[15]Cheng S. Z. D., Wu Z. Q., Wunderlich B., Macromolecules, 20, 2802 (1987)

[16]Cheng S. Z. D., Cao M.-Y., Wunderlich B., Macromolecules, 19, 1868 (1986)

[17]Huo P., Cebe P., Macromolecules, 25, 902 (1992)

[18]Kalika D. S., Krishnaswamy R. K., Macromolecules, 26, 4252 (1993)

[19]Michele A., Vittoria V., Polymer, 32, 232 (1991)

[20]Booth A., Hay J. H., Polymer, 10, 95 (1969)

[21]Schultz J. M., Scott R. D., J. Polym. Sci.: A-2, 7, 659 (1969)

[22]Hoffman J. D., Weeks J. J., J. Chem. Phys., 42, 4301 (1965)

[23]Wunderlich B., Mellilo J., Macromol. Chem., 118, 250 (1968)

[24]Banks W., Gordon M., Roe R.-J., Sharples A., Polymer, 4, 61 (1963)

[25]Buckser S., Tung L. H., J. Phys. Chem., 63, 763 (1959)

[26]Rybnikar F., J. Polym. Sci., 44, 517 (1960)

[27]Fischer E. W., Schmidt G. F., Angew. Chem. (Intern. Ed. Engl.), 1, 488 (1962)

[28]Grubb D. T., Liu J. J.-H., Caffrey M., Bilderback D. H., J. Polym. Sci.: Polym. Phys. Ed., 22, 367 (1984)

[29]Fischer E. W., Pure Appl. Chem., 31(1), 113 (1972)

[30]Collins R. L., J. Polym. Sci., 27, 75 (1958)

[31]Yue C. Y., Msuya W. F., J. Mat. Sci. Lett., 9, 985 (1990)

[32]Buckley C. P., Habibullah M., J. Appl. Polym. Sci., 26, 2613 (1981)

[33]Vittoria V., Polymer, 29, 1118 (1988)

[34]Kapur S., Rogers C. E., J. Polym. Sci.: Polym. Phys. Ed., 10, 2107 (1972)

[35]Baum J. S., Schultz J. M., J. Appl. Polym. Sci., 26, 1579 (1981)

[36]Groeninckx G., Reynaers H., Berghmans H., Smets G., J. Polym. Sci.: Polym. Phys. Ed., 18, 1311 (1980); Groeninckx G., Reynaers H., J. Polym. Sci.: Polym. Phys. Ed., 18, 1325 (1980)

[37]Bell J. P., Murayama T., J. Polym. Sci.: Part A-2, 7, 1059 (1969)

[38]Roberts R. C., Polymer, 10, 117 (1969)

[39]Holdsworth P. J., Turner-Jones A., Polymer, 12, 195 (1971)

[40]Fakirov S., Fischer E. W., Hoffmann R., Schmidt G. F., Polymer, 18, 1121 (1977)

[41]Fischer E. W., Fakirov S., J. Mat. Sci., 11, 1041 (1976)

[42]Wunderlich B., "*Macromolecular Physics, Crystal Melting*", Academic Press: New York, Vol. III (1980)

[43]Sakaguchi F., Mandelkern L., Maxfield J., J. Polym. Sci.: Polym. Phys. Ed., 14, 2137 (1976)

[44]Busfield W. K., Blake C. S., Polymer, 21, 35 (1980)

[45]Kriesten U., Ph. D. Thesis, University of Aberdeen, Aberdeen, UK (1993)

[46]Hutchinson J. M., Kriesten U., J. Non-Cryst. Sol., 172-174, 592 (1994)

[47]Hellinckx S., Coll. Polym. Sci., 273, 130 (1995)

[48]Lemstra P. J., Kooistra T., Challa G. J., Polym. Sci.: Part A-2, 10, 823 (1972)

[49]Pelzbauer Z., Manley R. St. J., J. Macromol. Sci. - Phys., B7, 345 (1973)

[50]Vivirito J., Iler H. D., Marand H., unpublished results

[51]Illers K. H., Makromol. Chem., 127, 1 (1969)

[52]Scherrenberg R. L., Reynaers H., Gondard C., Steeman P. A. M., J. Polym. Sci.: Part B: Polym. Phys., 32, 111 (1994)

[53]Bair H. E., Warren P. C., J. Macromol. Sci.-Phys., B20, 381 (1981)

[54]Weigel P., Hirte R., Ruscher C., Faserforsch. Textiltech., 25, 283 (1974)

[55]Bell J. P., Slade P. E., Dumbleton J. H., J. Polym. Sci.: Part A-2, 6, 1773 (1968)

[56]Shuren F., Guanghua Z., Qun T., Yuqin Y., J. Thermal Anal., 39, 875 (1993)

[57]Pecorini T. J., Hertzberg R. W., Polymer, 34, 5053 (1993)

[58]Yeh J. T., Runt J., J. Polym. Sci.: Part B: Polym. Phys., 27, 1543 (1989)

[59]Nichols M. E., Robertson R. E., J. Polym. Sci.: Part B: Polym. Phys., 30, 755 (1992)

[60]Kim J., Nichols M. E., Robertson R. E., J. Polym. Sci.: Part B: Polym. Phys., 32, 887 (1994)

[61]Chung J. S., Cebe P., Polymer, 33, 2312 (1992); Chung J. S., Cebe P., Polymer, 33, 2325 (1992)

[62]Huo P., Cebe P., Coll. Polym. Sci., 270, 840 (1992); Huo P., Cebe P., J. Polym. Sci.: Part B: Polym. Phys., 30, 239 (1992)

[63]Blundell D. J., Osborn B. A., Polymer, 24, 953 (1983)

[64]Blundell D. J., Polymer, 28, 2248 (1987)

[65]Lee Y., Porter R. S., Lin J. S., Macromolecules, 22, 1756 (1989)

[66]Lee Y., Porter R. S., Macromolecules, 20, 1336 (1987)

[67]Jonas A., Legras R., Issi J.-P., Polymer, 32, 3364 (1991)

[68]Jonas A. M., Russell T. P., Yoon D. Y., Macromolecules, 28, 8491, (1995)

[69]Ostberg G. M. K., Seferis J.C., J. Appl. Polym. Sci., 33, 29 (1987)

[70]Bassett D. C., Olley R. H., Al Raheil I. A. M., Polymer, 29, 1745 (1988)

[71]Cebe P., Hong S.-D., Polymer, 27, 1183 (1986)

[72]Chang S.-S., Polymer, 29, 138 (1988)

[73]Lattimer M. P., Hobs J. K., Hill M. J., Barham P. J., Polymer, 33, 3971 (1992)

[74]Kruger K.-N., Zachmann H. G., Macromolecules, 26, 5202 (1993)

[75]Mehmet-Alkan A. A., Hay J. N., Polymer, 33, 3527 (1992)

[76]Mijovic J., Gsell T., SAMPE Q., 22, 42 (1990)

[77]Velikov V., Netopilik M., Marand H., ACS Polym. Preprints, 33(2), 239 (1992)

[78]Velikov V., Marand H., ACS Polym. Preprints, 34(2), 835 (1993)

[79]Velikov V., Marand H., Bull. Am. Phys. Soc., 39(1), 168 (1994)

[80]Velikov V., Vivirito J., Marand H., Bull. Am. Phys. Soc., 39(1), 168 (1994)

[81]Velikov V., Verma R., Prabhu V., Dillard D., Marand H., ACS Polymer Preprints, 36(1), 344 (1995)

[82]Verma R. K., Velikov V., Kander R., Marand H., Chu B., Hsiao B. S., Polymer, in press

[83]Lovinger A. J., Hudson S. D., Davis D. D., Macromolecules, 25, 1752 (1992)

[84]Hsiao B. S., Gardner K. H., Wu D. Q., Chu B., Polymer, 34, 3986 (1993); Hsiao B. S., Gardner K. H., Wu D. Q., Chu B., Polymer, 34, 3996 (1993)

[85]Wang J., Alvarez M., Zhang W., Wu Z., Li Y., Chu B., Macromolecules, 25, 6943 (1992)

[86]Struik L. C. E., "Physical Aging", in "*Encyclopedia of Polymer Science and Engineerin*g", ed. Kroschwitz J. I., Wiley: New York, 2nd ed., vol. 1, 595 (1984-1990)

[87]Struik L. C. E., "*Physical Aging of Amorphous Polymers and Other Materials*", Elsevier: Amsterdam (1978)

[88]Struik L. C. E., Polymer, 28, 1521 (1987)

[89]Struik L. C. E., Polymer, 28, 1534 (1987)

[90]Struik L. C. E., Polymer, 30, 799 (1989)

[91]Struik L. C. E., Polymer, 30, 815 (1989)

[92]Read B. E., Dean G. D., Tomlins P. E., Polymer, 29, 2159 (1988)

[93]Read B. E., Tomlins P. E., Dean G. D., Polymer, 31, 1204 (1990)

[94]Chai C. K., McCrum N. G., Polymer, 25, 291 (1984)

[95]Chai C. K., McCrum N. G., Polymer, 21, 706 (1980)

[96]Kemmish D. J., Hay J. N., Polymer, 26, 905 (1985)

[97]Ogale A. A., McCullough R. L., Comp. Sci. Tech., 30, 137 (1987)

[98]Ogale A. A., McCullough R. L., Comp. Sci. Tech., 30, 185 (1987)

[99]Carfagna C., Amendola E., D'Amore A., Nicolais L., Polym. Eng. Sci., 28(18), 1203 (1988)

[100]Wang S. F., Ogale A. A., Polym. Eng. Sci., 29(18), 1273 (1989)

[101]Jar P.-Y., Kausch H.-H., J. Polym. Sci.: Part B: Polym. Phys., 30, 775 (1992)

[102]Hay J. N., "*Progress in Colloid and Polymer Science*", v. 87, 74 (1992)

[103]Iler H. D., Ph.D. Dissertation, Virginia Tech, Blacksburg, VA (1995)

[104]Roovers J., Cooney J. D., Toporowski P. M., Macromolecules, 23, 1611 (1990)

[105]Bishop M. T., Karasz F. E., Russo P. S., Langley K. H., Macromolecules, 18, 86 (1985)

[106]Devaux J., Delimoy D., Daoust D., Legras R., Mercier J. P., Strazielle C., Nield E., Polymer, 26, 1994 (1985)

[107]Mullins M. J., Woo E. P., J. Macromol. Sci.: Rev. Macromol. Chem. Phys., C27(2), 313 (1987)

[108]Mohanty D. K., Lowery R. C., Lyle G. D., McGrath J. E., SAMPE Symp., 32, 408 (1987)

[109]Brink A. E., Gutzeit S., Lin T., Marand H., Lyon K., Hua T., Davis R., Riffle J. S., Polymer, 34, 826 (1993)

[110]Jonas A., Legras R., Polymer, 32, 2691 (1991)

[111]Mencer H. J., Polym. Eng. Sci., 28(8), 497 (1988)

[112]Kurata et al., "*Polymer Handbook*", ch. VII, eds. Brandrup J., Immergut E. H., Wiley: New York (1989)

[113]Wunderlich B., "*Thermal Analysis*", Academic Press: San Diego, CA (1990)

[114]Instructions for Specific Heat Kit, PE part No. 219-0136, rev. 12/68, The Perkin Elmer Corporation, Norwalk, CT (1990)

[115]Cheng S. Z. D., Wunderlich B., J. Polym. Sci.: Polym. Phys. Ed., 24, 1755 (1986)

[116]Séguéla R., Polymer, 34, 1761 (1993)

[117]Zoller P., Kehl T. A., Starkweather H. W., Jones G. A., J. Polym. Sci.: Part B: Polym. Phys., 27, 993 (1989)

[118]Rueda D. R., Ania F., Richardson A., Ward I. M., Balta Calleja F. J., Polym. Commun., 24, 258 (1983)

[119]Dawson P. C., Blundell D. J., Polymer, 21, 577 (1980)

[120]Hay J. N., Kemmish D. J., Langford J. I., Rae A. I. M., Polym. Commun., 25, 175 (1984)

[121]Fratini A. V., Cross E. M., Whitaker R. B., Adams W. W., Polymer, 27, 861 (1986)

[122]Wakelyn N. T., J. Polym. Sci.: Part C: Polym. Lett., 25, 25 (1987)

[123]Hay J. N., Langford J. I., Lloyd J. R., Polymer, 30, 489 (1989)

[124]Chung J. S., Bodziuch J., Cebe P., J. Mater. Sci., 27, 5609 (1992)

[125]Verma R. K., Marand H., Srinivas S., Wilkes G. L., in preparation

[126]Balta-Calleja F. J., Vonk C. G., "*X-Ray Scattering of Synthetic Polymers*", Elsevier: Amsterdam, New York (1989)

[127]Hall M. M., Veeraraghavan V. G., Rubin H., Winchell P. G., J. Appl. Cryst., 10, 66 (1977)

[128]Cullity B.D., "*Elements of X-Ray Diffraction*," 2nd ed., Addison-Wesley: Reading, MA (1978)

[129]Chen H.-L., Porter R.S., J. Polym. Sci.: Part B: Polym. Phys., 31, 1845 (1993)

[130]Day M., Deslandes Y., Roovers J., Suprunchuk T., Polymer, 132, 1258 (1991)

[131]Deslandes Y., Sabir F.-N., Roovers J., Polymer, 132, 1267 (1991)

[132]Hsiao B. S., Sauer B. B., J. Polym. Sci.: Part B: Polym. Phys., 31, 901 (1993)

[133]Lopez L. C., Wilkes G. L., Polymer, 29, 106 (1988)

[134]Chivers R. A., Moore D. R., Polymer, 35, 110 (1994)

[135]Buijs J. A. H. M., Vroege G. J., Polymer, 34, 4692 (1993)

[136]Boyd R. H., Polymer, 26, 323 (1985)

[137]Hirschinger J., Schaeter D., Spiess H. W., Lovinger A. J., Macromolecules, 24, 2428 (1991)

[138]Schaeter D., Spiess H. W., Suter U. W., Fleming W. W., Macromoleculs, 23, 3431 (1990)

[139]Quirk R. P., Alsamarraie M. A. A., "*Polymer Handbook*", ch. V, eds. Brandrup J., Immergut E. H., Wiley: New York (1989)

[140]McCrum N. G., Read B. E., Williams G., "*Anelastic and Dielectric Effects in Polymeric Solids*", Dover: New York (1991)

[141]McCullough R. L., "Anisotropic Elastic Behavior of Crystalline Polymers", in "*Treatise on Materials Science and Technology, Volume 10, Properties of Solid Polymeric Materials, Part B*," ed. Schultz J. M., Academic Press: New York (1977)

[142]Janzen J., Polym. Eng. Sci., 32, 1242 (1992)

[143]Takayanagi M., Uemura S., Minami S., J. Polym. Sci.: Part C, 5, 113 (1966?)

[144]Matsuoka S., "*Relaxation Phenomena in Polymers*", Hanser Publishers - Oxford University Press: New York (1992)

[145]Kerner E. H., Proc. Phys. Soc. (London), B69, 808 (1956)

[146]Halpin J. C., Kardos J. L., J. Appl. Phys., 43, 2235 (1972)

[147]Verma R. K., Marand H., Hsiao B., Macromolecules, 29, 7767 (1996)

[148]Verma R. K., Sholtz P., Marand H., in preparation

[149]Verma R. K., private communication

[150]Sauer B. B., "Dielectric Relaxation in Polymers", in "*Performance of Plastics*", ed. Brostow, W.; in preparation

[151]Marand H., Velikov V., Verma R. K., Cham P. M., Prabhu V., Dillard D., ACS Polym. Preprints, 36(1), 263 (1995)

[152]Marand H., in preparation

[153]Santa Cruz C., Stribeck N., Zachmann H. G., Balta Calleja F. J., Macromolecules, 24, 5980 (1991)

[154]Sauer B. B., Hsiao B. S., ACS Preprints: Div. Polym. Mat. Sci. Eng., 69, 35 (1993)

[155]Hsiao B. S., Sauer B. B., Verma R. K., Zachmann H. G., Seifert S., Chu B., Harney P., Macromolecules, 28, 6931 (1995)

[156]Sauer B. B., Hsiao B. S., Polymer Preprints, 36(1), 261 (1995)

[157]Jonas A., Legras R., Macromolecules, 26, 813 (1993)

[158]Schultz J. M., Fischer E. W., Schaumburg O., Zachmann H. A., J. Polym. Sci.: Polym. Phys. Ed., 18, 239 (1980)

[159]Wunderlich B., private communication

[160]Bassett D. C., "*Principles of Polymer Morphology*", Cambridge University Press: Cambridge (1981)

[161]Guerra G., Petracone V., Corradini P., De Rosa C., Napolitano R., Pirozzi B., Giunchi G., J. Polym. Sci.: Polym. Phys. Ed., 22, 1029 (1984)

[162]Zhou Y. Q., Tong G., Qi Z. N., Macromol. Chem., Macromol. Symp., 20-21, 383 (1988)

[163]Montserrat S., Cortes P., J. Mater. Sci., 30, 1790 (1995)

[164]Aref-Azar A., Arnoux F., Biddlestone F., Hay J. N., Thermochim. Acta, 273, 217 (1996)

[165]Vigier G., Tatibouet J., Polymer, 34, 4257 (1993)

[166]Pethrick R. A., Trends Polym. Sci., 1(8), 226 (1993)

[167]Berens A. R., Hodge I. M., Macromolecules, 15, 756 (1982); Hodge I. M., Berens A. R., Macromolecules, 15, 762 (1982)

[168]Mandelkern L., Allou A.L., Gopalan M., J. Phys. Chem., 72, 309 (1968)

[169]Mijovich J., Nicolais L., D.Amore A., Kenny J. M., Polym. Eng. Sci., 34, 381 (1994)

[170]Menczel J., Wunderlich B., J. Polym. Sci.: Polym. Lett. Ed., 19, 265 (1981)

[171]Blundell D. J., Beckett D. R., Willcocks P. H., Polymer, 22, 704 (1981)

[172]Samuels R. J., J. Polym. Sci.: Polym. Phys. Ed., 13, 1417 (1975)

[173]Uemura T., Abe K., Akiyama K., Couderc D., IEEE Trans. Electr. Insul., EI22(6), 735 (1987)

[174]Petraccone V., De Rosa C., Guerra G., Tuzi A., Macromol. Chem., Rapid Commun., 5, 631 (1984)

[175]Passingham C., Hendra P. J., Cudby M. E. A., Zichy V., Weller M., Eur. Polym. J., 26, 631 (1990)

[176]Vittoria V., Petrillo E., Russo R., J. Macromol. Sci. - Phys., B35(1), 147 (1996)

[177]Hatakeyama T., Quinn F. X., "*Thermal Analysis: Fundamentals and Applications to Polymer Science*", Wiley: Chichester, UK (1994)

[178]Pelzbauer Z., Manley R. St. J., J. Polym. Sci.: A-2, 8, 649 (1970)

[179]Overbergh N., Berghmans H., Smets G., J. Polym. Sci.: Part C, 38, 237 (1972)

[180]Bell J. P., Dumbleton J. H., J. Polym. Sci.: Part A-2, 7, 1033 (1969)

[181]Martucelly E., Riva F., Selitti C., Silvestre C., Polymer, 26, 270 (1985)

[182]Weigel P., Hirte R., Ruscher C., Faserforsch. Textiltech., 25, 440 (1974)

[183]Gray A., Gilbert M., Polymer, 17, 44 (1976)

[184]Sweet G. E., Bell J. P., J. Polym. Sci.: Part A-2, 10, 1273 (1972)

[185]Zhou C., Clough S. B., Polym. Eng. Sci., 28, 65 (1988)

[186]Doiullard A., Dumazet Ph., Chabert B., Guillet J., Polymer, 34, 1702 (1993)

[187]Jonas A. M., Russell T. P., Yoon D. Y., Coll. Polym. Sci., 272, 1344 (1994)

[188]Lin S. B., Koenig J. L., J. Polym. Sci. Polym Symp., 71, 121 (1984)

[189]Illers K.-H., Coll. Polym. Sci., 258, 117 (1980)

[190]Fakirov S., Avramova N., Schultz J., Angew. Macromol. Chem., 140, 63 (1986)

[191]Runt J., Miley D. M., Zhang X., Gallagher K. P., McFeaters K., Fishburn J., Macromolecules, 25, 1929 (1992)

[192]Yeh J. T., Runt J., J. Mater. Sci., 24, 2637 (1989)

[193]Wu S. S., Kalika D. S., Lamonte R. R., Makhija S., J. Macromol. Sci. - Phys., B35(2), 157 (1996)

[194]Lustig S. R., Van-Alsten J. G., Hsiao B., Macromolecules, 26, 3885 (1993)

[195]Phillips R. A., Cooper S. L., Macromolecules, 28, 5734 (1995)

[196]Laivins G. V., Macromolecules, 22, 3974 (1989)

[197]Hutchinson J. M., Prog. Polym. Sci., 20, 703 (1995)

[198]Zimmerman H. J., Konnecke K., Polymer, 32, 3162 (1991)

[199]Angell C. A., Science, 267, 1930 (1995)

[200]Hodge I. M., J. Non-Cryst. Solids, 169, 211 (1994)

[201]Hay J. N., Pure Appl. Chem., 67, 1855 (1995)

[202]Biddlestone F., Harris A., Hay J. N., Hammond T., Polymer International, 39, 221 (1996)

[203]Echeveria I., Su P.-C., Simon S. L., Plazek D. J., J. Polym. Sci.Part B: Polym. Phys., 33, 2457 (1995)

[204]Rigby R., Adv. Polym. Tech., 2(3), 163 (1982)

[205]Schael G. W., J. Appl. Polym. Sci., 10, 901 (1966)

[206]Karasz F. E., Bair H. E., O'Reilly J. M., J. Phys. Chem., 69(8), 2657 (1965)

[207]Angell C. A., J. Non-Cryst. Solids, 131-133, 13 (1991)

[208]K. L. Ngai et al., Ann. N.Y. Acad. Sci., 484, 3150 (1986); Macromolecules, 24, 1222, (1991); J. Non-Cryst. Solids, 131-133, 442 (1991); J. Chem. Phys., 88(8), 5086 (1988)

[209]Richter D., J. Phys.: Condens. Matter, 8, 9177 (1996)

[210]Sasabe H., Moynihan C., J. Polym. Sci.: Polym. Phys. Ed., 16, 1447 (1978)

[211]Tobolski A. V., "*Properties and Structure of Polymers*", Wiley: New York (1960)

[212]Kovacs A. J., Aklonis J. J., Hutchinson J. M., Ramos A. R., J. Polym. Sci.-Phys., 17, 1097 (1979)

[213]G. ten Brinke et al., Macromolecules, 22, 1761 (1989); Macromolecules, 25, 698 (1992)

[214]G. Williams et al., Trans. Far. Soc., 67, 1323 (1971)

[215]Verbiest T., Burland D. M., Walsh C. A., Macromolecules, 29, 6310 (1996)

[216]Marand H., Velikov V., Prabhu V., Srinivas S., Christian S., ACS Preprints: Div. Polym. Mat. Sci. Eng., 76 (1997)

[217]Velikov V., Marand H., J. Thermal Anal., 49(1), 375 (1997)

[218]Bershtein V. A., Egorov V. M., "*Differential Scanning Calorimetry of Polymers"*, Ellis Horwood: Chichester, UK (1994)

# APPENDIX

During the course of this study, the effect of annealing above $T_g$ on the DSC heating scan of semicrystalline PEEK has been studied under a wide variety of thermal histories (see figures 3.3 - 3.7). For any type of thermal history and its parameters - $\{T_a, t_a\}$, $\{T_c, t_c\}$, $\{T_x, t_x\}$, an endothermic peak in the DSC scan is observed above the annealing temperature. Similar observations are made for other semicrystalline polymers as well (see section 4.2.2 and references in section 2.4.1).

The universality of this observation demands a rigorous universal approach to the evaluation of the quantitative characteristics of the low temperature endothermic peak. In most of the studies of "multiple melting" of PEEK and other polymers the realization of such an approach has been inadvertently hindered by the choice of experimental conditions. Two types of thermal histories dominate these studies:

1. Isothermal crystallization from the melt.

For most of the polymers reviewed or investigated, such thermal history leads to a low temperature endothermic peak which is a relatively small shoulder at the beginning of the main melting peak of the polymer. As the latter is a broad asymmetric peak, the shape of which cannot be modeled with a simple analytical function, a rigorous definition of a "local baseline" for the low temperature endothermic peak is impossible. Due to this obstacle, the shape of the low temperature peak can not be examined. The peak enthalpy (and to some extent the peak maximum position) would depend on the choice of the local baseline or the procedure for resolving the two peaks.

2. Isothermal crystallization and/or annealing from the amorphous glassy state.

Under this thermal history, in most cases a well resolved peak appears at a significant distance below the beginning of the main melting peak. However, the temperature dependence of the peak shape and position is such that the observed peak is very small. In addition, a significant drop in the heat capacity after the peak is observed (figure 4.13 and references 14-16, 58, 68, 70, 71, 157, 189). The magnitude of this change appears larger than any possible changes in the heat capacity, due to changes in the composition of a multiphase

(semicrystalline) system (for example, melting and RAF transformation [16]). Its shape is uncharacteristic for a crystallization peak, despite earlier claims made to that effect. [63-66, 71]

The above mentioned features are probably the reason why a detailed characterization of the otherwise well separated peak has not been performed in the case of polymers, cold-crystallized or annealed at temperatures well below the main melting peak. The small magnitude of the peak has even lead few authors to make the erroneous statement that upon short time annealing at temperatures just above the glass transition no peak is observed. [70, 71]

A third type of thermal history - long and complete primary crystallization, followed by annealing down (between $T_g$ and $T_x/T_c$) leads to the observation of an "annealing" low temperature endothermic peak (see figure 4.25 and references 61, 72-74). Under this type of thermal history for PEEK, for annealing temperatures 210°C - 250°C, the peak appears to be superposed only to the linearly increasing with temperature heat capacity of the semicrystalline polymer. This allowed, despite the small magnitude of the peak, its complete characterization and firmly established the following characteristics of the peak:

- The low temperature endothermic peak is symmetrical in shape.

Direct evidence for this are DSC scans in which the peak is well separated from the strong main melting peak (figure 4.25). Further evidence is seen in scans in which the main melting peak is small compared to the "annealing" peak (figure 5.14) and after analysis of the shape and evolution of the low temperature peak in scans in which it is strong, although superposed to the large asymmetrical main melting peak (figures 4.15, 4.21, 5.13, 5.15).

- A local step-change in the heat capacity trace in the vicinity of the peak is detected.

Although different in magnitude, this change is present in samples with very different thermal histories (see figures 4.13 and 4.26). The magnitude of the change in the heat capacity evolves with annealing time and temperature, parallel to the evolution of the peak maximum and enthalpy (figure 4.29).

These two observations suggest that the presence of a local change in the heat capacity in the immediate vicinity of the peak is also an universal feature of the DSC scan and must be accounted for under other thermal histories as well.

These widely different conditions suggest that the symmetrical shape is a universal characteristic of the low temperature endothermic peak and should be accounted for even under conditions, when due to the presence of a complicated local baseline it is not immediately transparent in the scan.

As a result of these generalizations, at the end of section 4.2.1 a procedure for the evaluation of the peak parameters was suggested. It is based on fitting not only the peak itself, but also the heat capacity and its step-change in the vicinity of the peak. A combination of several functions is used:

- *linear function*, representing the unperturbed heat capacity trace of semicrystalline PEEK before the peak,

$$f_1(\mathrm{T}) = \mathrm{A}*\mathrm{T} + \mathrm{B} \qquad (4.4)$$

- *peak function*, characterizing the symmetrical peak profile,

$$f_2(\mathrm{T}) = a * f\left(\frac{T - T_{\max}}{b}\right) \qquad (4.5)$$

- *step function* which reflects the observed step-change in the heat capacity after the peak from its values below it.

$$f_3(\mathrm{T}) = a_s * f\left(\frac{T - T_{\max}}{b}\right) \qquad (4.6)$$

Justification for the use of a linear function to approximate the heat capacity of semicrystalline PEEK can be found in references 16 and 115 (the heat capacities of glassy and liquid amorphous PEEK are approximately linear functions of temperature). Although quantitatively this approximation does not agree with a two-phase model calculation of the heat capacity according to equation (2.2) (see review on the RAF of PEEK - section 2.3.2), the current experimental observations also support this approximation (figure 4.26). In the absence of noticeable thermal transitions below the low temperature peak (glass transition or other low temperature melting) the heat capacity below the peak is a linear function of temperature. For the purposes of our analysis the linear function is needed merely in order to establish the local heat capacity baseline before the peak.

The two other functions - *peak function* and *step function* which were defined in most general terms in section 4.2.1, are described, respectively, in parts A and B below.

## *Appendix A*

*Fitting of the peak profile*

Analytical investigation of the shape of the low temperature endothermic peak shows that it is narrower than a peak described with a Cauchy function - equation (A.1), but wider than an exponential (Gaussian) peak - equation (A.2):

$$f(T) = \frac{a}{1 + \left( \frac{T - T_{max}}{b} \right)^2} \qquad \text{(A.1)}$$

$$f_G(T) = a * exp\left[ -\left( \frac{T - T_{max}}{b} \right)^2 \right] \qquad \text{(A.2)}$$

A fit with the PEARSON type VII function, [127] defined in equation (3.9), would have been best, but would require one more parameter for the fit, than the other two peak functions mentioned above (the exponent *m* which controls the relative weight of the tail and central parts of the peak).

A fit with a peak-function, derived from the hyperbolic cosine function, was used instead. The functional dependence used is:

$$f(T) = \frac{2 * a}{1 + \cosh\left( 2 * \frac{T - T_{\max}}{b} \right)} \qquad \text{(A.3)}$$

$T_{max}$ is the peak maximum, *a* is the peak height and *b* controls the peak width (the peak width at half of the maximum is about 1.8**b*).

The function can be approximated with a PEARSON type VII function with $m \approx 3.4$. Its area, which corresponds to the peak enthalpy $\Delta H_m$(low), is S = 2**a***b*.

The adjustable parameters of the fit are $T_{max}$, *a*, and *b*.

## *Appendix B*

*Fitting of the step-change in the heat capacity*

The step-change function used is derived from the hyperbolic tangent function:

$$f(T) = a_s * b * \left[1 + \tanh\left(\frac{T - T_{max}}{b}\right)\right] \qquad \text{(A.4)}$$

It is centered at the peak maximum $T_{max}$. The magnitude of the step-change is $\Delta C_P(T_{max}) = 2*a_s$. The parameter *b*, which controls the steepness of the step-change is the same as in equation (A.3) for the peak function.

In fact, the peak function is the derivative of the step-function, normalized by a constant factor. As their widths are the same, only the height of the step function is added as an adjustable parameter for the combined fitting procedure (through $a_s$). In choosing the peak function as the derivative of the step-function with the same center of symmetry ($T_{max}$) and width (*b*), one assumes that the two physical changes - the peak and the step-change in the heat capacity are two different manifestations of the same phenomenon and obey the same kinetics. As the exact physical origin of the step change in the heat capacity remains unclear (see reference 16 and section 5.2.2), the half-height of the step function $a_s$ is added as an independent parameter of the fit.

The studies of the scanning rate dependence of the low temperature peak have shown (section 5.6.1) that some of the above mentioned parameters of the peak and step functions: $\Delta H_m$(low), $T_{max}$, *a*, and *b* are heating rate dependent. From the universality of the peak characteristics, intuitively one could expect that the height of the step function $2*a_s$ is a function of the heating rate as well.

In conclusion, the procedure for resolving the low temperature endothermic peak is as follows:

- The heat capacity data in the vicinity of the low temperature endothermic peak is fitted with the combination of: linear function - equation (4.4), peak-function - equation (A.3), and step-function - equation (A.4).

- The linear function is determined independently from fitting the portion of the scan before the peak and is subtracted from the data.

- The residual scan is fitted with the sum of the peak-function and the step-function. The parameters of the fit are $T_{max}$, $a$, $b$, and $a_s$.

When the low temperature endothermic peak is observed close to another thermal transition (close to the glass transition or to the main melting peak) the fitting procedure is modified as described at the end of section 4.2.1.

# VESSELIN HRISTOV VELIKOV

## VITA

Vesselin H. Velikov was born in Varna, Bulgaria on May 9, 1965. He spent his pre-school years at the University of Veliko Turnovo, Bulgaria - most of the time in the kindergarten next to it, but often - in the lecture halls, sitting next to his Mom and drawing battle cartoons in her history notebooks. To this day he owes her for putting up with that and for the encouragement and support received from her later in his more productive college years. He graduated from the Mathematical High School in the town of Shumen in 1982, where he participated actively in regional competitions in mathematics and the National Olympiads in physics and mathematics. From 1982 to 1987 he attended Sofia University, Sofia, Bulgaria, where he was recipient of a fellowship during the last year of his studies. In June 1987, after defending a thesis on the subject of "Effect of Gamma-Radiation on the Structure and Properties of Isotactic Polypropylene", he received a degree in Physics (certification in Solid State Physics) from the College of Physics at Sofia University. Upon discharge from the army, where he served his military duty for the next two years, he applied to the Ph. D. program in Physics at Virginia Tech, and joined it in January 1990 on a full teaching assistantship. In the fall semester of 1991 he transferred to the Materials Engineering Science Ph. D. program and began working in the department of Chemistry under the guidance of his advisor Prof. Hervé Marand. In November, 1996 he received the degree of Doctor of Philosophy in Materials Engineering Science.